Aus der Klinik und Poliklinik für Hals-Nasen-Ohrenheilkunde,
Kopf- und Halschirurgie "Otto Körner", Universitätsmedizin Rostock
Direktor: Univ.-Prof. Dr. med. Robert Mlynski

Hydrostatischer Hochdruck in der Kopf-Hals-Chirurgie: Neue Perspektiven für Gewebeersatz und Tumortherapie

Kumulative Dissertation
zur Erlangung des akademischen Grades
Doktor der Medizinwissenschaften
der Universitätsmedizin Rostock

vorgelegt von
Friederike Kalle (geb. Poosch),
wohnhaft in Pinnow

Rostock, 2025

https://doi.org/10.18453/rosdok_id00005502

Gutachter:

Univ.-Prof. Dr. med. Robert Mlynski
Klinik und Poliklinik für Hals-Nasen-Ohrenheilkunde, Kopf- und Halschirurgie „Otto Körner“;
Universitätsmedizin Rostock

PD Dr. Anika Jonitz-Heincke
Orthopädische Klinik und Poliklinik, Forschungslabor für Biomechanik und Implantattechnologie;
Universitätsmedizin Rostock

Univ.-Prof. Dr. med. Stephan Hackenberg
Klinik und Poliklinik für Hals-Nasen-Ohrenheilkunde, Kopf- und Hals-Chirurgie;
Universitätsklinikum Würzburg

Jahr der Einreichung: 2025
Jahr der Verteidigung: 2025

Zusammenfassung

Bei der Behandlung von Kopf-Hals-Tumoren bestehen komplexe Herausforderungen sowohl in der Heterogenität der Tumoren als auch auf physischer und emotionaler Ebene bei den Patienten. Besonders nach chirurgischen Eingriffen oder einer Radio(chemo)therapie können funktionelle Einschränkungen beim Sprechen und Schlucken auftreten. Im Rahmen der Patientenversorgung werden diese häufig durch Fragebögen zur Lebensqualität erfasst. Kontrovers wird dazu diskutiert, ob die subjektive Einschätzung der schluckbezogenen Lebensqualität mit den tatsächlichen, objektiv gemessenen Funktionseinschränkungen übereinstimmt. In der vorliegenden Arbeit bestand keine Korrelation zwischen den subjektiv (M. D. Anderson Dysphagia Inventory-Fragebogen) und objektiv (faseroptische endoskopische Beurteilung des Schluckens) gemessenen Parametern. Daher sollte ein ganzheitlicher Ansatz mit der Kombination beider Methoden in der Patientenversorgung etabliert werden.

Schluckstörungen und Luftnot können beispielsweise in der Larynxchirurgie auftreten, wenn durch den Verlust des knorpeligen Kehlkopfskeletts eine Querschnittsverengung entsteht. Aufgrund dieser Limitation ist es notwendig, die Therapie von Kopf-Hals-Tumoren weiterhin durch innovative Ansätze zu verbessern. Eine mögliche Option ist der Einsatz von hydrostatischem Hochdruck (HHD). Dieser könnte Tumorzellen spezifisch devitalisieren und damit eine autologe, anatomisch korrekte Rekonstruktion des ehemals tumorinfiltrierten Knorpels ermöglichen. Als sicherer Schwellenwert konnte eine Behandlung mit 315 MPa etabliert werden, der durch die Quantifizierung der Zellvitalität mit durchflusszytometrischen Analysen und einem Kristallviolettassay bestätigt wurde. Ist eine Reimplantation jedoch nicht möglich, kann auf allogenen Gewebeersatz zurückgegriffen werden. Bei solchen Materialien ist ein Devitalisierungsschritt während der Aufbereitung notwendig, was oft kostspielig und arbeitsintensiv ist sowie die Gewebeintegrität schädigt. Die HHD-Technologie könnte hierbei eine Devitalisierung der Spenderzellen bei gleichzeitigem Erhalt der Matrixintegrität bewirken und somit eine allogene oder xenogene Transplantation ermöglichen. Eine effektive Devitalisierung von Chondrozyten und hyalinem Knorpelgewebe erfolgte bei einer HHD-Behandlung mit 200 MPa. Bei diesem Druckniveau konnten weder Zell- und Matrixschäden bei der elektronenmikroskopischen Analyse noch biomechanische Beeinträchtigungen bei Kompressionstests des Knorpels nachgewiesen werden.

Insgesamt bietet der HHD gegenüber anderen Methoden Vorteile in Bezug auf Zeit, Aufwand und Kosten. Außerdem ermöglicht er eine spezifische, gleichmäßige und reproduzierbare Devitalisierung von isolierten Zellen und Gewebe. Die Anwendung der HHD-Technologie hat das Potenzial, eine sichere und zuverlässige Methode für die autologe Rekonstruktion in der Kopf-Hals-Chirurgie sowie für den allogenen und xenogenen Gewebeersatz zu sein. Somit könnte die Verfügbarkeit von Transplantationsmaterialien im klinischen Bereich erweitert und deren Bereitstellung verbessert werden.

Für die klinische Anwendbarkeit von HHD-behandeltem Gewebe ist, zur Prüfung komplexer Prozesse wie der Immunreaktion auf ein Transplantat, ein In-vivo-Versuch erforderlich. Dabei ist zu beachten, dass Tierversuche auf ein Minimum reduziert (replace), die Anzahl der Tiere möglichst gering gehalten (reduce) und deren Belastung minimiert werden sollen (refine). Die Rückenhautkammer (RHK) im Mausmodell ist eine etablierte Methode für die wiederholte Untersuchung von Gefäßveränderungen und Entzündungen. Daher wurde dieses Modell genutzt, um die Immunogenität des HHD-behandelten Knorpels zu untersuchen, wobei sich lediglich eine geringe Inflammation durch die Implantation des HHD-behandelten Gewebes zeigte. Meistens wird beim RHK-Modell eine mit Schrauben befestigte Titan-RHK genutzt. Bei der Verwendung einer kleineren und leichteren RHK aus Polyetheretherketon (PEEK) hingegen kann die Fixierung mit reißfesten Nähten erfolgen, wodurch ein geringeres Trauma verursacht wird. Bei Titan-RHK besteht zudem das Risiko, dass diese durch das relativ hohe Gewicht seitlich abkippen und damit die Bewegungsfreiheit der Versuchstiere eingeschränkt ist. Beim Vergleich der verschiedenen Materialien kippten in der dritten Woche 50 % der RHK aus Titan um mehr als 80°, während der Neigungswinkel bei allen RHK aus PEEK drei Wochen lang unter 80° blieb. Weiterhin war bei den Mäusen mit PEEK-RHK der postoperative Gewichtsverlust geringer und sie erzielten ihr Ausgangsgewicht bereits in der zweiten Woche wieder. Die Tiere mit einer RHK aus Titan hingegen erreichten ihr Ausgangsgewicht über den gesamten Versuchszeitraum nicht. Somit erweist sich PEEK als geeignetes Material für die Herstellung von kleineren und leichteren RHK, mit denen sowohl das Wohlbefinden der Tiere als auch die Versuchszeit gesteigert werden können.

Zusammenfassend ist für eine Verbesserung der Behandlungsmöglichkeiten in der Kopf-Hals-Chirurgie ein interdisziplinärer, umfassender Ansatz erforderlich, der sowohl innovative Technologien als auch ethische Aspekte berücksichtigt.

Inhaltsverzeichnis

1 Einleitung

In der Kopf-Hals-Chirurgie können Traumata, Infektionen und Krebserkrankungen zu Gewebedefekten führen, die sowohl die Funktion als auch das Aussehen beeinträchtigen und eine große Herausforderung für die Geweberekonstruktion darstellen [1–5]. Bei den Krebserkrankungen haben beispielsweise Plattenepithelzellkarzinome des Kopfes und Halses (head and neck squamous cell carcinoma, HNSCC) einen großen Anteil. Jedes Jahr gibt es weltweit etwa 890000 neue Fälle, womit es die siebthäufigste Krebsart ist [6,7]. Die Erstdiagnose erfolgt zu über 60 % in einem fortgeschrittenen Stadium, was zu einer schlechten Prognose und einer 5-Jahres-Überlebensrate von weniger als 50 % führt [8]. Die Risikofaktoren für HNSCC umfassen u. a. Rauchen, Alkoholkonsum, HPV-Infektionen und Betelquid-Konsum [9–12]. Bei den Behandlungsoptionen werden verschiedene Einflussgrößen wie die primäre Lokalisation, das Stadium, die chirurgische Zugänglichkeit, die damit verbundene Morbidität und der allgemeine Gesundheitszustand des Patienten berücksichtigt [6,13,14]. Bei vergleichbarer Überlebenswahrscheinlichkeit ist die Therapieentscheidung häufig von der zu erwartenden Funktionseinschränkung abhängig [15]. Für die Lebensqualität der Betroffenen sind die Ästhetik sowie die Qualität des Sprechens und Schluckens wichtige Faktoren. Bei Störungen des Schluckvorganges, einer Dysphagie, können die Folgen von Unterernährung über Abhängigkeit von Sondennahrung bis hin zum Risiko einer Aspiration und permanenten Luftröhrenschnitten reichen [16–19]. In der Diagnostik besteht die Möglichkeit, eine Dysphagie durch die Visualisierung des Schluckvorganges mit Hilfe von objektiven fiberendoskopischen oder Videofluoroskopie-Untersuchungen nachzuweisen. Weiterhin sind Fragebögen ein bewährtes Mittel, um die allgemeine und schluckbezogene Lebensqualität der Betroffenen zu ermitteln [20,21].

Die zumeist bei HNSCC angewendeten kurativen Therapieoptionen sind Radiotherapie und Chirurgie. Bei einer Radiotherapie wird neben dem eigentlichen Tumorgewebe auch das umliegende Gewebe der Bestrahlungstoxizität ausgesetzt. Hierbei kann es zu postradiogenen Narben, Fibrosen und Gefäßschäden sowie in der Folge zu Sensibilitätsstörungen, Lymphödemen und Xerostomien kommen [22–24]. In der Chirurgie wird der Tumor mit ausreichendem Sicherheitsabstand entfernt. Dadurch wird häufig eine Rekonstruktion erforderlich, welche sowohl lokale und mikrovaskuläre Lappenplastiken als auch die Transplantation von Stützgewebe (Knorpel/Knochen) umfasst. Vor allem bei größeren Tumorresektionen kann sowohl die Funktion als auch die Ästhetik des betroffenen Areals stark beeinträchtigt sein, was mit Hilfe eines Gewebeersatzmaterials verbessert oder wiederhergestellt werden kann. Der derzeitige Goldstandard ist autologes Gewebe, das natürlicherweise begrenzt ist und eine zweite Operation an der Spenderstelle erfordert [25]. Diese Entnahme kann eine Morbidität an der Spenderstelle verursachen, was zu weiteren Komplikationen und dem Risiko einer irreversiblen Funktionseinschränkung führen kann. Eine verzögerte Genesung widerspricht zudem dem aktuellen Trend hin zu kurzen Liegedauern und einer ambulanten Kopf- und Halschirurgie [26]. Allo- und Xenotransplantate sind in größerer Menge verfügbar als autologes Gewebe, allerdings müssen mögliche Übertragungen von Krankheitserregern und die Abstoßung des Transplantats aufgrund der erhöhten Antigenität beachtet werden [27]. Die Prozessierung von solchem Gewebe ist oft kostspielig, arbeitsintensiv und kann die biomechanische Integrität stören.

Der europäische Rechtsrahmen sieht für die Verwendung von allo- und xenogenem Gewebe strenge Beschränkungen vor. Zur Gewährleistung der biologischen Sicherheit sind obligatorische Sterilisationsverfahren vorgeschrieben [28]. Die heutigen Sterilisationsmethoden, einschließlich chemischer, enzymatischer und physikalischer Verfahren, beeinträchtigen jedoch die Integrität des Gewebes und wirken sich auf die Biomechanik und das biologische Remodeling aus, was sich direkt auf das funktionelle Ergebnis und den Erfolg der Rekonstruktion auswirkt [29–35]. Obwohl verschiedene Ansätze für die Aufbereitung von Allo- und Xenotransplantaten untersucht wurden, konnte noch keine optimale Methode gefunden werden [36–39]. Beispielsweise führten Ansätze zur Knorpelregeneration nicht zu einer hyalinen extrazellulären Matrix (EZM), sondern zur Bildung von Faserknorpel [40,41]. Aus diesem Grund besteht weiterhin ein klinischer Bedarf an einer verbesserten Transplantatverarbeitung.

Die Technologie des hydrostatischen Hochdrucks (HHD) wird in der Lebensmittelindustrie häufig zur Dekontamination bei gleichzeitigem Erhalt von Geschmack und Vitaminen eingesetzt [42–44]. HHD zeichnet sich zudem durch die Fähigkeit aus, die strukturelle und biomechanische Integrität von Gewebe zu erhalten, was für eine erfolgreiche Transplantation entscheidend ist [45–48]. Je nach angewandtem Druck löst HHD den apoptotischen oder nekrotischen Zelltod aus, indem die Plasmamembran geschädigt und die tertiäre/quaternäre Proteinstruktur verändert wird [45,48,49]. Die HHD-Behandlung ist kostengünstig und vermeidet den Einsatz toxischer Substanzen [50]. Ein weiterer Vorteil ist die hohe Standardisierung, da der Druck sofort und isostatisch auf jede Zelle in komplexen Geweben wirkt [45,51]. Daher bietet HHD ein erhebliches Potenzial für die Aufarbeitung von Gewebetransplantaten (Abb. 1) [52].

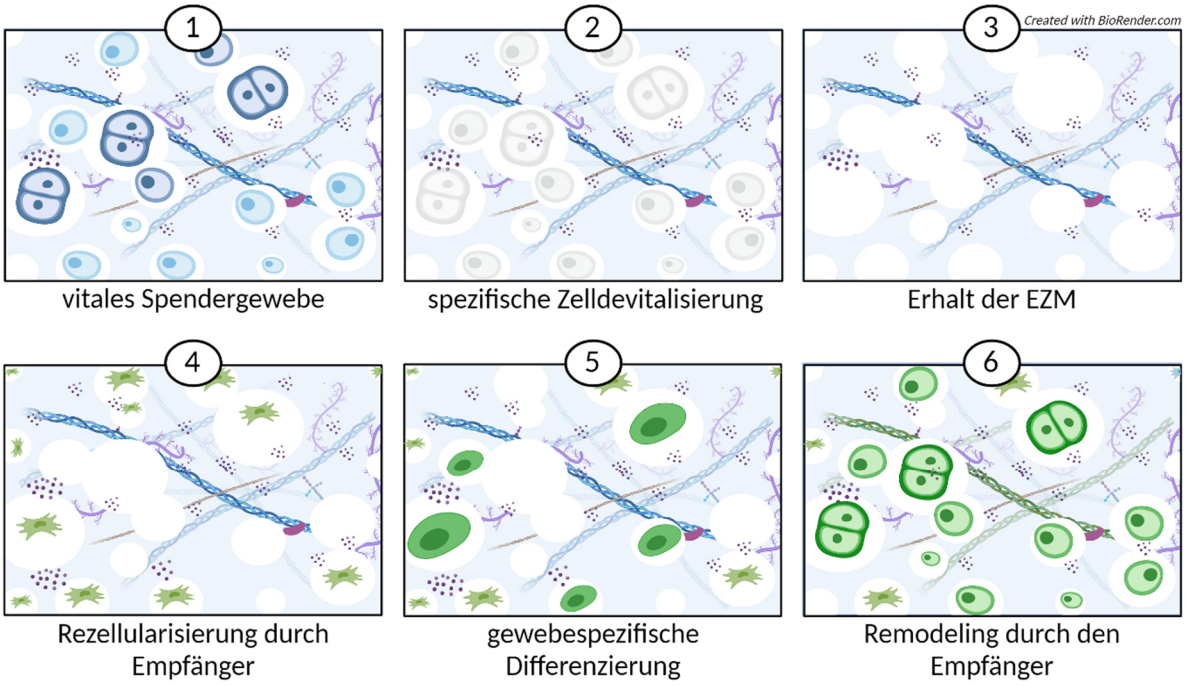

Abbildung 1: Gewebespezifische Rezellularisierung nach Devitalisierung mit Erhalt der extrazellulären Matrix.
Die Behandlung von vitalem Spendergewebe (1) mit hydrostatischem Hochdruck kann eine spezifische Zelldevitalisierung (2) bei gleichzeitigem Erhalt der extrazellulären Matrix (EZM, 3) bewirken. Bei der nachfolgenden Rezellularisierung durch Zellen des Empfängers (4) fungiert die EZM nicht als inertes Gewebe, sondern bedingt als Sekretionsprodukt der Zellen mit eingeschlossenen Mediatoren eine gewebespezifische Differenzierung der einwandernden Zellen (5). Dies führt wiederum zum Remodeling durch die Zellen des Empfängers, wodurch die Funktionalität des Gewebes erhalten bleibt (6). Modifiziert aus [52].

Um jedoch die klinische Anwendbarkeit und Sicherheit von HHD-behandeltem Gewebe gewährleisten zu können, ist es derzeit noch unerlässlich, die Effekte in präklinischen Modellen zu untersuchen. Entsprechende Forschungen zu Gewebeersatzmaterialien sind ohne Tierversuche noch nicht möglich, da derart komplexe Prozesse wie die Immunreaktion auf ein Transplantat nicht in vitro dargestellt werden können [52]. Um den ethischen Standards gerecht zu werden, müssen alle Versuche gemäß dem international anerkannten 3R-Prinzip (Europäische Richtlinie 2010/63/EU [53]) sorgfältig geplant und durchgeführt werden. Das 3R-Prinzip beinhaltet die Vorgaben, Tierversuche, wann immer es möglich ist, durch andere Methoden zu ersetzen (replace), die Anzahl der Versuchstiere auf ein Minimum zu reduzieren (reduce) sowie das Wohlbefinden der Versuchstiere zu steigern und gleichzeitig die Belastung für die Tiere möglichst gering zu halten (refine).

2 Zielsetzung und Fragestellungen

Kopf-Hals-Tumoren führen bei Betroffenen häufig zu physischen und emotionalen Herausforderungen. Bei der Therapie wird daher eine Balance zwischen effektiver Tumorbehandlung und dem Auftreten funktioneller Beeinträchtigungen gesucht. Beispielsweise ist eine Limitation in der Larynxchirurgie der Verlust des knorpeligen Kehlkopfskeletts. Dies führt zu einer Verkleinerung des Querschnittes sowie zur Störung des Ventilmechanismus zur Trennung von Luft- und Speiseweg und damit zu Aspiration, Luftnot und Schluckstörungen bei den Betroffenen. In klinischen Studien wird hierbei die schluckbezogene Lebensqualität häufig als primärer Endpunkt für den Behandlungserfolg gewählt. Bei subjektiven Verfahren besteht jedoch die Gefahr, dass Funktionsstörungen vom Patienten nicht bemerkt und somit übersehen werden, was wiederum zu gefährlichen Komplikationen wie einer stillen Aspiration führen kann. Das Ziel der Originalarbeit [I] war es, die schluckbezogene Lebensqualität in der Tumornachsorge zu erfassen und die Korrelation zwischen subjektiver Lebensqualität und der objektiven Schluckfunktion zu untersuchen.
Weiterhin wird eine stetige Verbesserung der Therapie von Kopf-Hals-Tumoren angestrebt. Eine mögliche Option ist der Einsatz der HHD-Technologie. Diese könnte die Tumorzellen devitalisieren und die strukturelle und biomechanische Integrität des tumorinfiltrierten Gewebes erhalten. Daher zielte die Originalarbeit [II] darauf ab, einen sicheren Schwellenwert für die Devitalisierung von HNSCC zu bestimmen, um die zukünftige Anwendung der HHD-Behandlung zur autologen anatomisch korrekten Rekonstruktion in der Kopf-Hals-Chirurgie zu ermöglichen. Das Ziel ist die orthotope Reimplantation von devitalisiertem Knorpel nach der kompletten Inaktivierung von Tumorzellen. Bei zu vielen Defekten ist eine Reimplantation jedoch nicht möglich, sodass auf allogenes oder xenogenes Transplantatmaterial zurückgegriffen werden muss. Bei solchen Materialien ist ein Devitalisierungsschritt während der Aufbereitung obligat. Häufig werden chemische, enzymatische oder physikalische Methoden angewandt, die jedoch die Matrixintegrität und die biomechanischen Eigenschaften der Gewebe verschlechtern. Die Originalarbeit [III] evaluierte deshalb, inwieweit eine HHD-Behandlung für die Aufbereitung von Gewebeersatzmaterialien geeignet ist. Hierfür wurde eine Druckamplitude identifiziert, welche eine effektive Devitalisierung von hyalinem Knorpelgewebe bei gleichzeitigem Erhalt der Matrixintegrität und der biomechanischen Eigenschaften bewirkt. Zudem wurde die Immunogenität des prozessierten Gewebes in einem Tiermodell, der Rückenhautkammer (RHK) der Maus, untersucht. Bei solchen Tierversuchen ist die Einhaltung des 3R-Prinzips essentiell. Die Originalarbeit [IV] zielte darauf ab, die Belastung der Mäuse im RHK-Modell zu minimieren und somit deren Wohlbefinden zu steigern. Hierfür wurde eine kleinere und leichtere RHK aus dem autoklavierbaren Material Polyetheretherketon (PEEK) entwickelt und in einem Pilotversuch getestet.
Mit den vorgelegten Arbeiten sollen daher folgende Fragestellungen beantwortet werden:

- Liegt eine Korrelation zwischen der subjektiven, schluckbezogenen Lebensqualität und der objektiv gemessenen Schluckfunktion nach Tumorbehandlung vor?
- Welcher Schwellenwert ist bei einer HHD-Behandlung von HNSCC onkologisch sicher?
- Ist der Einsatz von HHD-behandeltem xenogenem Gewebeersatz bei der Rekonstruktion größerer Defekte im Kopf-Hals-Bereich im Vergleich zu anderen Gewebeersatzmaterialien eine einfachere, zeitlich effektivere und dennoch sichere Behandlungsoption?
- Bei welcher HHD-Behandlung liegen eine vollständige Devitalisierung und zugleich eine intakte Matrixintegrität und Biomechanik bei Knorpelgewebe vor?
- Welche entzündlichen Veränderungen zeigen mit HHD-behandelte Knorpelgewebe in der RHK der Maus?
- Weist eine neuartige RHK aus PEEK gegenüber der herkömmlichen aus Titan Vorteile hinsichtlich der maximalen Versuchsdauer und des Wohlbefindens der Mäuse auf?

3 Methoden

3.1 Klinische Studie

3.1.1 Studiendesign

Für die Erfassung der Zusammenhänge zwischen der subjektiven allgemeinen und schluckbezogenen Lebensqualität sowie der objektiven Schluckfunktion nach Behandlung von HNSCC wurde eine Querschnittsstudie durchgeführt. Alle Patienten haben entsprechend der Vorgaben der Ethikkommission der Medizinischen Fakultät der Universität Rostock (A2018-0163) in Übereinstimmung mit der Deklaration von Helsinki aus dem Jahr 1964 zuvor eine schriftliche Einwilligung zur Verwendung ihrer Daten unterzeichnet. Zudem wurden unabhängig von der Behandlungsart Patienten jeden Alters und Geschlechts konsekutiv eingeschlossen, bei denen histologisch ein HNSCC nachgewiesen wurde.

3.1.2 Subjektive Erfassung der Lebensqualität mit Fragebögen

Die subjektive schluckbezogene Lebensqualität wurde durch die deutsche Version des M. D. Anderson Dysphagia Inventory- (MDADI) Fragebogens [20,54] erfasst (n = 307). Hierbei werden die Auswirkungen der Dysphagie auf globaler, emotionaler, funktionaler und physischer Ebene bewertet. Der Maximalwert von 100 bedeutet, dass keine Einschränkungen durch die Dysphagie vorliegen.
Die Fragebögen wurden zufällig entweder digital oder in Papierform über die Evasys Survey Software, Version 8.0 (Evasys GmbH, Lüneburg, Deutschland) zur Verfügung gestellt [5].

3.1.3 Objektive Beurteilung der Schluckfunktion durch fiberendoskopische Untersuchungen

Die objektive Beurteilung der Schluckfunktion fand mit Hilfe der endoskopischen Beurteilung des Schluckens (Fiberoptic Endoscopic Evaluation of Swallowing, FEES, n = 59) statt. Der Eingriff wurde nach einem standardisierten Protokoll durchgeführt: Es erfolgte eine anatomische, sensomotorische und endoskopische Untersuchung [5]. Letztere wurde für eine spätere Auswertung mit Video und Ton aufgezeichnet. Die Wirksamkeit und Sicherheit des Schluckens wurden anhand der Penetrations-Aspirations-Skala (PAS) zur Beurteilung der Tiefe der Bolusfehlleitung und der Reaktion des Patienten darauf (Skala von 1 bis 8, 1: unauffällige Schluckdynamik) sowie der Yale Pharyngeal Residue Severity Bewertungsskala (YPRSRS) zur Erfassung des Vorhandenseins und des Schweregrads von Rachenrückständen in den Valleculae und dem Sinus piriformis bewertet (Skala von 1 bis 5, 1: unauffällige Schluckdynamik, keine Rückstände) [5,55–57]. Die FEES und die anschließende Auswertung erfolgte gemäß validierter Richtlinien, um die Treue und Konsistenz des Bewertungsprozesses zu gewährleisten [58].

3.2 In-vitro-Analysen

3.2.1 Gewebeentnahme

Die Entnahme von Septumknorpel im Rahmen der Körperspende bis zu 72 h post mortem wurde von der Ethikkommission der Medizinischen Fakultät der Universität Rostock (A2018-0163) in Übereinstimmung mit der Deklaration von Helsinki aus dem Jahr 1964 genehmigt. Hierfür erfolgte die Lagerung auf dem Rücken. Nach der Freilegung des Knorpels mit einem Hemitransfixationsschnitt nach submukoperichondrialer Dissektion wurde ein 2 x 3 cm großes Fragment entnommen.
Der porcine Schildknorpel wurde von einer lokalen Landfleischerei von bis zu sechs Monate alten Tieren zur Verfügung gestellt. Es erfolgten die Präparation des Larynx und die Trennung des Schildknorpels vom umliegenden Perichondrium.
Anschließend fand die Lagerung der Knorpel in Dulbecco's phosphatgepufferter Salzlösung (phosphate buffered saline, PBS) mit Zusatz von 1 % Penicillin/Streptomycin (P/S, Sigma-Aldrich Chemie GmbH, Taufkirchen, Deutschland) bei 4 °C statt. Die PBS-Lösung wurde zuvor durch das Hinzufügen von 10x PBS (Sigma-Aldrich

Chemie GmbH, Taufkirchen, Deutschland) in Ampuwa® Spüllösung (Fresenius Kabi AG, Bad Homburg, Deutschland) im Verhältnis von 1:10 hergestellt.
Für weiterführende Experimente wurde der porcine Schildknorpel entsprechend dem gewünschten Durchmesser (10 mm: Ring-Stanzwerkzeug, Hoffmann Group, München, Deutschland; 2 mm: Biopsiestanze, GSK Consumer Healthcare, Dungaravan, Irland) und einer Höhe von 1 mm (Rhinogrid® Precisely Measure Dice & Slicing Grid, DrKhan´s™Creations, Maharahtra, Indien) geschnitten.

3.2.2 Zellkultur

3.2.2.1 Chondrozyten

Die Chondrozytenisolation erfolgte, indem der zerkleinerte, humane Septumknorpel zunächst für 20 min in Trypsin-Ethylendiamintetraessigsäure (EDTA) (Gibco™ - Thermo Fisher Scientific, Waltham, MA, USA) und dann für 3 h in Collagenase A (0,46 U/ml, Roche Diagnostics Deutschland GmbH, Mannheim, Deutschland) bei 37 °C im Thermoschüttler KS 4000 i control (75 rpm, IKA-Werke GmbH & Co. KG, Staufen, Deutschland) gelagert wurde. Die Zellkultivierung fand bei 37 °C und 5 % CO_2 in Dulbecco's Modifiziertem Eagle-Medium + GlutaMAX™ (DMEM, Gibco™ - Thermo Fisher Scientific, Waltham, MA, USA) unter Zusatz von 10 % fetalem Kälberserum (FKS, Sigma-Aldrich Chemie GmbH, Taufkirchen, Deutschland), 1 % P/S, 1 % Amphotericin B (PAN Biotech, Aidenbach, Deutschland) und 50 µg/ml Ascorbinsäure (Sigma-Aldrich, München, Deutschland) statt.

3.2.2.2 Tumorzellen

HNSCC-Zellen von der Zunge (UT-SCC-14) und vom Larynx (HNSCC16, patientenabgeleitete Zellen [59]) wurden bei 37 °C und 5 % CO_2 in DMEM/F12 (PAN-Biotech GmbH, Aidenbach, Deutschland) unter Zusatz von 10 % FKS und 1 % P/S kultiviert.
Alle Zellen wurden passagiert, wenn sie eine Konfluenz von 80 bis 90 % erreichten.

3.2.3 Hydrostatische Hochdrucktechnologie

Porciner Schildknorpel oder humane Chondrozyten und Tumorzellen wurden zusammen mit dem entsprechenden Medium in Kryotubes (1,8 ml, Thermo Fisher Scientific, Waltham, MA, USA) und diese wiederum in ein mit Wasser gefülltes 50 ml-Zentrifugenröhrchen überführt, bevor die HHD-Behandlung in der mit Glykol gefüllten Druckkammer der Druckprüfanlage "205797 - Druckprüfanlage 6000 bar" (Dustec Hochdrucktechnik GmbH, Wismar, Deutschland) erfolgte. Der Druck wurde mit dem Drucksensor HP-2-S 7000 bar (WIKA Alexander Wiegand SE & Co. KG, Klingenberg, Deutschland) überprüft und die Proben für 10 min behandelt. Die Kammertemperatur betrug 30 °C für Gewebeproben und Chondrozyten und 20 °C für Tumorzellen. Die Kontrollgruppen wurden in der Druckprüfanlage dem atmosphärischen Druck ausgesetzt.

3.2.4 Elektronenmikroskopie

Zellpellets von humanen Chondrozyten oder aufbereitete porcine Schildknorpel-Proben wurden mit HHD behandelt und anschließend in einer Lösung von 2 % Glutaraldehyd und 1 % Paraformaldehyd in 0,1 M Natriumphosphatpuffer fixiert. Nach einer Stunde bei Raumtemperatur erfolgte die Lagerung bei 4 °C. Die nachfolgende Feldemissions-Rasterelektronenmikroskopie (FESEM) wurde im Elektronenmikroskopischen Zentrum der Universitätsmedizin Rostock durchgeführt. Hierfür wurden die Proben zweimal mit Natriumphosphatpuffer gewaschen und ein Aliquot der Zellen für eine Stunde auf ein mit 0,1 %igem Poly-L-Lysin beschichtetes Deckglas aufgebracht. Anschließend fanden die Dehydratation in einer aufsteigenden Acetonreihe und die Kritisch-Punkt-Trocknung mit CO_2 als Zwischenmedium statt (Emitech K850, Quorum Technologies Ltd., East Sussex, Vereinigtes Königreich Großbritannien und Nordirland). Um die Strukturen sichtbar zu machen, wurden die getrockneten Schildknorpel in flüssigem Stickstoff tiefgefroren und mit Hilfe einer Pinzette aufgebrochen. Die Herstellung der Oberflächenleitfähigkeit erfolgte durch Sputterbeschichtung der Proben mit einer Goldschicht von etwa 10 – 15 nm Dicke (Leica SCD 500, Leica Microsystems, Wetzlar, Deutschland). Die Zelloberflächen wurden mit dem FESEM untersucht (MERLIN VP Compact, Carl Zeiss, Oberkochen, Deutschland, Detektor: HE-SE2, Beschleunigungsspannung: 5,0 kV, Arbeitsabstände ca. 5,2 - 5,3 mm).

Für die Transmissionselektronenmikroskopie (TEM) wurden im Elektronenmikroskopischen Zentrum der Universitätsmedizin Rostock die Zellpellets von humanen HHD-behandelten Chondrozyten mit vorgewärmter 2 %iger Agarose gemischt und erneut als Pellet in der Agarose gesammelt. Es erfolgten die Fixierung mit einer 1 %igen Osmiumtetroxidlösung, das Waschen mit destilliertem Wasser, eine Dehydratation mit einer aufsteigenden Acetonreihe und das Einbetten in Epon-Harz. Nach dem Aushärten des Harzes wurden auf einem Ultramikrotom (Ultracut S, Reichert, Wien, Österreich) mit einem Diamantmesser halbdünne und ultradünne Schnitte angefertigt. Ultradünnschnitte von ca. 70 nm Dicke wurden mit Bleicitrat und Uranylacetat kontrastiert und mit dem TEM (EM902, Carl Zeiss, Oberkochen, Deutschland) bei verschiedenen Vergrößerungen und einer Beschleunigungsspannung von 80 kV untersucht. Die Aufnahme der digitalen Bilder erfolgte mit der iTEM-Kamerasteuerungs- und Bildgebungssoftware (Olympus Soft Imaging Solutions, Münster, Deutschland) mit einer 1x2k FT-CCD-Kamera (Proscan, Scheuring, Deutschland).

3.2.5 Zellviabilität

Nach der HHD-Behandlung von Chondrozyten oder Tumorzellen (n = 5) fand die Inkubation der Zellen für 72 h in einer 24 Well-Platte bei 37 °C und 5 % CO_2 statt. Die Chondrozyten wurden im Anschluss für 1 h mit einer Lösung des wasserlöslichen Tetrazolium- (Water-Soluble Tetrazolium (WST) 1-Reagenz, Premix WST-1 Cell Proliferation Assay System, Takara Bio Europe SAS, Saint-Germain-en-Laye, Frankreich) und dem entsprechenden Kulturmedium im Verhältnis 1:10 inkubiert. Die Quantifizierung der Formazan-Farbstoffproduktion erfolgte durch Extinktionsmessungen mit einem Tecan Infinite® 200 Pro Reader (Tecan Group Ltd., Männerdorf, Schweiz) bei einer Absorptionswellenlänge von 450 nm mit einer Referenzwellenlänge von 600 nm. Die Tumorzellen wurden im Anschluss an die 72-stündige Inkubation mit einer 0,2 %igen Kristallviolettlösung für 10 min gefärbt, bevor die Zellen mit PBS gewaschen und letztlich mit einer 1 %igen Natriumdodecylsulfat-Lösung (Sodium Dodecyl Sulfate, SDS) für 10 min auf einem Schüttler inkubiert wurden. Die Absorptionsmessung erfolgte bei 560 nm mit einem Spektrophotometer (Tecan Reader Infinite M Plex, Tecan Group Ltd., Männerdorf, Schweiz).

3.2.6 Zelltodanalyse

Für die Bestimmung des Anteils von Apoptose und Nekrose wurden die Zellen 24 h nach der HHD-Behandlung bei 37 °C und 5 % CO_2 inkubiert. Anschließend fand die Färbung der Chondrozyten (n = 5) nach den Herstellerangaben mit dem APC Annexin-V (AxV) Apoptose-Nachweiskit mit Propidiumiodid (PI) (Biolegend, San Diego, CA, USA) statt. Nachdem dieser Ansatz für 15 min im Dunkeln inkubierte, erfolgte die Zugabe von 300 µl Annexin Binding Buffer. Die UT-SCC-14-Zellen (n = 15) wurden mit einer YoPro 1-Iodid-Färbelösung gefärbt und für 20 min inkubiert. Anschließend erfolgte die Zugabe von PI zu beiden Zelltypen. Die Analyse wurde mit dem FACS Calibur Durchflusszytometer (BD, Heidelberg, Deutschland) durchgeführt und die Daten mit der FloJo Software (v10.6.1, BD, Heidelberg, Deutschland) analysiert, um den Prozentsatz der Zellen mit positiven Signalen zu bestimmen.

3.2.7 DNA-Gehalt

Der porcine Schildknorpel (Durchmesser: 10 mm, Kontrolle: n = 11, HHD-behandelt: n = 8) wurde nach der HHD-Behandlung in kleine Stücke von etwa 1 x 1 mm geschnitten und bei -20 °C eingefroren, bevor die Gefriertrocknung für mindestens 7 h erfolgte. Im Anschluss fanden die Gewichtserfassung und der Verdau mit 3 ml Collagenase A über Nacht im Thermoschüttler (75 rpm) statt. Die DNA-Isolation wurde mit dem Quick-DNA Midiprep Plus Kit (Zymo Research, Irvine, CA, USA) durchgeführt und die Konzentration durch Extinktionsmessungen bei 260 und 280 nm (Tecan Infinite® F200 Pro Reader) bestimmt.

3.2.8 Kompressionstest

Der porcine Schildknorpel (Durchmesser: 10 mm) wurde mit HHD behandelt (Kontrolle: n = 11, 100 MPa: n = 9, 200 MPa: n = 8, 300 MPa: n = 10). Zur Ermittlung des Elastizitätsmoduls erfolgte anschließend ein Unconfined compression-Test mit der Mach-1 v500css (Biomomentum Inc., Montreal, Kanada) und einer Kraftmessdose mit einer Kapazität von 100 N (Honeywell, Charlotte, NC, USA) am Universitätsklinikum Freiburg, Abteilung Muskuloskelettale Forschung. Zur Auswertung wurde die Software Mach-1 Analysis (v4.1.0.17) genutzt.

3.3 In-vivo-Analysen

3.3.1 Ethische Voraussetzungen und Tierinformationen

Alle In-vivo-Experimente erfolgten gemäß dem deutschen Tierschutzgesetz (7221.3-1-012/20) und dem NIH Guide for the Care and Use of Laboratory Animals [60]. Für alle Experimente wurden männliche haarlose SKH1-hr-Mäuse verwendet (Crl:SKH1-Hrhr Outbred, 6 - 10 Wochen alt, 25 – 30 g schwer), welche einzeln in speziellen Käfigen untergebracht wurden, die so konstruiert waren, dass kein Kontakt der RHK mit dem Käfigdach möglich war. Der Gesundheitszustand der Tiere wurde täglich bewertet und sie hatten ad libitum Zugang zu Futter und Wasser, wobei letzteres 2,5 mg/ml Metamizol (Ratiopharm, Ulm, Deutschland) enthielt. Vor dem eigentlichen Versuchsbeginn gab es eine einwöchige Eingewöhnungsphase, um die Tiere mit den Versuchsbedingungen vertraut zu machen.

3.3.2 Studiendesign

Zur Beurteilung der Biokompatibilität von HHD-behandeltem porcinem Schildknorpel wurden 22 Mäuse zufällig in zwei Gruppen aufgeteilt: Kontrolle (n = 10) und 200 MPa (n = 12). Deren Beobachtung fand 2 Tage vor und über einen Zeitraum von 15 Tagen nach der Implantation des Knorpelgewebes statt. In einem weiteren Versuch zur Prüfung des Materials PEEK als Ersatz für die herkömmliche RHK aus Titan wurden 12 Mäuse zufällig in zwei Gruppen aufgeteilt: Titan- und PEEK-RHK (je n = 6) und sowohl 2 bis 3 Tage vor der Präparation der RHK als auch 20 bis 21 Tage danach beobachtet. Nach den Messungen am jeweils letzten Versuchstag erfolgte die Euthanasie der Mäuse entsprechend der EU-Empfehlungen mit einer intravenösen Überdosis Ketamin- (100 mg/kg Körpergewicht) und Xylazinhydrochlorid (Rompun; 6 mg/kg Körpergewicht) gefolgt von einer zervikalen Dislokation.

3.3.3 Herstellung der PEEK-Rückenhautkammer

Die PEEK-RHK wurde gemeinsam mit der Fakultät für Ingenieurwissenschaften der Hochschule Wismar mit SolidWorks (Dassault Systemes, MA, USA) entworfen und mit dem Fused Filament Fabrication-Verfahren und dem Drucker Minifactory ultra (miniFactory Oy LTD, Seinajoki, Finnland) angefertigt. Hierfür erfolgte die Verwendung des biokompatiblen und dampfsterilisierbaren PEEK-Filaments Intamsys Funmat HT (INTAMSYS Technology Co. Ltd, Shanghai, China) mit einem Biegemodul von 3738 MPa und einer Zugfestigkeit von 100 MPa. Das Slicing fand gemäß den Herstellereinstellungen mit einer Schichtdicke von 250 µm statt. Unregelmäßigkeiten auf der Oberseite (Fensterseite) wurden nach dem Druckvorgang manuell geschliffen und sieben Löcher mit 1 mm Durchmesser für die spätere Fixierung der RHK gebohrt. Vor der Verwendung fanden eine visuelle Prüfung der PEEK-RHK sowie eine Nachbehandlung durch Dampfsterilisation statt.

3.3.4 Präparation der Rückenhautkammer

Für die Präparation der RHK [61–63] wurden die Tiere durch intraperitoneale Injektion von Ketamin and Xylazin (90 und 25 mg/kg Körpergewicht, Medistar, Holzwickede and Bayer, Leverkusen, Germany) betäubt. Es erfolgte entlang der dorsalen Medianlinie das Aufspannen einer Doppelhautschicht und deren Fixierung. Anschließend wurde die RHK an der Hautfalte befestigt, wobei dies bei der Titan-RHK mit Schrauben, bei der PEEK-RHK mit Nahtmaterial (FiberWire®, Arthrex GmbH, München, Deutschland) erfolgte. Die RHK wurde abschließend mit 0,9 %iger Kochsalzlösung (B. Braun Melsungen AG, Melsungen, Germany) gefüllt und durch einen Sprengring mit einem Deckglas (Durchmesser: 12 mm, Gerhard Menzel B.V. & Co. KG, Braunschweig, Germany) verschlossen.

3.3.5 Gewebeimplantation

Zwei Tage nach der RHK-Präparation wurden die Mäuse mit Hilfe des UniVet Porta T8 Systems (Groppler, Deggendorf, Deutschland) mit Isofluran (2,5 l/min, Baxter, Unterschleißheim, Deutschland) narkotisiert, um die Implantation des porcinen Schildknorpels (Durchmesser: 2 mm) durchzuführen. Anschließend erfolgte die Entfernung des Deckgläschens, das Auflegen des Gewebes, die Füllung der RHK mit 0,9 %iger Kochsalzlösung und das erneute Verschließen mit einem Deckgläschen.

3.3.6 Intravitalmikroskopie

Für die Intravitalmikroskopie (IVM) wurde eine Anästhesie durch eine kontinuierliche Gabe von Isofluran (2,5 l/min) durchgeführt. Anschließend erfolgte die Verabreichung von 0,05 ml Fluorescein-Isothiocyanat-markiertem Dextran (5 %, MW: 150 kD, Sigma, Deisenhofen, Deutschland) und 0,05 ml Rhodamin 6G (2 %, MW: 496 D, Sigma, Deisenhofen, Deutschland). Die Injektion beider Farbstoffe fand mit einer 32-G-Mikroinjektionsnadel (Mesoram® Ri.mos SRL, Mirandola, Italien) direkt intravenös in die laterale Schwanzvene der Maus statt. Es wurden vier Messfelder eingerichtet, um die funktionelle Kapillardichte (functional capillary density, FCD) wiederholt zu messen. Zwei dieser Felder wurden zentral innerhalb der 10-fachen Vergrößerung um die Transplantationsstelle herum positioniert, während die übrigen Felder außerhalb dieses zentralen Bereichs lagen. Die Mikroskopie erfolgte bei 10-facher Vergrößerung (10x/0,30 W, Plan-NEOFLUAR, Zeiss, Jena, Deutschland) für 20 s in jedem Feld. Die automatische Bildanalyse fand mit ImageJ (v1.53t) und QuPath (v0.3.0, [64]) statt.
Die IVM erfolgte an den Tagen 3, 6, 10 und 15 zur Messung der FCD als Indikator für Entzündungen nach der Gewebeimplantation.

3.3.7 Kippwinkel der Rückenhautkammer

Für die Analyse der RHK-Neigung fand die Sedierung der Tiere an den Tagen 7, 12 und 20/21 für etwa 10 s in einer Isofluran-Kammer statt. Die Tiere wurden aufrecht positioniert und von hinten fotografiert. Die Messung der Kippwinkel erfolgte, indem mit der Software Photoshop (Adobe Inc., San Jose, USA.) die Abweichung von einer vertikalen Linie in Grad bestimmt wurde.

3.3.8 Gewichtsbestimmung

Die Gewichtsbestimmung der Mäuse fand auf einer Waage (EMB 200-2, Kern & Sohn, Balingen, Deutschland) zwischen 9:00 und 9:30 Uhr an den Tagen 7, 12 und 20/21 statt. Die Bestimmung der Gewichtsänderung erfolgte prozentual zum jeweiligen Ausgangsgewicht, indem das gemessene Gewicht des Tieres mit dem jeweiligen Ausgangsgewicht verglichen wurde.

3.4 Statistik

Die statistische Auswertung fand mit der Software GraphPad Prism 8 oder 9 (GraphPad Software, San Diego, CA, USA) statt. Eine statistische Signifikanz wurde für p-Werte unter 0,05 angenommen. Die Prüfung auf Normalverteilung erfolgte mit dem Shapiro-Wilk-Test, mit Ausnahme der unter „Klinische Studie“ beschriebenen Analysen, bei denen der D'Agostino-Pearson-Test Anwendung fand. Die Darstellungsform der abgebildeten Werte sowie die genaue verwendete statistische Analysemethode wurden in den Abbildungslegenden dargelegt.

4 Ergebnisse

4.1 Ergebnisse des schluckbezogenen Fragebogens

Insgesamt haben 59 Patienten sowohl den MDADI-Fragebogen ausgefüllt als auch die objektive Bewertung der Schluckfunktion durch FEES vornehmen lassen. Das Durchschnittsalter war in dieser Gruppe 63,20 Jahre und der Männeranteil 77,97 % (46/59). Insgesamt lag bei 16,95 % (10/59) der Patienten ein Tumor in der Mundhöhle (MDADI Gesamt-Score: 71,90 ± 14,66), zu 55,93 % (33/59) im Oropharynx (MDADI Gesamt-Score: 60,58 ± 14,90), zu 10,17 % (6/59) im Hypoharynx (MDADI Gesamt-Score: 61,33 ± 15,10) und zu 15,25 % (9/59) im Larynx (MDADI Gesamt-Score: 68,00 ± 20,55) vor. Zu 1,69 % (1/59) (MDADI Gesamt-Score: 78,00 ± 0,00) bestand eine unbekannte Primärlokalisation (Cancer of Unknown Primary, CUP). Es wurde zudem bei je 18,64 % (11/59) der Patienten das Tumorstadium 1 (MDADI Gesamt-Score: 63,27 ± 17,40) und 2 (MDADI Gesamt-Score: 59,27 ± 22,28), bei 28,81 % (17/59) das Tumorstadium 3 (MDADI Gesamt-Score: 61,71 ± 17,45) und bei 32,20 % (19/59) das Tumorstadium 4 (MDADI Gesamt-Score: 68,47 ± 8,07) festgestellt. Weiterhin war die primäre Behandlung zu 55,93 % (33/59) die Chirurgie (MDADI Gesamt-Score: 62,21 ± 16,02) und zu 44,07 % (26/59) die Radio(chemo)therapie (MDADI Gesamt-Score: 66,27 ± 16,13). Es lag weder ein signifikanter Unterschied im MDADI Gesamt-Score der verschiedenen Lokalisationen noch der Tumorstadien ($p > 0,05$, s. Anhang Tab. A1) im Vergleich zu Tumorstadium 1 (T2: $p = 0,88$, T3: $p = 0,99$, T4: $p = 0,71$) oder zwischen den Therapiemöglichkeiten ($p = 0,34$) vor (Abb. 2).

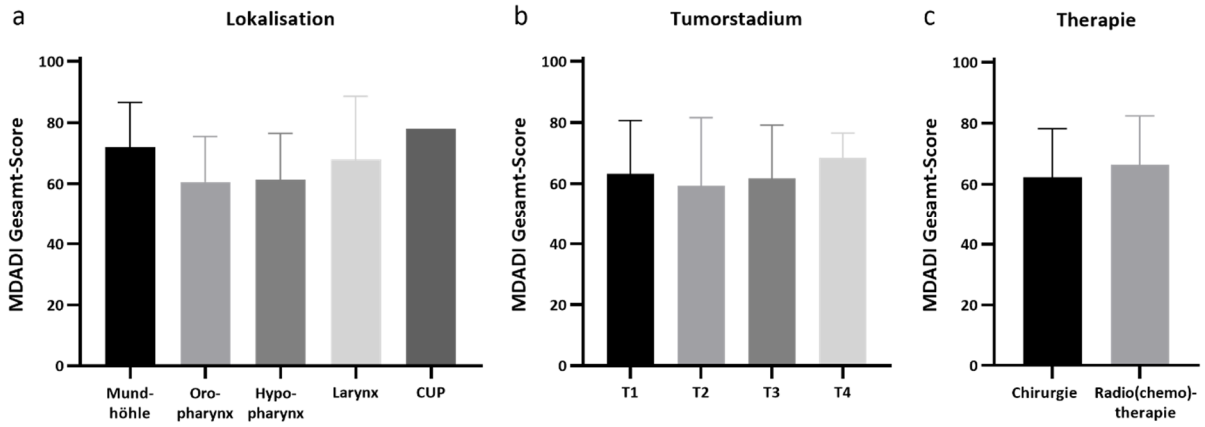

Abbildung 2: Verteilung der Lokalisation, Tumorstadien und Therapieoptionen bei Patienten mit Kopf-Hals-Tumoren
Der M. D. Anderson Dysphagia Inventory (MDADI) Gesamt-Score zeigt weder bei der Verteilung der Lokalisation (a) noch bei den Tumorstadien (T1 bis T4, b) oder bei den verschiedenen Therapieoptionen (c) einen signifikanten Unterschied. a: n – Mundhöhle = 10, n – Oropharynx = 33, n – Hypopharynx = 6, n – Larynx = 9, n – Karzinom unbekannter Primärlokalisation (Cancer of Unknown Primary, CUP) = 1, b: n – T1/T2 = 11, n – T3 = 17, n – T4 = 19, c: n – Chirurgie = 33, n – Radio(chemo)therapie = 26, Ordinary One-Way-ANOVA mit Dunnett's (a) oder Tukeys Test (c) für Mehrfachvergleiche, unabhängiger t-Test mit zweiseitiger p-Wert-Testung (b), $p < 0,05$: kein signifikanter Unterschied zwischen den verschiedenen Lokalisationen (a), T1 und T2 bis T4 (b) sowie zwischen den Therapieoptionen (c).

4.2 Korrelation zwischen subjektiver, schluckbezogener Lebensqualität und objektiv gemessener Schluckfunktion

Die objektive Bewertung der Schluckfunktion durch FEES ergab in der Studienkohorte (n = 59) einen medianen PAS-Score von 2 (Spannweite: 1 bis 8). Der mit der YPRSRS bestimmte Wert in den Valleculae zeigte einen Median von 4 (Spannweite: 1 bis 5), im Sinus piriformis von 2 (Spannweite: 1 bis 5). Die objektive Bewertung der Schluckfunktion durch FEES ergab keine signifikante Korrelation mit dem MDADI (Abb. 3). Zwischen dem MDADI und PAS-Score (n = 59) betrug der Spearman-Korrelationskoeffizient $r = 0,17$ und der zweiseitige p-Wert $p = 0,21$. Zwischen dem MDADI und der YPRSRS - Valleculae lagen die Werte bei $r = -0,04$ und $p = 0,81$ (n = 49) sowie zwischen dem MDADI und der YPRSRS - Sinus piriformis bei $r = 0,12$ und $p = 0,44$ (n = 48).

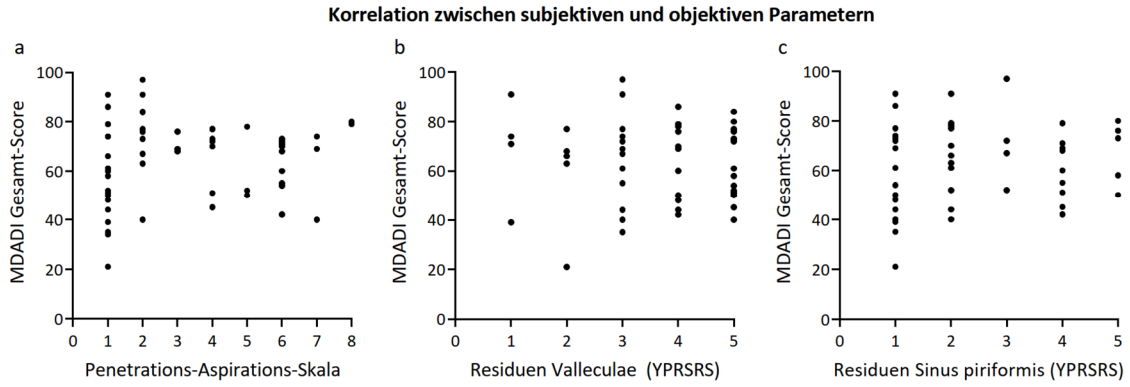

Abbildung 3: Korrelation zwischen der subjektiven, schluckbezogenen Lebensqualität (MDADI) und der objektiven, fiberendoskopischen Untersuchung des Schluckvorganges bei Patienten mit Kopf-Hals-Tumoren

Die Korrelation wurde zwischen dem MDADI und der Penetrations-Aspirations-Skala (a, n = 59, Spearman-Korrelationskoeffizient r = 0,17, zweiseitiger p-Wert p = 0,21), dem MDADI und der Yale Pharyngeal Residue Severity Bewertungsskala (YPRSRS) zur Erfassung des Vorhandenseins und des Schweregrads von Rachenrückständen in den Valleculae (b, n = 49, r = -0,04, p = 0,81) und dem Sinus piriformis (c, n = 48, r = 0,12, p = 0,44) bestimmt.

4.3 Analyse der Biomasse und Vitalität von humanen Tumorzellen

4.3.1 Biomasse

Die Bestimmung der Vitalität von etablierten (UT-SCC-14) und von Patienten abgeleiteten Zelllinien (HNSCC16) nach HHD-Behandlung erfolgte mit Hilfe des Kristallviolettassays (Abb. 4a). Hierfür wurde 72 Stunden nach der HHD-Behandlung die Absorption der vitalen Biomasse der Kontrollzellen auf 100 % normiert. Die berechnete relative Absorption zeigte für beide Zelllinien eine Verringerung bei der Behandlung bei 105 MPa im Vergleich zur unbehandelten Kontrolle. Die Werte betrugen nach Behandlung bei 105 MPa für UT-SCC-14 82,52 ± 8,16 % und für HNSCC16 63,81 ± 17,64 % ($p < 0,05$: 105 MPa vs. Kontrolle). Die relative Absorption von lebensfähiger Biomasse betrug nach 210 MPa-Behandlung 24,39 ± 3,91 % (UT-SCC-14) und 1,43 ± 2,20 % (HNSCC16) ($p < 0,05$: 210 MPa vs. Kontrolle/105 MPa). Auch nach der Anwendung von 315 MPa HHD wurde lebensfähige Biomasse mit relativen Absorptionen von 1,64 ± 3,01 % (UT-SCC-14) und 1,12 ± 1,69 % (HNSCC16) ($p < 0,05$: 315 MPa vs. Kontrolle/105 MPa) nachgewiesen.

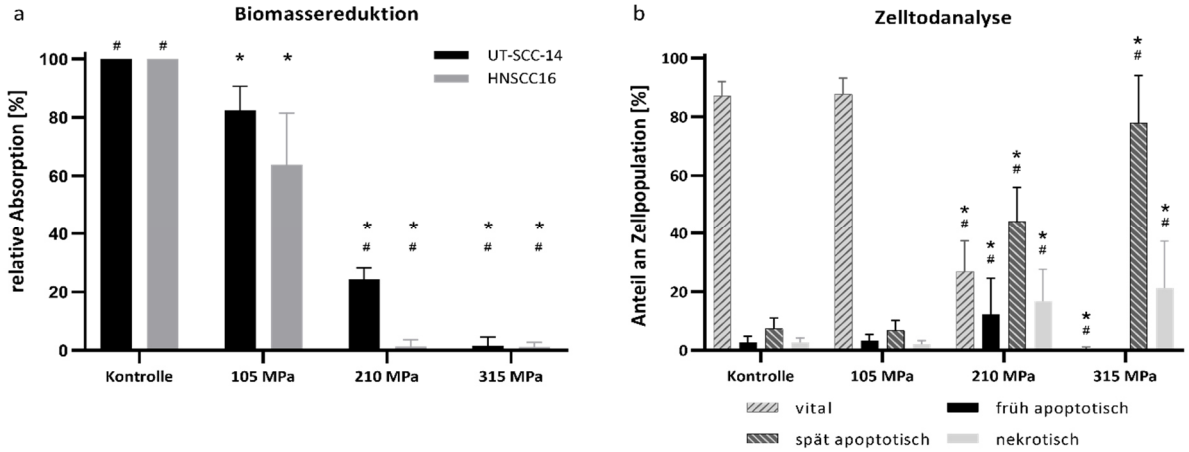

Abbildung 4: Auswirkungen des hydrostatischen Hochdrucks auf die Lebensfähigkeit von humanen Tumorzellen

Um Veränderungen von humanen Tumorzellen hinsichtlich der Biomasse (a) und der Vitalität (b) bewerten zu können, wurden UT-SCC-14 und HNSCC16-Zellen mit hydrostatischem Hochdruck von bis zu 315 MPa behandelt. Nach der Druckeinwirkung erfolgte die Inkubation der Zellen bei 37 °C und 5 % CO_2 für 24 (b) oder 72 h (a). Die Biomassereduktion wurde mit dem Kristallviolettassay bestimmt, während die Vitalität der UT-SSC-14-Zellen durchflusszytometrisch mit dem YoPro 1-Iodid/ Propidiumiodid-Assay analysiert wurde. Die Daten werden als Mittelwerte mit Standardabweichungen dargestellt. a: n = 5, b: n = 18, Two-Way-ANOVA mit Tukey's Test für Mehrfachvergleiche, *: $p < 0,05$ vs. unbehandelte Kontrolle, #: $p < 0,05$ vs. 105 MPa.

4.3.2 Vitalität

Mit Hilfe der Durchflusszytometrie wurde bei UT-SSC-14-Zellen zwischen verschiedenen Formen des Zelltodes, Apoptose und Nekrose, unterschieden (Abb. 4b). Die unbehandelte Kontrolle und die Zellen nach einer HHD-Behandlung bei 105 MPa hatten eine ähnliche Vitalität (Kontrolle: 87,06 ± 5,01 %, 105 MPa: 87,77 ± 5,46 %, $p > 0,99$) und es wurde keine Apoptose oder Nekrose induziert (frühe Apoptose: 2,70 ± 2,07 % (Kontrolle) und 3,33 ± 2,10 % (105 MPa), späte Apoptose: 7,49 ± 3,46 % (Kontrolle) und 6,81 ± 3,44 % (105 MPa), Nekrose: 2,75 ± 1,48 % (Kontrolle) und 2,09 ± 1,25 % (105 MPa), jeweils $p > 0,99$). Im Gegensatz dazu führte die HHD-Behandlung bei 210 MPa zu einem signifikant erhöhten Anteil an Apoptose und Nekrose im Vergleich zur Kontrolle und zur Behandlung mit 105 MPa (frühe Apoptose 12,22 ± 12,36 %, späte Apoptose 44,14 ± 11,68 %, Nekrose 16,70 ± 10,98 %; jeweils $p < 0,05$: 210 MPa vs. Kontrolle/105 MPa). Der Anteil vitaler Zellen verringerte sich signifikant auf 26,94 ± 10,37 % ($p < 0,05$: 210 MPa vs. Kontrolle/105 MPa). Wurden die Zellen mit HHD bei 315 MPa behandelt, blieben davon 0,67 ± 0,48 % vital ($p < 0,05$: 315 MPa vs. Kontrolle/105 MPa). Außerdem waren 0,06 ± 0,07 % der behandelten Zellen früh apoptotisch ($p = 0,78$ vs. Kontrolle, $p = 0,65$ vs. 105 MPa), 77,96 ± 16,11 % spät apoptotisch und 21,27 ± 16,00 % nekrotisch (jeweils $p < 0,05$ vs. Kontrolle/105 MPa).

4.4 Analyse der Zellmorphologie

Für die Beurteilung der Auswirkungen der HHD-Behandlung auf die Morphologie der Chondrozyten und deren Zellintegrität wurden FESEM- und TEM-Aufnahmen angefertigt (Abb. 5). Unbehandelte Zellen wiesen eine intakte Membranoberfläche mit zahlreichen Filopodien und Lamellipodien auf, die als glatte, kugelförmige bis knopfartige Erhebungen ersichtlich sind (Abb. 4a). Die Exposition bei 100 MPa führte zu keinen offensichtlichen morphologischen Veränderungen (Abb. 4b). Ab 200 MPa kam es zu einer Aufrauung der Zelloberfläche und kleine Perforationen der Zellmembran waren bei höherer Vergrößerung sichtbar. An einigen Stellen entwickelten sich auch größere Perforationen in der Zellmembran (Abb. 4c). Höhere Drücke bis zu 400 MPa verstärkten zunehmend diese Oberflächenveränderungen und führten zu zahlreichen Perforationen (Abb. 4d).

Außerdem wurden TEM-Aufnahmen von Chondrozyten zur Bewertung der Auswirkungen der HHD-Behandlungen auf die Integrität der Zellorganellen angefertigt (Abb. 4). Die Exposition bei 100 MPa verursachte Umlagerungen des Zytoskeletts mit Ansammlungen von Mikrofilamenten und Intermediärfilamenten, die als helle Flecken in den Schnitten sichtbar sind. Zudem wurde eine leichte mitochondriale Schwellung festgestellt, während das raue endoplasmatische Retikulum (rER) im Vergleich zu Kontrollzellen keine offensichtlichen strukturellen Veränderungen aufwies (Abb. 4e, f). Im Zellkern erschienen zusätzliche Stellen mit kondensiertem Heterochromatin (Abb. 4f). Die HHD-Behandlung bei 200 MPa verursachte ähnliche Auswirkungen auf das Zytoskelett und zudem eine Schädigung und Auflösung der mitochondrialen Struktur und des rER. Im Zellkern wurde eine starke Zunahme des Heterochromatins sowohl entlang der Kernlamina als auch an anderen Stellen ersichtlich, was auf eine erhebliche Chromatinschädigung hinweist (Abb. 4g). Nach einer Behandlung der Chondrozyten bei 300 MPa waren die meisten Organellen desintegriert und es waren nur noch Reste der inneren Struktur vorhanden. Ebenso sind Perforationen in der Zellmembran ersichtlich und das ehemalige Kerngebiet ist durch unscharfe Chromatinflecken gekennzeichnet (Abb. 4h).

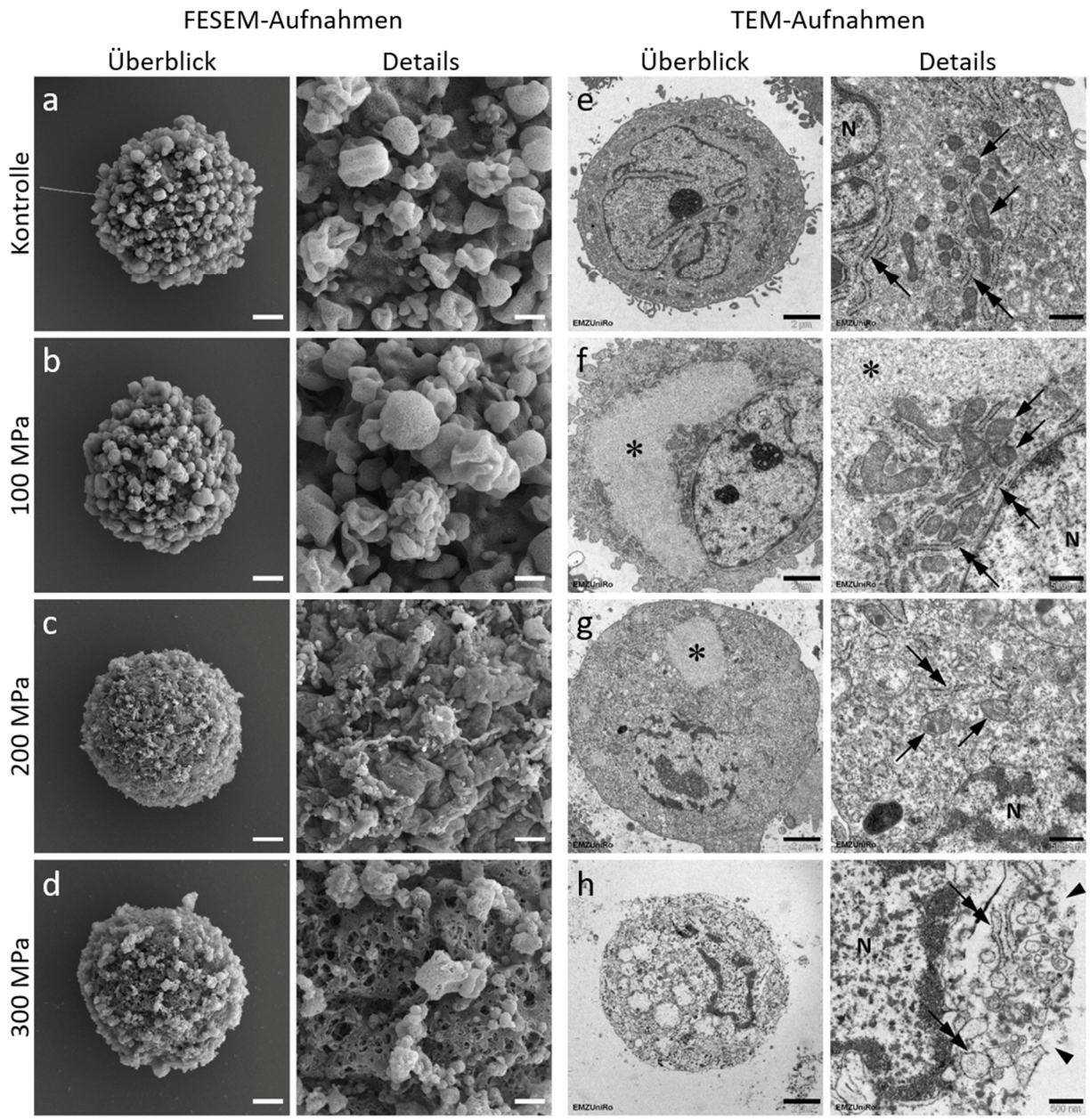

Abbildung 5: Elektronenmikroskopische Analyse von humanen Chondrozyten nach hydrostatischer Hochdruckbehandlung
Zur Detektion von Zellschädigungen wurden zum einen repräsentative Übersichtsaufnahmen der Chondrozyten und Detailansichten ihrer Zelloberfläche (a – d, Feldemissions-Rasterelektronenmikroskopie (FESEM)) angefertigt. Zum anderen erfolgte die Aufnahme von repräsentativen Querschnitten der Zellen und deren Organellen (e – h, Transmissionselektronenmikroskopie (TEM)). Die Chondrozyten wurden mit 100 MPa (b, f), 200 MPa (c, g) und 300 MPa (d, h) behandelt und mit der entsprechenden unbehandelten Kontrolle (a, e) verglichen. Im Gegensatz zur Kontrolle sind bei einem Druck von 100 und 200 MPa Anhäufungen von Zytoskelettelementen (Sternchen) sowie fortschreitende Organellenschädigungen zu beobachten. Die Veränderungen an Mitochondrien (Pfeile) und rauem endoplasmatischem Retikulum (Doppelpfeile) sowie Heterochromatinanhäufungen in den Nuclei (N) weisen auf eine allgemeine Organellen- und Membrankompartimentschädigung, einschließlich großer Membranperforationen (Pfeilspitzen) bei 300 MPa, hin. Maßstab Übersicht: 2 µm, Details: 500 nm.

4.5 Analyse der metabolischen Aktivität und Vitalität von humanen Chondrozyten

4.5.1 Metabolische Aktivität

Die metabolische Aktivität der humanen Chondrozyten wurde mit Hilfe eines WST-1-Assays bestimmt (Abb. 6a). Hierfür wurde 24 Stunden nach der HHD-Behandlung die relative Absorption der Stoffwechselaktivität der Kontrollzellen auf 100 % normiert. Die Stoffwechselaktivität verringerte sich nach der Behandlung bei 100 MPa auf 72,42 ± 10,83 % ($p = 0,52$) und lag nach der Exposition bei 200, 300 und 400 MPa unterhalb der Nachweisgrenze (jeweils $p < 0,05$ vs. Kontrolle/100 MPa). Die Entwicklung der Absorption der Stoffwechselaktivität war nach 48 und 72 Stunden ähnlich, wobei sie nach 48 Stunden in der Kontrollgruppe bei 233,80 ± 73,33 % lag. Sie verringerte sich signifikant weiter auf 134,20 ± 71,70 % (100 MPa), 5,05 ± 6,69 % (200 MPa), 0,72 ± 0,99 % (300 MPa) und 3,92 ± 5,82 % (400 MPa) (jeweils $p < 0,05$ vs. Kontrolle/100 MPa). Nach 72 Stunden betrug die relative Absorption der Stoffwechselaktivität 435,10 ± 107,50 % für die unbehandelte Kontrolle. Der Wert verringerte sich signifikant auf 242,10 ± 61,57 % (100 MPa), fiel unter die Nachweisgrenze (200 und 300 MPa) und betrug 1,21 ± 2,70 % nach der HHD-Behandlung bei 400 MPa (jeweils $p < 0,05$ vs. Kontrolle/100 MPa).

Im Zeitverlauf stieg die relative Absorption der Stoffwechselaktivität in der Kontrollgruppe signifikant auf 233,80 ± 73,33 % nach 48 Stunden und auf 435,10 ± 107,50 % nach 72 Stunden (jeweils $p < 0,05$ vs. 24 h). In der 100 MPa-Gruppe stieg die Stoffwechselaktivität von 72,42 ± 10,83 % nach 24 Stunden auf 134,20 ± 71,70 % nach 48 Stunden ($p = 0,18$ vs. 24 h) und signifikant auf 242,10 ± 61,57 % nach 72 Stunden ($p < 0,05$ vs. 24 h). In den 200-, 300- und 400 MPa-Gruppen gab es keinen signifikanten Anstieg über die Zeit ($p > 0,05$ vs. 24 h, s. Anhang Tab. A2).

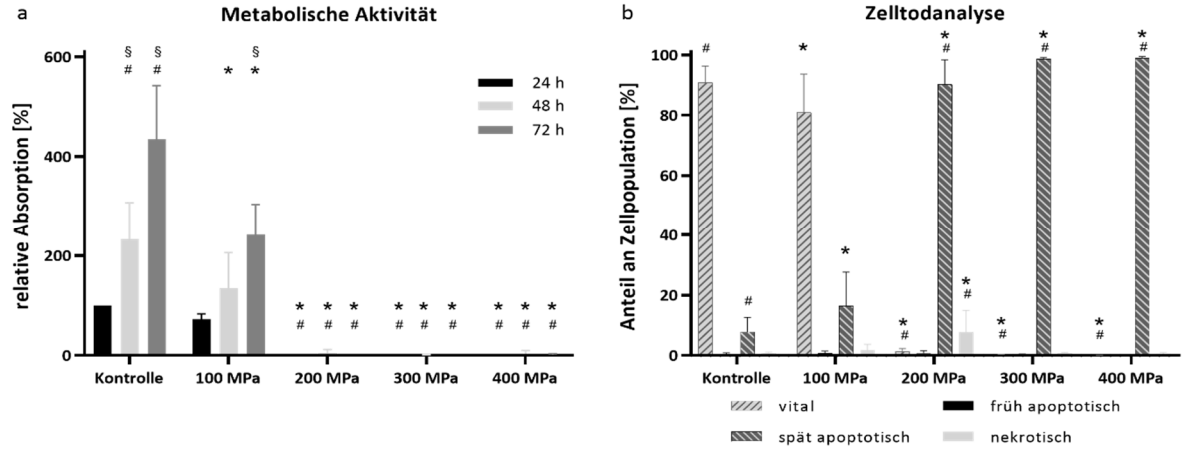

Abbildung 6: Auswirkungen des hydrostatischen Hochdrucks auf die Lebensfähigkeit von humanen Chondrozyten
Um Veränderungen von humanen Chondrozyten hinsichtlich der metabolischen Aktivität (a) und der Vitalität (b) bewerten zu können, wurden die Zellen mit hydrostatischem Hochdruck von bis zu 400 MPa behandelt. Nach der Druckeinwirkung erfolgte die Inkubation der Chondrozyten bei 37 °C und 5 % CO_2 für 24, 48 und 72 h. Die metabolische Aktivität wurde mit dem wasserlöslichen Metrazolium-1-Assay bestimmt, während die Vitalität der Zellen 24 h nach der hydrostatischen Hochdruckbehandlung durchflusszytometrisch mit dem APC-Annexin-V/Propidiumiodid-Assay analysiert wurde. Die Daten werden als Mittelwerte mit Standardabweichungen dargestellt. n = 5, Two-Way-ANOVA mit Dunnett's Test für Mehrfachvergleiche, *: $p < 0,05$ vs. unbehandelte Kontrolle, #: $p < 0,05$ vs. 100 MPa (a, b); Two-Way-ANOVA mit Tukey's Test für Mehrfachvergleiche §: $p < 0,05$: 24 vs. 48 oder 72 h (a).

4.5.2 Vitalität

Mit Hilfe der Durchflusszytometrie wurde bei Chondrozyten zwischen verschiedenen Formen des Zelltodes, Apoptose und Nekrose, unterschieden (Abb. 6b). 24 Stunden nach der HHD-Behandlung waren 90,88 ± 5,47 % der unbehandelten Chondrozyten vital und 7,84 ± 4,82 % spät apoptotisch. Nach der HHD-Behandlung bei 100 MPa waren die Werte ähnlich mit 81,02 ± 12,63 (vital, $p = 0,14$ vs. Kontrolle) und 16,37 ± 11,28 (spät apoptotisch, $p = 0,14$ vs. Kontrolle). Die Behandlung der Chondrozyten bei 200 MPa verringerte den Anteil vitaler Zellen signifikant auf 1,30 ± 1,02 % mit einem entsprechenden signifikanten Anstieg der spät apoptotischen

Zellen auf 90,28 ± 8,14 % (jeweils $p < 0,05$ vs. Kontrolle/100 MPa). Behandlungen bei 300 und 400 MPa ergaben ähnliche Ergebnisse, wobei die Vitalität bei 300 MPa auf 0,22 ± 0,12 % und bei 400 MPa auf 0,11 ± 0,04 % sank (jeweils $p < 0,05$ vs. Kontrolle/100 MPa) und der Anteil spät apoptotischer Zellen bei 300 MPa auf 98,68 ± 0,48 % und bei 400 MPa auf 99,00 ± 0,50 % stieg (jeweils $p < 0,05$ vs. Kontrolle/100 MPa). Die Anteile früh apoptotischer und nekrotischer Zellen blieben über den gesamten Druckverlauf unter 8 % ($p > 0,05$ vs. Kontrolle/100 MPa, s. Anhang Tab. A3 und A4).

4.6 Analyse der Gewebedezellularisierung und der Matrixintegrität

4.6.1 DNA-Gehalt

Um eine mögliche Dezellularisierung infolge der HHD-Behandlung zu beurteilen, wurde der DNA-Gehalt von porcinen Schildknorpel bestimmt (Abb. 7a). Der gemessene DNA-Gehalt betrug 269,20 ± 38,08 ng/mg Knorpel in der unbehandelten Kontrolle und 268,50 ± 45,88 ng/mg Knorpel nach einer Behandlung mit 100 MPa, 299,70 ± 32,87 ng/mg Knorpel nach 200 MPa-, 325,80 ± 47,66 ng/mg Knorpel nach 300 MPa- und 281,80 ± 44,21 ng/mg Knorpel nach 400 MPa-Behandlung ($p > 0,05$, s. Anhang Tab. A5, außer Kontrolle/100 MPa vs. 300 MPa: $p < 0,05$). Trotz einer signifikanten Behandlungsstärke bei 300 MPa gab es keinen druckabhängigen Trend.

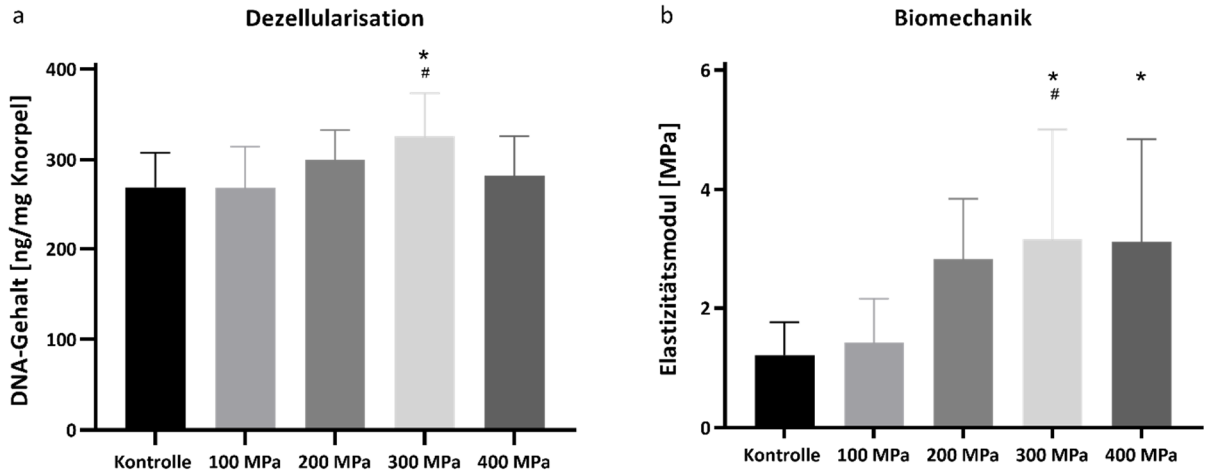

Abbildung 7: Analyse der Gewebedezellularisierung und biomechanischen Eigenschaften des porcinen Schildknorpels nach hydrostatischer Hochdruckbehandlung

Zum Nachweis des Dezellularisierungspotentials der hydrostatischen Hochdruckbehandlung wurde der DNA-Gehalt von porcinen Schildknorpel nach deren Druckbehandlung bei bis zu 400 MPa untersucht (a). Auch die biomechanischen Eigenschaften des Gewebes wurden nach der Druckbehandlung analysiert, indem die Bestimmung des Elastizitätsmoduls durch einen Unconfined compression-Test erfolgte (b). Die Daten werden als Mittelwerte mit Standardabweichungen dargestellt. a: n – Kontrolle = 11, n – behandelt = 8, b: n – Kontrolle = 11, n – 100 MPa = 9, n – 200 MPa = 8, n – 300/400 MPa = 10. Ordinary One-Way-ANOVA mit Dunnett's (a) oder Tukey's Test (b) für Mehrfachvergleiche, *: $p < 0,05$ vs. unbehandelte Kontrolle, #: $p < 0,05$ vs. 100 MPa.

4.6.2 Biomechanik

Die biomechanischen Eigenschaften von porcinen Schildknorpel wurden durch die Messung des Elastizitätsmoduls mit Hilfe eines Unconfined compression-Tests analysiert (Abb. 7b). Das Elastizitätsmodul zeigte einen schrittweisen Anstieg, ausgehend von 1,21 ± 0,55 MPa für die unbehandelte Kontrolle. Es stieg auf 1,42 ± 0,73 MPa (100 MPa, $p > 0,99$ vs. Kontrolle) und 2,82 ± 1,03 MPa (200 MPa, $p = 0,08$ vs. Kontrolle, $p = 0,19$ vs. 100 MPa). Weiterhin stieg das Elastizitätsmodul signifikant auf 3,17 ± 1,84 MPa nach der Behandlung bei 300 MPa ($p < 0,05$ vs. Kontrolle/100 MPa) und betrug 3,11 ± 1,73 MPa nach der Behandlung bei 400 MPa ($p < 0,05$ vs. Kontrolle, $p = 0,05$ vs. 100 MPa). Die statistische Analyse ergab einen signifikanten Unterschied zur Kontrollgruppe ab einem Behandlungsniveau von 300 MPa, was auf eine zunehmende Steifigkeit und reduzierte Dämpfungseigenschaften des Knorpels hinweist.

4.6.3 Gewebemorphologie

Zur Bewertung der Auswirkungen der HHD-Behandlung auf die Morphologie der Chondrozyten (Pfeile) und deren Matrixintegrität wurden FESEM-Aufnahmen von porcinen Schildknorpel angefertigt (Abb. 8). Ab einer Druckbehandlung mit 200 MPa sind deutliche strukturelle Schäden an den Chondrozyten ersichtlich. Die Anzahl der Perforationen in der Zellmembran nimmt mit steigender Druckbelastung kontinuierlich zu, bis die Membran bei einem Druck von 400 MPa ihre vollständige Integrität verliert. Im Gegensatz dazu blieb die Struktur der EZM weitgehend unverändert.

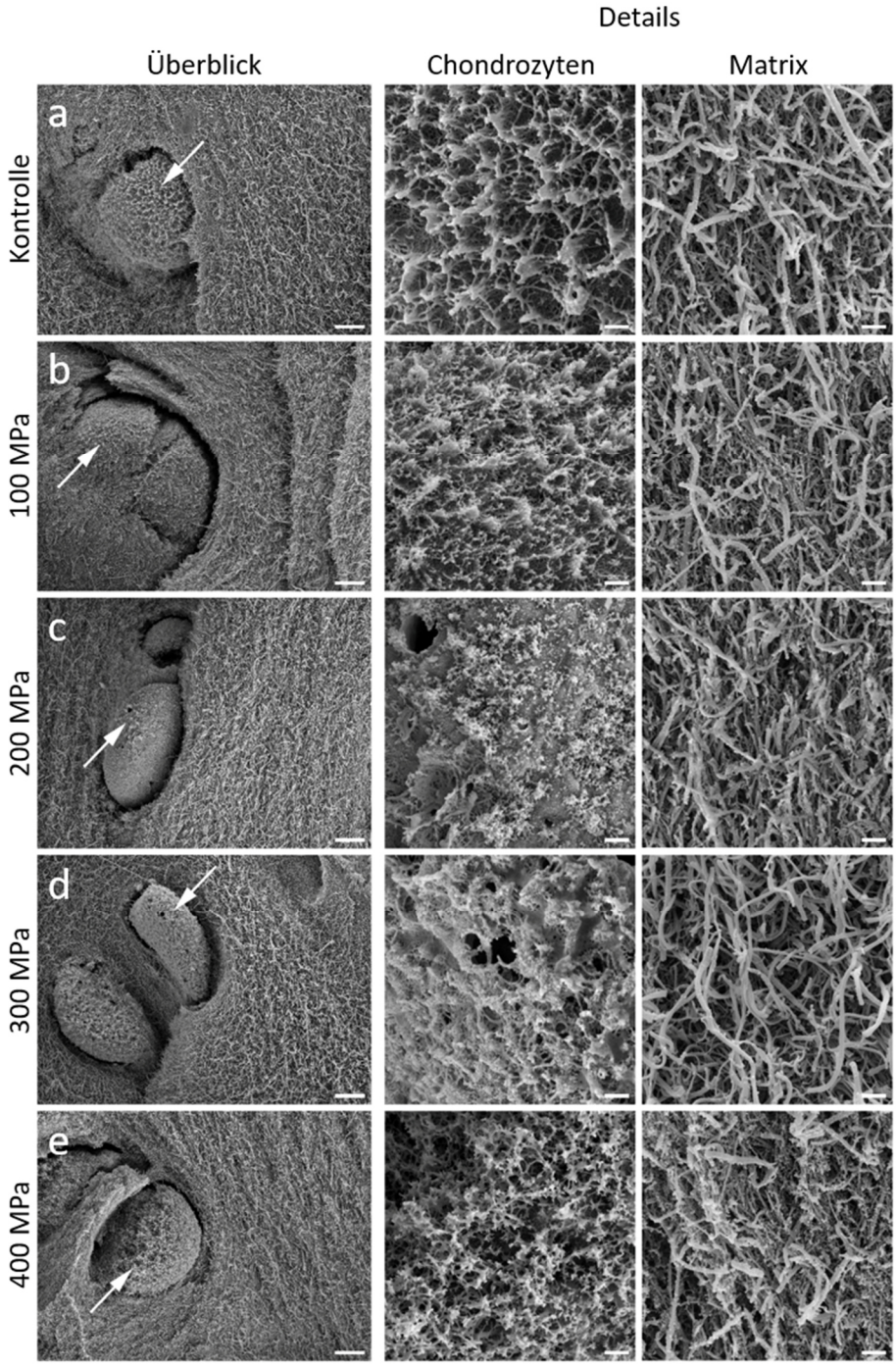

Abbildung 8: Feldemissions-Rasterelektronenmikroskopie von porcinem Schildknorpel nach hydrostatischer Hochdruckbehandlung

Zur Detektion von Gewebeschädigungen wurden Übersichtsaufnahmen von repräsentativen Bereichen des Schildknorpels mit Detailaufnahmen der Chondrozyten (Pfeile) und der umgebenden extrazellulären Matrix (a – e) angefertigt. Unbehandelter Knorpel (a, Kontrolle) wurde mit solchem verglichen, der bei 100 MPa (b), 200 MPa (c), 300 MPa (d) oder 400 MPa (e) mit hydrostatischem Hochdruck behandelt wurde. Maßstab Übersicht: 2 µm, Details: 500 nm.

4.7 In-vivo-Analyse entzündlicher Veränderungen

HHD-behandelter porciner Schildknorpel wurde in der RHK der Maus untersucht. Die FCD diente als Biomarker für die Inflammation (Abb. 9). Weder in der unmittelbaren Nähe des Schildknorpels noch in weiter entfernten Bereichen konnte über den gesamten Zeitverlauf ein signifikanter Unterschied der FCD zwischen der Kontrollgruppe und der 200 MPa-Gruppe festgestellt werden. Die FCD-Messungen in der Nähe des Knorpels ergaben drei Tage nach der Implantation Werte von 22,73 ± 3,14 cm/cm^2 (Kontrolle) und 25,99 ± 6,93 cm/cm^2 (200 MPa). Die FCD stieg bis Tag 15 auf 28,03 ± 6,50 cm/cm^2 (Kontrolle) und 28,95 ± 5,02 cm/cm^2 (200 MPa) ($p > 0,05$: Kontrolle vs. 200 MPa, s. Anhang Tab. A6 und A7). Die FCD in der Peripherie betrug drei Tage nach der Implantation 24,15 ± 1,80 cm/cm^2 in der unbehandelten Kontrolle und 25,12 ± 4,62 cm/cm^2 bei der 200 MPa-Gruppe. Die FCD stieg auf 31,80 ± 5,83 cm/cm^2 (Kontrolle) und 34,13 ± 11,05 cm/cm^2 (200 MPa) an Tag 15 ($p > 0,05$: Kontrolle vs. 200 MPa, s. Anhang Tab. A6 und A7). Weiterhin gab es keinen signifikanten Unterschied beim Vergleich der FCD in der Nähe und im peripheren Bereich des implantierten Knorpels ($p > 0,05$, s. Anhang Tab. A8).

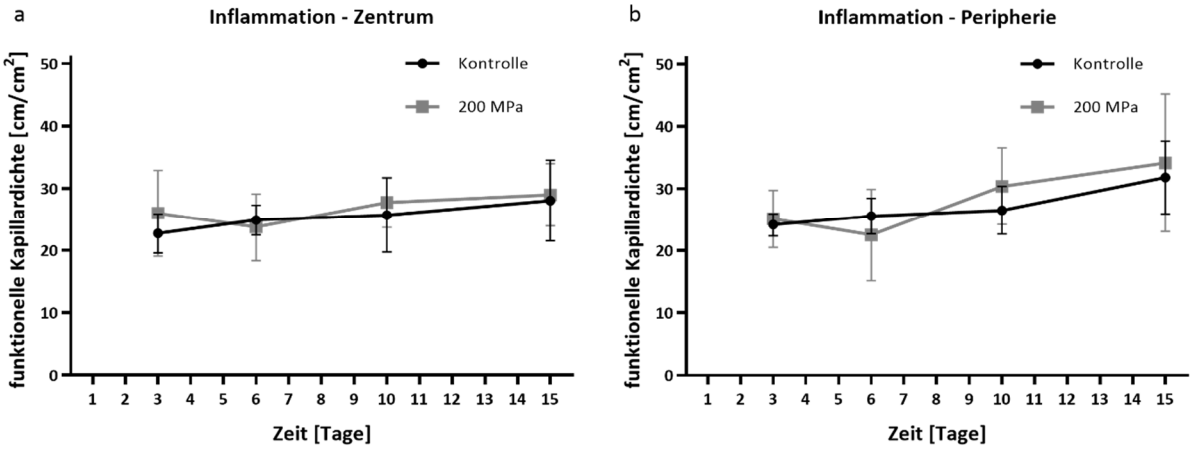

Abbildung 9: Analyse der entzündlichen Veränderungen nach der Implantation von mit hydrostatischem Hochdruck behandeltem porcinen Schildknorpelgewebe im Mausmodell

Die möglicherweise nach der Implantation von mit hydrostatischem Hochdruck behandelten Schildknorpel auftretende Entzündungsreaktion wurde mit Hilfe des Rückenhautkammermodells der Maus untersucht. Behandelte (200 MPa) und unbehandelte (Kontrolle) Gewebeproben wurden implantiert und die funktionelle Kapillardichte (FCD) mit Hilfe der Intravitalmikroskopie an Tag 3, 6, 10 und 15 nach der Implantation bestimmt. Die FCD wurde innerhalb eines Sichtfeldes (20-fache Vergrößerung) zum implantierten Gewebe (Zentrum) und in dessen Peripherie bestimmt. Die Daten werden als Mittelwerte mit Standardabweichungen dargestellt. a: n – Kontrolle = 10, n – 200 MPa = 12, b: n – Kontrolle = 6, n – 200 MPa = 7. Two-Way-ANOVA mit Sidak's Test für Mehrfachvergleiche, $p < 0,05$: kein signifikanter Unterschied zwischen Kontrolle und 200 MPa sowie zwischen der FCD in der Nähe und im peripheren Bereich des Transplantats.

4.8 Vergleichende Analyse der Rückenhautkammern aus Titan und PEEK

4.8.1 Vergleich von PEEK- und Titankammer

Die klassische Titankammer hat eine Größe von 36 x 24 mm und wiegt 3,8 g. Die PEEK-Kammer ist mit 24 x 20 mm und 1,5 g kleiner und leichter. Außerdem wird die Titankammer mit drei transdermalen Schrauben befestigt und kostet 30 bis 110 €, während die PEEK-Kammer mit Nahtmaterial fixiert wird und für 5 € angefertigt werden kann.

4.8.2 Kippwinkel

Um die Effekte einer PEEK-RHK zu evaluieren, wurde der Kippwinkel als Abweichung von der Medianebene gemessen und mit dem von Titankammern verglichen (Abb. 10a). In der ersten Woche war der Kippwinkel aller Kammern nicht höher als 35°, wobei die Titankammer insgesamt eine etwas geringere Neigung hatte (Titan: 5,0°/0,0° bis 28,0°, PEEK: 15,0°/9,0° bis 35,0°, p = 0,17; Median/Spannweite). In der zweiten Woche verstärkte sich die Neigung einer PEEK-Kammer auf 72° und die einer Titankammer auf 101°. Alle anderen Kammern wiesen einen Kippwinkel von unter 20° auf (Titan: 13,0°/6,0° bis 101,0°, PEEK: 9,0°/3,0° bis 72,0°, p > 0,05). Die stärker geneigte PEEK-Kammer aus der zweiten Woche blieb in der dritten Woche stabil, jedoch zeigte eine weitere PEEK-Kammer einen Winkel von 62°. Die anderen vier PEEK-Kammern wiesen nach 21 Tagen einen Kippwinkel von höchstens 13° auf. In der Titangruppe führten die Neigungswinkel zwischen 87 und 129° bei drei Tieren zu Hautdefekten aufgrund der Hautdehnung (Titan: 67,5°/10,0° bis 129,0°, PEEK: 8,5°/0,0° bis 62,0°, p < 0,05).

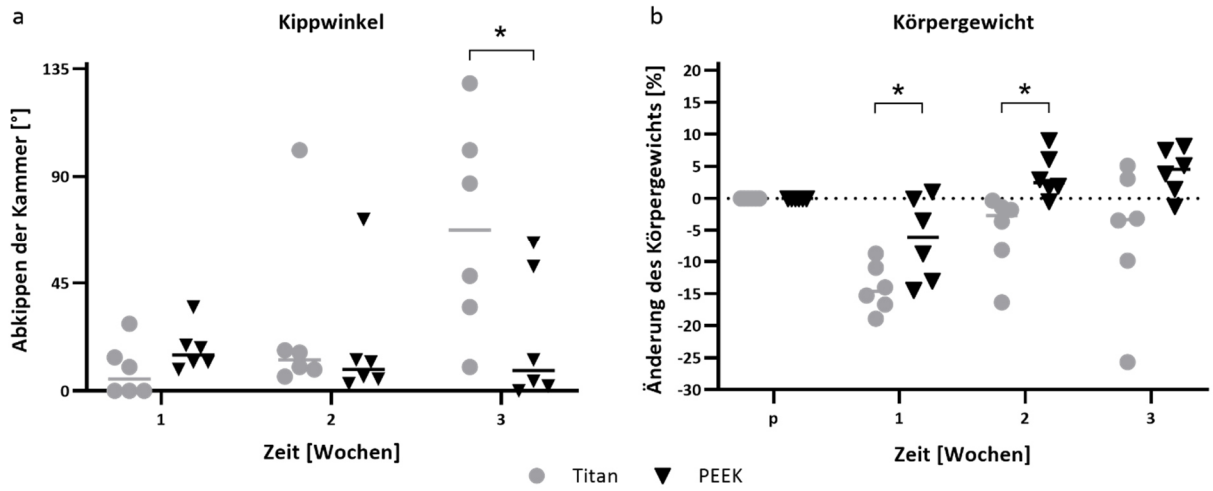

Abbildung 10: Analyse der postoperativen Kippwinkel und der Gewichtsveränderung nach der Präparation von Titan- und PEEK-Rückenhautkammern

Um die Unterschiede zwischen einer herkömmlichen Titan- und einer neu erstellten Polyetheretherketon (PEEK)-Kammer zu beurteilen, wurden zum einen die von der Medianebene aus gemessenen Kippwinkel der Kammern über 3 Wochen (a) und zum anderen das Gewicht der Mäuse (b) präoperativ (p) und bis zu 3 Wochen postoperativ bestimmt. Die Daten werden als individuelle Werte mit Median dargestellt. n – Titan = 6, n – PEEK = 6, a: multipler t-Test mit Holm-Sidak-Korrektur für Mehrfachvergleiche, b: unabhängiger t-Test mit zweiseitiger p-Wert-Testung, *: p < 0,05: Titan vs. PEEK.

4.8.3 Gewicht

Zur Analyse der Auswirkungen von Titan- und PEEK-RHK auf die Mäuse wurde deren Gewicht regelmäßig gemessen (Abb. 10b). Postoperativ trat bei 11 von 12 Tieren ein Gewichtsverlust in der ersten Woche auf, wobei dieser bei Tieren mit PEEK-Kammern im Vergleich zu den Titankammern geringer war (Titan: -14,69 %/-18,95 bis -8,77 %, PEEK: -6,11 %/-14,46 bis 1,06 %, p < 0,05, Median/Spannweite). Das Gewicht der Mäuse mit PEEK-Kammern erholte sich bereits in der zweiten Woche (Titan: -1,79 %/-16,36 bis 3,73 %, PEEK: 2,46 %/-0,47 bis 9,07 %, p < 0,05). Die meisten Mäuse mit Titankammern hingegen haben sich erst in der dritten Woche vollständig vom anfänglichen Gewichtsverlust erholt. Bei einer Maus wurde ein Abbruchkriterium erreicht, da das Körpergewicht mehr als 20 % vom Ursprungsgewicht abwich, was den niedrigen Medianwert erklärt (Titan: -3,33 %/-25,68 % bis 5,10 %, PEEK: 2,46 %/-0,47 bis 9,07 %, p = 0,07).

5 Diskussion

Bei der Therapie von HNSCC können neben Schmerzen auch ästhetische und funktionelle Einschränkungen auftreten. Daher ist bei einer vergleichbaren Überlebenswahrscheinlichkeit die Therapieentscheidung häufig von der zu erwartenden Funktionseinschränkung abhängig [15]. Für die Lebensqualität der Betroffenen sind unter anderem die Qualität des Sprechens und Schluckens wichtige Faktoren. Beispielsweise ist eine Limitation in der Larynxchirurgie der Verlust des knorpeligen Kehlkopfskeletts. Dies führt zu einer Verkleinerung des Querschnittes sowie zur Störung des Ventilmechanismus zur Trennung von Luft- und Speiseweg und damit zu Aspiration, Luftnot und Schluckstörungen bei den Betroffenen. In klinischen Studien werden zur Erfassung subjektiver, schluckbezogener Daten Fragebögen wie der MDADI eingesetzt [65,66]. Eine parallele objektive Bewertung der Schluckfunktion wie etwa durch eine fiberendoskopische Untersuchung fehlt jedoch häufig [19,67,68].
Die kontinuierliche Verbesserung der Therapiemöglichkeiten für HNSCC beispielsweise mit dem Ziel, den Verlust des knorpeligen Kehlkopfskeletss zu begrenzen, erfordert innovative Ansätze. Die HHD-Technologie wird in der Lebensmittelindustrie bereits zur Dekontamination bei gleichzeitigem Erhalt von Geschmack und Vitaminen verwendet [42–44]. In der Kopf-Hals-Chirurgie könnte HHD folglich eine spezifische Devitalisierung von Tumorzellen bei gleichzeitigem Erhalt der strukturellen und biomechanischen Integrität von tumorinfiltriertem Gewebe ermöglichen. Eine autologe, anatomisch korrekte Rekonstruktion wäre damit realisierbar. Für größere Defekte wird hingegen ein geeigneter Gewebeersatz mit erhaltener Matrixintegrität und ursprünglichen biomechanischen Eigenschaften benötigt. Die Prozessierung von Gewebe ist jedoch oft kostspielig, arbeitsintensiv und kann die biomechanische Integrität stören. Solch eine Beeinträchtigung der Gewebequalität wirkt sich direkt auf das funktionelle Ergebnis und den Erfolg der Rekonstruktion aus [36]. Die HHD-Technologie könnte hierbei eine Devitalisierung der Spenderzellen bei gleichzeitigem Erhalt der Matrixintegrität bewirken, was allogene oder xenogene Transplantationen ermöglichen würde [49,69,70].

In dieser kumulativen Dissertation soll die Korrelation zwischen subjektiven (MDADI) und objektiven (FEES) Messverfahren zur Schluckfunktion bei Patienten mit HNSCC untersucht werden. Weiterführend ist es das Ziel, die HHD-Technologie sowohl für die Aufbereitung von tumorinfiltriertem Gewebe zur autologen Rekonstruktion als auch von allogenen und xenogenen Gewebeersatzmaterialien zu verifizieren. Letztlich soll die Immunogenität HHD-behandelter Transplantate im Tierversuch geprüft werden, wobei die konsequente Umsetzung des 3R-Prinzips beachtet wird.

5.1 Korrelation zwischen subjektiver, schluckbezogener Lebensqualität und objektiv gemessener Schluckfunktion

Bei der Therapieentscheidung von HNSCC werden zunehmend auch zu erwartende funktionelle Beeinträchtigungen berücksichtigt. Für die Lebensqualität der Patienten sind beispielsweise das Sprechen und Schlucken wichtige Faktoren, die in der Tumornachsorge zumeist mit Fragebögen erfasst werden. In der klinischen Forschung werden jedoch bei bis zu 80 % der Studien zum Thema Dysphagie nach der Behandlung von Kopf-Hals-Tumoren keine zusätzlichen objektiven Befunde erhoben [19]. Außerdem führt die bisherige Forschung zur Korrelation zwischen objektiven Befunden und subjektiver Lebensqualität zu inkonsistenten Ergebnissen. So gibt es einige Studien, die eine signifikante Korrelationen zeigen (Schluckeffizienz im Oropharynx, Bolustransportzeit, pharyngeale Residuen und Aspiration) und mehrheitlich solche, die keine wesentliche Korrelation, insbesondere im Hinblick auf Penetration und Aspiration, nachweisen [71–75]. Die Inkonsistenz ist auf mehrere Faktoren zurückzuführen. Einerseits spielen die Stichprobengröße und die Studienart eine Rolle, wobei häufig Querschnittsanalysen verwendet werden. Andererseits gibt es auch Unterschiede in den Populationsvariablen, wie etwa die Heterogenität bei der HPV-Positivität, die Behandlungsmodalitäten, der Schweregrad der vorliegenden Symptome und der Zeitpunkt der Datenerhebung nach der Behandlung.
Der in der vorliegenden Originalarbeit [I] verwendete MDADI hat sich als der am häufigsten verwendete Fragebogen zur schluckbezogenen Lebensqualität von Kopf-Hals-Tumorpatienten in klinischen Studien

(u. a. ORATOR, E3311, PATHOS, HN002) etabliert [5,72,73,75–82]. Dieser ermöglicht die Bewertung des Behandlungserfolgs und der Anpassung von Maßnahmen zur Verbesserung der funktionellen Ergebnisse der Patienten. Fragebögen haben allerdings auch Nachteile: Die Länge ist begrenzt und Komplikationen, die von Patienten nicht bemerkt werden, können auch nicht erfasst werden. Weiterhin können Nervenverletzungen, Tracheotomien und Strahlentherapien die subjektive Wahrnehmung von Dysphagie aufgrund von Sensibilitätsverlusten verändern [83]. Diese Störung der Sensibilität kann zum Verlust der Schutzreflexe führen, wodurch stille Aspirationen gefördert werden. Die Inzidenz stiller Aspirationen wird auf 50 – 75 % geschätzt [83–86]. Die subjektive Lebensqualität ist weiterhin ein multifaktorielles Konstrukt, welches beispielsweise durch die physische und psychische Gesundheit sowie die soziale Umgebung beeinflusst wird. In der Studie von Chen et al. gaben Patienten mit Depression im MDADI eine schlechte schluckbezogene Lebensqualität an [87]. Zudem können Komplikationen wie Aspiration, Penetration oder das Zurückbleiben von Speiseresten weniger einschränkend für die schluckbezogene Lebensqualität sein als eine Störung der oralen Phase. Unbemerkte Komplikationen wie eine stille Aspiration können jedoch zu gefährlichen Aspirationspneumonien führen. Daher ist es umso wichtiger, objektive Messverfahren einzubeziehen. FEES und Videofluoroskopie des Schluckens sind etablierte Methoden zur Untersuchung der Schluckfunktion [73–75,81,88,89]. Beide Methoden sind jedoch zeit- und ressourcenaufwändig, weshalb sie nur in 30 % der Studien zur Messung der Schluckfunktion eingesetzt werden [19].

In der vorliegenden Arbeit wurde die Korrelation zwischen der subjektiven, schluckbezogenen Lebensqualität (MDADI) und der objektiven Schluckfunktion (FEES) bei Patienten mit HNSCC bestimmt. Dabei zeigte sich, dass keine Korrelation zwischen den Ergebnissen der FEES und der Wahrnehmung des Grades der Pathophysiologie durch die Patienten anhand des MDADI-Fragebogens bestand (Spearman-Korrelationskoeffizient r = 0,17 (PAS), r = -0,04 (Rückstände Valleculae), r = 0,12 (Rückstände Sinus piriformis), p > 0,05) [5]. Während Instrumente zur Selbstbeurteilung vor allem Einblicke in die Perspektive des Patienten bieten, liefern objektive Messwerte klinische Informationen. Es ist jedoch entscheidend, dass beide Methoden nicht isoliert für Behandlungsentscheidungen, Interventionen und Rehabilitationsstrategien herangezogen werden, sondern eine Kombination angewendet wird, um ein ganzheitliches Krankheitsbild zu erlangen und gefährliche Komplikationen wie z. B. eine stille Aspiration zu erkennen [5].

5.2 Hydrostatische Hochdruckbehandlung

Die funktionelle und ästhetische Rekonstruktion in der Kopf-Hals-Chirurgie stellt eine große Herausforderung dar [4]. Bei einer Tumorbehandlung wird das Gewebe mit einem ausreichenden Sicherheitsabstand entfernt, wodurch Rekonstruktionen erforderlich werden, welche sowohl lokale und mikrovaskuläre Lappenplastiken als auch die Transplantation von Stützgewebe umfassen. Bei invasiven Tumoren an der Ohrmuschel, Nase oder am Kehlkopf können durch die notwendige Resektion Defekte am knorpeligen Stützgerüst entstehen. Die Infiltration des Knorpels begrenzt beim Kehlkopfkarzinom entscheidend die möglichen Therapieansätze und führt für die Patienten oft zu einem dauerhaften Luftröhrenschnitt oder zur vollständigen Entfernung des Kehlkopfes. Tumoren der Stimmlippen in der vorderen Kommissur zeigen dabei eine besonders frühe Infiltration des Schildknorpels [90]. Selbst bei einer geringen Infiltration des Schildknorpels ist die onkologisch sicherste organerhaltende Operationstechnik eine offene Larynxteilresektion [91–93]. Diese kann zur Verkleinerung des Querschnittes und zu Luftnot und Schluckstörungen führen [94]. Um dies zu verhindern, ist es das Ziel, zukünftig eine orthotope Reimplantation von devitalisiertem Knorpel nach der kompletten Inaktivierung von Tumorzellen durchzuführen. Die HHD-Technologie könnte hierbei eine spezifische Devitalisierung von Zellen bei gleichzeitigem Erhalt der strukturellen und biomechanischen Integrität des Gewebes bewirken [46,52,70,95]. Die natürliche EZM spielt eine entscheidende Rolle bei der Regulierung der chondrogenen Differenzierung, der Proliferation und der Migration von Zellen [96]. Derzeit wird die Reimplantation autologer EZM als der Goldstandard betrachtet, da sie ein förderliches biologisches Remodeling unterstützt [97–100]. Dieses Gewebe ist jedoch nur begrenzt verfügbar und bei zu starken Defekten nicht ausreichend vorhanden. Synthetische Materialien sind eine Option, jedoch weisen diese derzeit im Vergleich zu autologen Materialien eine geringere Qualität auf, was auf das häufigere Auftreten von Extrusion, Schrumpfung, Abbau oder Infektion zurückzuführen

ist [2,29,101]. Eine weitere Alternative stellt allogenes oder xenogenes Transplantatmaterial dar, welches entsprechend aufbereitetet werden muss, beispielsweise durch den Einsatz von HHD. Derartige Gewebe sind in größerer Menge verfügbar, wobei mögliche Übertragungen von Krankheitserregern und die Fremdkörperreaktion zu beachten sind [45].

In der vorliegenden Originalarbeit [III] wurde zunächst die Devitalisierungseffizienz der HHD-Behandlung untersucht und eine Devitalisierungsschwelle bei 200 MPa für Chondrozyten ermittelt. Dieses Ergebnis stimmt mit anderen Forschungsergebnissen überein, die zeigen, dass verschiedene Säugetierzellen auf diese Druckbereiche ähnlich reagieren [49,52,102,103]. In der Studie von Waletzko et al. wurde etwa festgestellt, dass ein Druck von 100 – 150 MPa keinen signifikanten Einfluss auf die Vitalität humaner Chondrozyten und Osteoblasten hat [49,102]. In Übereinstimmung damit wurde in der Originalarbeit [III] kein signifikanter Rückgang der Vitalität der Chondrozyten nach einer HHD-Behandlung bei 100 MPa festgestellt. Ein Druck von 200 MPa war erforderlich, um die Vitalität der Chondrozyten auf 1,30 ± 1,02 % zu reduzieren [52]. Ähnliche Ergebnisse wurden in anderen Studien berichtet, bei denen weniger als 5 % der Chondrozyten und Osteoblasten nach einer Druckeinwirkung von 250 bis 300 MPa vital waren [49]. Bei einer ausreichend hohen Druckamplitude erwies sich HHD im Vergleich zu anderen Devitalisierungsmethoden als wirksame Alternative. In einer vergleichenden Analyse von HHD, Gammabestrahlung und Ethanol-Behandlung von Tumorzellen in Originalarbeit [II] wurde festgestellt, dass eine Bestrahlung mit Dosen von bis zu 150 Gy zu einer Verringerung der Vitalität der Zellen um 50 % führte. Während die Behandlung mit Ethanol eine signifikante Toxizität aufwies, waren die Zellen, die vital blieben, in der Lage, anschließend zu proliferieren. Im Gegensatz dazu wurde bei der HHD-Behandlung bei 315 MPa eine vollständige Devitalisierung erreicht [95]. Bei 210 MPa reduzierte sich der Anteil vitaler Zellen zwar signifikant, jedoch blieben mehr als 20 % der Zellen lebensfähig. Bei der Kristallviolettfärbung hingegen wurden bereits nach einer HHD-Behandlung bei 210 MPa keine vitalen Zellen nachgewiesen. Daher ist eine Kombination verschiedener Methoden wichtig, um fundierte und zuverlässige Rückschlüsse auf die Wirksamkeit der HHD-Devitalisierung zu ermöglichen und Tumorrezidive zu vermeiden. In anderen Studien wurden HHD-Behandlungen zwischen 250 und 300 MPa für eine vollständige Devitalisierung von Tumoren beschrieben [51,104–113]. Insgesamt deuten die Ergebnisse darauf hin, dass die HHD-Devitalisierung eine Zellspezifität aufweist und Tumorzellen im Vergleich zu Chondrozyten resistenter gegen HHD sind [52,95,102,103]. Die genauen Mechanismen, die dem Zelltod zugrunde liegen, sind noch nicht vollständig geklärt. Es wurde festgestellt, dass Schäden bei Säugetierzellen, die aus HHD-Behandlungen bis 300 MPa resultieren, tendenziell reversibel sind, während Schäden bei Überschreitung dieses Schwellenwerts irreversibel werden. Das Fehlen eines reversiblen Zelltods nach einer Behandlung bei 300 MPa wurde in verschiedenen Studien auf eine Beeinträchtigung der Membran- und Proteinstruktur bei diesem Druckniveau zurückgeführt [45,49]. Signifikante Schäden der Membran und Zellorganellen sind in Originalarbeit [III] bei Chondrozyten bereits bei einem Druck von 200 MPa in FESEM- und TEM-Aufnahmen sichtbar. Es sind mit steigender Druckhöhe zudem Veränderungen in der Chromatin- und Kernstruktur erkennbar, die schließlich zu irreversiblen funktionellen Schäden führen können [52]. Darüber hinaus ist eine mögliche Ursache der irreversiblen Schädigung das Auftreten von DNA-Doppelstrangbrüchen, ein Phänomen, das in Originalarbeit [II] bei Tumorzellen beobachtet wurde. DNA-Doppelstrangbrüche nahmen nach HHD-Behandlung bei 315 MPa im Vergleich zur unbehandelten Kontrolle signifikant zu [95]. In jedem Fall ermöglicht die HHD-Technologie eine spezifische Devitalisierung, die mit den Sterilisationsanforderungen der Richtlinie 2004/23/EG des Europäischen Parlaments und des Rates übereinstimmt.

Neben der erfolgreichen Devitalisierung durch HHD ist die Erhaltung der Matrixintegrität wichtig, um die strukturellen und funktionellen Eigenschaften des Gewebes beizubehalten. Die in Originalarbeit [III] dargestellten FESEM-Aufnahmen vom Schildknorpel nach HHD-Behandlung zeigten deutliche strukturelle Schäden der Chondrozyten in der EZM ab einem Druck von 200 MPa. Ähnlich wie bei den Beobachtungen an isolierten Chondrozyten umfassten diese Veränderungen Perforationen der Zellmembran, die mit der Druckbelastung bei 200 und 300 MPa an Häufigkeit zunahmen und bei 400 MPa zu einer vollständigen Desintegration der Membran führten. Im Gegensatz dazu blieb die Struktur der EZM weitgehend unverändert [52]. Darüber hinaus gab es keine signifikanten Veränderungen der biomechanischen Eigenschaften des Schildknorpels bei Druckversuchen bis zu 200 MPa [52]. Watanabe et al. zeigten, dass sich das Druckmodul von

Menisken auch nach einer 30-minütigen Behandlung mit 1000 MPa nicht signifikant veränderte [114]. Darüber hinaus wiesen Hiemer et al. durch histologische, immunhistochemische und FESEM-Analysen nach, dass HHD bei 480 MPa die Integrität von Knorpelgewebe und der EZM-Proteine wie Kollagen Typ II und Aggrecan erhält und keine strukturellen Veränderungen auftreten [96]. Salti et al. stellten weiterhin fest, dass die EZM-Struktur und der Kollagengehalt von Rattennieren durch HHD nicht verändert werden, aber bei allen getesteten Methoden (chemische Reagenzien, HHD, Gefrier-Auftauzyklus, Ultraschallbadsystem) ein erheblicher Verlust an Glykosaminoglykanen auftrat [70]. Diehl et al. bestätigten, dass HHD-behandeltes Fibronektin, Vitronectin und Typ-I-Kollagen in Knochengewebe keine nachteiligen Auswirkungen hatten, ihre Funktionalität beibehielten und sogar die Zellproliferation förderten [115]. In ähnlicher Weise beobachteten Waletzko-Hellwig et al. keine signifikanten Unterschiede im Kollagen-Typ-I-Gehalt im Knochengewebe nach einer HHD-Behandlung bei 300 MPa, was darauf hindeutet, dass die Kollagenstruktur intakt blieb [46]. Nach der Anwendung des HHD war in der vorliegenden Originalarbeit [III] die strukturelle Integrität des Schildknorpels gegeben, jedoch erfolgte keine Dezellularisierung. Über den gesamten Druckverlauf bis 400 MPa war der DNA-Gehalt des Schildknorpels ähnlich [52]. Ein stabiler DNA-Gehalt nach HHD-Behandlung wurde auch in anderen Arbeiten nachgewiesen [114,116]. In der Studie von Sutherland et al. wurde festgestellt, dass die HHD-Behandlung allein lediglich zur Devitalisierung des Gewebes führt, aber ein anschließender Waschschritt für eine erfolgreiche Dezellularisierung erforderlich ist [117]. Eine Zelldevitalisierung ohne Dezellularisierung impliziert das Vorhandensein von zellulären Komponenten in der Matrix, die nach der Transplantation möglicherweise eine Entzündung auslösen können [118]. In der von Hiemer et al. durchgeführten Studie wurde jedoch im Laufe der Zeit nach einer HHD-Behandlung ein Abbau der DNA beobachtet, während der DNA-Gehalt der unbehandelten Kontrollgruppe unverändert blieb [96]. Dieser Befund sollte bei künftigen Forschungen berücksichtigt werden.

Weiterhin ist die Art des Zelltodes ein Faktor, der immunologische Prozesse auslösen kann. Gewebeersatzmaterialien sollten höchstens eine geringe Immunogenität aufweisen und möglichst immunologisch inert sein, um eine Abstoßung durch den Empfänger zu vermeiden. Sowohl in Originalarbeit [II] als auch [III] wurde hauptsächlich ein spät apoptotischer Zelltod identifiziert [52,95]. Ein nekrotischer Devitalisierungsprozess kann zu Entzündungsreaktionen führen, indem schadensassoziierte molekulare Muster (DAMPS, Damage-Associated Molecular Patterns) freigesetzt werden, die die proinflammatorische Reaktion stimulieren und damit starke Immunreaktionen hervorrufen können [119–121]. Weiterhin kann der Einsatz von Gewebeersatzmaterialien eine Fremdkörperreaktion hervorrufen, wobei dessen Ausßmaß durch eine Reihe von Faktoren bestimmt wird. Die Art der Transplantation ist der wichtigste Faktor, wobei zwischen Gewebe- und Organtransfer unterschieden wird. Weitere wichtige Aspekte sind die genetische Disparität zwischen Spender und Empfänger, die durch die Histokompatibilität der Chromosomen gekennzeichnet ist, die Menge des transplantierten Gewebes, die gewebespezifische Antigenität, das Empfängerorgan bzw. das Transplantatbett und der Grad der Immunreaktivität des Empfängers. Generell ist aus immunologischer Sicht bei Knorpeltransplantationen nur eine geringe Fremdkörperreaktion zu erwarten [122]. Es wird angenommen, dass die dichte Knorpel-EZM Immunzellen daran hindert, Chondrozytenantigene zu erkennen. Darüber hinaus besteht die EZM überwiegend aus Typ-II-Kollagen, das phylogenetisch hoch konserviert ist [123,124]. In der vorliegenden Originalarbeit [III] wurden xenogene Schildknorpeltransplantate vom Schwein verwendet. Die im Schildknorpel nach der HHD-Behandlung verbliebenen devitalisierten Zellen scheinen in vivo biologisch unbedeutend zu sein, was wahrscheinlich auf die geringe Zelldichte im Knorpel und die artenübergreifende Erhaltung der Matrixkomponenten zurückzuführen ist. Dafür spricht auch die Tatsache, dass die Transplantation von Frischgewebe in einigen Ländern erlaubt ist [125,126]. Es scheint, dass die allo- oder xenogene Transplantation von Stützgewebe überwiegend bioinert ist. Dies deutet darauf hin, dass HHD-devitalisiertes Gewebe ohne zusätzliche Verarbeitungsschritte direkt transplantiert werden kann. Weiterhin ist der porcine Schildknorpel in großen Mengen verfügbar und stammt von jungen Tieren, wodurch dieses Material für den zukünftigen Einsatz in der regenerativen Medizin geeignet ist. Es muss jedoch stets beachtet werden, dass sowohl das Risiko einer Immunreaktion besteht, wenn das xenogene Material als körperfremd erkannt wird als auch eine Übertragung von artfremden Krankheiten möglich ist [127,128]. Im Gegensatz dazu ist allogenes Gewebe nur in begrenzteren Mengen verfügbar, stammt in der Regel von älteren Spendern und ist qualitativ wenig standardisiert.

Im Vergleich zur Standardaufarbeitung von Gewebetransplantaten bietet HHD eine effiziente und schnelle Devitalisierung bei gleichzeitigem Erhalt der Matrixintegrität und Biomechanik [52]. Konventionelle Verarbeitungsmethoden sind chemische (z. B. Tris-HCl und SDS) oder physikalische (z. B. Gefrier-Auftau-Zyklen oder γ-Bestrahlung) Verfahren [29–34,129,130]. Diese Prozesse dauern mehrere Tage bis Wochen, während die HHD-Behandlung nur 10 Minuten in Anspruch nimmt [52,95]. Außerdem kann die konventionelle Verarbeitung zu einer Verschlechterung der biomechanischen Eigenschaften führen [33]. Gefrier-Auftau-Zyklen können zur Kristallbildung in den Geweben führen, was in der Folge die Integrität des Kollagennetzwerks beeinträchtigt [29]. In ähnlicher Weise führt Gammabestrahlung zu Veränderungen der biomechanischen Eigenschaften von Weichgewebe, was die Verringerung der Festigkeit und Steifigkeit zur Folge hat [131]. Im Gegensatz dazu hatte die HHD-Behandlung von Knochenzylindern für 30 min bei 300 MPa keinen negativen Einfluss auf die Biomechanik [69]. Darüber hinaus zeigten histologische Analysen von Nierenschnitten die beste Matrixintegrität und -stabilität nach einer HHD-Behandlung im Vergleich zu anderen gängigen Methoden wie Gefrier-Auftau-Zyklen oder chemischer Behandlung [70]. Insgesamt bietet der HHD gegenüber anderen Methoden Vorteile in Bezug auf Zeit, Aufwand und Kosten. Außerdem ermöglicht der HHD eine standardisierte und gleichmäßige Devitalisierung gemäß dem Pascalschen Gesetz, da der Druck in einem geschlossenen System isostatisch und sofort wirkt [132]. Diese gleichmäßige Druckverteilung ist wesentlich, um eine vollständige Devitalisierung von Zellen und Geweben zu erreichen. In den Originalarbeiten [II] und [III] wurde eine Reproduzierbarkeit der Ergebnisse mit der HHD-Technologie für kommerzielle sowie patientenabgeleitete Tumorzellen und Chondrozyten nachgewiesen.
Die Anwendung der HHD-Technologie hat somit das Potenzial, eine sichere und zuverlässige Methode für die autologe Rekonstruktion in der Kopf-Hals-Chirurgie sowie für den allogenen und xenogenen Gewebeersatz zu sein. Weiterhin besteht so die Möglichkeit, die Verfügbarkeit von Transplantationsmaterialien im klinischen Bereich zu erweitern und deren Bereitstellung zu verbessern.

5.3 Refinement der Rückenhautkammer aus Titan

Translationale Forschung im Themengebiet der Gewebeersatzmaterialien ist ohne Tierversuche noch nicht gänzlich möglich, da u. a. sehr komplexe Prozesse wie die Immunreaktion auf ein Transplantat nicht in vitro dargestellt werden können [52,133]. Bei einem Tierversuch ist darzulegen, wie die ethischen Standards gemäß dem international anerkannten 3R-Prinzip (Europäische Richtlinie 2010/63/EU [53]) umgesetzt werden. Tierversuche sollen, wann immer es möglich ist, durch andere Methoden ersetzt (replace), die Anzahl der Versuchstiere reduziert (reduce) und die Belastung der Tiere minimiert werden (refine).
Die in Originalarbeit [IV] verwendete RHK ist ein wichtiges Modell für die wiederholte Untersuchung von Gefäßveränderungen und Entzündungen, wobei in den meisten Fällen eine klassische Titankammer verwendet wird [52,61,134–142]. Die Kammer hat eine Größe von 36 x 24 mm, wiegt 3,8 g und wird im Tierversuch mit Schrauben befestigt. Die Belastung der Tiere wird zumeist mit mäßig bewertet [63]. Durch das Gewicht der Kammer und die Fixierung durch Schrauben kann es zur Dehnung und Defektbildung der Haut kommen, was in der Folge zu Schmerzen, Immobilisierung und eingeschränkter Atmung führt. Es gibt bereits einige Bestrebungen im Sinne von „Refine“, um die Belastung der Tiere zu minimieren. Eine Variante ist die Entwicklung eines dünneren Titanrahmens mit gleichbleibend großem Beobachtungsfenster. Diese kleineren RHK werden bereits kommerziell vermarktet (Small Dorsal Kit SM100, APJ Trading Co., Ventura, CA, USA) [143–145]. Schreiter et al. konzipierten ebenfalls eine kleinere Titankammer, durch welche postoperativ keine Erholungsphase notwendig war und das Stresslevel der Tiere verringert werden konnte [118]. Titankammern sind jedoch grundsätzlich nicht MRT-kompatibel und die Herstellung kann in den meisten biowissenschaftlichen Einrichtungen nicht vor Ort erfolgen [146]. Die in Originalarbeit [IV] entwickelte 3D-gedruckte PEEK-Kammer ist kleiner und 2,3 g leichter als die klassische Titankammer. Die chirurgischen Anforderungen, der Versuchsablauf und die Qualität der Intravitalmikroskopie sind bei PEEK- und Titankammern gleich. Bei der Präparation der PEEK-Kammer kann aufgrund des geringeren Gewichts auf die Fixierung mit Schrauben verzichtet werden. An deren Stelle kommen reißfeste Nähte zur Anwendung, die ein geringeres Trauma verursachen [63]. Die häufigste Komplikation bei Experimenten mit der RHK aus Titan ist das seitliche Abkippen der Kammer [134]. Beim Vergleich der Titan- und PEEK-Kammer in Originalarbeit [IV] kippten in der dritten Woche 50 % der Titankammern um mehr als 80°, was

zu einer Immobilisierung der Tiere führte. Bei allen PEEK-Kammern blieb der Neigungswinkel drei Wochen lang unter 80°, was auf das geringere Gewicht zurückzuführen ist. Die RHK aus PEEK könnte damit die maximale Versuchsdauer auf vier oder fünf Wochen verlängern, wie es auch schon bei anderen leichteren Kammern beobachtet wurde [147]. Dies ist besonders für die Biomaterialentwicklung von Vorteil, da somit die Untersuchung der Biomaterialintegration (Fibrose, Riesenzellbildung, Vaskularisierung des Implantats) länger ermöglicht wird [133]. Weiterhin könnte die Eignung des Modells für onkologische Untersuchungen verbessert werden, da das Wachstum von Tumorzellen bereits einen großen Teil der bisherigen maximalen Beobachtungszeit in Anspruch nimmt [148].
Neben dem geringeren Neigungswinkel bei PEEK-Kammern im Vergleich zu Titankammern konnte in Originalarbeit [IV] auch der postoperative Gewichtsverlust verringert werden. Bei den Tieren mit Titankammern wurden die Ausgangswerte nicht wieder erreicht, während die Mäuse mit PEEK-Kammern diese bereits in der zweiten Woche erzielten. In Übereinstimmung mit diesen Daten wurde in früheren Untersuchungen ein postoperativer Gewichtsverlust von bis zu 15 % bei Titankammern und ein geringerer Gewichtsverlust bei nichtmetallischen RHK beschrieben [149–151].
Die Entwicklung einer Kunststoffkammer wurde bereits 2003 aus dem Material Duracon, einem Copolymer aus Polypropylen, beschrieben [134]. Diese frühen Kunststoffkammern wurden noch mit Schrauben befestigt, sodass dadurch Hautdefekte entstanden [134]. Die ersten PEEK-Kammern wurden von Gaustad et al. und Seynhaeve et al. entwickelt [146,152]. Diese Kammern wogen ca. 1 g und wurden mit Nähten oder kleinen Schrauben fixiert. Bei der additiven Fertigung von PEEK ist ein hoher Grad an geometrischer Freiheit gegeben, die Produktionskosten sind gering und es ist eine schnelle Herstellung von Einzelstücken möglich [63,153].
Insgesamt gesehen ist PEEK ein geeignetes Material für die Herstellung von RHK, da kleinere und leichtere Kammern hergestellt werden können, mit denen sowohl das Wohlbefinden der Tiere als auch die Versuchszeit gesteigert werden. Zudem ist PEEK autoklavierbar und hält Nagetierbissen stand. Weiterhin ist eine MRT-Bildgebung möglich und durch die Anwendung der 3D-Drucktechnologie zur Herstellung können die Kammern weit verbreitet und kostengünstig hergestellt werden.

5.4 Schlussfolgerung

Bei der Therapie von HNSCC können ästhetische und funktionelle Einschränkungen auftreten. Hierbei sind besonders das Sprechen und Schlucken wichtige Faktoren für die Lebensqualität der Betroffenen. Der häufig in der Klinik eingesetzte MDADI bietet Einblicke in die Bewertung der schluckbezogenen Lebensqualität der Patienten, die jedoch in der vorliegenden Studie nicht mit der objektiv ermittelten Schluckfunktion korreliert. Daher sollte die Erfassung der Lebensqualität sowohl im klinischen Alltag als auch in Studien durch eine Kombination aus standardisierten Fragebögen und einer objektiven Funktionsanalyse erfolgen.

Innovative Therapieansätze zur Behandlung von HNSCC könnten die Anwendung des HHD beinhalten. Bei einer HHD-Behandlung mit 315 MPa können HNSCC onkologisch sicher devitalisiert werden, was HHD zu einer sicheren und zuverlässigen Technologie zur Ergänzung der autologen Kopf-Hals-Rekonstruktion macht. Auch bei größeren Defekten des Stützgewebes kann HHD eingesetzt werden, um allo- und xenogenen Gewebeersatz zu prozessieren. Eine HHD-Behandlung bei 200 MPa führt zur Devitalisierung von Chondrozyten ohne strukturelle Veränderungen auf zellulärer Ebene. Außerdem bleiben bei diesem Druckniveau die EZM und die biomechanischen Eigenschaften des Schildknorpels erhalten. In einem xenogenen RHK-Modell in der Maus konnte keine Entzündungsreaktion beobachtet werden, was auf eine günstige biologische Reaktion auf HHD-behandeltes Gewebe hinweist. Somit ist der HHD eine vielversprechende Technologie, die die vorhandene Bandbreite der Methoden für die Aufbereitung von Gewebeersatzmaterialien innovativ ergänzt.

Weiterhin werden Versuchstiere durch Titan-RHK besonders belastet. Gemäß dem 3R-Prinzip konnte gezeigt werden, dass leichtere PEEK-RHK die Belastung der Tiere erheblich verringern und die maximale Versuchsdauer verlängern. Zudem sind die PEEK-RHK autoklavierbar, halten Nagetierbissen stand, sind kostengünstig und durch 3D-Druck weithin verfügbar, was sie zu einer vielversprechenden Alternative zur klassischen Titankammer macht. Zusammenfassend ist für eine Verbesserung der Behandlungsmöglichkeiten in der Kopf-Hals-Chirurgie ein interdisziplinärer, umfassender Ansatz erforderlich, der sowohl innovative Technologien als auch ethische Aspekte berücksichtigt.

A Anhang

A.1 Literaturverzeichnis

1. Tarhan E., Cakmak O., Ozdemir B.H., et al. (2008): Comparison of AlloDerm, fat, fascia, cartilage, and dermal grafts in rabbits. *Arch Facial Plast Surg*(3) 187–193. DOI:10.1001/archfaci.10.3.187.
2. Firat C., Gurlek A., Aydin N.E. (2011): Viability of cartilage grafts in various forms. *J Craniofac Surg*(5) 1666–1670. DOI:10.1097/SCS.0b013e31822f3b1f.
3. Liu Y., Zhou G., Cao Y. (2017): Recent Progress in Cartilage Tissue Engineering—Our Experience and Future Directions. *Engineering*(1) 28–35. DOI:10.1016/J.ENG.2017.01.010.
4. Albrecht T., Wallner F. (2023): Rekonstruktionsmöglichkeiten nach Verletzungen der Kopf-Hals-Region. *HNO*(1) 57–62. DOI:10.1007/s00106-022-01230-5.
5. Strüder D., Ebert J., Kalle F., et al. (2023): Head and Neck Cancer: A Study on the Complex Relationship between QoL and Swallowing Function. *Curr Oncol*(12) 10336–10350. DOI:10.3390/curroncol30120753.
6. Johnson D.E., Burtness B., Leemans C.R., et al. (2020): Head and neck squamous cell carcinoma. *Nat Rev Dis Primers*(1) 92. DOI:10.1038/s41572-020-00224-3.
7. Sung H., Ferlay J., Siegel R.L., et al. (2021): Global Cancer Statistics 2020: GLOBOCAN Estimates of Incidence and Mortality Worldwide for 36 Cancers in 185 Countries. *CA Cancer J Clin*(3) 209–249. DOI:10.3322/caac.21660.
8. Leemans C.R., Braakhuis B.J.M., Brakenhoff R.H. (2011): The molecular biology of head and neck cancer. *Nat Rev Cancer*(1) 9–22. DOI:10.1038/nrc2982.
9. Talamini R., Bosetti C., La Vecchia C., et al. (2002): Combined effect of tobacco and alcohol on laryngeal cancer risk: a case-control study. *Cancer Causes Control*(10) 957–964. DOI:10.1023/A:1021944123914.
10. Cogliano V.J., Baan R., Straif K., et al. (2011): Preventable exposures associated with human cancers. *J Natl Cancer Inst*(24) 1827–1839. DOI:10.1093/jnci/djr483.
11. Hashibe M., Brennan P., Benhamou S., et al. (2007): Alcohol drinking in never users of tobacco, cigarette smoking in never drinkers, and the risk of head and neck cancer: pooled analysis in the International Head and Neck Cancer Epidemiology Consortium. *J Natl Cancer Inst*(10) 777–789. DOI:10.1093/jnci/djk179.
12. Di Credico G., Polesel J., Dal Maso L., et al. (2020): Alcohol drinking and head and neck cancer risk: the joint effect of intensity and duration. *Br J Cancer*(9) 1456–1463. DOI:10.1038/s41416-020-01031-z.
13. Chow L.Q.M. (2020): Head and Neck Cancer. *N Engl J Med*(1) 60–72. DOI:10.1056/NEJMra1715715.
14. Mody M.D., Rocco J.W., Yom S.S., et al. (2021): Head and neck cancer. *Lancet*(10318) 2289–2299. DOI:10.1016/S0140-6736(21)01550-6.
15. Klinghammer K., Raguse J.-D., Plath T., et al. (2015): A comprehensively characterized large panel of head and neck cancer patient-derived xenografts identifies the mTOR inhibitor everolimus as potential new treatment option. *Int J Cancer*(12) 2940–2948. DOI:10.1002/ijc.29344.
16. Eisbruch A. (2004): Dysphagia and aspiration following chemo-irradiation of head and neck cancer: major obstacles to intensification of therapy. *Ann Oncol*(3) 363–364. DOI:10.1093/annonc/mdh117.
17. Nguyen N.P., Moltz C.C., Frank C., et al. (2004): Dysphagia following chemoradiation for locally advanced head and neck cancer. *Ann Oncol*(3) 383–388. DOI:10.1093/ANNONC/MDH101.
18. Nguyen N.P., Frank C., Moltz C.C., et al. (2006): Aspiration rate following chemoradiation for head and neck cancer: an underreported occurrence. *Radiother Oncol*(3) 302–306. DOI:10.1016/j.radonc.2006.07.031.
19. Li P., Constantinescu G.C., Nguyen N.-T.A., et al. (2020): Trends in Reporting of Swallowing Outcomes in Oropharyngeal Cancer Studies: A Systematic Review. *Dysphagia*(1) 18–23. DOI:10.1007/S00455-019-09996-7.
20. Bauer F., Seiss M., Grässel E., et al. (2010): Schluckbezogene Lebensqualität bei Mundhöhlenkarzinomen. Anderson-Dysphagia-Inventory, deutsche Version. *HNO*(7) 692–697. DOI:10.1007/s00106-010-2117-7.

21. Ludwig K., Graf von der Schulenburg J.-M., Greiner W. (2018): German Value Set for the EQ-5D-5L. *Pharmacoeconomics*(6) 663–674. DOI:10.1007/s40273-018-0615-8.
22. Moussa L., Usunier B., Demarquay C., et al. (2016): Bowel Radiation Injury: Complexity of the Pathophysiology and Promises of Cell and Tissue Engineering. *Cell Transplant*(10) 1723–1746. DOI:10.3727/096368916X691664.
23. Brook I. (2020): Late side effects of radiation treatment for head and neck cancer. *Radiat Oncol J*(2) 84–92. DOI:10.3857/ROJ.2020.00213.
24. Liu Y.-Q., Wang X.-L., He D.-H., et al. (2021): Protection against chemotherapy- and radiotherapy-induced side effects: A review based on the mechanisms and therapeutic opportunities of phytochemicals. *Phytomedicine*(80) 153402. DOI:10.1016/J.PHYMED.2020.153402.
25. Staudenmaier R. (2006): Optimierung der Ohrmuschelrekonstruktion mit autologem Rippenknorpel. Erfahrung aus 120 Fällen. *HNO*(10) 749–755. DOI:10.1007/s00106-005-1372-5.
26. Kashkouli M.B. (2007): A novel technique for small-incision fascia lata harvesting without a fasciatome for the frontalis suspension procedure. *Orbit*(3) 203–206. DOI:10.1080/01676830701376122.
27. Shibuya N., Jupiter D.C. (2015): Bone graft substitute: allograft and xenograft. *Clin Podiatr Med Surg*(1) 21–34. DOI:10.1016/j.cpm.2014.09.011.
28. Europäisches Parlament und der Rat (2004): Richtlinie 2004/23/EC zur Festlegung von Qualitäts- und Sicherheitsstandards für die Spende, Beschaffung, Testung, Verarbeitung, Konservierung, Lagerung und Verteilung von menschlichen Geweben und Zellen.
29. Benders K.E.M., van Weeren P.R., Badylak S.F., et al. (2013): Extracellular matrix scaffolds for cartilage and bone regeneration. *Trends Biotechnol*(3) 169–176. DOI:10.1016/j.tibtech.2012.12.004.
30. Fawzi-Grancher S., Goebbels R.M., Bigare E., et al. (2009): Human tissue allograft processing: impact on in vitro and in vivo biocompatibility. *J Mater Sci Mater Med*(8) 1709–1720. DOI:10.1007/s10856-009-3726-0.
31. Lansdown D.A., Riff A.J., Meadows M., et al. (2017): What Factors Influence the Biomechanical Properties of Allograft Tissue for ACL Reconstruction? A Systematic Review. *Clin Orthop Relat Res*(10) 2412–2426. DOI:10.1007/s11999-017-5330-9.
32. Putzer D., Huber D.C., Wurm A., et al. (2014): The mechanical stability of allografts after a cleaning process: comparison of two preparation modes. *J Arthroplasty*(8) 1642–1646. DOI:10.1016/j.arth.2014.03.028.
33. Mickiewicz P., Binkowski M., Bursig H., et al. (2014): Preservation and sterilization methods of the meniscal allografts: literature review. *Cell Tissue Bank*(3) 307–317. DOI:10.1007/s10561-013-9396-7.
34. Shang X., Wang H., Li J., et al. (2019): Progress of sterilization and preservation methods for allografts in anterior cruciate ligament reconstruction. *Chinese Journal of Reparative and Reconstructive Surgery*(9) 1102–1107. DOI:10.7507/1002-1892.201903078.
35. Arzi B., DuRaine G.D., Lee C.A., et al. (2015): Cartilage immunoprivilege depends on donor source and lesion location. *Acta Biomater*(23) 72–81. DOI:10.1016/j.actbio.2015.05.025.
36. Fischer M., Bortel E., Schoon J., et al. (2023): Cold physical plasma treatment optimization for improved bone allograft processing. *Front Bioeng Biotechnol*(11) 1264409. DOI:10.3389/fbioe.2023.1264409.
37. Kani K.K., Porrino J.A., Chew F.S. (2022): Meniscal Allograft Transplantation: A Pictorial Review. *Curr Probl Diagn Radiol*(5) 779–786. DOI:10.1067/j.cpradiol.2021.09.008.
38. Theodoulou M.H., Bohman L. (2018): Allograft Cartilage Replacements. *Clin Podiatr Med Surg*(3) 281–293. DOI:10.1016/j.cpm.2018.02.003.
39. Kurokawa S., Hashimoto Y., Funamoto S., et al. (2021): In vivo recellularization of xenogeneic vascular grafts decellularized with high hydrostatic pressure method in a porcine carotid arterial interpose model. *PLoS One*(7) e0254160. DOI:10.1371/journal.pone.0254160.
40. Hindle P., Hendry J.L., Keating J.F., et al. (2014): Autologous osteochondral mosaicplasty or TruFit plugs for cartilage repair. *Knee Surg Sports Traumatol Arthrosc*(6) 1235–1240. DOI:10.1007/s00167-013-2493-0.
41. Krueger S., Achilles S., Zimmermann J., et al. (2019): Re-Differentiation Capacity of Human Chondrocytes in Vitro Following Electrical Stimulation with Capacitively Coupled Fields. *J Clin Med*(11) 1771. DOI:10.3390/jcm8111771.

42. San Martín M.F., Barbosa-Cánovas G.V., Swanson B.G. (2002): Food processing by high hydrostatic pressure. *Crit Rev Food Sci Nutr*(6) 627–645. DOI:10.1080/20024091054274.
43. Rendueles E., Omer M.K., Alvseike O., et al. (2011): Microbiological food safety assessment of high hydrostatic pressure processing: A review. *LWT - Food Science and Technology*(5) 1251–1260. DOI:10.1016/j.lwt.2010.11.001.
44. Yamamoto K. (2017): Food processing by high hydrostatic pressure. *Biosci Biotechnol Biochem*(4) 672–679. DOI:10.1080/09168451.2017.1281723.
45. Rivalain N., Roquain J., Demazeau G. (2010): Development of high hydrostatic pressure in biosciences: pressure effect on biological structures and potential applications in biotechnologies. *Biotechnol Adv*(6) 659–672. DOI:10.1016/j.biotechadv.2010.04.001.
46. Waletzko-Hellwig J., Pohl C., Riese J., et al. (2021): Effect of High Hydrostatic Pressure on Human Trabecular Bone Regarding Cell Death and Matrix Integrity. *Front Bioeng Biotechnol*(9) 730266. DOI:10.3389/fbioe.2021.730266.
47. van de Sande M.A.J., Bovée J.V.M.G., van Domselaar M., et al. (2018): Successful disinfection of femoral head bone graft using high hydrostatic pressure. *Cell Tissue Bank*(3) 333–340. DOI:10.1007/s10561-017-9678-6.
48. Frey B., Janko C., Ebel N., et al. (2008): Cells under pressure - treatment of eukaryotic cells with high hydrostatic pressure, from physiologic aspects to pressure induced cell death. *Curr Med Chem*(23) 2329–2336. DOI:10.2174/092986708785909166.
49. Waletzko J., Dau M., Seyfarth A., et al. (2020): Devitalizing Effect of High Hydrostatic Pressure on Human Cells-Influence on Cell Death in Osteoblasts and Chondrocytes. *Int J Mol Sci*(11) 3836. DOI:10.3390/ijms21113836.
50. Weiss E.-M., Frey B., Rödel F., et al. (2010): Ex vivo- and in vivo-induced dead tumor cells as modulators of antitumor responses. *Ann N Y Acad Sci*(1209) 109–117. DOI:10.1111/j.1749-6632.2010.05743.x.
51. Seitz C., Rückert M., Deloch L., et al. (2019): Tumor Cell-Based Vaccine Generated With High Hydrostatic Pressure Synergizes With Radiotherapy by Generating a Favorable Anti-tumor Immune Microenvironment. *Front Oncol*(9) 805. DOI:10.3389/fonc.2019.00805.
52. Kalle F., Stadler V.P., Brach J.K., et al. (2024): High hydrostatic pressure treatment for advanced tissue grafts in reconstructive head and neck surgery. *J Biomed Mater Res A*(113(1)) e37791. DOI:10.1002/jbm.a.37791.
53. Europäisches Parlament und der Rat (2010): Richtlinie 2010/63/EU zum Schutz der für wissenschaftliche Zwecke verwendeten Tiere.
54. Hutcheson K.A., Barrow M.P., Lisec A., et al. (2016): What is a clinically relevant difference in MDADI scores between groups of head and neck cancer patients? *Laryngoscope*(5) 1108–1113. DOI:10.1002/lary.25778.
55. Rosenbek J.C., Robbins J.A., Roecker E.B., et al. (1996): A penetration-aspiration scale. *Dysphagia*(2) 93–98. DOI:10.1007/BF00417897.
56. Hey C., Pluschinski P., Zaretsky Y., et al. (2014): Penetrations-Aspirations-Skala nach Rosenbek. Validierung der deutschen Version für die endoskopische Dysphagiediagnostik. *HNO*(4) 276–281. DOI:10.1007/s00106-013-2815-z.
57. Neubauer P.D., Rademaker A.W., Leder S.B. (2015): The Yale Pharyngeal Residue Severity Rating Scale: An Anatomically Defined and Image-Based Tool. *Dysphagia*(5) 521–528. DOI:10.1007/s00455-015-9631-4.
58. Langmore S.E., Schatz K., Olsen N. (1988): Fiberoptic endoscopic examination of swallowing safety: a new procedure. *Dysphagia*(4) 216–219. DOI:10.1007/BF02414429.
59. Schoenwaelder N., Krause M., Freitag T., et al. (2022): Preclinical Head and Neck Squamous Cell Carcinoma Models for Combined Targeted Therapy Approaches. *Cancers (Basel)*(10) 2484. DOI:10.3390/cancers14102484.
60. Institute for Laboratory Animal Research, National Research Council (2011): Guide for the Care and Use of Laboratory Animals (8th Edition): National Academies Press. ISBN: 978-0-309-15400-0.
61. Laschke M.W., Vollmar B., Menger M.D. (2011): The dorsal skinfold chamber: window into the dynamic interaction of biomaterials with their surrounding host tissue. *Eur Cell Mater*(22) 147-167. DOI:10.22203/eCM.v022a12.

62. Grambow E., Leppin C., Leppin K., et al. (2017): The effects of hydrogen sulfide on platelet-leukocyte aggregation and microvascular thrombolysis. *Platelets*(5) 509–517. DOI:10.1080/09537104.2016.1235693.
63. Xie W., Lorenz M., Poosch F., et al. (2022): 3D-printed lightweight dorsal skin fold chambers from PEEK reduce chamber-related animal distress. *Sci Rep*(1) 11599. DOI:10.1038/s41598-022-13924-5.
64. Bankhead P., Loughrey M.B., Fernández J.A., et al. (2017): QuPath: Open source software for digital pathology image analysis. *Sci Rep*(1) 16878. DOI:10.1038/s41598-017-17204-5.
65. Aggarwal V.V., Waghmare C.M., Lolage S.N., et al. (2023): Subjective and perceptive assessment of speech/voice and swallowing function before and after radiation therapy in patients of head-and-neck squamous cell cancer. *J Cancer Res Ther*(19(Suppl 1)) 373-379. DOI:10.4103/jcrt.jcrt_621_21.
66. Toft K., McLachlan K., Winton M., et al. (2024): Global assessment of swallow function (GASF) following VMAT radiotherapy for head and neck squamous cell carcinoma. *Tech Innov Patient Support Radiat Oncol*(32) 100272. DOI:10.1016/j.tipsro.2024.100272.
67. D'Andréa G., Bordenave L., Nguyen F., et al. (2022): A prospective longitudinal study of quality of life in robotic-assisted salvage surgery for oropharyngeal cancer. *Eur J Surg Oncol*(6) 1243–1250. DOI:10.1016/j.ejso.2022.01.017.
68. McDowell L., King M.T., Hutcheson K.A., et al. (2024): A Hard Truth to Swallow: Critically Evaluating the MD Anderson Dysphagia Inventory (MDADI) as an Endpoint in Human Papillomavirus-associated Oropharyngeal Cancer Trials. *Int J Radiat Oncol Biol Phys*(3) 805–822. DOI:10.1016/j.ijrobp.2024.05.005.
69. Waletzko-Hellwig J., Saemann M., Schulze M., et al. (2021): Mechanical Characterization of Human Trabecular and Formed Granulate Bone Cylinders Processed by High Hydrostatic Pressure. *Materials (Basel)*(5) 1069. DOI:10.3390/ma14051069.
70. Salti H., Kramer L., Nelz S.-C., et al. (2023): Decellularization of precision-cut kidney slices-application of physical and chemical methods. *Biomed Mater*(18) 25004. DOI:10.1088/1748-605X/acb02e.
71. Hedström J., Tuomi L., Finizia C., et al. (2018): Correlations Between Patient-Reported Dysphagia Screening and Penetration-Aspiration Scores in Head and Neck Cancer Patients Post-oncological Treatment. *Dysphagia*(2) 206–215. DOI:10.1007/s00455-017-9847-6.
72. Da Silva G.M., Portas J., López R.V.M., et al. (2019): Study of Dysphagia in Patients with Advanced Oropharyngeal Cancer Subjected to an Organ Preservation Protocol Based on Concomitant Radiotherapy and Chemotherapy. *Asian Pac J Cancer Prev*(3) 977–982. DOI:10.31557/APJCP.2019.20.3.977.
73. Kirsh E., Naunheim M., Holman A., et al. (2019): Patient-reported versus physiologic swallowing outcomes in patients with head and neck cancer after chemoradiation. *Laryngoscope*(9) 2059–2064. DOI:10.1002/lary.27610.
74. Liou H.-H., Tsai S.-W., Hsieh M.H.-C., et al. (2022): Evaluation of Objective and Subjective Swallowing Outcomes in Patients with Dysphagia Treated for Head and Neck Cancer. *J Clin Med*(3) 692. DOI:10.3390/jcm11030692.
75. Wishart L.R., Harris G.B., Cassim N., et al. (2022): Association Between Objective Ratings of Swallowing and Dysphagia-Specific Quality of Life in Patients Receiving (Chemo)radiotherapy for Oropharyngeal Cancer. *Dysphagia*(4) 1014–1021. DOI:10.1007/s00455-021-10364-7.
76. Owadally W., Hurt C., Timmins H., et al. (2015): PATHOS: a phase II/III trial of risk-stratified, reduced intensity adjuvant treatment in patients undergoing transoral surgery for Human papillomavirus (HPV) positive oropharyngeal cancer. *BMC Cancer*(15) 602. DOI:10.1186/s12885-015-1598-x.
77. Nichols A.C., Theurer J., Prisman E., et al. (2019): Radiotherapy versus transoral robotic surgery and neck dissection for oropharyngeal squamous cell carcinoma (ORATOR): an open-label, phase 2, randomised trial. *Lancet Oncol*(10) 1349–1359. DOI:10.1016/S1470-2045(19)30410-3.
78. Yom S.S., Torres-Saavedra P., Caudell J.J., et al. (2021): Reduced-Dose Radiation Therapy for HPV-Associated Oropharyngeal Carcinoma (NRG Oncology HN002). *J Clin Oncol*(9) 956–965. DOI:10.1200/JCO.20.03128.
79. Ferris R.L., Flamand Y., Weinstein G.S., et al. (2022): Phase II Randomized Trial of Transoral Surgery and Low-Dose Intensity Modulated Radiation Therapy in Resectable p16+ Locally Advanced Oropharynx Cancer: An ECOG-ACRIN Cancer Research Group Trial (E3311). *J Clin Oncol*(2) 138–149. DOI:10.1200/JCO.21.01752.

80. Jensen K., Lambertsen K., Torkov P., et al. (2007): Patient assessed symptoms are poor predictors of objective findings. Results from a cross sectional study in patients treated with radiotherapy for pharyngeal cancer. *Acta Oncol*(8) 1159–1168. DOI:10.1080/02841860701491041.
81. Gillespie M.B., Brodsky M.B., Day T.A., et al. (2004): Swallowing-related quality of life after head and neck cancer treatment. *Laryngoscope*(8) 1362–1367. DOI:10.1097/00005537-200408000-00008.
82. Pedersen A., Wilson J., McColl E., et al. (2016): Swallowing outcome measures in head and neck cancer - How do they compare? *Oral Oncol*(52) 104–108. DOI:10.1016/j.oraloncology.2015.10.015.
83. Strojan P., Hutcheson K.A., Eisbruch A., et al. (2017): Treatment of late sequelae after radiotherapy for head and neck cancer. *Cancer Treat Rev*(59) 79–92. DOI:10.1016/j.ctrv.2017.07.003.
84. Langerman A., MacCracken E., Kasza K., et al. (2007): Aspiration in chemoradiated patients with head and neck cancer. *Arch Otolaryngol Head Neck Surg*(12) 1289–1295. DOI:10.1001/archotol.133.12.1289.
85. Feng F.Y., Kim H.M., Lyden T.H., et al. (2010): Intensity-modulated chemoradiotherapy aiming to reduce dysphagia in patients with oropharyngeal cancer: clinical and functional results. *J Clin Oncol*(16) 2732–2738. DOI:10.1200/JCO.2009.24.6199.
86. Jagtap M., Karnad M. (2019): Swallowing Skills and Aspiration Risk Following Treatment of Head and Neck Cancers. *Indian J Surg Oncol*(2) 402–405. DOI:10.1007/s13193-019-00912-x.
87. Chen S.-C., Huang B.-S., Hung T.-M., et al. (2018): Swallowing ability and its impact on dysphagia-specific health-related QOL in oral cavity cancer patients post-treatment. *Eur J Oncol Nurs*(36) 89–94. DOI:10.1016/j.ejon.2018.07.002.
88. Florie M., Pilz W., Kremer B., et al. (2021): EAT-10 Scores and Fiberoptic Endoscopic Evaluation of Swallowing in Head and Neck Cancer Patients. *Laryngoscope*(1) E45-E51. DOI:10.1002/lary.28626.
89. Rogus-Pulia N.M., Pierce M.C., Mittal B.B., et al. (2014): Changes in swallowing physiology and patient perception of swallowing function following chemoradiation for head and neck cancer. *Dysphagia*(2) 223–233. DOI:10.1007/s00455-013-9500-y.
90. Gómez Serrano M., Iglesias Moreno M.C., Gimeno Hernández J., et al. (2016): Cartilage invasion patterns in laryngeal cancer. *Eur Arch Otorhinolaryngol*(7) 1863–1869. DOI:10.1007/s00405-015-3687-5.
91. Pfister D.G., Laurie S.A., Weinstein G.S., et al. (2006): American Society of Clinical Oncology clinical practice guideline for the use of larynx-preservation strategies in the treatment of laryngeal cancer. *J Clin Oncol*(22) 3693–3704. DOI:10.1200/JCO.2006.07.4559.
92. Patel U.A., Howell L.K. (2011): Local response to chemoradiation in T4 larynx cancer with cartilage invasion. *Laryngoscope*(1) 106–110. DOI:10.1002/lary.21181.
93. Wagner M.M., Curé J.K., Caudell J.J., et al. (2012): Prognostic significance of thyroid or cricoid cartilage invasion in laryngeal or hypopharyngeal cancer treated with organ preserving strategies. *Radiat Oncol*(7) 219. DOI:10.1186/1748-717X-7-219.
94. Harréus U. (2013): Fehler und Gefahren: Onkochirurgie im Kopf-Hals-Bereich. *Laryngorhinootologie*(92(Suppl 1)) 177-198. DOI:10.1055/s-0032-1333250.
95. Maletzki C., Freiin Grote V., Kalle F., et al. (2023): Establishing safe high hydrostatic pressure devitalization thresholds for autologous head and neck cancer vaccination and reconstruction. *Cell Death Discov*(1) 390. DOI:10.1038/S41420-023-01671-z.
96. Hiemer B., Genz B., Jonitz-Heincke A., et al. (2016): Devitalisation of human cartilage by high hydrostatic pressure treatment: Subsequent cultivation of chondrocytes and mesenchymal stem cells on the devitalised tissue. *Sci Rep*(6) 33747. DOI:10.1038/srep33747.
97. Badylak S.F., Freytes D.O., Gilbert T.W. (2009): Extracellular matrix as a biological scaffold material: Structure and function. *Acta Biomater*(1) 1–13. DOI:10.1016/j.actbio.2008.09.013.
98. Londono R., Gorantla V.S., Badylak S.F. (2016): Emerging Implications for Extracellular Matrix-Based Technologies in Vascularized Composite Allotransplantation. *Stem Cells Int*(2016) 1541823. DOI:10.1155/2016/1541823.
99. Swinehart I.T., Badylak S.F. (2016): Extracellular matrix bioscaffolds in tissue remodeling and morphogenesis. *Dev Dyn*(3) 351–360. DOI:10.1002/dvdy.24379.

100. Hiemer B., Genz B., Ostwald J., et al. (2019): Repair of cartilage defects with devitalized osteochondral tissue: A pilot animal study. *J Biomed Mater Res B Appl Biomater*(7) 2354–2364. DOI:10.1002/jbm.b.34329.
101. Sharpe P., Wang X.-P., Vishwakarma A. et al. (2015): Stem Cell Biology and Tissue Engineering in Dental Sciences: Academic Press. ISBN: 9780123971579.
102. Diehl P., Schmitt M., Blümelhuber G., et al. (2003): Induction of tumor cell death by high hydrostatic pressure as a novel supporting technique in orthopedic surgery. *Oncol Rep*(6) 1851–1855. DOI:10.3892/or.10.6.1851.
103. Naal F.-D., Mengele K., Schauwecker J., et al. (2005): High hydrostatic pressure-induced cell death in human chondrocytes and chondrosarcoma cells. *Anticancer Res*(3B) 1977–1982. PMID: 16158933.
104. Eisenthal A., Ramakrishna V., Skornick Y., et al. (1993): Induction of cell-mediated immunity against B16-BL6 melanoma in mice vaccinated with cells modified by hydrostatic pressure and chemical crosslinking. *Cancer Immunol Immunother*(5) 300–306. DOI:10.1007/BF01741168.
105. Korn A., Frey B., Sheriff A., et al. (2004): High hydrostatic pressure inactivated human tumour cells preserve their immunogenicity. *Cell Mol Biol (Noisy-le-grand)*(4) 469–477. PMID: 15529756.
106. Schauwecker J., Wirthmann L., Schmitt M., et al. (2006): Effect of extracorporeal high hydrostatic pressure on cellular outgrowth from tumor-afflicted bone. *Anticancer Res*(1A) 85–89. PMID: 16475683.
107. Weiss E.M., Meister S., Janko C., et al. (2010): High hydrostatic pressure treatment generates inactivated mammalian tumor cells with immunogeneic features. *J Immunotoxicol*(3) 194–204. DOI:10.3109/15476911003657414.
108. Adkins I., Fucikova J., Garg A.D., et al. (2014): Physical modalities inducing immunogenic tumor cell death for cancer immunotherapy. *Oncoimmunology*(12) e968434. DOI:10.4161/21624011.2014.968434.
109. Chen S.-K., Chung C.-A., Cheng Y.-C., et al. (2014): Hydrostatic pressure enhances mitomycin C induced apoptosis in urothelial carcinoma cells. *Urol Oncol*(1) 26.e17-24. DOI:10.1016/J.UROLONC.2012.09.004.
110. Fucikova J., Moserova I., Truxova I., et al. (2014): High hydrostatic pressure induces immunogenic cell death in human tumor cells. *Int J Cancer*(5) 1165–1177. DOI:10.1002/ijc.28766.
111. Mikyšková R., Štěpánek I., Indrová M., et al. (2016): Dendritic cells pulsed with tumor cells killed by high hydrostatic pressure induce strong immune responses and display therapeutic effects both in murine TC-1 and TRAMP-C2 tumors when combined with docetaxel chemotherapy. *Int J Oncol*(3) 953–964. DOI:10.3892/ijo.2015.3314.
112. Morimoto N., Jinno C., Mahara A., et al. (2016): Verification of the Inactivation of Melanocytic Nevus in vitro Using a Newly Developed Portable High Hydrostatic Pressure Device. *Cells Tissues Organs*(3) 170–179. DOI:10.1159/000444048.
113. Urbanova L., Hradilova N., Moserova I., et al. (2017): High hydrostatic pressure affects antigenic pool in tumor cells: Implication for dendritic cell-based cancer immunotherapy. *Immunol Lett*(187) 27–34. DOI:10.1016/j.imlet.2017.05.005.
114. Watanabe N., Mizuno M., Matsuda J., et al. (2019): Comparison of High-Hydrostatic-Pressure Decellularized Versus Freeze-Thawed Porcine Menisci. *J Orthop Res*(11) 2466–2475. DOI:10.1002/jor.24350.
115. Diehl P., Schmitt M., Schauwecker J., et al. (2005): Effect of high hydrostatic pressure on biological properties of extracellular bone matrix proteins. *Int J Mol Med*(2) 285–289. PMID: 16012763.
116. Zemmyo D., Yamamoto M., Miyata S. (2021): Efficient Decellularization by Application of Moderate High Hydrostatic Pressure with Supercooling Pretreatment. *Micromachines (Basel)*(12) 1486. DOI:10.3390/mi12121486.
117. Sutherland A.J., Converse G.L., Hopkins R.A., et al. (2015): The bioactivity of cartilage extracellular matrix in articular cartilage regeneration. *Adv Healthc Mater*(1) 29–39. DOI:10.1002/adhm.201400165.
118. Schreiter J., Meyer S., Schmidt C., et al. (2017): Dorsal skinfold chamber models in mice. *GMS Interdiscip Plast Reconstr Surg DGPW*(6) Doc10. DOI:10.3205/iprs000112.
119. Elmore S. (2007): Apoptosis: a review of programmed cell death. *Toxicol Pathol*(4) 495–516. DOI:10.1080/01926230701320337.
120. Kono H., Rock K.L. (2008): How dying cells alert the immune system to danger. *Nat Rev Immunol*(4) 279–289. DOI:10.1038/nri2215.

121. Yang Y., Jiang G., Zhang P., et al. (2015): Programmed cell death and its role in inflammation. *Mil Med Res*(2) 12. DOI:10.1186/s40779-015-0039-0.
122. Brusis T. (2023): Die erste allogene Trachealtransplantation beim Menschen vor 45 Jahren. *HNO*(12) 763–766. DOI:10.1007/s00106-023-01374-y.
123. Niemietz T., Zass G., Hagmann S., et al. (2014): Xenogeneic transplantation of articular chondrocytes into full-thickness articular cartilage defects in minipigs: fate of cells and the role of macrophages. *Cell Tissue Res*(3) 749–761. DOI:10.1007/s00441-014-1982-x.
124. Smith B., Sigal I.R., Grande D.A. (2015): Immunology and cartilage regeneration. *Immunol Res*(1-3) 181–186. DOI:10.1007/s12026-015-8720-7.
125. Milkovich J., Ahmad J. (2022): A Canadian Experience With Off-the-Shelf, Aseptically Processed, Costal Cartilage Segment Allografts in Complex Rhinoplasty. *Aesthet Surg J Open Forum*(4) ojac085. DOI:10.1093/asjof/ojac085.
126. Rohrich R.J., Abraham J., Alleyne B., et al. (2022): Fresh Frozen Rib Cartilage Grafts in Revision Rhinoplasty: A 9-Year Experience. *Plast Reconstr Surg*(1) 58–62. DOI:10.1097/PRS.0000000000009203.
127. Sicari B.M., Johnson S.A., Siu B.F., et al. (2012): The effect of source animal age upon the in vivo remodeling characteristics of an extracellular matrix scaffold. *Biomaterials*(22) 5524–5533. DOI:10.1016/j.biomaterials.2012.04.017.
128. Wang R.M., Johnson T.D., He J., et al. (2017): Humanized mouse model for assessing the human immune response to xenogeneic and allogeneic decellularized biomaterials. *Biomaterials*(129) 98–110. DOI:10.1016/j.biomaterials.2017.03.016.
129. Yang Q., Peng J., Guo Q., et al. (2008): A cartilage ECM-derived 3-D porous acellular matrix scaffold for in vivo cartilage tissue engineering with PKH26-labeled chondrogenic bone marrow-derived mesenchymal stem cells. *Biomaterials*(15) 2378–2387. DOI:10.1016/j.biomaterials.2008.01.037.
130. Kheir E., Stapleton T., Shaw D., et al. (2011): Development and characterization of an acellular porcine cartilage bone matrix for use in tissue engineering. *J Biomed Mater Res A*(2) 283–294. DOI:10.1002/jbm.a.33171.
131. Rihn J.A., Irrgang J.J., Chhabra A., et al. (2006): Does irradiation affect the clinical outcome of patellar tendon allograft ACL reconstruction? *Knee Surg Sports Traumatol Arthrosc*(9) 885–896. DOI:10.1007/s00167-006-0036-7.
132. Halliday D., Resnik R., Walker J. (2001): Fundamentals of physics. 6th ed. Hoboken: Wiley. ISBN: 111823071X.
133. Laschke M.W., Menger M.D. (2016): The dorsal skinfold chamber: A versatile tool for preclinical research in tissue engineering and regenerative medicine. *Eur Cell Mater*(32) 202–215. DOI:10.22203/eCM.v032a13.
134. Ushiyama A., Yamada S., Ohkubo C. (2004): Microcirculatory parameters measured in subcutaneous tissue of the mouse using a novel dorsal skinfold chamber. *Microvasc Res*(2) 147–152. DOI:10.1016/j.mvr.2004.05.004.
135. Dahmke I.N., Ampofo E., Menger M.D., et al. (2019): The dorsal skinfold chamber: A valuable model for the in vivo evaluation of topical formulations. *Exp Dermatol*(8) 940–947. DOI:10.1111/exd.13983.
136. McLuckie M., Robotti F., Sanchez-Macedo N., et al. (2020): Lipoconstruct surface topography grating size influences vascularization onset in the dorsal skinfold chamber model. *Acta Biomater*(106) 136–144. DOI:10.1016/j.actbio.2020.01.050.
137. Menger M.M., Nalbach L., Roma L.P., et al. (2020): Erythropoietin accelerates the revascularization of transplanted pancreatic islets. *Br J Pharmacol*(7) 1651–1665. DOI:10.1111/bph.14925.
138. Kihm A., Quint S., Laschke M.W., et al. (2021): Lingering Dynamics in Microvascular Blood Flow. *Biophys J*(3) 432–439. DOI:10.1016/j.bpj.2020.12.012.
139. Weinzierl A., Harder Y., Schmauss D., et al. (2021): Improved Vascularization and Survival of White Compared to Brown Adipose Tissue Grafts in the Dorsal Skinfold Chamber. *Biomedicines*(1) 23. DOI:10.3390/biomedicines10010023.

140. Weinzierl A., Harder Y., Schmauss D., et al. (2022): Boosting Tissue Vascularization: Nanofat as a Potential Source of Functional Microvessel Segments. *Front Bioeng Biotechnol*(10) 820835. DOI:10.3389/fbioe.2022.820835.
141. Strüder D., Lachmann C., van Bonn S.M., et al. (2023): The Dorsal Skinfold Chamber as a New Tympanic Membrane Wound Healing Model: Intravital Insights into the Pathophysiology of Epithelialized Wounds. *Eur Surg Res*(2) 286–300. DOI:10.1159/000519774.
142. Limido E., Weinzierl A., Ampofo E., et al. (2024): Nanofat Accelerates and Improves the Vascularization, Lymphatic Drainage and Healing of Full-Thickness Murine Skin Wounds. *Int J Mol Sci*(2). DOI:10.3390/ijms25020851.
143. Kang C., Cho A.-R., Lee H.J., et al. (2021): Feasibility study of incident dark-field video microscope for measuring microcirculatory variables in the mouse dorsal skinfold chamber model. *Acute Crit Care*(1) 29–36. DOI:10.4266/acc.2020.00969.
144. Currie S.M., Stegmeyer R.I., Mildner K., et al. (2022): Confocal Real-Time Analysis of Cutaneous Platelet Recruitment during Immune Complex–Mediated Inflammation. *J Invest Dermatol*(10) 2724-2732.e3. DOI:10.1016/j.jid.2022.03.011.
145. Kang C., Cho A.-R., Kim H., et al. (2024): Sedation with propofol and isoflurane differs in terms of microcirculatory parameters: A randomized animal study using dorsal skinfold chamber mouse model. *Microvasc Res*(153) 104655. DOI:10.1016/j.mvr.2024.104655.
146. Gaustad J.-V., Brurberg K.G., Simonsen T.G., et al. (2008): Tumor vascularity assessed by magnetic resonance imaging and intravital microscopy imaging. *Neoplasia*(4) 354–362. DOI:10.1593/neo.08162.
147. Axelsson H., Bagge U., Lundholm K., et al. (1997): A one-piece plexiglass access chamber for subcutaneous implantation in the dorsal skin fold of the mouse. *Int J Microcirc Clin Exp*(6) 328–329. DOI:10.1159/000179248.
148. Boucher Y., Leunig M., Jain R.K. (1996): Tumor angiogenesis and interstitial hypertension. *Cancer Res*(18) 4264–4266. PMID: 8797602.
149. Leunig M., Yuan F., Gerweck L.E., et al. (1997): Effect of basic fibroblast growth factor on angiogenesis and growth of isografted bone: quantitative in vitro-in vivo analysis in mice. *Int J Microcirc Clin Exp*(1) 1–9. DOI:10.1159/000179199.
150. Gelaw B., Levin S. (2001): Wound-induced angiogenesis and its pharmacologic inhibition in a murine model. *Surgery*(3) 497–501. DOI:10.1067/msy.2001.115833.
151. Shan S., Flowers C., Peltz C.D., et al. (2006): Preferential extravasation and accumulation of liposomal vincristine in tumor comparing to normal tissue enhances antitumor activity. *Cancer Chemother Pharmacol*(2) 245–255. DOI:10.1007/s00280-005-0145-x.
152. Seynhaeve A.L.B., Hagen T.L.M. ten (2018): Intravital Microscopy of Tumor-associated Vasculature Using Advanced Dorsal Skinfold Window Chambers on Transgenic Fluorescent Mice. *J Vis Exp*(131) 55115. DOI:10.3791/55115.
153. Vaezi M., Yang S. (2015): Extrusion-based additive manufacturing of PEEK for biomedical applications. *Virtual and Physical Prototyping*(3) 123–135. DOI:10.1080/17452759.2015.1097053.

A.2 Abkürzungsverzeichnis

AxV: Annexin-V
CUP: Cancer of Unknown Primary, Karzinom unbekannter Primärlokalisation
DAMPS: Damage-Associated Molecular Patterns, schadensassoziierte molekulare Muster
DNA: Deoxyribonucleic Acid, Desoxyribonucleinsäure
DMEM: Dulbecco's Modifiziertes Eagle-Medium
EDTA: Ethylenediaminetetraacetic Acid, Ethylendiamintetraessigsäure
EZM: Extrazelluläre Matrix
FCD: Functional Capillary Density, funktionelle Kapillardichte
FESEM: Field Emission Scanning Electron Microscopy, Feldemissions-Rasterelektronenmikroskopie
FEES: Fiberoptic Endoscopic Evaluation of Swallowing, Faseroptische endoskopische Beurteilung des Schluckens
FKS: Fetales Kälberserum
HHD: Hydrostatischer Hochdruck
HNSCC: Head and Neck Squamous Cell Carcinoma, Kopf-Hals-Plattenepithelkarzinom
IVM: Intravitalmikroskopie
MDADI: M. D. Anderson Dysphagia Inventory
MRT: Magnetresonanztomographie
NIH: National Institutes of Health
PAS: Penetrations-Aspirations-Skala
PEEK: Polyetheretherketon
PBS: Phosphate Buffered Saline, phosphatgepufferte Salzlösung
PI: Propidiumiodid
P/S: Penicillin/Streptomycin
rER: Raues endoplasmatisches Retikulum
RHK: Rückenhautkammer
rpm: revolutions per minute, Umdrehungen pro Minute
SDS: Sodium Dodecyl Sulfate, Natriumdodecylsulfat
TEM: Transmissionselektronenmikroskopie
Tris-HCl: Tris(hydroxymethyl)aminomethan-Hydrochlorid
WST: Water-Soluble Tetrazolium, wasserlösliches Tetrazolium
YPRSRS: Yale Pharyngeal Residue Severity Rating Scale, Yale Pharyngeal Residue Severity Bewertungsskala

A.3 Abbildungsverzeichnis

A.4 Tabellenverzeichnis

A.5 Zusätzliche Tabellen

Tabelle A1: P-Werte des Vergleichs der MDADI Gesamt-Scores der verschiedenen Tumorlokalisationen von Patienten mit Kopf-Hals-Tumoren

Fragebogen	Vergleich	p-Wert
MDADI	Mundhöhle vs. Oropharynx	0,29
	Mundhöhle vs. Hypopharynx	0,70
	Mundhöhle vs. Larynx	0,98
	Mundhöhle vs. CUP	> 0,99
	Oropharynx vs. Hypopharynx	> 0,99
	Oropharynx vs. Larynx	0,72
	Oropharynx vs. CUP	0,81
	Hypopharynx vs. Larynx	0,93
	Hypopharynx vs. CUP	0,87
	Larynx vs. CUP	0,97

Die M. D. Anderson Dysphagia Inventory (MDADI) Gesamt-Scores wurden den verschiedenen Tumorlokalisationen zugeordnet und die p-Werte zwischen den verschiedenen Lokalisationen bestimmt. Ein p-Wert unter 0,05 zeigt einen signifikanten Unterschied zwischen den verglichenen Gruppen an.

Tabelle A2: P-Werte der relativen Absorption der metabolischen Aktivität humaner Chondrozyten 24, 48 und 72 Stunden nach hydrostatischer Hochdruckbehandlung

Zelltyp	HHD-Behandlung	Vergleich	p-Wert
Chondrozyten	200 MPa	24 vs. 48 h	0,32
		24 vs. 72 h	-
	300 MPa	24 vs. 48 h	0,34
		24 vs. 72 h	-
	400 MPa	24 vs. 48 h	0,38
		24 vs. 72 h	0,62

Die metabolische Aktivität wurde mit Hilfe des WST-1-Assays 24, 48 und 72 h nach der hydrostatischen Hochdruck (HHD)-Behandlung bei bis zu 400 MPa gemessen. Die Bestimmung der p-Werte erfolgte zwischen den relativen Absorptionen nach 24 Stunden und denjenigen nach 48 und 72 Stunden. Ein p-Wert unter 0,05 zeigt einen signifikanten Unterschied zwischen den verglichenen Gruppen an.
-: Der p-Wert konnte nicht bestimmt werden, da die entsprechenden Gruppen keine Schwankungen aufweisen und es keine Unterschiede zwischen den Daten der jeweiligen Gruppen gibt.

Tabelle A3: Gemessene Werte der durchflusszytometrischen Bestimmung der Vitalität humaner Chondrozyten 24 Stunden nach der hydrostatischen Hochdruckbehandlung

Zelltyp	HHD-Behandlung	Vitalitätslevel	Anteil an Zellpopulation [%]
Chondrozyten	Kontrolle	früh apoptotisch	0,43 ± 0,42
		nekrotisch	0,82 ± 0,29
	100 MPa	früh apoptotisch	0,83 ± 0,66
		nekrotisch	1,77 ± 1,96
	200 MPa	früh apoptotisch	0,74 ± 0,88
		nekrotisch	7,69 ± 7,33
	300 MPa	früh apoptotisch	0,34 ± 0,20
		nekrotisch	0,77 ± 0,29
	400 MPa	früh apoptotisch	0,28 ± 0,13
		nekrotisch	0,63 ± 0,39

Die Durchflusszytometrie wurde eingesetzt, um 24 h nach der Behandlung mit hydrostatischem Hochdruck (HHD) bei bis zu 400 MPa zwischen vitalen, früh und spät apoptotischen sowie nekrotischen Zellen zu unterscheiden.

Tabelle A4: P-Werte der durchflusszytometrischen Bestimmung der Vitalität humaner Chondrozyten 24 Stunden nach der hydrostatischen Hochdruckbehandlung

Zelltyp	Vitalitätslevel	Vergleich	p-Wert
Chondrozyten	früh apoptotisch	Kontrolle vs. 100 MPa	0,26
		Kontrolle vs. 200 MPa	0,84
		Kontrolle vs. 300 MPa	0,97
		Kontrolle vs. 400 MPa	0,81
		100 vs. 200 MPa	0,98
		100 vs. 300 MPa	0,35
		100 vs. 400 MPa	0,34
	nekrotisch	Kontrolle vs. 100 MPa	0,68
		Kontrolle vs. 200 MPa	0,24
		Kontrolle vs. 300 MPa	0,75
		Kontrolle vs. 400 MPa	0,62
		100 vs. 200 MPa	0,33
		100 vs. 300 MPa	0,65
		100 vs. 400 MPa	0,57

Die Durchflusszytometrie wurde eingesetzt, um 24 h nach der Behandlung mit hydrostatischem Hochdruck (HHD) bei bis zu 400 MPa zwischen vitalen, früh und spät apoptotischen sowie nekrotischen Zellen zu unterscheiden. Die Bestimmung der p-Werte erfolgte zwischen den prozentualen Anteilen der Vitalitätslevel der unbehandelten Kontrolle sowie 100 MPa und der Behandlung bei 100, 200, 300 und 400 MPa. Ein p-Wert unter 0,05 zeigt einen signifikanten Unterschied zwischen den verglichenen Gruppen an.

Tabelle A5: P-Werte der DNA-Gehaltsbestimmung porciner Schildknorpel nach hydrostatischer Hochdruckbehandlung

Gewebe	Vergleich	p-Wert
Schildknorpel	ctl vs. 100 MPa	> 0,99
	ctl vs. 200 MPa	0,36
	ctl vs. 400 MPa	0,92
	100 vs. 200 MPa	0,38
	100 vs. 400 MPa	0,92

Die Dezellularisierungseffizienz wurde anhand der DNA-Menge der porcinen Schildknorpel nach hydrostatischer Hochdruckbehandlung mit bis zu 400 MPa ermittelt. Die Bestimmung der p-Werte erfolgte zwischen dem DNA-Gehalt der unbehandelten Kontrolle sowie 100 MPa und der Behandlung bei 100, 200, 300 und 400 MPa. Ein p-Wert unter 0,05 zeigt einen signifikanten Unterschied zwischen den verglichenen Gruppen an.

Tabelle A6: In vivo gemessene Werte der funktionellen Kapillardichte in der Nähe und der Peripherie von Schildknorpel nach hydrostatischer Hochdruckbehandlung

Gewebe, Messort	Tag	HHD-Behandlung	FCD [cm/cm²]
Schildknorpel, zentral	6	Kontrolle	24,89 ± 2,42
		200 MPa	23,72 ± 5,38
	10	Kontrolle	25,70 ± 5,96
		200 MPa	27,71 ± 4,00
Schildknorpel, peripher	6	Kontrolle	25,56 ± 2,90
		200 MPa	22,51 ± 7,38
	10	Kontrolle	26,50 ± 3,88
		200 MPa	30,37 ± 6,18

Die funktionelle Kapillardichte (FCD) wurde als Entzündungsindikator nach der Implantation von mit hydrostatischem Hochdruck (HHD) behandelten porcinen Schildknorpel im Mausmodell bestimmt. Die Messung der FCD in der Nähe und in der Peripherie des implantierten Gewebes erfolgte an Tag 3, 6, 10 und 15.

Tabelle A7: Angabe der p-Werte der ermittelten funktionellen Kapillardichten von Schildknorpel nach hydrostatischer Hochdruckbehandlung zwischen den experimentellen Gruppen

Gewebe, Messort	Kontrolle vs. 200 MPa	p-Wert
Schildknorpel, zentral	Tag 3	0,47
	Tag 6	0,97
	Tag 10	0,84
	Tag 15	0,99
Schildknorpel, peripher	Tag 3	> 0,99
	Tag 6	0,86
	Tag 10	0,72
	Tag 15	0,94

Die funktionelle Kapillardichte (FCD) wurde als Entzündungsindikator nach der Implantation von mit hydrostatischem Hochdruck (HHD) behandelten porcinen Schildknorpel im Mausmodell bestimmt. Die Messung der FCD in der Nähe und in peripheren Bereichen des implantierten Gewebes erfolgte an Tag 3, 6, 10 und 15. Die p-Werte wurden zwischen der FCD der unbehandelten Kontrolle und der Behandlung bei 200 MPa ermittelt. Ein p-Wert unter 0,05 zeigt einen signifikanten Unterschied zwischen den verglichenen Gruppen an.

Tabelle A8: Angabe der p-Werte zwischen zentral und peripher gemessenen funktionellen Kapillardichten von Schildknorpel nach hydrostatischer Hochdruckbehandlung

Gewebe, experimentelle Gruppe	zentral vs. peripher	p-Wert
Schildknorpel,	Tag 3	0,96
Kontrolle	Tag 6	> 0,99
	Tag 10	> 0,99
	Tag 15	0,38
Schildknorpel,	Tag 3	> 0,99
200 MPa	Tag 6	> 0,99
	Tag 10	0,85
	Tag 15	0,31

Die funktionelle Kapillardichte (FCD) wurde als Entzündungsindikator nach der Implantation von mit hydrostatischem Hochdruck (HHD) behandelten porcinen Schildknorpel im Mausmodell bestimmt. Die Messung der FCD in der Nähe und in peripheren Bereichen des implantierten Gewebes erfolgte an Tag 3, 6, 10 und 15. Die p-Werte wurden zwischen der FCD in der Nähe und der Peripherie der Knorpel ermittelt. Ein p-Wert unter 0,05 zeigt einen signifikanten Unterschied zwischen den verglichenen Gruppen an.

A.6 Wissenschaftlicher Lebenslauf

Persönliche Daten

Name: **Friederike Kalle (geb. Poosch)**

Beruflicher Werdegang und Hochschulausbildung

aus Datenschutzgründen in dieser Version nicht enthalten

Publikationen

- **Kalle F.**, Stadler V.P., Brach J.K., Freiin Grote V., Pohl C., Schulz K., Seidenstücker M., Jonitz-Heincke A., Bader R., Mlynski R., Strüder D. (2024): High hydrostatic pressure treatment for advanced tissue grafts in reconstructive head and neck surgery. J Biomed Mater Res A. 113(1):e37791. DOI: 10.1002/jbm.a.37791
- Pohl C., Kunzmann M., Brandt N., Koppe C., Waletzko-Hellwig J., Bader R., **Kalle F.**, Kertsing S., Behrendt D., Schlosser M., Hoene A. (2024): Quantitative analysis of trabecular bone tissue cryosections via a fully automated neural network-based approach. PloS One. 19(4):e0298830. DOI: 10.1371/journal.pone.0298830.
- Maletzki C., Freiin Grote V., **Kalle F.**, Kleitke T., Zimpfer A., Becker A.S., Bergmann-Ewert W., Jonitz-Heincke A., Bader R., Vollmar B., Hackenberg S., Scherzad A., Mlynski R., Strüder D. (2023): Establishing safe high hydrostatic pressure devitalization thresholds for autologous head and neck cancer vaccination and reconstruction. Cell Death Discov. 2023 Oct 23;9(1):390. DOI: 10.1038/s41420-023-01671-z.
- Strüder D., Ebert J., **Kalle F.**, Schraven S.P., Eichhorst L., Mlynski R., Großmann W. (2023): Head and Neck Cancer: A Study on the Complex Relationship between QoL and Swallowing Function. Curr Oncol. 2023 Dec;30:10336-10350. DOI: 10.3390/curroncol30120753.
- Xie W., Lorenz M., **Poosch F.**, Palme R., Zechner D., Vollmar B., Grambow E., Strüder D. (2022): 3D-printed lightweight dorsal skin fold chambers from PEEK reduce chamber-related animal distress. Sci Rep. 2022 Jul 8;12(1):11599. DOI: 10.1038/s41598-022-13924-5.

Kongressbeiträge

- Kleitke T., Eichhorst L., **Kalle F.**, Maletzki C., Danko A., Lindner T., Mlynski R., Strüder D. (2024): Multimodale Bildgebung von Kopf-Hals-Tumoren im Chorion Allantois Membrane Assay als Basis für die Etablierung neuer onkologischer Therapien. Vortrag, Deutscher HNO-Kongress, Essen. Laryngorhinootologie 2024; 103(S 02): S53. DOI: 10.1055/s-0044-1784111.
- Eichhorst L., Kleitke T., **Kalle F.**, Maletzki C., Becker A.-S., Zimpfer A., Mlynski R., Strüder D. (2024): Etablierung Patienten-abgeleiteter Modelle (PDX) von Kopf-Hals-Tumoren im Chorion-Allantois-Membrane Assay (CAM-Assay). Vortrag, Deutscher HNO-Kongress, Essen. Laryngorhinootologie 2024; 103(S 02): S60. DOI: 10.1055/s-0044-1784136
- **Kalle F**., Stadler V., Pohl C., Jonitz-Heincke A., Springer A., Seidenstücker M., Bader R., Mlynski R., Strüder D. (2023): High hydrostatic pressure as a novel method for devitalization and quality enhancement of cartilage tissue grafts in head and neck surgery. Vortrag, Annual Meeting of the German Society for Biomaterials, Jena.

- **Poosch F.**, Kirchner L., Pohl C., Jonitz-Heincke A., Springer A., Seidenstuecker M., Bader R., Strüder D., Mlynski R. (2022): Neuartige Ansätze zur Bereitstellung verbesserter Binde- und Stützgewebetransplantate auf Basis der hydrostatischen Hochdrucktechnologie. Vortrag, Deutscher HNO-Kongress, Hannover. Laryngorhinootologie 2022; 101(S 02): S34. DOI: 10.1055/s-0042-1747188.
- Strüder D., Kleitke T., Christiansen A.-S., Schoenwaelder N., **Poosch F.**, Mlynski R., Maletzki C. (2022): Devitalisierung von Kopf-Hals-Tumoren durch hydrostatischen Hochdruck - Untersuchungen zur onkologischen Sicherheit und zum immunogenen Zelltod. Vortrag, Deutscher HNO-Kongress, Hannover. Laryngorhinootologie 2022; 101(S 02): S66. DOI: 10.1055/s-0042-1747275
- **Poosch F.**, Kirchner L., Waletzko J., Schulze M., Jonitz-Heincke A., Dau M., Bader R., Mlynski R., Strüder D. (2020): "Hochdruck-behandelte Knorpel- und Faszientransplantate zur Rekonstruktion von Gewebedefekten in der Kopf-Hals-Chirurgie: In vitro-Charakterisierung der Zellvitalität, Morphologie und Biomechanik. Poster, Deutscher HNO-Kongress, Berlin. Laryngorhinootologie 2020; 99(S 02): S401. DOI: 10.1055/s-0040-1711447.
- **Poosch F.,** Strüder D., Mlynski R. (2019): Hochdruck-behandelte Knorpel- und Faszientransplantate zur Rekonstruktion von Gewebedefekten in der Kopf-Hals-Chirurgie. Poster, Forschungscamp der Universität Rostock, Rostock.
- **Poosch F.**, Bahl H., Kriebel K. (2017): Biofilm formation of *C. acetobutylicum* is enhanced by oxidative stress. Poster, Gemeinsame Konferenz der Deutschen Gesellschaft für Hygiene und Mikrobiologie & Vereinigung für Allgemeine und Angewandte Mikrobiologie e. V.: Microbiology and Infection 2017, Würzburg.

A.7 Danksagung

An dieser Stelle möchte ich allen meinen herzlichen Dank und meine Wertschätzung aussprechen, die in vielfältiger Weise zur Anfertigung meiner Dissertation beigetragen haben.

Insbesondere möchte ich mich zuerst bei Herrn Prof. Dr. Robert Mlynski bedanken. Durch seine kontinuierliche Unterstützung, fachliche Expertise und konstruktiven Hinweise hat er die Entwicklung dieser Arbeit maßgeblich unterstützt.

Ebenso richte ich meinen Dank an Herrn Dr. Daniel Strüder, der mich durch seine fachliche Begleitung, wertvollen Input und hilfreichen Gespräche in allen Phasen der Promotion unterstützt hat. Seine stets offene Art sowie sein konstruktives Feedback waren eine große Hilfe.

Auch dem gesamten Team der Klinik und Poliklinik für Hals-Nasen-Ohrenheilkunde, Kopf- und Halschirurgie „Otto Körner“ gilt mein Dank, einschließlich des engagierten Sekretariats und ganz besonders der Forschungsabteilung, deren Unterstützung in vielerlei Hinsicht zum Gelingen meiner Arbeit beigetragen hat.

Weiterhin möchte ich mich beim gesamtem FORBIOMIT für die Unterstützung und wertvollen Hinweise während der gesamten Promotion bedanken, vor allem bei Herrn Prof. Dr. Rainer Bader und Frau Dr. Anika Jonitz-Heincke. Die Möglichkeit, von dem vorhandenen Wissen und der Erfahrung zu profitieren, war für mich von unschätzbarem Wert.

Ein besonderer Dank gilt zudem den Personen, die durch ihre Teilnahme an Fragebögen oder der Einwilligung zur Gewebespende meine Forschung unterstützt haben. Ihr Engagement für den Fortschritt der wissenschaftlichen Erkenntnisse ist von großer Bedeutung.

Zuletzt bedanke ich mich bei meiner Familie und meinen Freunden, die mich während der Anfertigung dieser Dissertation mit ihrem Zuspruch, ihrer Geduld und ihrer Unterstützung stets begleitet haben.

A.8 Eidesstattliche Erklärung

Hiermit versichere ich eidesstattlich, dass ich die eingereichte Dissertation selbstständig und ohne unerlaubte fremde Hilfe verfasst habe. Es wurden keine anderen als die angegebenen Quellen und Hilfsmittel verwendet. Alle aus Quellen wörtlich oder inhaltlich entnommenen Stellen sind als solche kenntlich gemacht. Die Arbeit wurde bisher in gleicher oder ähnlicher Form keinem anderen Prüfungsamt vorgelegt und auch nicht veröffentlicht.

Rostock, den

_____
Friederike Kalle

A.9 Verwendete Originalarbeiten

Die vorliegende Dissertation basiert auf den folgenden Originalarbeiten:

[I] Strüder D., Ebert J., **Kalle F.**, Schraven S.P., Eichhorst L., Mlynski R., Großmann W. (2023): Head and Neck Cancer: A Study on the Complex Relationship between QoL and Swallowing Function. Curr Oncol(12) 10336-10350. DOI: 10.3390/curroncol30120753.

[II] Maletzki C., Freiin Grote V., **Kalle F.**, Kleitke T., Zimpfer A., Becker A.S., Bergmann-Ewert W., Jonitz-Heincke A., Bader R., Vollmar B., Hackenberg S., Scherzad A., Mlynski R., Strüder D. (2023): Establishing safe high hydrostatic pressure devitalization thresholds for autologous head and neck cancer vaccination and reconstruction. Cell Death Discov(1) 390. DOI: 10.1038/s41420-023-01671-z.

[III] **Kalle F.**, Stadler V.P., Brach J.K., Freiin Grote V., Pohl C., Schulz K., Seidenstuecker M., Jonitz-Heincke A., Bader R., Mlynski R., Strüder D. (2024): High hydrostatic pressure treatment for advanced tissue grafts in reconstructive head and neck surgery. J Biomed Mater Res A(113(1)) e37791. DOI: 10.1002/jbm.a.37791.

[IV] Xie W., Lorenz M., **Poosch F.**, Palme R., Zechner D., Vollmar B., Grambow E., Strüder D. (2022): 3D-printed lightweight dorsal skin fold chambers from PEEK reduce chamber-related animal distress. Sci Rep(1) 11599. DOI: 10.1038/s41598-022-13924-5.

Current Oncology

MDPI

Article

Head and Neck Cancer: A Study on the Complex Relationship between QoL and Swallowing Function

Daniel Strüder [1,*], Johanna Ebert [1], Friederike Kalle [1], Sebastian P. Schraven [2], Lennart Eichhorst [1], Robert Mlynski [1] and Wilma Großmann [1]

[1] Department of Otorhinolaryngology, Head and Neck Surgery "Otto Körner", Rostock University Medical Center, D-18057 Rostock, Germany; johanna.ebert@uni-rostock.de (J.E.); friederike.kalle@med.uni-rostock.de (F.K.); lennart.eichhorst@med.uni-rostock.de (L.E.); robert.mlynski@med.uni-rostock.de (R.M.); wilma.grossmann@med.uni-rostock.de (W.G.)

[2] Department of Otorhinolaryngology, Head and Neck Surgery, RWTH Aachen University Hospital, D-52074 Aachen, Germany; spschraven@ukaachen.de

* Correspondence: daniel.strueder@med.uni-rostock.de

Abstract: Head and neck squamous cell carcinoma (HNSCC) is linked to significant morbidity, adversely affecting survival and functional capacity. Post-treatment challenges such as pain, dysphonia, and dysphagia are common, prompting increased attention in survivorship research. Quality of Life (QoL) questionnaires, especially the MD Anderson Dysphagia Inventory (MDADI), are prevalent outcome measures in clinical studies but often lack parallel objective swallowing function evaluations, leading to potential outcome discrepancies. This study aimed to illuminate the relationship between subjective QoL (EQ-5D-5L and MDADI) measures and objective swallowing function (evaluated via Fiberoptic Endoscopic Evaluation of Swallowing, FEES) in patients with HNSCC. The analysis revealed a notable discordance between objective measures of swallowing function, such as the Penetration–Aspiration Scale (PAS) and residue ratings in the vallecula or piriform sinus, and patients' subjective QoL assessments ($p = 0.21$). Despite the lack of correlation, swallowing-related QoL, as measured by the MDADI, was more indicative of disease severity than generic QoL assessments. Generic QoL scores did not demonstrate substantial variation between patients. In contrast, MDADI scores significantly declined with advancing tumor stage, multimodal therapy, and reliance on feeding tubes. However, the clinical significance of this finding was tempered by the less than 10-point difference in MDADI scores. The findings of this study underline the limitations of QoL measures as standalone assessments in patients with HNSCC, given their reliance on patient-perceived impairment. While subjective QoL is a crucial aspect of evaluating therapeutic success and patient-centric outcomes, it may fail to capture critical clinical details such as silent aspirations. Consequently, QoL assessments should be augmented by objective evaluations of swallowing function in clinical research and practice to ensure a holistic understanding of patient well-being and treatment impact.

Keywords: head and neck squamous cell carcinoma (HNSCC); quality of life (QoL); MD Anderson Dysphagia Inventory (MDADI); post-treatment challenges; swallowing function; fiberoptic endoscopic evaluation of swallowing (FEES); Penetration–Aspiration Scale (PAS); subjective vs. objective assessments; disease severity; therapeutic outcome evaluation

Citation: Strüder, D.; Ebert, J.; Kalle, F.; Schraven, S.P.; Eichhorst, L.; Mlynski, R.; Großmann, W. Head and Neck Cancer: A Study on the Complex Relationship between QoL and Swallowing Function. *Curr. Oncol.* **2023**, *30*, 10336–10350. https://doi.org/10.3390/curroncol30120753

Received: 19 November 2023
Revised: 2 December 2023
Accepted: 4 December 2023
Published: 6 December 2023

1. Introduction

Head and neck squamous cell cancer (HNSCC) is the 7th most common cancer worldwide and is associated with a poor outcome [1–4]. Despite aggressive surgery, radiation, and chemotherapy, ~50% of patients die, while survivors suffer from pain, dysphonia, and dysphagia [5].

Among these functional impairments, dysphagia assumes particular significance. Notably, 45–88% of patients endure dysphagia with pharyngeal residue, laryngeal penetration

and aspiration. A total of 70% of aspirations occur silently, escaping patient notice [6–10]. Consequently, dysphagia leads to malnutrition, aspiration, and tracheostomies. Given the comprehensive management of HNSCC, a standardized dysphagia diagnosis is imperative. Objective swallow assessments via Fiberoptic Endoscopic Evaluation of Swallowing (FEES) and videofluoroscopy (VFSS) offer direct visualization of the swallowing process, analysis of anatomical structure movements, anomaly detection, and support for treatment planning. Owing to dysphagia's high importance, swallowing function is increasingly employed as an endpoint in clinical studies. The Orator Study notably introduced swallowing function as a primary endpoint in a prospective randomized clinical trial, comparing primarily surgical and radiotherapeutic therapies [11,12]. Swallowing function was assessed using the MDADI questionnaire, which determines swallowing-related quality of life rather than an objective swallowing assessment. Likewise, 70% of studies on dysphagia in HNSCC solely rely on patient-reported outcomes (PRO) [13].

However, the validity of PROs in evaluating swallowing function in HNSCC is controversial: Some studies indicate significant correlations between subjective swallowing difficulties and objective parameters such as oropharyngeal swallowing efficiency, bolus transport time, residue, and aspiration [14–17]. Nevertheless, most research suggests a tenuous relationship between these measures, particularly concerning penetration and aspiration [18–29]. The present study aimed to determine if central European patients with tumors primarily attributable to smoking and/or alcohol can accurately assess their physiologic swallowing functioning using the most widely employed questionnaire, MDADI [12,30–32]. Therefore, this study explored the association of generic and swallowing-related QoL with patient characteristics such as tumor stage, therapy, nutritional mode, and tumor localization. Likewise, generic QoL (EQ-5D-5L) and swallowing-related QoL (MDADI) were correlated with objective swallowing function (FEES).

2. Materials and Methods

Study Design: A cross-sectional study was conducted to compare the generic QoL, swallowing-related QoL, and objective swallowing function among patients with HNSCC during their cancer aftercare. This study investigated the influence of therapy and patient characteristics on QoL and swallowing function. Additionally, the subjective QoL was correlated with the objective outcomes obtained from the FEES.

Participants: Patients were approached during cancer aftercare at a tertiary university hospital with a certified head and neck cancer center. Written informed consent was obtained from all participants following the local ethics committee (A 2021-0024) according to the 1964 Declaration of Helsinki. Only patients with histologically confirmed head and neck squamous cell carcinoma were included. Eligibility for the study was open to consecutive patients of any age, gender, and treatment modality. Due to the cross-sectional study design, these data (questionnaires and swallowing assessments) were collected at a single time point, without subsequent follow-up.

Assessment Protocol: The German adaptation of the EQ-5D-5L questionnaire was used to evaluate general health-related QoL comprehensively. This questionnaire is designed to explore a spectrum of life domains, specifically mobility, self-care, the performance of usual activities, the experience of pain or discomfort, and the presence of anxiety or depression. Each dimension is individually scored, culminating in an aggregated index value representing the patient's overall health status. A higher index value indicates a superior QoL. Simultaneously, the study incorporated the German MDADI [33]. The MDADI is an in-depth questionnaire divided into four subscales, each examining a different facet of the impact of dysphagia. The 'Global' subscale provides an immediate personal perception of the impact of dysphagia, while the 'Emotional' subscale addresses the psychological effects. The 'Functional' subscale considers how dysphagia affects daily activities, and the 'Physical' subscale measures the somatic aspects of swallowing difficulties. Together, these subscales converge to form a total score that ranges from 20, signaling severe dysphagia-related QoL impairment, to 100, which reflects no such impairment. Higher scores on this scale denote

a less affected swallowing-related QoL, providing a detailed understanding of the physical and emotional well-being of the patients in the context of their swallowing abilities [33,34]. Questionnaires were administered digitally or on paper via Evasys Survey Software, version 8.0 (Evasys GmbH, Lüneburg, Germany). Paper-based questionnaires were printed on DIN A4 sheets and distributed on clipboards. Digital questionnaires were presented on 12.9″ tablets (Apple iPad Pro, Cupertino, CA, USA) without a stylus, allowing responses to be marked using finger touch. All questions were displayed in a format consistent with the DIN A4 layout. The decision to use digital or paper-based questionnaires was made randomly, depending on the day of assessment.

FEES was performed to assess swallowing function. Consecutive patients assigned to phoniatrics were recruited. All patients with head and neck tumors were eligible. The procedure was conducted in the phoniatrics department by one experienced and trained laryngologist according to a standardized protocol: After an anatomical and sensory-motor assessment, a distal-chip endoscope was used for endoscopic evaluation of swallowing during the administration of three standard consistencies (International Dysphagia Diet Standardization Initiative [IDDSI] consistency, starting at 7 and then transitioning to 0): pureed solids (apple puree/plain yogurt; IDDSI consistency, 4), thin liquids (water; IDDSI consistency, 0), and solids (cracker; IDDSI consistency, 7) in successive boluses that increased in size, starting with a level teaspoon amount (puree/water) or small sip followed by larger boluses (heaped teaspoon puree/several sips of water out of medicinal cup). At least three teaspoon amounts were administered to evaluate spilling, residue, penetration, and aspiration. If aspiration occurred, the examiner decided if it was safe to administer another bolus of the same size and viscosity to determine whether the patient still demonstrated aspiration-otherwise the remaining boluses of this consistency were skipped, and the smallest amount of the next consistency was administered. In cases of gross aspiration, the examination was aborted. Food coloring was used to enhance contrast, and all FEES examinations were video and sound-recorded for later assessment. Swallowing efficacy and safety were quantified utilizing two scales: The Penetration–Aspiration Scale (PAS), an eight-point scale developed by Rosenbek, was employed to characterize the depth of bolus misdirection and the patient's response to it [35,36]. The highest PAS score achieved by a participant, indicative of the greatest impairment across all bolus consistencies, was recorded for subsequent analysis. Additionally, the Yale Pharyngeal Residue Severity Rating Scale (YPRSRS), a five-point scale, was used to evaluate the presence and severity of pharyngeal residue in the vallecula and piriform sinus [37]. The FEES and subsequent scoring were conducted in accordance with validated guidelines to ensure the fidelity and consistency of the evaluation process [38].

Statistics: Statistical analysis was conducted using GraphPad PRISM software, version 9 (GraphPad, San Diego, CA, USA). Quantitative variables were presented as means (±standard deviations) and medians (including ranges min. to max.). Descriptive statistics were used to summarize these data, and the D'Agostino–Pearson normality test was performed to assess normal distribution. T-tests were employed to compare two independent parametric samples. The ordinary one-way ANOVA with Tukey's T3 posthoc test was used for multiple comparisons. In the case of unequal variances, Welch's ANOVA, followed by Dunnett's T3 posthoc test, was conducted. For non-parametric data, the Mann–Whitney U test was applied. Non-parametric multiple comparisons were performed using the Kruskal–Wallis and Dunn's multiple comparisons tests. Spearman's non-parametric correlation was used to calculate correlations between individual parameters, and two-tailed p-values were reported. Statistical significance was defined as $p < 0.05$.

3. Results

3.1. Characteristics of the Study Cohort

This study enrolled 307 patients, with a significantly higher proportion of men (79.81%, $n = 245$) than women (20.33%, $n = 62$) (Table 1). The mean age of the participants was 65.88 years, with a standard deviation of 9.98 years. The most frequently affected sites

were the oropharynx (40.39%, n = 124) and the larynx (32.25%, n = 99). The distribution of primary tumor sizes was as follows: 29.97% (n = 92) of patients presented with T1 tumors, 26.38% (n = 81) with T2, and an equal prevalence of 18.24% for both T3 and T4 tumors (n = 56 for each category). The assessment of lymph node involvement (N-Stage) revealed that 44.95% (n = 138) of patients had no lymph node metastasis (N0), 15.31% (n = 47) were classified as N1, 35.83% (n = 110) as N2a/b/c, and a smaller subset of 3.58% (n = 11) as N3a/b. Regarding distant metastases (M-Stage), a vast majority of patients were classified as M0, with 91.53% (n = 281) showing no distant metastasis, while only 0.98% (n = 3) were M1 and 7.49% (n = 23) were denoted as Mx. The treatment modalities varied, with 24.10% (n = 74) undergoing only surgery, 18.89% (n = 58) having surgery plus radiotherapy, and 19.87% (n = 61) receiving surgery plus chemoradiotherapy. 36.72% (n = 113) received primary radiotherapy or chemoradiation without surgery. The timing for post-therapy evaluations was: 10.42% (n = 32) were evaluated at $\leq$5 months, 13.36% (n = 41) at 6–11 months, 45.93% (n = 141) between 1–5 years, and 30.29% (n = 93) were evaluated at >5 years after therapy. A subset of the population, representing 15.31% (n = 47), depended on feeding tubes for nutrition.

Table 1. Characteristics of the Study Cohort.

Group Characteristics	EQ-5D-5L, MDADI n = 307	FEES, EQ-5D-5L, MDADI n = 59
Age [years]	65.88 (±9.98)	63.20 (±9.32)
Female	62 (20.33%)	13 (22.03%)
Male	245 (79.81%)	46 (77.97%)
Primary tumor T size		
T1	92 (29.97%)	11 (18.64%)
T2	81 (26.38%)	11 (18.64%)
T3	56 (18.24%)	17 (28.81%)
T4	56 (18.24%)	19 (32.20%)
Tx	22 (7.21%)	1 (1.69%)
Primary tumor location		
Oral cavity	24 (7.82%)	10 (16.95%)
Nasopharynx	4 (1.30%)	0
Oropharynx	124 (40.39%)	33 (55.93%)
Hypopharynx	30 (9.77%)	6 (10.17%)
Larynx	99 (32.25%)	9 (15.25%)
CUP	22 (7.17%)	1 (1.69%)
Other	4 (1.30%)	0
Therapy		
Surgery only	74 (24.10%)	9 (15.25%)
(Chemo)Radiotherapy	113 (36.72%)	26 (44.06%)
Surgery + Radiotherapy	58 (18.89%)	13 (22.03%)
Surgery + Chemoradiotherapy	61 (19.87%)	11 (18.64%)
Time after therapy		
$\leq$5 months	32 (10.42%)	28 (47.46%)
6–11 months	41 (13.36%)	12 (20.34%)
1–5 years	141 (45.93%)	15 (25.41%)
>5 years	93 (30.29%)	4 (6.78%)
Feeding tube use	47 (15.31%)	33 (55.93%)

A total of 59 patients completed the EQ-5D-5L, MDADI, and standardized FEES assessments. This subgroup had an average age slightly lower than the broader group at 63.20 years (±9.32), with a male representation of 77.97% (n = 46). This subgroup showed a higher presence of advanced tumors, with 60% being classified as T3 or T4. Within the subgroup, the distribution of lymph node involvement (N-Stage) was comparable with the main cohort: 37.29% of patients (n = 22) had no lymph node metastasis (N0), while 13.56% (n = 8) were classified as N1, 37.29% (n = 22) as N2, and 11.86% (n = 7) as N3. Likewise, regarding the presence of distant metastases (M-Stage), a significant

majority, 93.22% (n = 55), had no distant metastasis (M0), with a minimal 1.69% (n = 1) showing distant metastasis (M1), and 5.08% (n = 3) were categorized as Mx. In the FEES subgroup, dependence on feeding tubes was higher at 55.93% (n = 33). Treatment types within this group were nearly evenly split between primary surgery (56.94%, n = 33) and prior (chemo)radiation (44.06%, n = 26), with a larger percentage evaluated within one year post-therapy (67.8%).

3.2. Generic and Swallowing-Related QoL

This study's analysis of general quality of life (QoL) through the EQ-5D-5L index suggested minimal variation across HNSCC patient groups, with consistently high scores averaging 0.88 ± 0.20 (Figure 1). In patients with T1 glottic laryngeal carcinoma, where minimal impact on quality of life is expected, the EQ-5D-5L score was found to be the same, at 0.89 ± 0.19. Notably, a significant difference emerged when comparing patients with oral nutrition to those with feeding tubes, indicating better QoL for the former group (0.89 ± 0.17 vs. 0.80 ± 0.28, $p < 0.05$). No significant differences were found when QoL was analyzed against tumor size, treatment method, tumor location, HPV status, or nutritional status.

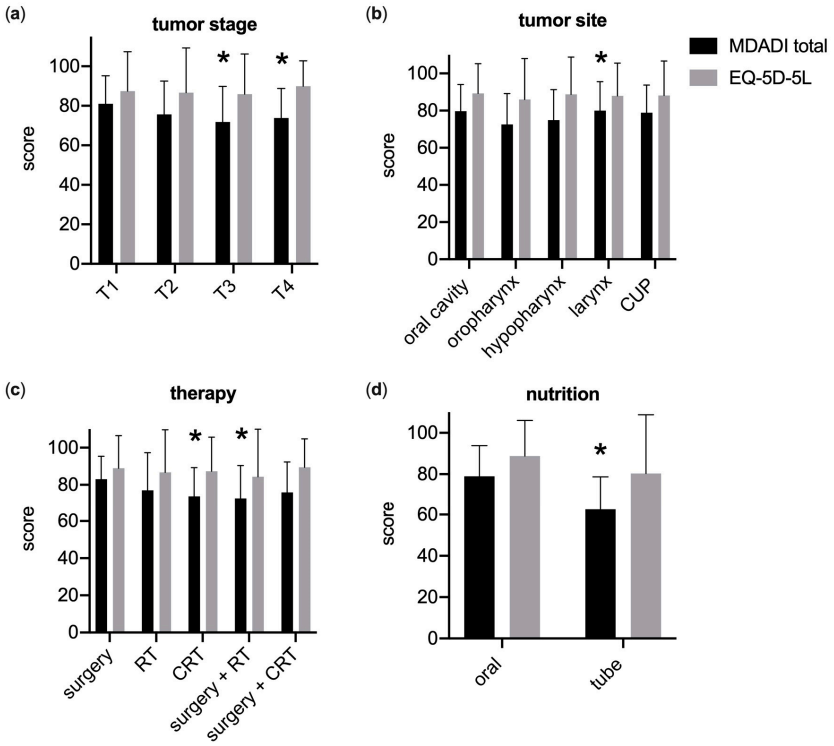

Figure 1. Swallowing-related QoL (MDADI total score) deteriorates in advanced head and neck cancer, while generic QoL (EQ-5D-5L) remains unrelated to cancer T-stage. (**a**) Low MDADI scores were associated with increasing cancer T-stage (* $p < 0.05$ vs. T1). (**b**) Cancer of the oral cavity, of the larynx, and unknown primary (CUP) were associated with high MDADI scores. Oropharyngeal and hypopharyngeal cancer scored a decrease (* $p < 0.05$ vs. oropharynx). (**c**) Among all patients and tumor locations, the MDADI score was highest for surgery only and significantly lower for combination therapies such as surgery + radiotherapy (RT) and chemoradiation (CRT) * $p < 0.05$ vs. surgery). (**d**) Feeding tube dependence scored a significant decrease for the MDADI (* $p < 0.05$ vs. oral nutrition). (**a**–**c**) However, generic quality of life did not change for increased cancer stage, cancer location, or therapy ($p < 0.05$). n = 59–112. Mean ± SD, (**a**–**c**) two-way ANOVA, Tukey; (**d**) Welch's t-test.

In contrast, swallowing-related QoL, measured by the MDADI, was notably affected in severe HNSCC. Patients with T1 tumors reported the highest swallowing-related QoL

(MDADI total score of 81.03 ± 14.20), while scores decreased in T3 (71.86 ± 17.99) and T4 (73.88 ± 14.94) tumors, indicating a statistically significant difference ($p < 0.05$). The highest scores were recorded for T1 glottic laryngeal carcinomas, with an average of 83.82 ± 11.60.

However, this disparity did not meet the clinically significant threshold of a 10-point difference. Surgery as a singular treatment modality was associated with better swallowing-related QoL than combined surgery + radiotherapy and primary radio(chemo)therapy, with significant and clinically meaningful differences noted.

QoL was also superior in patients who maintained oral nutrition (79.00 ± 14.82) as opposed to those dependent on tube feeding (62.55 ± 16.17), with both statistically and clinically significant findings ($p < 0.05$, r = 0.33). Tumor location influenced swallowing-related QoL, with the highest scores observed in patients with laryngeal (80.02 ± 15.59) and oral cavity cancer (79.71 ± 14.40). MDADI was lowest in oropharyngeal (72.60 ± 16.57; $p < 0.05$ vs. larynx) and hypopharyngeal cancers (74.87 ± 16.40).

Interestingly, HPV status showed no difference in swallowing-related QoL among patients with oropharyngeal cancer (72.58 ± 16.25 and 71.50 ± 16.16; $p = 0.48$). Additionally, treatment modality did not significantly affect MDADI scores in oropharyngeal tumors. When comparing treatment options, primary surgery + (chemo)radiotherapy yielded 73.31 ± 17, while primary (chemo)radiotherapy resulted in 71.45 ± 16. This similarity extended to MDADI subscales, the composite score, and global scores. For the time elapsed after therapy, a longer duration was associated with improvements in swallowing-related quality of life (QoL), with the association being statistically significant ($p < 0.05$). Patients surveyed more than five years after their treatment reported notably better scores (79.95 ± 14.43) compared with those surveyed less than six months post-therapy (70.86 ± 13.51, $p < 0.05$) and those surveyed between six to twelve months post-therapy (71.39 ± 15.29, $p < 0.05$). However, the statistical strength of this effect was relatively weak (f = 0.20). The Pearson correlation also revealed a weak positive correlation between time after treatment and the total MDADI score (r = 0.13, $p < 0.05$).

3.3. Fiberoptic Endoscopic Evaluation of Swallowing

The objective evaluation of swallowing function via FEES across the study cohort ($n = 59$) yielded a median PAS score of 2 (range 1 to 5.25). Residue in the valleculae, as measured by the YPRSRS, was scored at 4 (range 3/5), and residue in the pyriform sinus at 2 (range 1/4). There was no observed correlation between the MDADI and objective measures of swallowing function; Spearman's ρ between the MDADI total score and PAS was 0.20 ($p = 0.27$) (Figure 2). Mean MDADI scores did not significantly differ between patients with and without aspiration as per FEES (64.79 ± 12.71 vs. 63.76 ± 17.08, respectively; $p = 0.94$), nor did YPRSRS correlate with MDADI (valleculae residue: r = −0.05, $p = 0.8$; pyriform sinus residue: r = 0.12, $p = 0.44$).

The analysis also revealed that larger tumors were associated with higher PAS scores, indicating more pronounced penetration or aspiration events (Figure 3). Stage T1 tumors had significantly lower PAS scores (median 1, range 1/2) compared to stage T4 tumors (median 4, range 2/6) ($p < 0.05$). Tumors classified as T2 and T3 showed a median PAS of 2 (range 1/5), with an effect size (r) of 0.4, suggesting a moderate effect. Patients receiving oral nutrition demonstrated significantly better PAS scores (median 1, range 1/3.5) compared to those on PEG feeding ($p < 0.05$). The distribution of PAS scores was not significantly influenced by tumor location ($p = 0.29$) or treatment modality ($p = 0.26$). The most significant swallowing impairments were noted in hypopharyngeal tumors (PAS 6, range 3.2/7), followed by tumors in the oral cavity (median PAS 2.5, range 1/5.3), oropharynx (median PAS 2, range 1/4.5), and larynx (median PAS 1, range 1/2). Moreover, the type of therapy administered did not significantly affect penetration or aspiration rates ($p = 0.26$). However, a slight correlation was found with primary surgery showing a lower median PAS than definitive radio(chemo)therapy (median 2, range 1/4 vs. median 3, range 1/6), although this was not statistically significant.

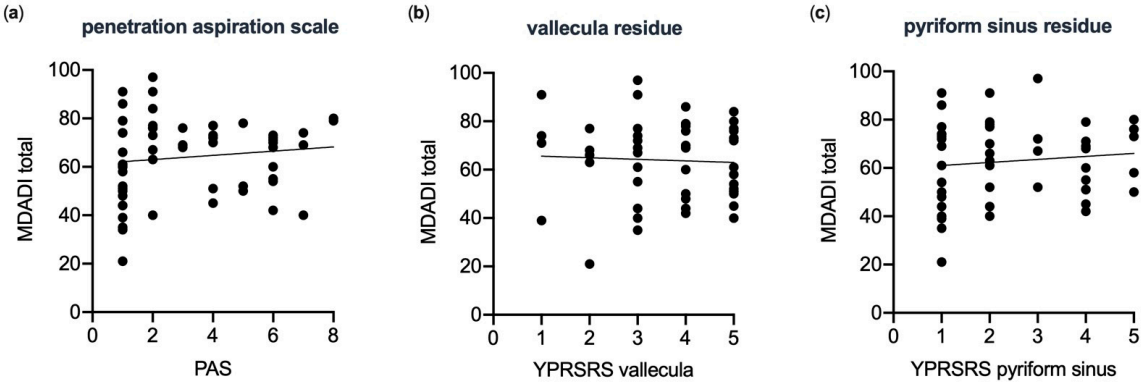

Figure 2. The correlation between the subjective swallowing-related quality of life (MDADI) and the objective fiber endoscopic evaluation of swallowing (FEES) is weak in head and neck cancer patients. No significant correlation was found between (**a**) MDADI and Rosenbek Penetration–Aspiration Scale (PAS) (n = 59, Spearman r = 0.17, p = 0.2); (**b**) MDADI and Yale Pharyngeal Residue Severity Rating Scale (YPRSRS) vallecula residues (n = 49, Spearman r = −0.035, p = 0.8); (**c**) MDADI and YPRSRS pyriform sinus residues (n = 48, Spearman r = 0.12, p = 0.44).

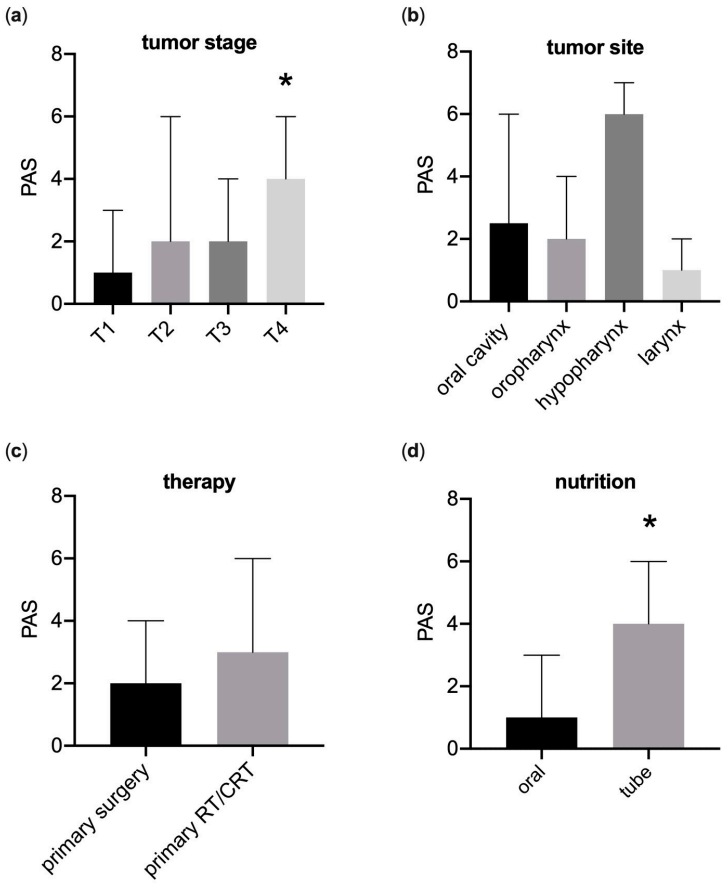

Figure 3. Fiberendoscopic swallow examination demonstrates a high specificity in identifying severely affected patients. (**a**) High Rosenbeks Penetration–Aspiration scale (PAS) scores were associated with advanced cancer T-stages (* p < 0.05 vs. T1). (**b**) PAS scores were comparable in patients after primary surgery and primary radiation (RT) or chemoradiation (CRT) (p = 0.15). (**c**) Impact of tumor location on penetration and aspiration scale (p = 0.10). (**d**) Association between feeding tube dependence on penetration and aspiration scale (* p < 0.05). n = 5–25. Median (95% CI); (**a**,**c**) Kruskal–Wallis test, Dunn's multiple comparisons; (**b**,**d**) Mann–Whitney-U test.

3.4. Completion Rates of Digital Questionnaires in Cancer Aftercare

Regarding adopting digital technology for completing the questionnaires, of the 204 patients who attempted, 79% (n = 161) did so independently, and 21% (n = 43) needed help. Among those who completed it independently, 88% (n = 143) answered all questions. The completion rate for digital questionnaires (88%) was similar to the completion rate for paper-based questionnaires (82%, n = 75), with no significant difference in completion rates (p = 0.25). The ability to use the tablet decreased with age, with a 91% proficiency rate (n = 11 out of 12) for those under 50 years, 83% (n = 35 out of 42) for those aged 50 to 59 years, 85% (n = 75 out of 88) for the 60 to 69 age group, 68% (n = 27 out of 40) for those aged 70 to 79 years, and 59% (n = 13 out of 22) for those over 80 years old, showing a significant correlation with age ($p < 0.05$, $R^2 = 0.076$).

4. Discussion

The present study investigated the correlation between subjective swallowing-related QoL and objective swallowing function in HNSCC. While the swallowing-related QoL correlated with the severity of the tumor disease, generic QoL remained unchanged in advanced disease. Notably, this study revealed an absence of correlation between objective swallowing measures (PAS; vallecula or piriform sinus residue) and patients' perception of their level of pathophysiology using questionnaires. Due to this absence of correlation, in studies and clinical practice, the swallowing function should be assessed objectively alongside the patients' subjective perception of swallowing.

In this context, generic QoL does not provide insight into the severity of head and neck cancer nor the functional success of the therapy. The generic QoL scores were relatively elevated across the entire group (0.88 ± 0.20). T1 glottic laryngeal carcinoma patients also demonstrated stable EQ-5D-5L values at 0.89 ± 0.19. Given the low disease burden and the effects of therapy, this group is not expected to experience a considerable impact on generic and, specifically, swallowing-related quality of life, thereby serving as a potential internal control group with similar socioeconomic status, age, and risk factors. The scores exceeded the German elderly population norms (0.84 ± 0.22) recently reported by Marten et al., indicating that the EQ-5D-5L questions are unsuitable for the head and neck cancer study cohort [39]. Additionally, no substantial disparities were detected among the different groups. For example, the QoL for T1 tumors was 0.87 ± 0.20, and for T4 tumors, it was 0.89 ± 0.13 (p = 0.95). Only tube feeding had such a negative impact on the QoL that it even reached significance in the generic quality of life assessment. This disparity highlights the complex nature of patients' experiences, where their perception of well-being may differ from measurable physiological indicators. It underscores the need to incorporate a more comprehensive and nuanced approach to evaluating treatment outcomes.

Swallowing-related QoL (such as MDADI) is better suited to assess the severity of tumor disease and therapy success. While generic QoL offers insights into overall well-being, swallowing-related QoL assessments provide a deeper understanding of the specific challenges faced by head and neck cancer patients, particularly about their ability to swallow and maintain proper nutrition. This specialized focus makes swallowing-related QoL a more appropriate and informative tool for assessing treatment success and tailoring interventions to improve patients' functional outcomes and, therefore, the overall QoL. In contrast to generic QoL, extensive tumors, feeding tube dependency, and a short time after therapy were significantly associated with low swallowing-related QoL. This correlation becomes particularly evident when examining tumor size in terms of T-Stage. Patients with T1 tumors, and especially those with glottic T1 tumors, exhibited significantly better quality of life (QoL) scores compared to those with advanced tumors. Specifically, patients with T1 tumors reported the highest swallowing-related QoL, as reflected in the MDADI total score of 81.03 ± 14.20. In contrast, QoL scores for T3 and T4 tumors were lower, at 71.86 ± 17.99 and 73.88 ± 14.94, respectively ($p < 0.05$). Notably, the highest scores were observed in T1 glottic laryngeal carcinomas, which averaged 83.82 ± 11.60. Overall, the values presented in the MDADI were relatively high compared to the head and neck cancer

patients validation cohort of the German MDADI (60.9 ± 25.7) [33]. The values, however, are only limitedly comparable as the validation study included only patients with oral cavity carcinoma, and these patients were significantly younger.

The therapy itself had a low impact on the swallowing-related QoL. In the oropharyngeal carcinoma group, <12 months after the treatment, a similar pattern emerged as in the Orator study, with higher swallowing-related QoL among primarily irradiated patients [11,12]. Beyond 12 months, the benefit diminished, with surgery patients experiencing better swallowing-related QoL. Thus, these data support the hypothesis that function and QoL are independent of the treatment decision, except when the therapy is transoral surgery only. This finding aligns with previous research reporting that surgery only in oropharyngeal cancer is beneficial and highlights the potential of reducing radiation doses in HNSCC [40–43]. However, it is important to consider that the stage of the tumor correlates with the escalation of therapy. Surgery-only is typically indicated for T1/T2 N0 stage tumors.

However, data regarding subjective swallowing function must be interpreted with caution; to gauge the extent of dysphagia, it is essential to measure objective parameters. For instance, the MDADI was similar for patients with and without aspiration (63.94 ± 12.86; 64.02 ± 17.33, $p = 0.20$). Thus, the MDADI may not reliably identify severely affected patients with a potentially dangerous swallowing disorder. An objective examination, such as FEES, was essential to identify patients with severe impairments, such as silent aspiration. This emphasizes the need for a more robust evaluation that considers objective indicators. Incorporating both patient-reported outcomes and objective parameters in dysphagia assessment allows for a more comprehensive and nuanced approach to understanding the condition. While self-assessment tools provide valuable insights into the patient's perspective, objective measures offer crucial clinical information that can guide treatment decisions, interventions, and rehabilitation strategies. This holistic approach enables patients to receive appropriate care that addresses both their individual experiences and the underlying physiological challenges they may be facing.

Several factors can diminish the validity of patient-reported outcome measures in HNSCC. Nerve injuries, tracheotomies, and radiotherapy can alter the subjective perception of dysphagia due to sensory loss [44]. This sensory loss can lead to a cessation of protective reflexes, thereby promoting silent aspirations. The incidence of silent aspirations is estimated to be 50–75% [44–47]. Additionally, QoL is a multifactorial construct: Swallowing-related QoL may be affected by dysphagia and other symptoms of oral dysfunction, such as dry mouth or loss of taste. Patients with oral cavity carcinoma and depression reported poor swallowing-related QoL in the MDADI [48]. Statements such as "I take longer to eat because of my swallowing problem" or "I feel like I have to swallow large amounts at once" can also be influenced by the presence of dry mouth. For patients, aspiration, penetration, or residue may be less restrictive to swallowing-related QoL than a disruption in the oral phase. This is supported by the finding that patients with oral cavity and oropharyngeal cancer, which frequently involve oral phase dysfunction, reported significantly worse swallowing-related QoL than patients with laryngeal or hypopharyngeal cancer [48]. In the present study, however, swallowing-related QoL was better in oral cavity cancer than in oro- and hypopharyngeal cancer. This discrepancy can be explained by the heterogeneity in the respective experimental groups, with more advanced hypopharyngeal than oral cavity cancer in this study (58% vs. 32%).

Previous research on the correlation between objective findings and QoL is highly controversial. In head and neck cancer patients, this limited correlation was observed when comparing multiple questionnaires alongside different accurate diagnostic methods in heterogeneous patient cohorts [18–29,49,50]. Standardized objective diagnostics, such as FEES [17,20–24] or VFSS [18,19,22,25–29], were commonly utilized, primarily focusing on measuring penetration and aspiration during swallowing. Among the questionnaires employed, the MD Anderson Dysphagia Inventory (MDADI) emerged as the most frequently used [17,19,20,22,23,26,27,34]. Further less often used questionnaires are Eating

Assessment Tool (Eat-10) [18], Head and Neck 35 (H&N35) [21,28], and study-specific questionnaires [24,29]. Florie et al. found a lack of correlation using the Dutch MDADI and FEES in a cross-sectional design. Pedersen et al. used a prospective design to confirm the weak correlation between MDADI and FEES. Despite the overall weak correlation between the MDADI scores and objective diagnostic results in severely affected patients, statistically significant and occasionally clinically relevant differences of 10 points were observed by other studies: A substantial study on mainly oropharyngeal squamous cell carcinoma (OPSCC) (HPV Status not given) by Hutcheson et al. found associations between dysphagia in VFSS and the MDADI. A difference of 10 points in the MDADI composite was considered clinically significant [34]. Wishart et al. revealed significant correlations between objective measurements of pharyngeal swallow physiology and swallowing-related QoL [27]. These findings suggest a more robust concordance between VFSS and MDADI, primarily during the first three months after (C)RT. Hedström (FEES) and Pauloski (VFSS) found similar moderate correlations using study-specific questionnaires. The patient cohort was primarily composed of HPV-positive cases (88%) [15,24]. Studies that have identified a correlation between objective and subjective results are mainly from the Anglo–American region and included a high proportion of OPSCC cases. Overall, up to 88% were HPV-associated. However, Kendall et al. found a remarkable lack of correlation in a similar group of OPSCC patients [26]. The current understanding of the agreement between clinician-rated and patient-reported measures of dysphagia in HNSCC is still limited. The inconsistencies in study findings are attributed to several factors: sample sizes, cross-sectional analyses used in most studies, and population variables, including the heterogeneity in HPV positivity, treatment modalities, the severity of presenting symptoms, and the timing of data collection post-treatment. The present study further enhances the evidence that subjective QoL is a poor indicator of swallowing function, especially in predominantly HPV-negative patient populations.

In the discourse surrounding the adequacy of collecting subjective parameters related to swallowing function, the current study's findings illustrate that disease-related QoL is considerably more appropriate than generic QoL. Nevertheless, this study further proves that disease-specific QoL, as observed in the ORATOR study, falls short of adequately assessing outcomes in everyday practice and clinical investigations.

The assessment of PROs in clinical studies and everyday practice should complement the objective measurement of swallowing function. Capturing disease-specific QoL is valid for eliciting the patient's perspective on the issue of functional impairment. However, a comprehensive evaluation of the therapeutic success and determining the need for intervention requires the inclusion of objective functional assessments. This approach is essential to detect dangerous complications, such as silent aspiration. FEES and VFSS are the established methods of choice for this purpose. However, both methods have the drawback of being time-consuming and resource-intensive, leading to their utilization in only 30% of studies focusing on swallowing function [13]. In the present study, FEES was chosen as the standard examination due to its ability to allow multiple assessments without radiation exposure and its direct visualization of laryngeal function, including aspiration and penetration. FEES facilitates the visualization of aspiration and allows for assessing airway protection mechanisms. However, its capabilities have significant limitations. The evaluation of the oral phase of swallowing is constrained. The visualization of the larynx during the pharyngeal phase is interrupted due to the transient 'white out' effect, which occurs when the soft palate elevates and pharyngeal constriction occurs. In instances of intradeglutitive aspiration, the quantity of aspirated material can only be estimated. Factors such as secretions and post-therapeutic alterations in anatomy can impair visibility. Additionally, FEES does not provide the ability to assess disturbances in the esophageal phase of swallowing.

Conversely, VFSS offers dynamic imaging that extends from the oral to the esophageal phases. This modality provides comprehensive insights into the movement of all pertinent structures and the bolus, including the precise quantification of aspirated material.

However, it has drawbacks; VFSS necessitates the use of radiation and contrast medium, which can alter the viscosity of the bolus. Moreover, research indicates that VFSS tends to systematically underrate the presence of residue and penetration/aspiration events.

Despite these drawbacks, VFSS is exceptionally suited for specific inquiries concerning swallowing functions. It is essential to recognize that FEES and VFSS are complementary diagnostic tools for a comprehensive evaluation of swallowing function.

Regarding skills in handling information technology, the patient cohort performed well. The acceptance and proficiency in managing tablet-based questionnaires were high within the HNSCC patient group. A total of 79% of the patients could independently complete the questionnaires, and the level of completeness was comparable with that of analog questionnaires. The ability to engage with digital questionnaires was significantly associated with age. The age group of 60 to 69 years, which also exhibited the highest incidence of HNSCC in this study and the general population, demonstrated an 85% capability in independently completing the digital questionnaire. The findings support the implementation of digital questionnaires with automated analysis, enabling the sustainable collection of PROs.

This study encompasses a heterogeneous cross-section of Central European head and neck cancer patients: This patient cohort comprised various age groups, tumors from diverse locations, and a broad post-treatment period. The patients differ significantly from previous studies due to a high proportion of cancer attributable to smoking and/or alcohol (-non-HPV) in advanced stages. This group of patients substantially diverges from the typical Anglo–American study subjects and necessitates supplementary evaluation. Therefore, the examined patients provide an overview of this often-underrepresented clientele. Notable parallels are evident with Dutch patients, where only a modest association between H&N35 and VFSS could be established [28]. However, an actual swallowing-related questionnaire was yet to be available in Dutch at the time of the study. Recently, the MDADI has established itself as the most widely used QoL questionnaire for head and neck tumor patients in clinical studies (ORATOR, E3311, Pathos, HN002) [12,30–32]. Hence, the examination of an evaluated and translated MDADI was imperative.

This study design is primarily suited to provide an overview of HNSCC patients. The heterogeneous etiology, varying treatments, and a limited number of patients with MDADI and FEES made sufficient stratification into etiological and treatment groups unfeasible. Moreover, each patient was assessed only at a single time point. Although this approach demonstrated minimal changes in functional impairment after one year, the repeated evaluation of the same patients, especially regarding MDADI, could have eliminated patient-specific variations. This limitation partly explains the detection of <10 points differences in MDADI, particularly given that MDADI was designed as a prospective study component [34]. Therefore, the transferability of these data to other patient groups and different diseases is limited due to the heterogeneity in the study participants and the design as a cross-sectional study (including lack of causality, time-dependent biases, and cohort effects).

A significant limitation of this study is its exclusive reliance on FEES. The predominance of previous research utilizing VFSS affects comparability due to its advanced capabilities in analyzing bolus movement and detailed structure assessment. However, FEES was selected for this study's swallowing assessments for its thorough anatomical evaluation of the pharynx and larynx. FEES is a recognized, safe (radiation-free), and commonly used diagnostic tool in the management and therapeutic planning of swallowing disorders [51]. It enables frequent re-evaluations with minimal patient risk, proving particularly beneficial for tailoring therapeutic interventions to meet oncological treatment patients' evolving needs and symptoms.

Despite these advantages, it's important to note that FEES may underrepresent challenges encountered during the oral swallowing phase, which can significantly impact the patient's quality of life. Therefore, a comprehensive clinical assessment of the oral phase remains essential to understand and address swallowing difficulties fully.

The study results have practical implications, indicating that an objective assessment is essential for each swallowing evaluation in clinical studies. We recommend FEES due to its repetitive applicability and ability to identify hazardous complications reliably. Through standardized execution, according to Langmore, the amount of residue and risk of penetration/aspiration can be examined for different consistencies [38].

To accommodate limited resources, an initial screening assessment can be carried out. The 100 mL swallowing test [52,53] and the Water Swallowing Test (WST) [54] exhibit high sensitivity and specificity in diagnosing dysphagia. In the presence of abnormal findings, an indication for further assessment using FEES or VFSS is warranted. However, the screening tests above possess limited predictive ability for detecting (silent) aspirations due to sensory impairments following treatment.

Silent aspiration is also a limitation for the revision of questionnaires to identify potentially dangerous complications. The commonly used swallowing-related QoL questionnaires include specific questions about aspiration. For instance, the MD Anderson Dysphagia Inventory (MDADI) asks, 'I cough when I try to drink liquids,' and the recently updated extensive EORTC QLQ–H&N43 includes questions such as 'Have you had problems with coughing?' and 'Have you had problems swallowing liquids?'. These questions could potentially be refined to more precisely inquire about dangerous complications such as aspiration, or they could be given greater weight in the analysis. However, this approach does not address the critical issue of silent aspiration. Questionnaires are limited in their length and cannot effectively capture complications that are not noticed by patients.

Further research should confirm the findings in a multicentric fashion on stratified patients (based on localization, therapy, and HPV status). Additionally, future investigations should employ a prospective design with different evaluation time points (e.g., pre-therapeutic, at 3-, 6-, and 12-months post-therapy) to account for the slight differences in MDADI scores and find specific functional problems during the post-therapy stages. Furthermore, research on MDADI should examine whether more minor differences than 10 points hold clinical significance.

5. Conclusions

This study's results indicate that patient-rated questionnaires, such as the MDADI, can provide valuable insights into assessing swallowing-related QoL among patients with Head and Neck Squamous Cell Carcinoma (HNSCC). However, these findings do not correspond with objective measures of swallowing function. Relying solely on PROs leads to omitting crucial aspects of swallowing function, which needs to be improved in clinical studies, registries, and everyday situations. This lack of correlation underscores the significance of adopting a comprehensive approach that considers both PROs and objective evaluations, such as FEES or VFSS.

Author Contributions: Conceptualization, D.S. and J.E.; methodology, D.S. and W.G.; formal analysis, D.S., J.E. and W.G.; investigation, J.E., L.E. and W.G.; data curation, J.E., L.E. and W.G.; writing—original draft preparation, D.S.; writing—review and editing, J.E., S.P.S., R.M., W.G. and F.K.; visualization, J.E. and D.S.; supervision, S.P.S. and R.M. All authors have read and agreed to the published version of the manuscript.

Funding: This research received no external funding.

Institutional Review Board Statement: The study was conducted in accordance with the Declaration of Helsinki, and approved by the Ethics Committee of the Rostock University Medical Center (protocol code A2021-0024, approved 11 February 2021).

Informed Consent Statement: Informed consent was obtained from all subjects involved in the study.

Data Availability Statement: The data presented in this study are available on request from the corresponding author.

Conflicts of Interest: The authors declare no conflict of interest.

References

1. Malone, E.; Siu, L.L. Precision Medicine in Head and Neck Cancer: Myth or Reality? *Clin. Med. Insights Oncol.* **2018**, *12*, 1179554918779581. [CrossRef] [PubMed]
2. Guo, T.; Califano, J.A. Molecular Biology and Immunology of Head and Neck Cancer. *Surg. Oncol. Clin. N. Am.* **2015**, *24*, 397–407. [CrossRef] [PubMed]
3. Specenier, P.; Vermorken, J.B. Optimizing Treatments for Recurrent or Metastatic Head and Neck Squamous Cell Carcinoma. *Expert Rev. Anticancer Ther.* **2018**, *18*, 901–915. [CrossRef] [PubMed]
4. Billard-Sandu, C.; Tao, Y.G.; Sablin, M.P.; Dumitrescu, G.; Billard, D.; Deutsch, E. CDK4/6 Inhibitors in P16/HPV16-Negative Squamous Cell Carcinoma of the Head and Neck. *Eur. Arch. Otorhinolaryngol.* **2020**, *277*, 1273–1280. [CrossRef]
5. Ordoñez, R.; Otero, A.; Jerez, I.; Medina, J.A.; Lupiañez-Pérez, Y.; Gomez-Millan, J. Role of Radiotherapy in the Treatment of Metastatic Head and Neck Cancer. *OncoTargets Ther.* **2019**, *12*, 677–683. [CrossRef] [PubMed]
6. Hutcheson, K.A.; Nurgalieva, Z.; Zhao, H.; Gunn, G.B.; Giordano, S.H.; Bhayani, M.K.; Lewin, J.S.; Lewis, C.M. Two-Year Prevalence of Dysphagia and Related Outcomes in Head and Neck Cancer Survivors: An Updated SEER-Medicare Analysis. *Head Neck* **2019**, *41*, 479–487. [CrossRef]
7. Eisbruch, A. Dysphagia and Aspiration Following Chemo-Irradiation of Head and Neck Cancer: Major Obstacles to Intensification of Therapy. *Ann. Oncol.* **2004**, *15*, 363–364. [CrossRef]
8. Nguyen, N.P.; Frank, C.; Moltz, C.C.; Vos, P.; Smith, H.J.; Bhamidipati, P.V.; Karlsson, U.; Nguyen, P.D.; Alfieri, A.; Nguyen, L.M.; et al. Aspiration Rate Following Chemoradiation for Head and Neck Cancer: An Underreported Occurrence. *Radiother. Oncol.* **2006**, *80*, 302–306. [CrossRef]
9. Nguyen, N.P.; Moltz, C.C.; Frank, C.; Vos, P.; Smith, H.J.; Karlsson, U.; Dutta, S.; Midyett, F.A.; Barloon, J.; Sallah, S. Dysphagia Following Chemoradiation for Locally Advanced Head and Neck Cancer. *Ann. Oncol.* **2004**, *15*, 383–388. [CrossRef]
10. Abdelhafiz, N.; Mahmoud, D.; Gad, M.; Essa, H.; Morsy, A. Effect of Definitive Hypo-Fractionated Radiotherapy Concurrent with Weekly Cisplatin in Locally Advanced Squamous Cell Carcinoma of the Head and Neck. *J. Med. Life* **2023**, *16*, 743–750. [CrossRef]
11. Nichols, A.C.; Theurer, J.; Prisman, E.; Read, N.; Berthelet, E.; Tran, E.; Fung, K.; de Almeida, J.R.; Bayley, A.; Goldstein, D.P.; et al. Randomized Trial of Radiotherapy Versus Transoral Robotic Surgery for Oropharyngeal Squamous Cell Carcinoma: Long-Term Results of the ORATOR Trial. *J. Clin. Oncol.* **2022**, *40*, 866–875. [CrossRef] [PubMed]
12. Nichols, A.C.; Theurer, J.; Prisman, E.; Read, N.; Berthelet, E.; Tran, E.; Fung, K.; de Almeida, J.R.; Bayley, A.; Goldstein, D.P.; et al. Radiotherapy versus Transoral Robotic Surgery and Neck Dissection for Oropharyngeal Squamous Cell Carcinoma (ORATOR): An Open-Label, Phase 2, Randomised Trial. *Lancet Oncol.* **2019**, *20*, 1349–1359. [CrossRef]
13. Li, P.; Constantinescu, G.C.; Nguyen, N.T.A.; Jeffery, C.C. Trends in Reporting of Swallowing Outcomes in Oropharyngeal Cancer Studies: A Systematic Review. *Dysphagia* **2020**, *35*, 18–23. [CrossRef] [PubMed]
14. Campbell, B.H.; Spinelli, K.; Marbella, A.M.; Myers, K.B.; Kuhn, J.C.; Layde, P.M. Aspiration, Weight Loss, and Quality of Life in Head and Neck Cancer Survivors. *Arch. Otolaryngol. Head Neck Surg.* **2004**, *130*, 1100. [CrossRef] [PubMed]
15. Pauloski, B.R.; Rademaker, A.W.; Logemann, J.A.; Lazarus, C.L.; Newman, L.; Hamner, A.; MacCracken, E.; Gaziano, J.; Stachowiak, L. Swallow Function and Perception of Dysphagia in Patients with Head and Neck Cancer. *Head Neck* **2002**, *24*, 555–565. [CrossRef] [PubMed]
16. Agarwal, J.; Palwe, V.; Dutta, D.; Gupta, T.; Laskar, S.G.; Budrukkar, A.; Murthy, V.; Chaturvedi, P.; Pai, P.; Chaukar, D.; et al. Objective Assessment of Swallowing Function After Definitive Concurrent (Chemo)Radiotherapy in Patients with Head and Neck Cancer. *Dysphagia* **2011**, *26*, 399–406. [CrossRef] [PubMed]
17. Florie, M.; Pilz, W.; Kremer, B.; Verhees, F.; Waltman, G.; Winkens, B.; Winter, N.; Baijens, L. EAT-10 Scores and Fiberoptic Endoscopic Evaluation of Swallowing in Head and Neck Cancer Patients. *Laryngoscope* **2021**, *131*, E45–E51. [CrossRef] [PubMed]
18. Arrese, L.C.; Carrau, R.; Plowman, E.K. Relationship Between the Eating Assessment Tool-10 and Objective Clinical Ratings of Swallowing Function in Individuals with Head and Neck Cancer. *Dysphagia* **2017**, *32*, 83–89. [CrossRef]
19. Gillespie, M.B.; Brodsky, M.B.; Day, T.A.; Lee, F.-S.; Martin-Harris, B. Swallowing-Related Quality of Life After Head and Neck Cancer Treatment. *Laryngoscope* **2004**, *114*, 1362–1367. [CrossRef]
20. Pedersen, A.; Wilson, J.; McColl, E.; Carding, P.; Patterson, J. Swallowing Outcome Measures in Head and Neck Cancer—How Do They Compare? *Oral Oncol.* **2016**, *52*, 104–108. [CrossRef]
21. Jensen, K.; Lambertsen, K.; Torkov, P.; Dahl, M.; Bonde Jensen, A.; Grau, C. Patient Assessed Symptoms Are Poor Predictors of Objective Findings. Results from a Cross Sectional Study in Patients Treated with Radiotherapy for Pharyngeal Cancer. *Acta Oncol.* **2007**, *46*, 1159–1168. [CrossRef] [PubMed]
22. Kirsh, E.; Naunheim, M.; Holman, A.; Kammer, R.; Varvares, M.; Goldsmith, T. Patient-reported versus Physiologic Swallowing Outcomes in Patients with Head and Neck Cancer after Chemoradiation. *Laryngoscope* **2019**, *129*, 2059–2064. [CrossRef]
23. da Silva, G.M.; Portas, J.; López, R.V.M.; Côrrea, D.F.; Arantes, L.M.R.B.; Carvalho, A.L. Study of Dysphagia in Patients with Advanced Oropharyngeal Cancer Subjected to an Organ Preservation Protocol Based on Concomitant Radiotherapy and Chemotherapy. *Asian Pac. J. Cancer Prev.* **2019**, *20*, 977–982. [CrossRef] [PubMed]
24. Hedström, J.; Tuomi, L.; Finizia, C.; Olsson, C. Correlations Between Patient-Reported Dysphagia Screening and Penetration–Aspiration Scores in Head and Neck Cancer Patients Post-Oncological Treatment. *Dysphagia* **2018**, *33*, 206–215. [CrossRef]

25. Liou, H.-H.; Tsai, S.-W.; Hsieh, M.H.-C.; Chen, Y.-J.; Hsiao, J.-R.; Huang, C.-C.; Ou, C.-Y.; Chang, C.-C.; Lee, W.-T.; Tsai, S.-T.; et al. Evaluation of Objective and Subjective Swallowing Outcomes in Patients with Dysphagia Treated for Head and Neck Cancer. *J. Clin. Med.* **2022**, *11*, 692. [CrossRef]
26. Kendall, K.A.; Kosek, S.R.; Tanner, K. Quality-of-life Scores Compared to Objective Measures of Swallowing after Oropharyngeal Chemoradiation. *Laryngoscope* **2014**, *124*, 682–687. [CrossRef] [PubMed]
27. Wishart, L.R.; Harris, G.B.; Cassim, N.; Alimin, S.; Liao, T.; Brown, B.; Ward, E.C.; Nund, R.L. Association Between Objective Ratings of Swallowing and Dysphagia-Specific Quality of Life in Patients Receiving (Chemo)Radiotherapy for Oropharyngeal Cancer. *Dysphagia* **2022**, *37*, 1014–1021. [CrossRef] [PubMed]
28. van der Molen, L.; van Rossum, M.A.; Ackerstaff, A.H.; Smeele, L.E.; Rasch, C.R.; Hilgers, F.J. Pretreatment Organ Function in Patients with Advanced Head and Neck Cancer: Clinical Outcome Measures and Patients' Views. *BMC Ear Nose Throat Disord.* **2009**, *9*, 10. [CrossRef]
29. Rogus-Pulia, N.M.; Pierce, M.C.; Mittal, B.B.; Zecker, S.G.; Logemann, J.A. Changes in Swallowing Physiology and Patient Perception of Swallowing Function Following Chemoradiation for Head and Neck Cancer. *Dysphagia* **2014**, *29*, 223–233. [CrossRef]
30. Ferris, R.L.; Flamand, Y.; Weinstein, G.S.; Li, S.; Quon, H.; Mehra, R.; Garcia, J.J.; Chung, C.H.; Gillison, M.L.; Duvvuri, U.; et al. Phase II Randomized Trial of Transoral Surgery and Low-Dose Intensity Modulated Radiation Therapy in Resectable P16+ Locally Advanced Oropharynx Cancer: An ECOG-ACRIN Cancer Research Group Trial (E3311). *J. Clin. Oncol.* **2022**, *40*, 138–149. [CrossRef]
31. Owadally, W.; Hurt, C.; Timmins, H.; Parsons, E.; Townsend, S.; Patterson, J.; Hutcheson, K.; Powell, N.; Beasley, M.; Palaniappan, N.; et al. PATHOS: A Phase II/III Trial of Risk-Stratified, Reduced Intensity Adjuvant Treatment in Patients Undergoing Transoral Surgery for Human Papillomavirus (HPV) Positive Oropharyngeal Cancer. *BMC Cancer* **2015**, *15*, 602. [CrossRef] [PubMed]
32. Yom, S.S.; Torres-Saavedra, P.; Caudell, J.J.; Waldron, J.N.; Gillison, M.L.; Xia, P.; Truong, M.T.; Kong, C.; Jordan, R.; Subramaniam, R.M.; et al. Reduced-Dose Radiation Therapy for HPV-Associated Oropharyngeal Carcinoma (NRG Oncology HN002). *J. Clin. Oncol.* **2021**, *39*, 956–965. [CrossRef] [PubMed]
33. Bauer, F.; Seiss, M.; Gräßel, E.; Stelzle, F.; Klotz, M.; Rosanowski, F. Schluckbezogene Lebensqualität Bei Mundhöhlenkarzinomen: Anderson-Dysphagia-Inventory, Deutsche Version. *HNO* **2010**, *58*, 692–697. [CrossRef] [PubMed]
34. Hutcheson, K.A.; Barrow, M.P.; Lisec, A.; Barringer, D.A.; Gries, K.; Lewin, J.S. What Is a Clinically Relevant Difference in MDADI Scores between Groups of Head and Neck Cancer Patients? *Laryngoscope* **2016**, *126*, 1108–1113. [CrossRef] [PubMed]
35. Rosenbek, J.C.; Robbins, J.A.; Roecker, E.B.; Coyle, J.L.; Wood, J.L. A Penetration-Aspiration Scale. *Dysphagia* **1996**, *11*, 93–98. [CrossRef] [PubMed]
36. Hey, C.; Pluschinski, P.; Zaretsky, Y.; Almahameed, A.; Hirth, D.; Vaerst, B.; Wagenblast, J.; Stöver, T. Penetration-Aspiration Scale According to Rosenbek: Validation of the German Version for Endoscopic Dysphagia Diagnostics. *HNO* **2014**, *62*, 276–281. [CrossRef]
37. Neubauer, P.D.; Rademaker, A.W.; Leder, S.B. The Yale Pharyngeal Residue Severity Rating Scale: An Anatomically Defined and Image-Based Tool. *Dysphagia* **2015**, *30*, 521–528. [CrossRef]
38. Langmore, S.E.; Kenneth, S.M.A.; Olsen, N. Fiberoptic Endoscopic Examination of Swallowing Safety: A New Procedure. *Dysphagia* **1988**, *2*, 216–219. [CrossRef]
39. Marten, O.; Greiner, W. EQ-5D-5L Reference Values for the German General Elderly Population. *Health Qual. Life Outcomes* **2021**, *19*, 76. [CrossRef]
40. Amit, M.; Hutcheson, K.; Zaveri, J.; Lewin, J.; Kupferman, M.E.; Hessel, A.C.; Goepfert, R.P.; Brandon Gunn, G.; Garden, A.S.; Ferraratto, R.; et al. Patient-Reported Outcomes of Symptom Burden in Patients Receiving Surgical or Nonsurgical Treatment for Low-Intermediate Risk Oropharyngeal Squamous Cell Carcinoma: A Comparative Analysis of a Prospective Registry. *Oral Oncol.* **2019**, *91*, 13–20. [CrossRef]
41. Barbon, C.E.A.; Yao, C.M.K.L.; Alvarez, C.P.; Goepfert, R.P.; Fuller, C.D.; Lai, S.Y.; Gross, N.D.; Hutcheson, K.A. Dysphagia Profiles after Primary Transoral Robotic Surgery or Radiation for Oropharyngeal Cancer: A Registry Analysis. *Head Neck* **2021**, *43*, 2883–2895. [CrossRef] [PubMed]
42. Dohopolski, M.J.; Diao, K.; Hutcheson, K.A.; Akhave, N.S.; Goepfert, R.P.; He, W.; Lei, X.J.; Peterson, S.K.; Shen, Y.; Sumer, B.D.; et al. Long-Term Patient-Reported Outcomes in a Population-Based Cohort Following Radiotherapy vs Surgery for Oropharyngeal Cancer. *JAMA Otolaryngol. Head Neck Surg.* **2023**, *149*. [CrossRef] [PubMed]
43. Choby, G.W.; Kim, J.; Ling, D.C.; Abberbock, S.; Mandal, R.; Kim, S.; Ferris, R.L.; Duvvuri, U. Transoral Robotic Surgery Alone for Oropharyngeal Cancer: Quality-of-Life Outcomes. *JAMA Otolaryngol. Head Neck Surg.* **2015**, *141*, 499–504. [CrossRef] [PubMed]
44. Strojan, P.; Hutcheson, K.A.; Eisbruch, A.; Beitler, J.J.; Langendijk, J.A.; Lee, A.W.M.; Corry, J.; Mendenhall, W.M.; Smee, R.; Rinaldo, A.; et al. Treatment of Late Sequelae after Radiotherapy for Head and Neck Cancer. *Cancer Treat. Rev.* **2017**, *59*, 79. [CrossRef] [PubMed]
45. Feng, F.Y.; Kim, H.M.; Lyden, T.H.; Haxer, M.J.; Worden, F.P.; Feng, M.; Moyer, J.S.; Prince, M.E.; Carey, T.E.; Wolf, G.T.; et al. Intensity-Modulated Chemoradiotherapy Aiming to Reduce Dysphagia in Patients With Oropharyngeal Cancer: Clinical and Functional Results. *J. Clin. Oncol.* **2010**, *28*, 2732. [CrossRef] [PubMed]
46. Jagtap, M.; Karnad, M. Swallowing Skills and Aspiration Risk Following Treatment of Head and Neck Cancers. *Indian J. Surg. Oncol.* **2019**, *10*, 402. [CrossRef]

47. Langerman, A.; MacCracken, E.; Kasza, K.; Haraf, D.J.; Vokes, E.E.; Stenson, K.M. Aspiration in Chemoradiated Patients with Head and Neck Cancer. *Arch. Otolaryngol. Head Neck Surg.* **2007**, *133*, 1289–1295. [CrossRef]
48. Chen, S.C.; Huang, B.S.; Hung, T.M.; Chang, Y.L.; Lin, C.Y.; Chung, C.Y.; Wu, S.C. Swallowing Ability and Its Impact on Dysphagia-Specific Health-Related QOL in Oral Cavity Cancer Patients Post-Treatment. *Eur. J. Oncol. Nurs.* **2018**, *36*, 89–94. [CrossRef]
49. Weymuller, E.A.; Yueh, B.; Deleyiannis, F.W.B.; Kuntz, A.L.; Alsarraf, R.; Coltrera, M.D. Quality of Life in Patients With Head and Neck Cancer. *Arch. Otolaryngol. Head Neck Surg.* **2000**, *126*, 329. [CrossRef]
50. Morton, R.P. Studies in the Quality of Life of Head and Neck Cancer Patients: Results of a Two-Year Longitudinal Study and a Comparative Cross-Sectional Cross-Cultural Survey. *Laryngoscope* **2003**, *113*, 1091–1103. [CrossRef]
51. Lehner, U.; Zaretsky, E.; Goeze, A.; Wermter, L.; Stuck, B.A.; Birk, R.; Neff, A.; Fischer, I.; Ghanaati, S.; Sader, R.; et al. Prätherapeutische Dysphagie Bei Kopf-Hals-Tumor-Patienten. *HNO* **2022**, *70*, 533. [CrossRef] [PubMed]
52. Patterson, J.M.; Hildreth, A.; McColl, E.; Carding, P.N.; Hamilton, D.; Wilson, J.A. The Clinical Application of the 100 ML Water Swallow Test in Head and Neck Cancer. *Oral Oncol.* **2011**, *47*, 180–184. [CrossRef] [PubMed]
53. Watson, L.J.; Woodman, S.H.; Ganderton, D.; Hutcheson, K.A.; Pringle, S.; Patterson, J.M. Development of the Remote 100 Ml Water Swallow Test versus Clinical Assessment in Patients with Head and Neck Cancer: Do They Agree? *Head Neck* **2022**, *44*, 2769–2778. [CrossRef] [PubMed]
54. Hey, C.; Goeze, A.; Sader, R.; Zaretsky, E. FraMaDySc: Dysphagia Screening for Patients after Surgery for Head and Neck Cancer. *Eur. Arch. Oto-Rhino-Laryngol.* **2023**, *280*, 2585. [CrossRef]

CDDpress

www.nature.com/cddiscovery

ARTICLE OPEN

Check for updates

Establishing safe high hydrostatic pressure devitalization thresholds for autologous head and neck cancer vaccination and reconstruction

Claudia Maletzki[1,9], Vivica Freiin Grote[2,9], Friederike Kalle[3], Thoralf Kleitke[3], Annette Zimpfer[4], Anne-Sophie Becker[4], Wendy Bergmann-Ewert[5], Anika Jonitz-Heincke[2], Rainer Bader[2], Brigitte Vollmar[6], Stephan Hackenberg[7], Agmal Scherzad[8], Robert Mlynski[3] and Daniel Strüder[3]✉

High hydrostatic pressure specifically devitalizes cells and tissues without major changes in their molecular structure. Hence, high hydrostatic pressure may enhance the development of whole-cell anti-tumor vaccines, representing tumor heterogeneity and thus (neo-) antigen diversity. Moreover, safe devitalization of tumor-infiltrated supporting tissue may facilitate reimplantation for functional reconstruction. However, precise high hydrostatic pressure thresholds for safe cancer cell killing are unknown. Here, we show that high hydrostatic pressure of at least 315 MPa is necessary to safely devitalize head and neck squamous cell cancer. A pressure of 210 MPa, which has been used frequently in cancer vaccine preparation, resulted in partial devitalization with 27% live cells in flow cytometry and 4% remaining autofluorescence in cell culture after one week. The remaining cells could form vital tumors in the chorioallantoic membrane assay. In contrast, 315 MPa killed all cells in vitro and prevented tumor outgrowth in ovo. The effectiveness of 315 MPa was attributed to the induction of DNA double-strand breaks, independent of apoptosis, autophagy, or methuosis. Furthermore, 315 MPa continued to induce immunogenic cell death. Our results demonstrate that 315 MPa of high hydrostatic pressure induces safe and sustained devitalization of head and neck cancer cells and tissues. Because of the heterogeneity in pressure resistance, we propose our approach as a starting point for determining the precise thresholds for other cancer entities. Further studies on head and neck cancer should focus on immunological co-cultures, combinations of immune checkpoint inhibition, and accurate anatomical reconstruction with pressure-treated autografts.

Cell Death Discovery (2023)9:390 ; https://doi.org/10.1038/s41420-023-01671-z

INTRODUCTION

High hydrostatic pressure (HHP) enables complete devitalization of complex tissues of any origin without major changes in structure and biomechanics [1–9]. On the one hand, HHP triggers specific cell death by altering the plasma membrane and the tertiary/quaternary protein structure [1, 2]. In contrast, HHP preserves the biomechanics of the extracellular matrix and tumor neoantigens [2–9]. In addition, HHP treatment is cost-effective and avoids toxic substances [4]. Another advantage is the high standardization according to Pascal's law: pressure acts isostatically and immediately at any cell within complex tissues [10]. Therefore, dose gradients and build-up effects were not observed in this study [4]. At the same time, HHP acts rapidly and can be applied to tissues ex situ during surgery.

Two significant complications in head and neck squamous cell cancer (HNSCC) are loss of function due to tissue defects and recurrence, with a low response to secondary treatment options, including immunotherapy. Therefore, head and neck surgeons can use HHP to kill all tumor cells while preserving a biomechanically stable extracellular matrix for reimplantation. In addition, the natural extracellular matrix and preserved cytokines can induce tissue-specific remodeling, proliferation, and migration into bone, cartilage, and skin. Hence, HHP may be highly beneficial for anatomical and functional reconstruction of head and neck defects [11–19].

The second application of HHP could be autologous anticancer vaccination for re-activating antigen-specific immune responses. HHP constitutes an excellent alternative to devitalization methods, such as radiotherapy, freeze-drying, and solvents [8, 20]. Indeed, dendritic cells loaded with HHP-treated tumor cells elicited specific anti-tumor immune responses in co-culture with immune cells [20–24]. Furthermore, the injection of HHP-treated melanoma

[1]Department of Internal Medicine, Medical Clinic III - Hematology, Oncology, Palliative Medicine, Rostock University Medical Center, Rostock, Germany. [2]Research Laboratory for Biomechanics and Implant Technology, Department of Orthopedics, Rostock University Medical Centre, Rostock, Germany. [3]Department of Otorhinolaryngology, Head and Neck Surgery "Otto Körner", Rostock University Medical Center, Rostock, Germany. [4]Institute of Pathology, Rostock University Medical Center, Rostock, Germany. [5]Core Facility for Cell Sorting and Cell Analysis, University Medical Center Rostock, Rostock, Germany. [6]Institute for Experimental Surgery, Rostock University Medical Center, Rostock, Germany. [7]Department of Otorhinolaryngology-Head and Neck Surgery, RWTH Aachen University Hospital, Aachen, Germany. [8]Department of Oto-Rhino-Laryngology, Plastic, Aesthetic and Reconstructive Head and Neck Surgery, University of Wuerzburg, Wuerzburg, Germany. [9]These authors contributed equally: Claudia Maletzki, Vivica Freiin Grote. ✉email: Daniel.strueder@med.uni-rostock.de

Received: 6 March 2023 Revised: 13 September 2023 Accepted: 3 October 2023
Published online: 23 October 2023

Table 1. Cancer devitalization using high hydrostatic pressure.

Authors	Pressure amplitude [MPa]	Complete devitalization [MPa]	Time [min]	Cancer	Remaining viable cells
Rückert et al. [25]	200	N/A	5	Melanoma, mammary	N/A
Seitz et al. [10]	100–500	300	10–15	Melanoma, colon	None
Urbanova et al. [20]	150–350	200	10–15	Prostate, ovary, lung	None
Hradilova et al. [22]	250	250	10	Lung	N/A
Mikyskova et al. [21]	200	N/A	10	Lung, prostate	<10%
Chen et al. [26]	0.01–0.1	N/A	>60	Urothelial	75×10^4
Fucikova et al. [23]	150–350	250	10	Leukemia, ovary prostate	N/A
Weiss et al. [4]	100–500	300	5	Melanoma, colon, lymphoma	"Few viable cells"'
Schauwecker et al. [27]	150–300	300	10	Chondrosarcoma, ostesarcoma	None
Eisenthal et al. [7]	60–120	N/A	15	Melanoma	N/A

cells into mice inhibited tumor growth when combined with irradiation [9, 10, 25]. Hence, HHP is promising for anatomical reconstruction using tumor-infiltrated tissue autografts and immunotherapy for restoring immunosurveillance.

A precondition for the clinical application of HHP-treated tumor cells is safe devitalization. The threshold for the complete devitalization of various cancer entities has been reported to be 250–210 MPa [4–10, 17, 20, 21, 23, 26–32]. However, most studies do not specify a threshold, leaving great uncertainty about the amplitude required to yield complete devitalization (Table 1). Owing to their immunological focus, most previous studies recommend 200 and 210 MPa to achieve an optimal balance between devitalization and preservation of the tumor-specific immune response [9, 20, 21]. However, the use of low pressure carries the risk of transplanting the remaining vital cells. Such residual cells pose a high risk of tumor recurrence; indeed, viable cells have remained in some studies. Therefore, to minimize the risk of vital tumor cell transplantation, it is necessary to define safe devitalization thresholds for each tumor entity.

In this study, a safe threshold for the devitalization of HNSCC was determined to enable the future application of HHP treatment in clinical trials. Commercial and patient-derived cell lines were treated at pressures between 105–420 MPa for 10–60 min. The percentage of dead cells and markers of processes involved in cell death were analyzed in vitro. In addition, engraftment was analyzed using the chorioallantoic membrane (CAM) in ovo model. Compared to previous research, a significantly higher threshold of 315 MPa was identified for safe devitalization. The application of this HHP amplitude is a precondition for the use of HHP in further studies on reconstruction and autologous anti-tumor vaccination.

RESULTS

HHP treatment with 210 and 315 MPa devitalized established (UT-SCC-14) and patient-derived cell lines (HNSCC16 and HNSCC46) in the crystal violet assay

Both cell growth (Supplementary Fig. 1) and viability (Fig. 1A) were moderately reduced following exposure to 105 MPa for 10 min; however, the cells recovered completely over time. Quantification of the viable biomass showed a reduction with 105 MPa treatment compared to 0 MPa (100%) for all three cell lines: UT-SCC-14 82 ± 8%, HNSCC16 64 ± 18%, and HNSCC46 73 ± 5%; $P < 0.05$, 105 MPa vs. 0 MPa (Fig. 1A). The absorption of viable biomass after 210 MPa was 2 ± 4% (UT-SCC-14), 1 ± 2% (HNSCC16), and 1 ± 2% (HNSCC46); $P < 0.05$, 210 MPa vs. 0 and 105 MPa. Even after the application of 315 MPa HHP, viable biomass was detected with absorptions of 2 ± 3% (UT-SCC-14), 1 ± 1% (HNSCC16), and 1 ± 1% (HNSCC46); $P < 0.05$, 315 MPa vs. 0 and 105 MPa (Fig. 1A).

Flow cytometric apoptosis/necrosis analysis revealed complete devitalization for HHP treatment with 315 MPa, but not for 210 MPa

HHP treatment at 105 MPa had no persistent impact on viability, as compared to the 0 MPa control (87.1 ± 5.0%), and a similar percentage of vital cells (87.7 ± 5.5%) was detected after 105 MPa (Fig. 1B). In addition, no induction of apoptosis or necrosis was observed (0 MPa: early apoptosis 2.6 ± 2.1%, late apoptosis 7.5 ± 3.5%, necrosis 2.8 ± 1.5%; 105 MPa: early apoptosis 3.3 ± 2.1%, late apoptosis 6.9 ± 3.4%, necrosis 2.1 ± 1.3%). In contrast, 210 MPa induced significant apoptotic cell death, but 26.9 ± 10.4% of the cells remained viable (210 MPa: early apoptosis 12.2 ± 12.4%, late apoptosis 44.1 ± 11.7%, necrosis 16.7 ± 11.0%; $P < 0.05$, 210 MPa vs. 0 and 105 MPa). HNSCC cell treatment at 315 MPa resulted in complete devitalization. As a result of the pressure exposure, only 0.6 ± 0.5% of treated cancer cells were identified as viable ($P < 0.05$, 315 MPa vs. 0, 105, and 210 MPa). Furthermore, 12.2 ± 12.4% of the treated cells were early apoptotic ($P < 0.05$, 315 MPa vs. 210 MPa), while a late apoptotic phenotype was characterized for 44.0 ± 11.7% of the treated cells ($P < 0.05$, 315 MPa vs. 0, 105 and 210 MPa), and 16.7 ± 11.0% were necrotic ($P < 0.05$, 315 MPa vs. 0 and 105 MPa). The significance of the remaining viable cells was examined in further experiments using autofluorescent cells.

315 MPa HHP was the threshold for complete suppression of NIR680 autofluorescence in transfected PE/CA/PJ-15

After treatment with 105 MPa for 10 min, colony formation was delayed (Fig. 2A), and relative viability decreased moderately to 85.9 ± 1.2% at 120 h post-treatment (compared to 100% fluorescence following 0 MPa, Fig. 2B). As most cells remained viable, continued proliferation led to 108.9 ± 21.9% viability at 168 h (Fig. 2B). A more extended HHP treatment significantly enhanced cell death: In cells treated with 105 MPa for 60 min, viability decreased to 12.1 ± 0.8% at 120 h ($P < 0.05$, 105 MPa, 60 min vs. 105 MPa, 10 min). However, at 168 h, cells recovered to 48.3 ± 30.2%

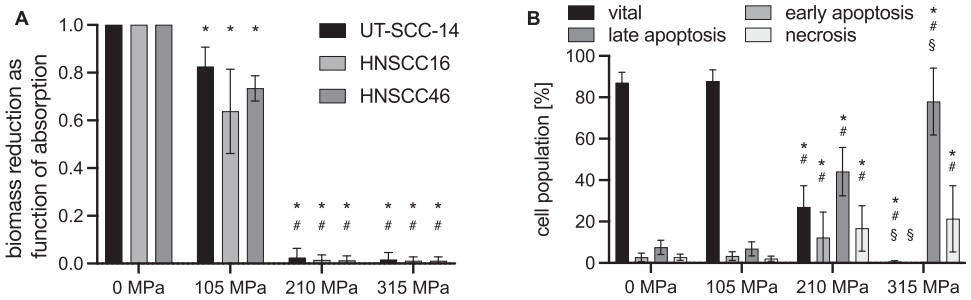

Fig. 1 High hydrostatic pressure (HHP) leads to the devitalization of head and neck cancer cells (HNSCC). A Biomass reduction as function of relative crystal violet absorption measurement 72 h after treatment. HHP caused dose-dependent cell death in UT-SCC-14 and HNSCC16/46. At 105 MPa, relative absorption reduced by 18–27%. Cytotoxicity increased at 210 MPa and 315 MPa with a maximum absorption for UT-SCC-14: 2.4 ± 4% (210 MPa) and 1.6 ± 3% (315 MPa). Results shown as means and standard deviations; $n = 5$. Statistical analysis: two-way ANOVA, Tukey's multiple comparison post hoc test; $^{*}P < 0.05$, vs. 0 MPa (UT-SCC-14/HNSCC16/46); $^{\#}P < 0.05$, vs. 105 MPa. **B** Cell death analysis using Yo-Pro 1 iodide/propidium iodide (Yo-Pro 1/PI) flow cytometry 24 h after treatment with UT-SCC-14. HHP at 105 MPa had no effect on vital, apoptotic, and necrotic cell populations. At 210 MPa, the number of apoptotic and necrotic cells increased significantly, but 27 ± 10% remained viable. At 315 MPa, viable cells reduced to 0.6 ± 0.5%. Values are given as means and standard deviations; $n = 18$; two-way ANOVA, Tukey's multiple comparison post hoc test; $^{*}P < 0.05$, vs. 0 MPa; $^{\#}P < 0.05$, vs. 105 MPa; $^{\S}P < 0.05'$ vs. 210 MPa.

viability ($P < 0.05$, 105 MPa, 60 min *vs.* 105 MPa, 10 min). Cytotoxicity of 210 MPa for 10 min (20.3 ± 0.3%) was slightly lower than 105 MPa for 60 min at 120 h (12.1 ± 0.8%). However, cells treated at 210 MPa did not recover over time, and viability further decreased to 8.3 ± 10.9% at 168 h ($P < 0.05$, 210 MPa, 10 min *vs.* 105 MPa, 10 min). Pressures of 315 and 420 MPa for 10 min led to a depression of autofluorescence, indicating extensive cell death. Viability decreased to 1.1 ± 1.6% following 315 MPa treatment ($P < 0.05$, 315 MPa, 10 min vs. 105 MPa, 10 min) and further decreased after 420 MPa (0.9 ± 1.3%; $P < 0.05$, 420 MPa, 10 min vs. 105 MPa, 10 min) at 120 h. Notably, no recovery was seen, and viability remained low even after 168 h of re-culture (315 MPa: 0.4 ± 1.1%, 420 MPa: 1.6 ± 3.8%; $P < 0.05$, 315/420 MPa, 10 min vs. 105 MPa, 10 min). In conclusion, at least 315 MPa was necessary for all-out HNSCC cell death in vitro.

Devitalization by HHP was more effective than high irradiation doses (75 and 150 Gy) and ethanol treatment

To compare the devitalization efficiency of HHP, irradiation as a clinically established method and 70% ice-cold ethanol, which is recommended for cell killing in live/dead assays, were used as cell death controls. NIR-680 fluorescence of PE/CA-PJ15 cells was moderately reduced at 120 h after irradiation with 75 Gy (85.4 ± 6.6%) and following treatment with 150 Gy (70.6 ± 15.3%; $P < 0.05$, 75/150 Gy vs. 210, 315, 420 MPa and 105 MPa, 60 min) (Fig. 2B). At 168 h, the cells were viable, but did not proliferate. Consequently, compared to the untreated control, fluorescence decreased to 61.1 ± 44.4% after exposure to 75 Gy and 59.9 ± 39.3% after irradiation with 150 Gy ($P > 0.05$, 75/150 Gy, 168 h vs. 75/150 Gy, 120 h). At 120 h, ethanol treatment (12.6 ± 6.5%) was more effective than irradiation and as effective as 210 MPa ($P > 0.05$). However, the remaining cells continued to grow after ethanol treatment, and viability increased to 49.1 ± 36.3% at 168 h.

210 MPa HHP was insufficient to prevent tumor growth in the CAM assay

To verify whether HHP-treated HNSCC cells are capable of proliferating and forming tumors in ovo, CAM assays were performed. Macroscopic and histological examination revealed that untreated HNSCC cells were able to proliferate and form tumors in ovo, while cells treated with 315 MPa showed no growth (Fig. 3A). The tumor engraftment rates of stable NIR-expressing PE/CA-PJ15 cells detected by fluorescence imaging were high at 0 MPa and 105 MPa (Fig. 3B). 0 MPa treatment led to 17 tumor engraftments out of 21 implantations. Fluorescence counts were 722 cts/s median, 25%/75%-percentile: 58/1283 cts/s. 105 MPa treatment led to 10 tumor engraftments out of 19 implantations (554 cts/s median, 25%/75%–percentile: 0/1933 cts/s). After 210 MPa treatment, moderate tumor growth was observed, and the engraftment was 7 tumor engraftments out of 19 implantations with a low fluorescence median of 0 cts/s (25%/75%-percentile: 0/470 cts/s). However, some tumors were viable with high fluorescence of 1334, 1654, and 1666 cts/s ($P > 0.05$, 210 MPa vs. 0 MPa, and 105 MPa, respectively). Finally, 315 MPa prevented tumor engraftment (0 tumor engraftments out of 19 implantations, 0 cts/s median, 25%/75%-percentile: 0/0 cts/s; $P < 0.05$, 315 MPa vs. 0 MPa and 105 MPa). One CAM exhibited a minimal fluorescence of 9 cts/s at 315 MPa. H&E histology revealed an empty Matrigel matrix without viable tumor cells (Supplementary Fig. 2). HHP at 315 MPa led to comprehensive cell death and prevented in ovo tumor growth, whereas HHP up to 210 MPa was not safe for HNSCC devitalization. There were no differences in susceptibility to pressure between the cell lines.

HHP treatment with 315 MPa was associated with DNA double-strand breaks and induction of immunogenic cell death

A comprehensive cell death panel confirmed the decreased viability and proliferation of UT-SCC-14, HNSCC16, and HNSCC46 after HHP treatment at 210 MPa and 315 MPa ($P < 0.05$, 315 MPa vs. 0 MPa) (Fig. 4A, B). Hallmarks of immunogenic cell death, such as calreticulin translocation and adenosine triphosphate (ATP) release, remained high with increased pressure amplitudes (Fig. 4C, D). Notably, calreticulin showed a pressure amplitude-dependent increase (Fig. 4C). HHP exposure had no effect on programmed death-ligand 1 (PD-L1) abundance, which remained high in all treatments ($P > 0.05$) (Fig. 4E). A significant difference between 210 and 315 MPa was found in phosphorylated histone variant H2A.X (pH2A.X) positive cells (for HNSCC16/46: $P < 0.05$, 315 MPa vs. 0 and 210 MPa), indicating DNA double-strand breaks (Fig. 4F). Considering the results of UT-SCC-14 cells, pH2A.X was detected in 2.9 ± 1.4% of the 0 MPa control cells. pH2A.X positive cells increased to 5.0 ± 0.7% after 210 MPa ($P < 0.05$, 210 MPa vs. 0 MPa). Moreover, 315 MPa HHP led to a significant increase: 25.5 ± 10.0% ($P < 0.05$, 315 MPa vs. 210 MPa). Pressure-related changes in pH2A.X were consistent in all cell lines (UT-SCC-14, HNSCC16, and HNSCC46).

In addition, BCL2-independent and PARP-dependent apoptosis was observed after 210 MPa, but no apoptotic cells (cleaved PARP/Apotracker Green positive) were observed after 315 MPa HHP (Fig. 4G, H). Autophagy levels were not increased by HHP ($P > 0.05$),

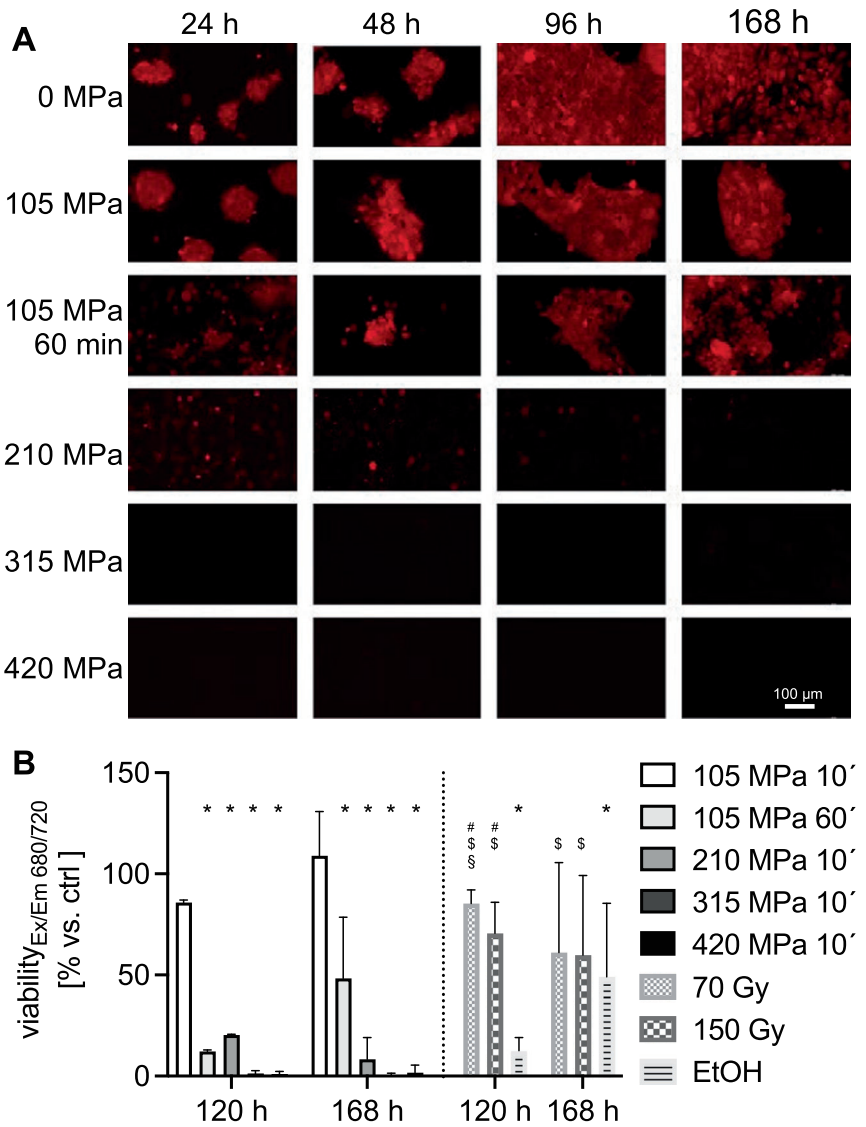

Fig. 2 At least 315 MPa of hydrostatic pressure (HHP) is needed for the complete devitalization of PE/CA/PJ-15-NIR-680 autofluorescent head and neck cancer (HNSCC) cells. A Colony formation of autofluorescent HNSCC cells after HHP treatment ($n = 3$): 105 MPa treatment for 10 and 60 min delayed but did not stop colony formation. 210 MPa showed no colony formation but fluorescent cells remained for 168 h. No fluorescence occurred after 315 and 420 MPa treatment. **B** Viability measured through NIR-680 fluorescence after HHP, irradiation, and ethanol (EtOH) treatment. Relative fluorescence shown compared to 0 MPa at 120 and 168 h. Values are given as means and standard deviations; $n = 3$; two-way ANOVA, Tukey's multiple comparison post hoc test; $^{*}P < 0.05$, vs. 105 MPa 10 min; $^{\#}P < 0.05$, vs. 105 MPa 60 min; $^{\$}P < 0.05$, vs. 210 MPa 10 min; $^{\$}P < 0.05$, vs. 315/420 MPa 10 min.

but LAMP-1/Rab7a expression as a methuosis marker was elevated at 210 MPa and 315 MPa (Fig. 4I, J). Compared to treatment with 315 MPa, 350 MPa caused significantly higher LAMP-1/Rab7a expression ($P < 0.05$) (Fig. 4J). Cell cycle analysis showed viable or proliferating cells in the G1 phase (red) and S/G2/M phases (green) 24 h after exposure to 0 and 210 MPa (Fig. 5). However, viability decreased and no proliferating cells were observed after 48 h. At 315 MPa, no cells in the S/G2/M phase were observed at 24 and 48 h.

315 MPa HHP devitalized human HNSCC tissue from surgical resections

To verify whether HHP treatment can devitalize cells in the tissue association, fragments of tumor resections were investigated. The patient characteristics were as follows: An 88-year-old female with pT4a pN0 cM0 HPV^{-} laryngeal squamous cell cancer (A, D, G & J), a 59-year-old male with pT3 pN0 cM0 HPV^{+} laryngeal squamous cell cancer (B, E, H & K), and a 55-year-old male with pT3 pN0 cM0 HPV^{-} oropharyngeal squamous cell cancer (C, F, I & L). Figure 6 displays the live/dead staining and light microscopic images. Neither viable cancer cells nor viable fibroblasts were observed at 72 and 168 h, respectively. The devitalization of complex HNSCC tissues confirmed the transferability of the results at the individual cell level.

DISCUSSION

Devitalization is a crucial step for autologous reconstruction with tumor-infiltrated tissue and whole-tumor cell vaccination. Devitalization must be safe, induce immunogenic cell death, and comply with the legal requirements [10]. The present study aimed to establish a safe threshold for HHP treatment in HNSCC devitalization. The underlying mechanisms and immunogenic cell death were investigated using four HNSCC cell lines.

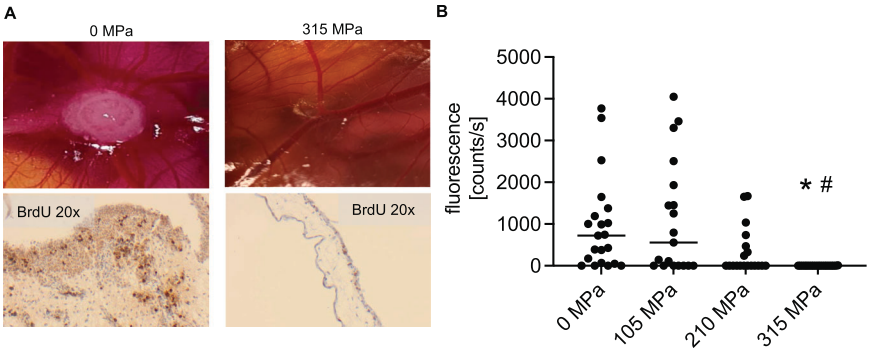

Fig. 3 315 MPa high hydrostatic pressure (HHP) treatment prevents tumor growth on the chicken chorioallantoic membrane (CAM). **A** UT-SCC-14, HNSCC16, and HNSCC46 cells were treated with 0, 105, 210, and 315 MPa ($n = 9$–21). In all, 1×10^6 cells in Matrigel were seeded on the CAM surface on embryonic development day 7. Tumors were harvested on day 14 (after 7 days of tumor growth and 1 day after topical bromodeoxyuridine (BrdU) application) for histological assessment. No tumor growth was observed after 315 MPa treatment. Representative images of HNSCC16 are shown. **B** NIR-680 fluorescence of PE/CA-PJ15 after CAM implantation at day 14 (after 7 days of tumor growth). Cancer cells could form fluorescent tumors in vivo after 105 MPa and 210 MPa treatment. Neither fluorescence nor tumor growth was observed following 315 MPa HHP. Individual values (photon counts per second (cts/s)) are plotted with median of 25% percentile/75% percentile; $n = 19$ for 105, 210, and 315 MPa; $n = 21$ for 0 MPa). Kruskal–Wallis test, Dunn's multiple comparisons; $^{*}P < 0.05$, 315 MPa vs. 0 MPa; $^{\#}P < 0.05$, 315 MPa vs. 105 MPa.

The scale and type of cell death were dependent on HHP amplitude. The cells recovered and continued proliferating at 105 MPa for 10 min and 60 min, respectively. The 60-min treatment was significantly more effective than the 10-min treatment. Reversible cell death after pressures ≤105 MPa is in line with previous research showing decent changes in membrane and protein structure [1]. In our study, high-pressure amplitudes (rather than treatment duration) were critical for irreversible devitalization; at higher pressures of 210 MPa for 10 min, the cells did not recover, and viability decreased substantially. Increasing pressure initially triggered apoptosis and, to an ascending extent, late apoptosis and necrosis. Flow cytometry confirmed a significant decrease in viable tumor cells after HHP treatment at 210 MPa; however, some cells remained alive. A minimum pressure of 315 MPa was required for sufficient cell death. In contrast to the autofluorescence measurements and flow cytometry, standard assays, such as colony formation and crystal violet staining, showed no viable cells after 210 and 315 MPa. Given that even small numbers of viable cancer cells can cause recurrence, a combination of different methods is crucial to allow reliable conclusions on the efficacy of HHP devitalization. Using a CAM assay, HNSCC cells were found to form solid tumors in ovo following treatment with 210 MPa. In contrast, no growth was observed at 315 MPa pressure.

Still, in vitro assays identified vital cell remnants. These cell remnants were reduced 10–20 times compared to those at 210 MPa. However, the importance of the few surviving cells required further investigations when evaluating oncological safety: Accompanying cell cycle analysis after HHP treatment at 210 MPa identified cells in the S/G2/M phase at 24 h. These proliferating cells could cause tumor growth under favorable in vivo conditions, such as microenvironmental niches. No S/G2/M phase labeling was observed at 315 MPa. Based on the decrease in apoptosis and methuosis at increasing pressures, it can be assumed that 315 MPa immediately causes severe cell damage. No form of programmed cell death or resilience was observed. Mechanistically, the failure to recover from 315 MPa is supported by profound DNA damage. pH2A.X DNA double-strand breaks increased significantly after 210 MPa HHP, whereas DNA damage remained low. This finding contrasts with previous studies on non-malignant cells in which DNA was reported to be the most resistant to HHP [1, 33]. DNA damage occurred only at higher pressures of >1000 MPa, whereas membrane and protein damage were critical for cell killing at pressures >200 MPa [1]. Impaired DNA repair in cancer cells could explain distinct intrinsic pressure resistance.

The effects of HHP were highly reproducible. Cell death and underlying mechanisms were consistent in commercial cell lines, patient-derived cell lines, and primary tumor tissue from surgical resections. According to Pascal's law, the same pressure is applied at each location in an enclosed space. There are no dose gradients during HHP treatment. Each cell in suspension or tissue is exposed to a precise amplitude for a similar time. These properties lead to complete devitalization. In contrast, alternative methods, such as 75 and 150 Gy irradiation, only reduced viability, but half of the cells remained viable after irradiation. The effectiveness of HHP was also confirmed in comparison with ethanol treatment (which is recommended as a dead control in live/dead assays); ethanol was initially toxic, but the surviving cells continued to proliferate. In contrast, virtually all HHP-treated cells were devitalized.

Finally, a proof-of-concept approach was developed for complex tissues obtained from patients with HNSCC after surgery. Cell culture results were confirmed for all tumor specimens. HHP-treated HNSCC (including cartilage infiltration) did not contain any vital cells after 315 MPa in short-term culture. The devitalization and reimplantation of non-malignant complex tissues have already been tested. Subcutaneous implantation of melanocytic nevi after HHP treatment at 200 MPa resulted in fading of the nevi in a mouse model [16, 34]. Subsequently, a clinical trial was initiated to reconstruct the donor site using HHP-treated autologous nevi [18]. In orthopedics, Schauwecker et al. showed that no cells grew out of the resected tumor-infiltrated bone after 210 MPa [27, 31]. However, devitalization was only confirmed by light microscopy. Based on the present results, the threshold of 210 MPa for complete devitalization should be revised in vitro and in vivo prior to clinical application.

Most oncology studies on HHP have focused on immune activation and whole-cell vaccination using distinct HHP-treated cancer cells [4–10, 20, 21, 23, 26, 27, 29, 31]. The research groups of Adkins et al. [8, 20, 22] and Gaipl et al. [2, 4, 6, 9, 10] contributed significantly to progress in this field. However, the methodology was limited in the examination of oncological safety. In vitro methods, such as clonogenic assays, WST-8, Annexin-V/PI flow cytometry, and basic histology, were used to establish 200–210 MPa as the threshold for cellular devitalization [4, 6, 8–10, 20, 21, 23]. This threshold was supported by only one in vivo study with three mice, confirming the absence of tumor outgrowth at 200 MPa [10]. Thus, relatively low thresholds

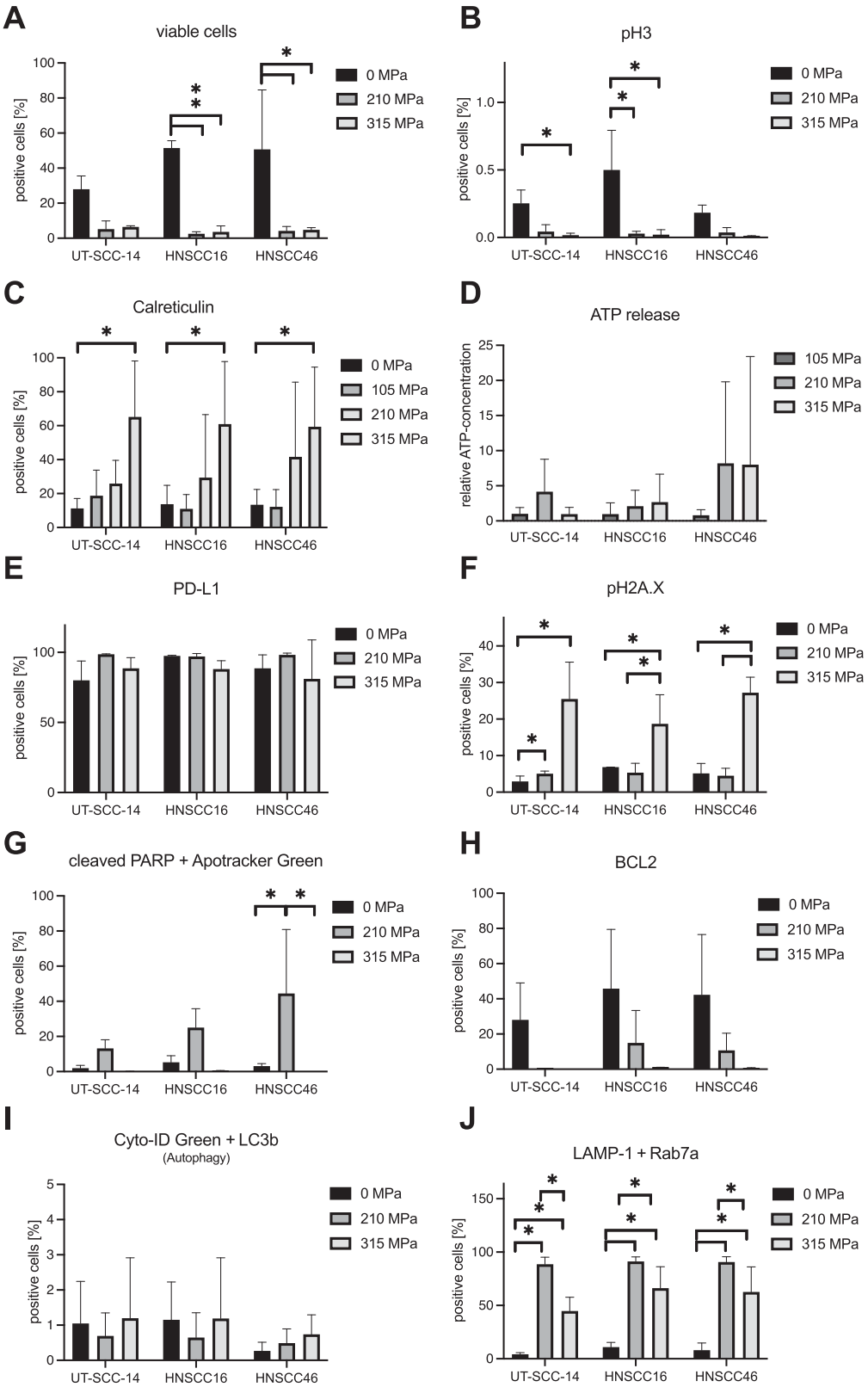

of 300 MPa maximum were defined for devitalization and preservation of immunogenicity [20]. This is in line with the findings of the clonogenic assays, Zombie staining, and crystal violet quantification. However, the critical pressure for safe devitalization was increased to 315 MPa using more sensitive assays.

Although pressure effects were highly reproducible in the four HNSCC cell lines, the pressure resistance of previously used cancer cell lines was heterogeneous. Weiss et al. reported complete devitalization of mammary adenocarcinoma (MCF7) and melanoma (B16-F10) cells by 210 MPa, whereas colon carcinoma (CT26) cells remained viable even after 500 MPa [9]. In vivo, 200 MPa was

Fig. 4 Increasing high hydrostatic pressure (HHP) induces immunogenic cell death and DNA damage in spectral multicolor flow cytometry. HHP-induced cell death was confirmed by Zombie NIR™ ($n = 3$) (**A**) and inhibited cell proliferation using phosphor-histone H3 (pH3) ($n = 3$) (**B**). Immunogenic cell death was determined by an increase in calreticulin translocation ($n = 5$) (**C**) and adenosine triphosphate (ATP) release ($n = 7$) (**D**). Programmed death-ligand 1 (PD-L1) expression remained high in all groups ($n = 3$) (**E**). **F** DNA double-strand breaks, indicated by phosphorylated histone variant H2A.X (pH2A.X), were significantly increased after 315 MPa treatment ($n = 3$). Apoptosis marker cleaved poly (ADP-ribose) polymerase (PARP) was increased after 210 MPa (**G**), while anti-apoptotic marker B-cell lymphoma 2 (BCL2) decreased (**H**). After 315 MPa, all cells were negative for cleaved PARP and BCL2 ($n = 3$) (**G**, **H**). Cyto-ID autophagy detection did not show HHP-related autophagy ($n = 3$) (**I**). Methuosis markers lysosomal-associated membrane protein 1 (LAMP-1) and Ras-related protein Rab7a (Rab7a) increased following HHP treatment. Methuosis markers were higher following 210 MPa than 315 MPa ($n = 3$) (**J**). Values are given as means and standard deviations, two-way ANOVA, Tukey's multiple comparison post hoc test; *$P < 0.05$.

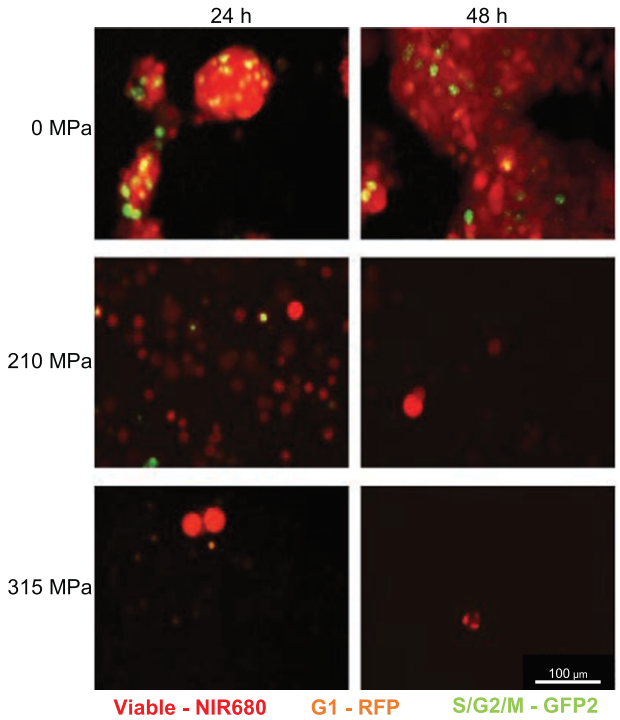

Fig. 5 Cell cycle analysis confirmed viable cells in the S/G2/M phase following 210 MPa high hydrostatic pressure compared to 315 MPa. NIR-680 autofluorescent cells were tagged with RFP in the G1 phase and GFP2 in the S/G2/M phase. Following 210 MPa and 315 MPa treatment, viability (red) decreased over time. After 315 MPa treatment, no proliferating cells (green) were observed.

reported to be safe, and no tumor growth was observed in mice. Urbanova et al. also found that only 0.8% of viable lung cancer cells (H522 and A549) remained after 250 MPa treatment [20]. Because the release of immunogenic cytokines was higher at 200 MPa than at 250 MPa, the authors proposed lower pressures for further experiments. Given the heterogeneity of cell lines and methods, no reliable thresholds have been established to date. Nevertheless, treatment at 200–210 MPa is frequently recommended for vaccination in preclinical [4, 8–10, 20, 21, 23] and clinical trials (*NCT03657966, NCT02470468, NCT02111577*). In this study, HNSCC was more resistant to HHP, and safe devitalization was observed only at pressures above 315 MPa.

Antigen loss was previously described to be dependent on cell origin and was particularly pronounced in lung cancer but low in prostate and ovarian cancer cells [20]. Other studies have reported that the shape was maintained and immunity was preserved at pressures up to 400 MPa [2]. Although the present study focused on oncological safety, it was found that 315 MPa could still trigger immunogenic cell death. Calreticulin translocation, which is essential for phagocytosis by dendritic cells, increased in a pressure-dependent manner, with a maximum at 315 MPa. ATP release, another hallmark of immunogenic cell death, was highly variable, but increased with pressure. In addition, PD-L1 abundance remained high.

Therapeutic application of whole-tumor cells passing through immunogenic cell death leads to immune activation and exposure to a variety of tumor-specific (neo-)antigens. Especially in tumors with a high mutational burden, such as HNSCC, relevant antigens do not need to be prospectively identified. HHP-treated tumor cells can be applied directly or used to load dendritic cells [4, 20]. With direct subcutaneous administration in mice, colon (CT26) and lung (LL2) cancer cells were able to elicit $CD4^+$ and $CD8^+$ T cell-dependent protective immunity [35]. In other tumor entities, co-treatment is necessary to bypass immune evasion. Concurrent radiotherapy, anti-CTLA4/PD1 immunotherapy, and immunoadjuvants showed promising additive effects in vivo [25]. Dendritic cells loaded with HHP tumor cells secrete proinflammatory cytokines and stimulate IFN-γ-producing tumor antigen-specific $CD4^+$ and $CD8^+$ T cells in non-small cell lung cancer [22].

The second indication for HHP is autologous reconstruction in oncological head and neck surgery. Invasive tumors of the auricle, nose, and larynx lead to defects in cartilaginous support due to infiltration and resection margins [36–39]. Only a few experimental studies have been conducted on autologous laryngeal reconstruction [40–42]. However, the complex requirements of form, function, and immunosuppression (in oncologic patients) forestall allogeneic or xenogeneic cartilage transplantation in humans. Therefore, autologous laryngeal reconstruction is an attractive option with a defined clinical need, success in a structurally related organ (trachea), and no need for immediate perfusion [14, 43]. For this purpose, HHP treatment could guarantee the devitalization of all tumor cells without permanently damaging the cartilage matrix.

This study comprehensively investigated cell death in HNSCC; however, no other tumor entities have been studied. Previous research has shown a heterogeneous response between tumor entities. Owing to this possible heterogeneity in intrinsic pressure resistance, devitalization thresholds should be determined separately for each tumor entity before clinical application. While previous studies have focused on the immunogenicity of HHP-treated tumors, this study addressed safety. Methodologically, our immunological studies only provided indications of persistent immunogenic cell death at pressures above 315 MPa. Follow-up studies are needed to investigate cytokine secretion and T-cell activation in co-culture experiments. Another limitation of this study is the lack of an in vivo study using a small animal model. The CAM assay is well suited to test tumor viability by fluorescence measurement and histology, with a low experimental animal burden and high growth rates. However, chicken is evolutionarily distant from mammals; moreover, the tumor grows on an extracorporeal membrane. Therefore, invasively growing (cartilage infiltrating) tumors should be generated, HHP-treated, and reimplanted in rodents before clinical application.

Conclusion

High hydrostatic pressure is suitable for the safe devitalization of head and neck cancer. Compared with previous studies on other entities using up to 210 MPa, higher hydrostatic pressures of more than 315 MPa are required to devitalize head and neck cancer safely. A significant difference between 210 and 315 MPa was

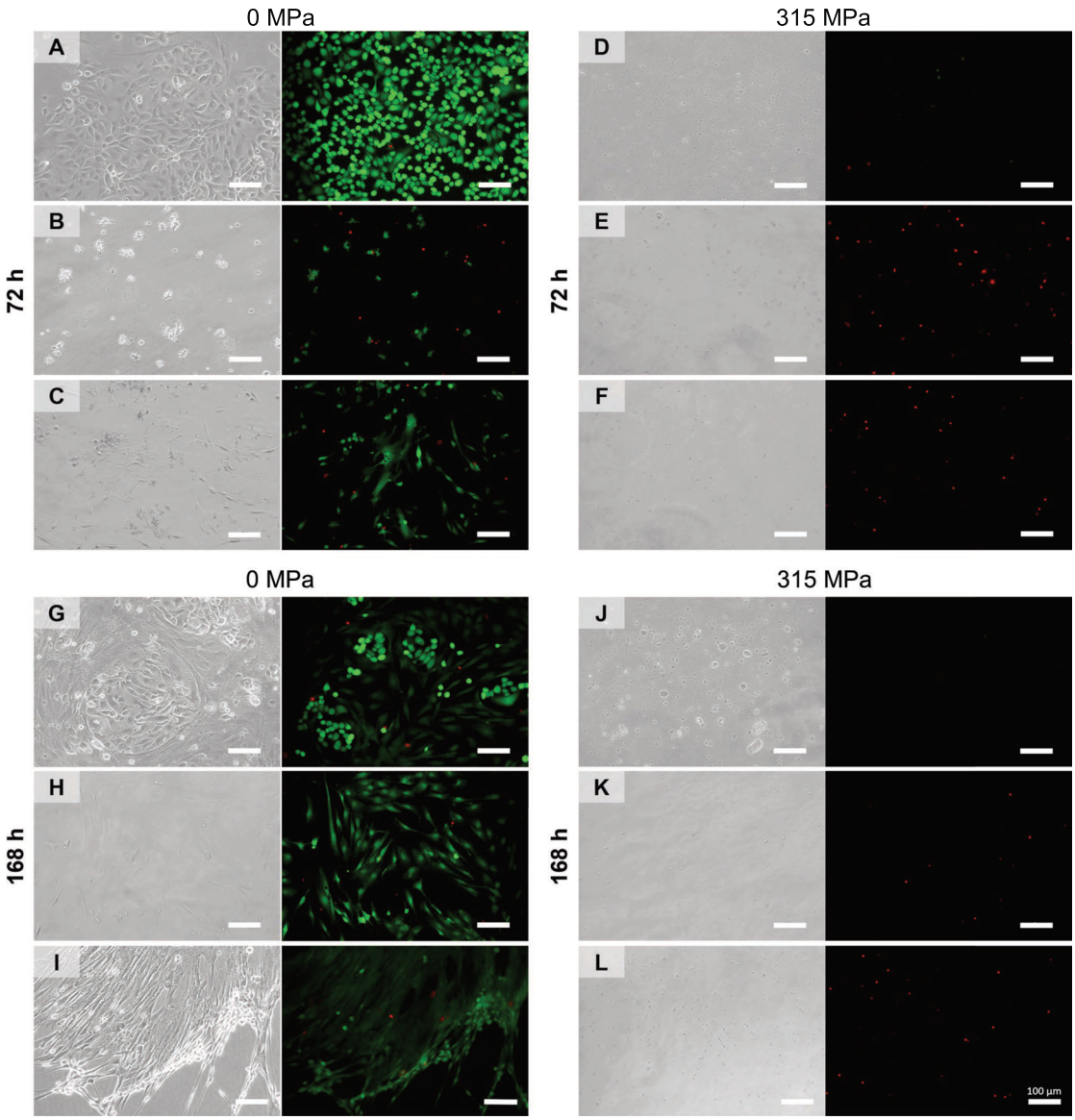

Fig. 6 Tissue devitalization by high hydrostatic pressure (HHP). Patient-derived HNSCC tissue culture following high hydrostatic pressure treatment. Fresh Tumor samples obtained from three different patients ($n = 3$) were used to analyze tissue devitalization by HHP treatment: 88-year old female, pT4a pN0 cM0 HPV- laryngeal squamous cell cancer (**A**, **D**, **G**, **J**), 59-year old male, pT3 cN0 cM0 HPV+ laryngeal squamous cell cancer (**B**, **E**, **H**, **K**) and 55-year old male pT3 pN0 cM0 HPV- oropharyngeal squamous cell cancer (**C**, **F**, **I**, **L**). All tissue fragments were treated with either 0 MPa (**A**–**C**, **G**-**I**) or 315 MPa (**D**–**F**, **J**–**L**) for 10 min, followed by enzymatic tissue dissociation and cultivation of isolated cells. After 72 h (**A**–**F**) and 168 h (**G**–**L**), tissue devitalization was analyzed by light microscopy and live/dead staining. As a result of the treatment with 315 MPa HHP, no living cells were identified. Bar: 100 µm.

observed in the induction of DNA double-strand breaks. In addition, immunogenic cell death accelerated with increasing pressure amplitude. These results demonstrate that HHP is a safe and reliable technology to complement autologous head and neck reconstruction and whole-cell anti-tumor immunotherapy for high mutational burden cancer.

MATERIALS AND METHODS

The full methods are described in the supplemental material (see Supplemental Methods) and are summarized herein.

Cell lines

HNSCC cells from the tongue (UT-SCC-14, PE/CA-PJ15), larynx (PDX-derived HNSCC16) [44], and hypopharynx (PDX-derived HNSCC46) [44] were used. The PE/CA-PJ15 cells were transduced to stably express iRFP680. All the cell lines were HPV-negative.

High hydrostatic pressure treatment

Cells were suspended in the culture medium and added to cryotubes for HHP treatment. Cryotubes were filled with medium, closed without air bubbles, sealed with Parafilm, and placed in water-filled centrifuge tubes. The samples were treated for 10 or 60 min at high hydrostatic pressures (Dustec Hochdrucktechnik GmbH, Germany) of 0, 105, 210, 315, or 420 MPa. The temperature was maintained at 20 °C. Cell pellets were resuspended after treatment.

Crystal violet assay for determination of cell viability

UT-SCC-14 and PDX-derived cell lines ($n = 5$) were incubated after HHP treatment and stained with 0.2% crystal violet for 10 min. The stained cells were washed with PBS, 1% SDS was added, and incubated for

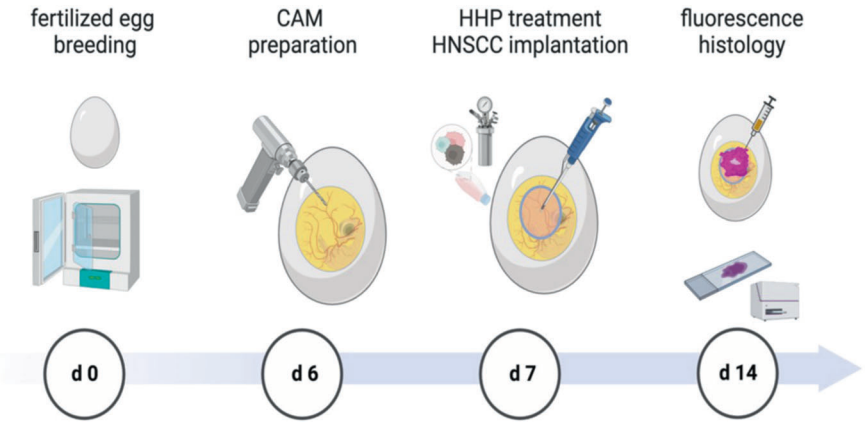

Fig. 7 Chorioallantoic membrane (CAM) assay experimental design. Breeding of the fertilized eggs with automatic rotation started from embryonic development day zero (d 0). Eggs were opened and the CAM was prepared at day 6. On day 7, 1×10^6 cells of the respective head and neck squamous cell carcinoma (HNSCC) cell line were treated with 0, 105, 210, and 315 MPa high hydrostatic pressure (HHP) at 20 °C for 10 min. Following 7 days of incubation and tumor growth, euthanasia and harvesting of the CAM were performed. Near-infrared (NIR) fluorescence was measured, and the CAM tissue was prepared for histology.

10 min. Absorbance was measured at 560 nm using a spectrophotometer after 72 h.

Apoptosis/necrosis and calreticulin flow cytometry

Apoptosis/necrosis was assessed 24 h after HHP treatment using a flow cytometer. UT-SCC-14 cells ($n = 15$) were stained with Yo-Pro 1 iodide (Yo-Pro 1) and propidium iodide (PI). For calreticulin (CalR) analysis, UT-SCC-14, HNSCC16 and HNSCC46 cells ($n = 5$) were incubated with primary antibody, labeled with FITC-conjugated secondary antibody, and analyzed by subtracting the secondary antibody-positive cells from CalR+ and secondary antibody-positive cells.

Autofluorescence measurement

The autofluorescence of PE/CA-PJ15-NIR-680 cells was measured after HHP, irradiation, or ethanol treatment using a fluorescence multi-well plate reader (Tecan Infinite® M200, Germany) at 680 nm excitation and 720 nm emission wavelengths. The fluorescence intensities were calculated by setting the untreated cells at 100%. Data from at least three independent experiments performed in duplicate are presented.

Spectral flow cytometry

This study utilized spectral flow cytometry with two custom-designed multicolor panels for functional analysis of non-transduced HNSCC cells ($n = 3$). Panel 1 was used to investigate apoptosis, necrosis, proliferation, and autophagy, while panel 2 was used to examine viability, methuosis, and immune regulation. To perform the analysis, 0.5×10^6 cells were taken per panel and processed using staining buffer (PBS, 2 mM EDTA, 2% BSA).

In Panel 1, extracellular staining was conducted using Apotracker green, Mitospy™ Orange CMTMRos, and Cyto-ID autophagy detection kit 2.0, and intracellular staining was performed using V450 rat anti-histone H3, Alexa Fluor 647 rabbit-anti-human light chain 3 B (LC3B), Alexa Fluor 700 mouse-anti-human cleaved poly (ADP-ribose) polymerase (PARP), and PE/Cyanine7 mouse anti-H2A.X phospho. In Panel 2, viability was assessed using Zombie NIR™, and extracellular staining was conducted using PE-Vio 770 REA anti-human CD274, FITC mouse anti-human CD107a (lysosomal-associated membrane protein 1 (LAMP-1)), and Alexa Fluor 594 rat anti-human Ras-related protein Rab7a (Rab7a). Intracellular staining was performed using APC REA anti-human B-cell lymphoma 2 (BCL2) and Alexa Fluor 405 mouse anti-human Hif1α. After staining, the cells were washed and treated with the True Nuclear Transcription Factor Buffer Set for membrane permeabilization and intracellular staining. The associated flow cytometry gating strategy is shown in Supplemental Fig. 3.

Chorioallantoic membrane assay

Animal procedures were conducted in accordance with national regulations (TierSchG, Germany). Lohmann Deutschland GmbH & Co. KG provided fertilized eggs, which were incubated for six days. The CAM was dropped, and a 1 cm diameter window was opened under sterile conditions [45]. The window was sealed with wound dressing, and the eggs were incubated without rotation. On day 7, the pellet of 1×10^6 HHP-treated or untreated cancer cells was suspended in 20 µL Matrigel and pipetted onto the CAM. Embryos were monitored daily for one week, euthanized, and CAM tissue was harvested for ex vivo fluorescence measurements and histology. CAMs were resected and measured using a NightOWL LB 983 imaging system (Berthold Technologies, Germany) with a 630-nm excitation filter and a 700-nm emission filter (PE/CA-PJ15; $n = 19$ for 105, 210 and 315 MPa; $n = 21$ for 0 MPa). The sample size was calculated using G-Power software (HHU, Germany). Based on the in vitro experiments, the effect size was estimated to be high with Cohen $\eta^2 = 0.14$/ $f = 0.403$. Photon counts per second (cts/s) were analyzed using Indigo Software. The CAM tissue was embedded in paraffin after fixation in 4% phosphate-buffered formalin for three days. Paraffin-embedded tissue blocks were cut into 4 µm sections and stained with hematoxylin and eosin (H&E). For the experimental groups with non-fluorescent PDX-derived cell lines, 100 µL BrdU (20 mg/mL) was topically administered onto the CAM membrane 24 h before euthanasia to assess tumor tissue viability ($n = 9$–21). BrdU immunohistochemistry was performed using the DAB method, with mouse anti-BrdU as the primary antibody and goat anti-mouse HRP as the secondary antibody. The histology was analyzed by a clinical pathologist Fig. 7.

Patient-derived HNSCC tissue culture and live/dead staining

To study the effect of HHP treatment on tumor tissue, tumor samples were obtained during surgery (Ethics Committee reference number A2018-000). After dissection, the samples were sent to the Institute of Pathology, Rostock University Medical Center, for instantaneous H&E staining. The pathologist removed the tumor tissue for routine diagnosis and provided macroscopically vital tumor tissue. Fresh tumor samples (n = 3) were then treated with 0 or 315 MPa for 10 min in air-free cryotubes within 90 min of resection. Next, the tumor tissue was dissociated using 2 mg/mL collagenase A at 37 °C under constant agitation for 2 h. The cell suspension was filtered and washed before resuspension in the cell culture medium before seeding into 12-well cell culture plates. Live/dead staining was performed after 72 or 168 h (LIVE/DEAD™ Viability/Cytotoxicity Kit).

Statistics

All values are given as mean ± standard deviation (in vitro) or as individual values with a median of 25% percentile/75% percentile (CAM assay). Statistical evaluation was performed using GraphPad PRISM software, version 8.0.2 (GraphPad Software, USA). The criterion for significance was set at $P < 0.05$. After proving the assumption of normality (Shapiro–Wilk test), two-way ANOVA with Tukey's multiple comparison post hoc test was performed. If the normality test failed, the Kruskal–Wallis test with Dunn's multiple comparison test was performed.

DATA AVAILABILITY

The datasets generated for this study are available on request to the corresponding author.

REFERENCES

1. Rivalain N, Roquain J, Demazeau G. Development of high hydrostatic pressure in biosciences: pressure effect on biological structures and potential applications in biotechnologies. Biotechnol Adv. 2010;28:659–72.
2. Frey B, Janko C, Ebel N, Meister S, Schlücker E, Meyer-Pittroff R, et al. Cells under pressure-treatment of eukaryotic cells with high hydro-static pressure, from physiologic aspects to pressure induced cell death. Curr Med Chem. 2008; https://doi.org/10.2174/092986708785909166.
3. Waletzko-Hellwig J, Pohl C, Riese J, Schlosser M, Dau M, Engel N, et al. Effect of High hydrostatic pressure on human trabecular bone regarding cell death and matrix integrity. Front Bioeng Biotechnol. 2021;9. https://doi.org/10.3389/fbioe.2021.730266.
4. Weiss E-M, Frey B, Rödel F, Herrmann M, Schlücker E, Voll RE, et al. Ex vivo- and in vivo-induced dead tumor cells as modulators of antitumor responses. Ann N. Y Acad Sci. 2010;1209:109–17.
5. van de Sande MAJ, Bovée JVMG, van Domselaar M, van Wijk MJ, Sanders I, Kuijper E. Successful disinfection of femoral head bone graft using high hydrostatic pressure. Cell Tissue Bank. 2018;19:333–40.
6. Korn A, Frey B, Sheriff A, Gaipl US, Franz S, Meyer-Pittroff R, et al. High hydrostatic pressure inactivated human tumour cells preserve their immunogenicity. Cell Mol Biol. 2004;50:469–77.
7. Eisenthal A, Ramakrishna V, Skornick Y, Shinitzky M. Induction of cell-mediated immunity against B16-BL6 melanoma in mice vaccinated with cells modified by hydrostatic pressure and chemical crosslinking. Cancer Immunol Immunother. 1993;36:300–6.
8. Adkins I, Fucikova J, Garg AD, Agostinis P, Špíšek R. Physical modalities inducing immunogenic tumor cell death for cancer immunotherapy. Oncoimmunology. 2014;3:e968434.
9. Weiss EM, Meister S, Janko C, Ebel N, Schlücker E, Meyer-Pittroff R, et al. High hydrostatic pressure treatment generates inactivated mammalian tumor cells with immunogeneic features. J Immunotoxicol. 2010;7:194–204.
10. Seitz C, Rückert M, Deloch L, Weiss EM, Utz S, Izydor M, et al. Tumor cell-based vaccine generated with high hydrostatic pressure synergizes with radiotherapy by generating a favorable anti-tumor immune microenvironment. Front Oncol. 2019;9. https://doi.org/10.3389/fonc.2019.00805.
11. Zhi L, Wenli W, Pengfei G, Pengcheng C, Wenxian C, Jiasheng L, et al. Laryngotracheal reconstruction with autogenous rib cartilage graft for complex laryngotracheal stenosis and/or anterior neck defect. Eur Arch Otorhinolaryngol. 2014;271:317–22.
12. Yamashita M, Omori K, Kanemaru S-I, Magrufov A, Tamura Y, Umeda H, et al. Experimental regeneration of canine larynx: a trial with tissue engineering techniques. Acta Otolaryngol Suppl. 2007;127:66–72.
13. Ringel RL, Kahane JC, Hillsamer PJ, Lee AS, Badylak SF. The application of tissue engineering procedures to repair the larynx. J Speech, Lang, Hearing Res. 2006;49:194–208.
14. Macchiarini P, Jungebluth P, Go T, Asnaghi MA, Rees LE, Cogan TA, et al. Clinical transplantation of a tissue-engineered airway. Lancet. 2008;372:2023–30.
15. Kiyotake EA, Beck EC, Detamore MS. Cartilage extracellular matrix as a biomaterial for cartilage regeneration. Ann N. Y Acad Sci. 2016;1383:139–59.
16. Sakamoto M, Morimoto N, Jinno C, Mahara A, Ogino S, Suzuki S, et al. Melanin pigments in the melanocytic nevus regress spontaneously after inactivation by high hydrostatic pressure. PLoS ONE. 2017;12:e0186958.
17. Morimoto N, Jinno C, Mahara A, Kakudo N, Fujisato T, Kusumoto K, et al. Verification of the inactivation of melanocytic nevus in vitro using a newly developed portable high hydrostatic pressure device. Cells Tissues Organs. 2016;201:170–9.
18. Morimoto N, Jinno C, Sakamoto M, Kakudo N, Yamaoka T, Kusumoto K. An exploratory clinical trial of a novel treatment for giant congenital melanocytic nevi combining inactivated autologous nevus tissue by high hydrostatic pressure and a cultured epidermal autograft: study protocol. JMIR Res Protoc. 2016;5:e162.
19. Kitamura M, Hirano S, Kanemaru S-I, Kitani Y, Ohno S, Kojima T, et al. Glottic regeneration with a tissue-engineering technique, using acellular extracellular matrix scaffold in a canine model. J Tissue Eng Regen Med. 2016;10:825–32.
20. Urbanova L, Hradilova N, Moserova I, Vosahlikova S, Sadilkova L, Hensler M, et al. High hydrostatic pressure affects antigenic pool in tumor cells: implication for dendritic cell-based cancer immunotherapy. Immunol Lett. 2017;187:27–34.
21. Mikyšková R, Štěpánek I, Indrová M, Bieblová J, Šímová J, Truxová I, et al. Dendritic cells pulsed with tumor cells killed by high hydrostatic pressure induce strong immune responses and display therapeutic effects both in murine TC-1 and TRAMP-C2 tumors when combined with docetaxel chemotherapy. Int J Oncol. 2016;48:953–64.
22. Hradilova N, Sadilkova L, Palata O, Mysikova D, Mrazkova H, Lischke R, et al. Generation of dendritic cell-based vaccine using high hydrostatic pressure for non-small cell lung cancer immunotherapy. PLoS ONE. 2017;12. https://doi.org/10.1371/JOURNAL.PONE.0171539.
23. Fucikova J, Moserova I, Truxova I, Hermanova I, Vancurova I, Partlova S, et al. High hydrostatic pressure induces immunogenic cell death in human tumor cells. Int J Cancer. 2014;135:1165–77.
24. Mikyskova R, Indrova M, Stepanek I, Kanchev I, Bieblova J, Vosahlikova S, et al. Dendritic cells pulsed with tumor cells killed by high hydrostatic pressure inhibit prostate tumor growth in TRAMP mice. Oncoimmunology. 2017;6. https://doi.org/10.1080/2162402X.2017.1362528.
25. Rückert M, Deloch L, Frey B, Schlücker E, Fietkau R, Gaipl US. Combinations of radiotherapy with vaccination and immune checkpoint inhibition differently affect primary and abscopal tumor growth and the tumor microenvironment. Cancers. 2021;13:1–29.
26. Chen SK, Chung CA, Cheng YC, Huang CJ, Ruaan RC, Chen WY, et al. Hydrostatic pressure enhances mitomycin C induced apoptosis in urothelial carcinoma cells. Urol Oncol: Semin Orig Investig. 2014;32:26.e17–26.e24.
27. Schauwecker J, Schmitt M, Tuebel J, Wirthmann L. Effect of extracorporeal high hydrostatic pressure on cellular outgrowth from tumor-afflicted bone. Anticancer Res. 2006;2006:85–90.
28. Mahara A, Morimoto N, Sakuma T, Fujisato T, Yamaoka T. Complete cell killing by applying high hydrostatic pressure for acellular vascular graft preparation. Biomed Res Int. 2014;2014:379607.
29. Hiemer B, Genz B, Jonitz-Heincke A, Pasold J, Wree A, Dommerich S, et al. Devitalisation of human cartilage by high hydrostatic pressure treatment: Subsequent cultivation of chondrocytes and mesenchymal stem cells on the devitalised tissue. Sci Rep. 2016;6:33747.
30. Dommerich S, Frickmann H, Ostwald J, Lindner T, Zautner AE, Arndt K, et al. Effects of high hydrostatic pressure on bacterial growth on human ossicles explanted from cholesteatoma patients. PLoS ONE. 2012;7:e30150.
31. Diehl P, Schauwecker J, Mittelmeier W, Schmitt M. High hydrostatic pressure, a novel approach in orthopedic surgical oncology to disinfect bone, tendons and cartilage. Anticancer Res. 2008;28:3877–83.
32. Shinitzky M, Goldman Y. Immunotherapy of cancer with pressure modified cells. Israel Med Assoc J IMAJ. 2000;2:615–20.
33. Demazeau G, Rivalain N. High hydrostatic pressure and biology: a brief history. Appl Microbiol Biotechnol. 2011;89:1305–14.
34. Liem PH, Morimoto N, Mahara A, Jinno C, Shima K, Ogino S, et al. Preparation of inactivated human skin using high hydrostatic pressurization for full-thickness skin reconstruction. PLoS ONE 2015;10. https://doi.org/10.1371/journal.pone.0133979.
35. Moserova I, Truxova I, Garg AD, Tomala J, Agostinis P, Cartron PF, et al. Caspase-2 and oxidative stress underlie the immunogenic potential of high hydrostatic pressure-induced cancer cell death. Oncoimmunology. 2016;6. https://doi.org/10.1080/2162402X.2016.1258505.
36. Pfister DG, Laurie SA, Weinstein GS, Mendenhall WM, Adelstein DJ, Ang KK, et al. American Society of Clinical Oncology clinical practice guideline for the use of larynx-preservation strategies in the treatment of laryngeal cancer. J Clin Oncol. 2006;24:3693–704.
37. Wagner M, Curé J, Caudell J, Spencer S, Nabell L, Carroll W, et al. Prognostic significance of thyroid or cricoid cartilage invasion in laryngeal or hypopharyngeal cancer treated with organ preserving strategies. Radiat Oncol. 2012;7:219.
38. Patel UA, Howell LK. Local response to chemoradiation in T4 larynx cancer with cartilage invasion. Laryngoscope. 2011;121:106–10.
39. Terrell JE, Ronis DL, Fowler KE, Bradford CR, Chepeha DB, Prince ME, et al. Clinical predictors of quality of life in patients with head and neck cancer. Arch Otolaryngol Head Neck Surg. 2004;130:401–8.
40. Loos E, Meulemans J, Vranckx J, Poorten V, vander, Delaere P. Tracheal autotransplantation for functional reconstruction of extended hemilaryngectomy defects: a single-center experience in 30 patients. Ann Surg Oncol. 2016;23:1674–83.
41. Piazza C, Paderno A, Nicolai P. Conservative surgery for laryngeal chondrosarcoma: a review of the most recently proposed approaches. Curr Opin Otolaryngol Head Neck Surg. 2017;25:93–100.
42. Navach V, Chu F, Cattaneo A, Zorzi S, Scelsi D, Ansarin M. Cartilage framework reconstruction after resection of thyroid cartilage chondrosarcoma: a case report. Otolaryngol Case Rep. 2017;4:12–14.
43. Ansari T, Lange P, Southgate A, Greco K, Carvalho C, Partington L, et al. Stem cell-based tissue-engineered laryngeal replacement. Stem Cells Transl Med. 2017;6:677–87.
44. Schoenwaelder N, Krause M, Freitag T, Schneider B, Zonnur S, Zimpfer A, et al. Preclinical head and neck squamous cell carcinoma models for combined targeted therapy approaches. Cancers 2022;14. https://doi.org/10.3390/CANCERS14102484.
45. Li M, Pathak RR, Lopez-Rivera E, Friedman SL, Aguirre-Ghiso JA, Sikora AG. The in ovo chick chorioallantoic membrane (CAM) assay as an efficient xenograft model of hepatocellular carcinoma. JoVE. 2015;104. https://doi.org/10.3791/52411.

ACKNOWLEDGEMENTS

The UT-SCC-14 cell line was obtained initially from Prof. Reidar Grenman, University of Turku, Finland. The PE/CA-PJ15-NIR-680 cells were provided by Dr. Troschke-Meurer, Department of Pediatric Oncology and Hematology, Greifswald University Medicine, Greifswald, Germany. Figures were created with biorender.com.

AUTHOR CONTRIBUTIONS

All authors contributed to the study, conception, and design. The study was planned by DS, RB, AJH, SH, and AS. The experiments were performed by VFG, CM, FK, and TK. AZ and AB performed patient tissue preparation and histology analysis. VFG, CM, WBE, and DS analyzed and interpreted the data. VFG, CM, and DS wrote the manuscript. RB, AJH, SH, RM, BV, and AS participated in manuscript finalization and critically revised the manuscript. All authors read and approved the final manuscript.

FUNDING

The study was supported by Deutsche Forschungsgemeinschaft (GZ: STR 1603/1-1, BA 3347/15-1, HA 7315/5-1). Open Access funding enabled and organized by Projekt DEAL.

COMPETING INTERESTS

The authors declare no competing interests.

ETHICS APPROVAL AND CONSENT TO PARTICIPATE

All procedures performed in studies involving human participants were in accordance with the ethical standards of the institutional and/or national research committee and with the 1964 Helsinki Declaration and its later amendments or comparable ethical standards. Informed consent was obtained from all individual participants involved in the study. Written informed consent was obtained according to the local Ethics Committee (reference number A2018-0003).

ADDITIONAL INFORMATION

Supplementary information The online version contains supplementary material available at https://doi.org/10.1038/s41420-023-01671-z.

Correspondence and requests for materials should be addressed to Daniel Strüder.

Reprints and permission information is available at http://www.nature.com/reprints

Publisher's note Springer Nature remains neutral with regard to jurisdictional claims in published maps and institutional affiliations.

Received: 10 April 2024 | Revised: 19 August 2024 | Accepted: 23 August 2024

DOI: 10.1002/jbm.a.37791

RESEARCH ARTICLE

High hydrostatic pressure treatment for advanced tissue grafts in reconstructive head and neck surgery

Friederike Kalle[1] | Valentin Paul Stadler[1] | Julia Kristin Brach[2] | Vivica Freiin Grote[3] | Christopher Pohl[4] | Karoline Schulz[5] | Michael Seidenstuecker[6] | Anika Jonitz-Heincke[3] | Rainer Bader[3] | Robert Mlynski[1] | Daniel Strüder[1]

[1]Department of Otorhinolaryngology, Head and Neck Surgery "Otto Körner", Rostock University Medical Center, Rostock, Germany

[2]Department of Otorhinolaryngology – Head and Neck Surgery, RWTH Aachen University Hospital, Aachen, Germany

[3]Research Laboratory for Biomechanics and Implant Technology, Department of Orthopedics, Rostock University Medical Center, Rostock, Germany

[4]Department of General Surgery, Visceral, Thoracic and Vascular Surgery, University Medical Center Greifswald, Greifswald, Germany

[5]Medical Biology and Electron Microscopy Center, Rostock University Medical Center, Rostock, Germany

[6]G.E.R.N. Center for Tissue Replacement, Regeneration & Neogenesis, Department of Orthopedics and Trauma Surgery, Medical Center-Albert-Ludwigs-University of Freiburg, Faculty of Medicine, Albert-Ludwigs-University of Freiburg, Freiburg, Germany

Correspondence
Friederike Kalle, Department of Otorhinolaryngology, Head and Neck Surgery "Otto Körner", Rostock University Medical Center, Doberaner Straße 137 – 139, 18057 Rostock, Germany.
Email: friederike.kalle@med.uni-rostock.de

Funding information
European Social Fund, Grant/Award Number: ESF/14-BM-A55-0016/18; Ministry of Education, Science and Culture of Mecklenburg-Vorpommern, Germany; German Research Foundation, Grant/Award Number: 456590961

Abstract

The increasing importance of regenerative medicine has resulted in a growing need for advanced tissue replacement materials in head and neck surgery. Allo- and xenogenic graft processing is often time-consuming and can deteriorate the extracellular matrix (ECM). High hydrostatic pressure (HHP)-treatment could allow specific devitalization while retaining the essential properties of the ECM. Porcine connective tissue and cartilage were HHP-treated at 100–400 MPa for 10 min. Structural modifications following HHP-exposure were examined using electron microscopy, while devitalization was assessed through metabolism and cell death analyses. Furthermore, ECM alterations and decellularization were evaluated by histology, biomechanical testing, and DNA content analysis. Additionally, the inflammatory potential of HHP-treated tissue was evaluated in vivo using a dorsal skinfold chamber in a mouse model. The devitalization effects of HHP were dose-dependent, with a threshold identified at 200 MPa for fibroblasts and chondrocytes. At this pressure level, HHP induced structural alterations in cells, with a shift toward late-stage apoptosis. HHP-treatment preserved ECM structure and biomechanical properties, but did not remove cell debris from the tissue. This study observed a pressure-

Abbreviations: APC, allophycocyanine; AxV, annexin V; ctl, untreated control; ECM, extracellular matrix; EDTA, ethylenediaminetetraacetic acid; FCD, functional capillary density; FCS-H, forward scatter height; FESEM, field emission scanning electron microscopy; FL, fluorescence; HHP, high hydrostatic pressure; IL, interleukin; IVM, intravital microscopy; MCP-1, monocyte chemoattractant protein-1; PBS, phosphate buffered saline; PI, propidium iodide; P/S, penicillin/streptomycin; RT, room temperature; SDF-1, stromal cell-derived factor-1; SSC-H, side scatter height; TEM, transmission electron microscopy; WST, Water Soluble Metrazolium.

dependent increase of markers suggesting the occurrence of immunogenic cell death. In vivo investigations revealed an absence of inflammatory responses to HHP-treated tissue, indicating a favorable biological response to HHP. In conclusion, application of HHP devitalizes fibroblasts and chondrocytes at 200 MPa while retaining the essential properties of the ECM. Prospectively, HHP may simplify the preparation of allo- and xenogenic tissue replacement materials and increase the availability of grafts in head and neck surgery.

KEYWORDS
allogenic and xenogenic tissues, fascia and cartilage regeneration, high hydrostatic pressure devitalization, reconstructive head and neck surgery, regenerative medicine

1 | INTRODUCTION

In head and neck surgery, trauma, cancer, and infection can lead to tissue defects that impact both function and appearance, presenting a substantial challenge in tissue reconstruction.[1–5] The current gold standard is autologous tissue, which is naturally limited and requires a second surgery at the donor site.[6] Donor site morbidity, particularly when involving fascia lata or costal and auricle cartilage tissue, may increase complications carrying the risk of irreversible functional impairment. Moreover, delayed recovery conflicts with the trend toward outpatient head and neck surgery.[7]

European legal frameworks impose tight constraints on use of allo- and xenogenic tissue. The application of fresh or fresh-frozen tissue is restricted and mandatory sterilization processes are required to guarantee biological safety.[8] However, contemporary sterilization methods, including chemical, enzymatic, and physical methods compromise the integrity of the tissue and affect biomechanical behavior and biological remodeling.[9–14]

In reconstructive procedures addressing various defects, including those of the skull base and facial nerve paralysis, the use of allogenic and xenogenic tissues has become an established standard of high-quality.[15] In addition, allo- and xenografts are available in greater quantity than autologous tissue. However, pathogen transmission and graft rejection due to increased antigenicity must be avoided.[16] Processing of soft tissue is often costly, labor-intensive, and critically, it can compromise biomechanical integrity. This reduction in tissue quality directly affects the functional outcome and success of the reconstruction.[17]

Various approaches for allo- and xenograft processing have been investigated.[18–21] However, an optimal method has not been found. For example, the cartilage regeneration approaches mostly resulted in fibrous tissue instead of a hyaline extracellular matrix (ECM).[22,23] For this reason, there is a clinical need for advanced graft processing.

High Hydrostatic Pressure (HHP)-technology is widely used in the food industry for decontamination while simultaneously retaining taste and vitamins.[24–26] HHP is notable for its ability to maintain the structural and biomechanical integrity of tissues, which is crucial for successful transplantations.[25,27–30] Depending on the applied pressure, HHP triggers apoptotic or necrotic cell death, by plasma membrane damage and the tertiary/quaternary protein structure change.[27,30,31] HHP-treatment is cost-efficient and avoids the use of toxic substances.[32] Another advantage is the high standardization, as the pressure is applied isostatically and instantaneously on every cell within complex tissues.[27,33] Therefore, HHP offers significant potential in tissue graft processing (Figure 1).

The present study focused on HHP's application in fascia and cartilage graft processing. The effects of HHP from 100 to 400 MPa on cell structure, cell death, biomechanical properties, and immunogenicity were investigated. The primary objective was to assess the potential of HHP in advanced processing of tissue replacement materials, with a particular focus on its relevance in head and neck reconstructive surgery.

2 | MATERIALS AND METHODS

For further methods, please refer to the supplementary material section "Materials and Method."

2.1 | In vitro experiments

2.1.1 | Tissue extraction

Human fascia lata and septal nasal cartilage were harvested from body donors up to 72 h post mortem. This was endorsed by the Ethics Committee at the Medical Faculty of the University of Rostock (A2018-0163) in accordance with the 1964 Declaration of Helsinki, and the body donors provided autonomous consent free from coercion during their lifetime. For preparation of the fascia lata, the body donor was positioned in a supine orientation, and the lateral thigh was identified. A longitudinal incision parallel to the femur bone was made, thereby exposing the fascia lata. The subcutaneous tissue was carefully dissected to reveal the tough, fibrous fascia lata, which was subsequently separated from the underlying muscle tissue and trimmed to a rectangle shape of at least 5 × 10 cm. For the preparation of the nasal septal cartilage, the body donor was left in the supine position. A hemitransfixation incision was made to access the septal cartilage,

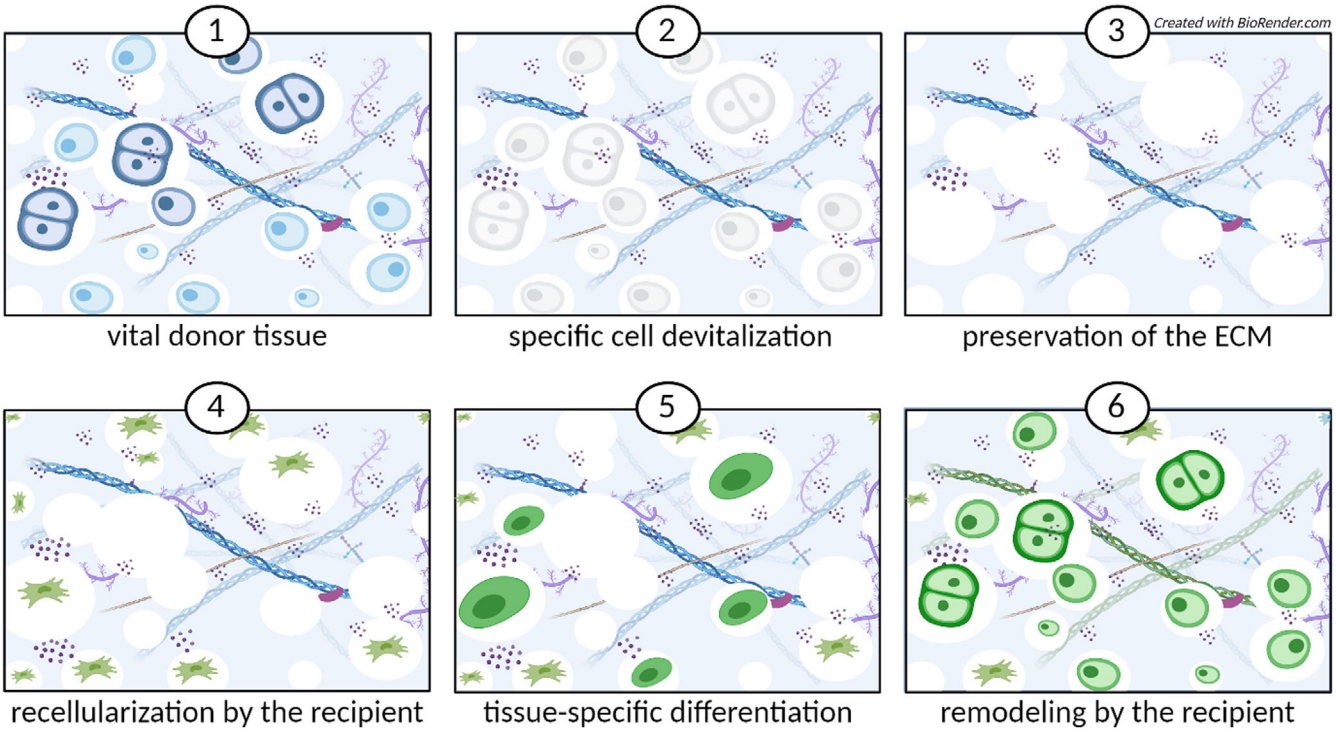

FIGURE 1 Tissue-specific recellularization of tissue while preserving the matrix. The treatment of vital donor tissue (1) by high hydrostatic pressure may enable specific devitalization (2) while preserving the extracellular matrix (ECM) (3). During recellularization by recipient cells (4), the ECM does not function as an inert tissue, but as a secretion product of the cells containing tissue-specific signaling mediators. The retained ECM may lead to tissue-specific differentiation of infiltrating cells (5) leading to remodeling by the recipient's cells, which preserves the tissue's functionality (6).

and a submucoperichondrial dissection was used to expose the cartilage. The 2 × 3 cm septal cartilage was then separated and harvested. Remaining perichondrium was removed by using a gauze compress (Gazin, Lohmann & Rauscher GmbH Co. KG, Rengsdorf, Germany). Subsequently, both tissues were stored in Dulbecco's Phosphate Buffered Saline (PBS) solution supplemented with 1% penicillin/streptomycin (P/S, Sigma-Aldrich Chemie GmbH, Taufkirchen, Germany) at 4°C. The PBS solution was previously prepared by mixing 10× PBS (Sigma-Aldrich Chemie GmbH, Taufkirchen, Germany) and Ampuwa® rinse solution (Fresenius Kabi AG, Bad Homburg, Germany) in a ratio of 1:10.

Porcine dura mater and thyroid cartilage were provided by a local abattoir. For the dura mater preparation, the tissue was gently detached from the cranial cavity. For thyroid cartilage preparation, the larynx was dissected, and the thyroid cartilage from the surrounding tissue separated. Both dura mater and thyroid cartilage were stored in PBS supplemented with 1% P/S at 4°C until further processing. Animals were up to 6 months old. For the experiments, the perichondrium was removed from the cartilage and dura mater and thyroid cartilage were punched out according to the required diameter (10 mm: Wad punch set, Hoffmann Group, Munich, Germany; 2 mm: biopsy punch, GSK Consumer Healthcare, Dungaravan, Ireland). The cartilage was cut to the height of 1 mm (Rhinogrid® Precisely Measure Dice & Slicing Grid, DrKhan's™ Creations, Maharashtra, India).

2.1.2 | Cell culture

Fibroblasts were harvested from fascia lata by cell outgrowth experiments at 37°C and 5% CO_2 in Dulbecco's Modified Eagle Medium + GlutaMAX™ (DMEM, GibcoTM, Paisley, UK) supplemented with 10% fetal calf serum (Sigma-Aldrich Chemie GmbH, Taufkirchen, Germany), 1% P/S, and 1% amphotericin B (PAN Biotech, Aidenbach, Germany). Chondrocytes from nasal septal cartilage were harvested by incubation of minced cartilage for 20 min in Trypsin-ethylenediaminetetraacetic acid (EDTA) (GibcoTM, Grand Island, NY, USA) and 3 h in collagenase A (0.46 U/mL, Roche Diagnostics Deutschland GmbH, Mannheim, Germany) at 37°C in the thermoshaker KS 4000 i control (75 rpm, IKA-Werke GmbH & Co. KG, Staufen, Germany). Cell cultivation was conducted under identical conditions to those used for fibroblasts, except for the addition of 50 µg/mL ascorbic acid (Sigma-Aldrich, Munich, Germany). The cells were passaged when they reached 80%–90% confluency.

2.1.3 | High hydrostatic pressure-treatment

Tissue samples or fibroblasts and chondrocytes were transferred into 1.8 mL cryotubes (Thermo Fisher Scientific, Waltham, MA, USA) filled with the corresponding medium. The cryotubes were inserted into a 50 mL centrifuge tube filled with water and placed in the glycol-filled

pressure chamber of the high-pressure device "205797—Pressure Testing System 6000 bar" (Dustec Hochdrucktechnik GmbH, Wismar, Germany). The pressure is measured by the pressure sensor model HP-2-S 7000 bar (WIKA Alexander Wiegand SE & Co. KG, Klingenberg, Germany; calibration curve—Supplement Figure A1 and Table A1). The samples were treated at 100, 200, 300, or 400 MPa, each for 10 min. The temperature in the chamber was set to 30°C. Control groups (ctl) were exposed to atmospheric pressure in the device.

2.1.4 | Electron microscopy

Cell pellets of human fibroblasts (9×10^5 cells) and chondrocytes (1×10^6 cells) were HHP-treated, the supernatant discarded and overlaid with a solution containing 2% glutaraldehyde and 1% paraformaldehyde in 0.1 M sodium phosphate buffer at pH 7.3. Then, cell pellets were incubated for 1 h at room temperature (RT) and stored at 4°C. Porcine cartilage specimens were fixed after preparation in the same fixative solution as above and stored at 4°C. For subsequent processing for field emission scanning electron microscopy (FESEM) with critical-point drying the cell pellets or the cartilage specimens were washed twice with sodium phosphate buffer, then an aliquot of the cells was attached to glass coverslips coated with 0.1% poly-L-lysine for 1 h. Subsequently, samples were dehydrated in an ascending acetone series, followed by critical point drying using CO_2 as an intermedium (Emitech K850, Quorum Technologies Ltd., East Sussex, UK). In order to visualize the structure of the cartilage cells with the extracellular matrix, the dried cartilage pieces were rapidly frozen in liquid nitrogen and were broken open with the help of tweezers to obtain cross fracture surfaces, respectively. Surface conductivity was established by sputter coating the samples with a gold layer of approximately 10–15 nm thickness (Leica SCD 500, Leica Microsystems, Wetzlar, Germany). Cell surfaces were examined with FESEM (MERLIN VP Compact, Carl Zeiss, Oberkochen, Germany, applied detector: HE-SE2, accelerating voltage: 5.0 kV, working distances approximately 5.2–5.3 mm).

For transmission electron microscopy (TEM), chondrocyte cell pellets were mixed with pre-warmed 2% low melting agarose and collected again as a pellet in the agarose. After post-fixation with a 1% osmium-tetroxide solution these specimen blocks were washed with distilled water and were dehydrated with an ascending acetone series and embedded in Epon resin. After hardening of the resin, semithin and ultrathin sections were cut on an ultramicrotome (Ultracut S, Reichert, Wien, Austria) with a diamond knife. Ultrathin sections of approximately 70 nm thickness were contrasted with lead citrate and uranyl acetate and were inspected with TEM at different magnifications using an acceleration voltage of 80 kV (EM902, Carl Zeiss, Oberkochen, Germany). Digital images were acquired using iTEM camera control and imaging software (Olympus Soft Imaging Solutions, Münster, Germany) with an 1x2k FT-CCD camera (Proscan, Scheuring, Germany).

2.1.5 | Metabolic activity

After HHP-treatment of 1×10^4 fibroblasts/chondrocytes ($n = 5$), cells were cultivated in a 24-well plate. Following a 24-, 48-, and 72-h incubation period at 37°C and 5% CO_2, the supernatants were removed. The cells were incubated for 1 h with a solution of Water Soluble Metrazolium (WST)-1 reagent (Premix WST-1 Cell Proliferation Assay System, Takara Bio Europe SAS, Saint-Germain-en-Laye, France) and the respective culture medium in relation 1:10. The quantification of formazan dye production was carried out through extinction measurements using a Tecan Infinite® 200 Pro Reader (Tecan, Maennedorf, Switzerland) at an absorption wavelength of 450 nm with a reference wavelength of 600 nm.

2.1.6 | Cell death analysis

The APC Annexin-V (AxV) Apoptosis Detection Kit with propidium iodide (PI) (Biolegend, San Diego, CA, USA) was used for apoptosis/necrosis analysis ($n = 5$). HHP-treatment was applied to 2×10^5 fibroblasts/chondrocytes before half of the samples were analyzed immediately (0 h-samples), while the other half underwent a 24 h cultivation in 6-well plates at 37°C and 5% CO_2. In both cases, samples were washed twice with 100 µL of autoMACS® Running Buffer (Miltenyi Biotec, Bergisch Gladbach, Germany) followed by addition of 1 µL AxV and 2 µL PI. After 15 min incubation at RT in darkness, 300 µL Annexin Binding buffer was added. Analysis was carried out with the FACS Calibur flow cytometer (BD, Heidelberg, Germany), with data analyzed using FloJo software (v10.6.1, BD, Heidelberg, Germany) to determine the percentage of cells displaying positive signals.

2.1.7 | Immunogenic cell death analysis

The cell pellet of 2×10^5 fibroblasts/chondrocytes ($n = 5$) was resuspended after HHP-treatment in 100 µL PBS supplemented with 2% bovine serum albumin and 2 mM EDTA, Carl Roth GmbH & Co. KG, Karlsruhe, Germany. Calreticulin monoclonal antibody (FMC 75, phycoerythrin conjugate, Enzo Life Sciences GmbH, Lörrach, Germany) was added in a ratio of 1:100, and the solution was incubated at 4°C for 30 min. Then, the cell pellet was washed twice with PBS and resuspended in 200 µL PBS for measurement at a wave length of 580 nm using the FACSVerse™ flow cytometer (BD, Heidelberg, Germany). The software FloJo was employed for analysis of the percentage of calreticulin-positive cells.

The supernatant of the cells was frozen at −20°C following HHP-treatment. ATP release was analyzed using the ATP Determination Kit (Molecular Probes, Eugene, OR, USA). The luminescence was determined with the Tecan Infinite® F200Pro Reader.

2.1.8 | DNA content

The dura mater (diameter: 12 mm, ctl: $n = 16$, treated: $n = 8$) and thyroid cartilage (diameter: 10 mm, ctl: $n = 11$, treated: $n = 8$) were fragmented into small sections to a size of approximately 1 × 1 mm and frozen at −20°C post HHP-treatment for subsequent freeze-drying for a minimum duration of 7 h. Then, the samples were weighed and digested overnight at 37°C within a thermoshaker (75 rpm) using 3 mL of collagenase A. The DNA isolation was done using the Quick-DNA Midiprep Plus Kit (Zymo Research, Irvine, CA, USA) and its concentration was determined through absorbance measurements at 260 and 280 nm (Tecan Infinite® F200Pro).

2.1.9 | Hematoxylin and eosin stain

Dura mater and thyroid cartilage were fixated for 24 h with buffered 4% formaldehyde-solution (Grimm med. Logistik GmbH, Torgelow, Germany) at RT immediately after HHP-treatment or after 15 days in the dorsal skinfold chamber of the mouse. This was followed by washing for 2 h in running tap water. Tissue samples were placed in Tissue-Tek (Sakura, Osaka, Japan) and snap frozen in liquid nitrogen. Cryosections of 6 µm thickness were prepared with a Leica CM 3050S Cryotome (Leica Mikrosysteme Vertrieb GmbH, Wetzlar, Germany). To assure secure attachment of the samples, loaded slides were baked for 60 min at 60°C. After cooling down to RT, they were placed in ice-cold acetone (J.T. Baker, Phillipsburg, PA, USA) for 10 min and dried overnight. Afterwards, the slides were put into PBS for 5 min followed by 2 min in A. dest. The slides were then stained with filtered Mayer's Hematoxylin Solution (Sigma Aldrich, St. Louis, MO, USA) for 15 min followed by washing with flowing tap water for 4 min until nuclei were stained blue. Counterstaining was performed with aqueous Eosin Y solution (Sigma Aldrich, St. Louis, MO, USA) for 2 min, followed by another washing step in tap water for 4 min. After drying, slices were analyzed with a light microscope CX41 or BX51 (Olympus, Tokyo, Japan) combined with a digital color camera DP23 (1600 × 1200 pixel, Olympus, Tokyo, Japan).

2.1.10 | Tensile strength and compression test

Porcine dura mater, human fascia lata and Tutoplast® Fascia lata Tissue Matrix (Tutogen Medical GmbH, Neunkirchen am Brand, Germany) were cut into pieces of 1 × 5 cm. Except for the gamma-irradiated Tutoplast® Fascia lata, all other tissues were treated with HHP up to 400 MPa (ctl: $n = 24$, treated: $n = 9$). The specimens were then clamped in the Zwick Roel Z1.0 (ZwickRoell GmbH & Co. KG, Ulm, Germany) with a test length of 3 cm and an uniaxial tensile test was performed in the direction of the fibers whenever possible (pre-tension: 3 N, testing speed: 5 mm/min, measurement of tensile strength: 0.05%–0.25% strain). The evaluation was performed using the testXpert® II software (ZwickRoell GmbH & Co. KG, Ulm, Germany). Thyroid cartilage (diameter: 10 mm, height: 1 mm) was HHP-treated with up to 400 MPa (ctl: $n = 11$, 100 MPa: $n = 9$, 200 MPa: $n = 8$, 300/400 MPa: $n = 10$) and an unconfined compression test was conducted on the Mach-1 v500css (Biomomentum Inc., Montreal, Canada) with 100 N load cell (Honeywell, Charlotte, NC, USA). The evaluation was performed using the Mach-1 Analysis software (v4.1.0.17).

2.2 | In vivo experiments

All in vivo experiments were conducted in accordance with the German legislation on protection of animals (7221.3-1-012/20) and the NIH Guide for the Care and Use of Laboratory Animals (Institute of Laboratory Animal Resources, National Research Council). Male hairless SKH1-hr mice without detrimental phenotype (Crl: SKH1-Hrhr Outbred, 6 weeks of age and weight of 25–30 g) were used for all experiments. The mice were individually housed under a 12 h light–dark cycle, with daily health checks and scoring. They had ad libitum access to food and water, with the latter containing 2.5 mg/mL metamizole (Ratiopharm, Ulm, Germany). The animals were housed in special cages designed to prevent contact of the dorsal skin chamber with the cage roof. Housing multiple animals in the cage after preparation of the dorsal skin chamber is not possible due to the risk of injury from the animals' social behavior. Before the actual start of the experiment, a 1-week adaptation to the housing and experimental conditions was conducted. Nesting materials were provided to the animals. A negative impact on the standardization of wound healing and dorsal skin chamber due to enrichment was neither described nor expected.

Fifty-two mice were randomly allocated into four groups: dura mater ctl ($n = 14$) and 200 MPa ($n = 16$) as well as thyroid cartilage ctl ($n = 10$) and 200 MPa ($n = 12$). For the calculation of the sample size, the methodology is predicated upon an analysis of the extant literature, which suggests a mean group size of 9.7.[34–39]

Preparation of the dorsal skinfold chamber was carried out 2 days before tissue implantation to minimize irritation.[40–42] This involved anesthetizing the mice by intraperitoneal injection of ketamine and xylazine (90 and 25 mg/kg bodyweight, Medistar, Holzwickede, Germany and Bayer, Leverkusen, Germany), stretching a median dorsal skin double fold along the median line, and securing it dorsally if congruent intracutaneous vessels were present. A chamber was then fixed to the skinfold, filled with 0.9% saline (B. Braun Melsungen AG, Melsungen, Germany) and sealed with a cover slip (diameter: 12 mm, Gerhard Menzel B.V. & Co. KG, Braunschweig, Germany).

For the tissue implantation, porcine dura mater or thyroid cartilage sample (diameter: 2 mm) were placed in the prepared skinfold chamber. This procedure was done under anesthesia using isoflurane (2.5 L/min, Baxter, Unterschleissheim, Germany) with a UniVet Porta T8 system (Groppler, Deggendorf, Germany). The coverslip was removed, tissue inserted, refilled with 0.9% saline, and the chamber resealed with a new cover slip. Repetitive intravital microscopy (IVM) was performed on day 3, 6, 10, and 15. The mice were sacrificed after the last IVM according to EU recommendations through an overdose of ketamine hydrochloride (100 mg/kg body weight) and xylazine

hydrochloride (Rompun; 6 mg/kg body weight) intravenously followed by cervical dislocation. For the purpose of histological examination, all components of the dorsal skinfold chamber were removed and the tissue under the coverslips, including the implanted tissue, was dissected out and fixed in 4% formaldehyde-solution.

Cumulatively, in cases of repeated low to moderate stress, a medium level of stress for the experimental animals was assumed. Severe distress was prevented by the application of consistent termination criteria.

IVM was performed as previously described.[43] For this procedure, anesthesia was achieved with a continuous application of isoflurane (2.5 L/min) using the UniVet Porta T8. This was followed by the administration of 0.05 mL fluorescein isothiocyanate-labeled-dextran (5%, MW: 150 kD, Sigma, Deisenhofen, Germany) and 0.05 mL Rhodamine 6G (2%, MW: 496 D, Sigma, Deisenhofen, Germany). Both dyes were injected directly intravenously into the lateral tail vein of the mouse using a 32G microinjection needle (Mesoram® Ri.mos SRL, Mirandola, Italy). Four measurement fields were established to repeatedly assess the functional capillary density (FCD). Specifically, two of these fields were positioned centrally within the 10× magnification view around the graft site, while the remaining fields were situated outside of this central area. Microscopy was conducted at 10× magnification (10×/0.30 W, Plan-NEOFLUAR, Zeiss, Jena, Germany) for 20 s in each field. Image analysis was performed automated with ImageJ (v1.53t) and QuPath (v0.3.0,[44]) or manual by tracing the individual capillaries with the ImageJ's Freehand Line Tool.

The exclusion criteria, such as reduction in body weight, deterioration of general condition and spontaneous behavior, as well as early chamber dropout, anesthesia complications, wound healing disorders, ascites, and infections, were defined but did not occur within the experiments.

2.3 | Statistics

All values are presented as means with standard deviations. Statistical significance was evaluated using GraphPad Prism 8 software (GraphPad Software, San Diego, CA, USA) with *p*-values below .05. Following the assumption of normality, as determined by the Shapiro–Wilk test, each statistical analysis method utilized in the study is elucidated in the figure legends.

3 | RESULTS

For further results, please refer to the supplementary material section "Results."

This study aimed to investigate the effects of HHP on cell structure and viability, with a specific focus on fibroblasts and chondrocytes. The morphological changes through FESEM, cellular metabolic activity, and cell death were investigated. Additionally, immunogenic cell death markers and the potential for decellularization following HHP-treatments were analyzed. These analyses were complemented by in vivo studies assessing the inflammatory response elicited by HHP-treated tissue.

3.1 | Analysis of cell morphology

Scanning electron micrographs were taken to assess the impact of 10 min HHP-treatments on fibroblast and chondrocyte cell morphology and membrane integrity (Figure 2). Untreated cells exhibited an intact membrane surface characterized by numerous smooth, spherical knob-like elevations corresponding to filopodia and lamellipodia processes of the cells retracted during detachment from the culture dish (Figure 2A,F). Exposure to 100 MPa resulted in no obvious morphological alterations (Figure 2B,G). However, when subjected to 200 MPa, these knob-like processes started to collapse leading to a pronounced roughening of the cell surface and small cell membrane perforations were clearly visible at higher magnifications. At places, larger-sized perforations in the cell membranes had developed as well (Figure 2C,H). Higher pressures up to 400 MPa progressively intensified these surface alterations, abolishing membrane integrity with numerous perforations present (Figure 2D,E,I,J).

Further, transmission electron micrographs on sections of embedded chondrocytes were taken and used to assess the alterations of the HHP-treatments on the integrity of organelles within the cell and on the cellular ultrastructure compared to control treated cells (Figure 3). Exposure to 100 MPa caused rearrangements of the cytoskeleton with striking accumulations of microfilaments and intermediate filaments visible as bright spots in the sections. Mild mitochondrial swelling was noted whereas the rough endoplasmatic reticulum (rER) did not show obvious structural changes compared to control cells (Figure 3A,B). In the nucleus some additional spots of condensed heterochromatin appeared (Figure 3B). HHP-treatment of 200 MPa caused similar detrimental effects on the cytoskeleton, in addition damage and disintegration of mitochondrial structure and of the rER were obvious. Also, in the nucleus marked changes were noted, specifically a strong increase of heterochromatin along the nuclear lamina and in other spots, which indicates significant chromatin damage (Figure 3C). At 300 MPa most organelles were disrupted with few remnants of their internal structure and large perforations in the cell membrane as well as in the nuclear membrane were obvious, complementing the results from the FESEM analysis. Fuzzy chromatin spots marked the former nuclear territory (Figure 3D).

3.2 | Pressure-dependent metabolic activity assessment

Cell viability was determined using a metabolic assay (Figure 4A,B). Twenty-four hours after HHP-treatment, the control cells' relative absorption of metabolic activity was normalized to 100%. For the fibroblasts, the metabolic activity significantly decreased to 62.48 ± 26.47% after treatment at 100 MPa, further decreased to 0.83 ± 1.44% at 200 MPa, to 0.65 ± 1.09% at 300 MPa, and to 0.09

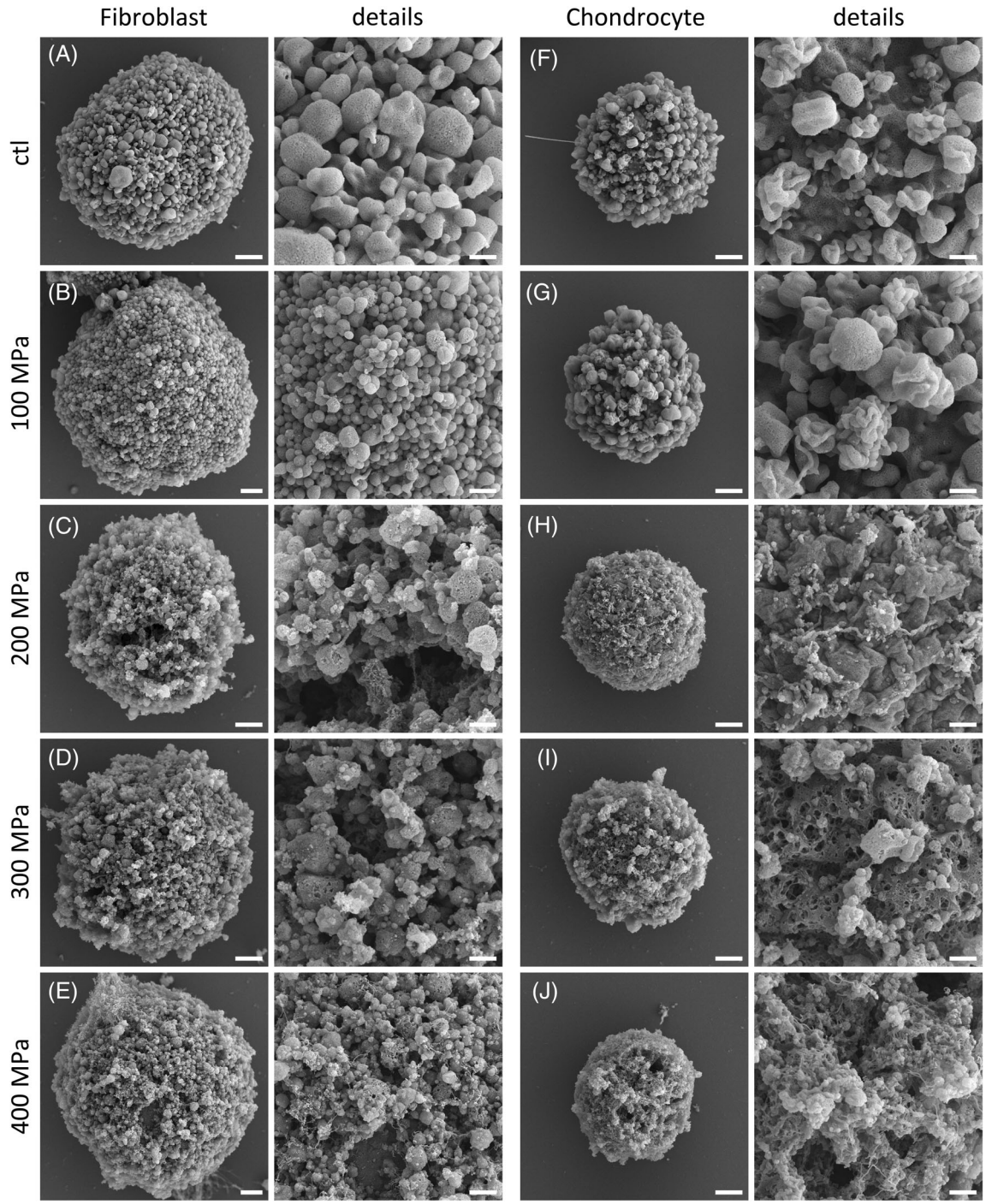

FIGURE 2 Field emission scanning electron microscopy analysis of human fibroblasts and chondrocytes treated with high hydrostatic pressure. Overview images of representative cells and details of their cell surface appearance are shown (A–J). Fibroblasts (A–E) and chondrocytes (F–J) were treated at 100 MPa (B, G), 200 MPa (C, H), 300 MPa (D, I), 400 MPa (E, J), and compared to their untreated controls (ctl) (A, F). Scale bar: 2 μm and 500 nm for details.

± 0.21% at 400 MPa ($p < .05$ vs. ctl/150 MPa). For the chondrocytes, similar patterns were observed. The metabolic activity decreased to 72.42 ± 10.83% after treatment at 100 MPa ($p = .52$) and further significantly below the detection limit at 200, 300, and 400 MPa ($p < .05$ vs. ctl/100 MPa). The development of the absorption of metabolic activity after HHP-treatment was similar after 48 and 72 h, whereby after 72 h it started for the fibroblasts at 171.60 ± 43.70% for the untreated control. The metabolic activity decreased significantly to 118.30 ± 30.49% (100 MPa), 1.34 ± 1.51% (200 MPa), 0.77 ± 0.87% (300 MPa), and 1.02 ± 1.51% (400 MPa) ($p < .05$ vs. ctl/100 MPa). For the chondrocytes, the metabolic activity was 435.10 ± 107.50% after 72 h for the untreated control. The metabolic activity decreased

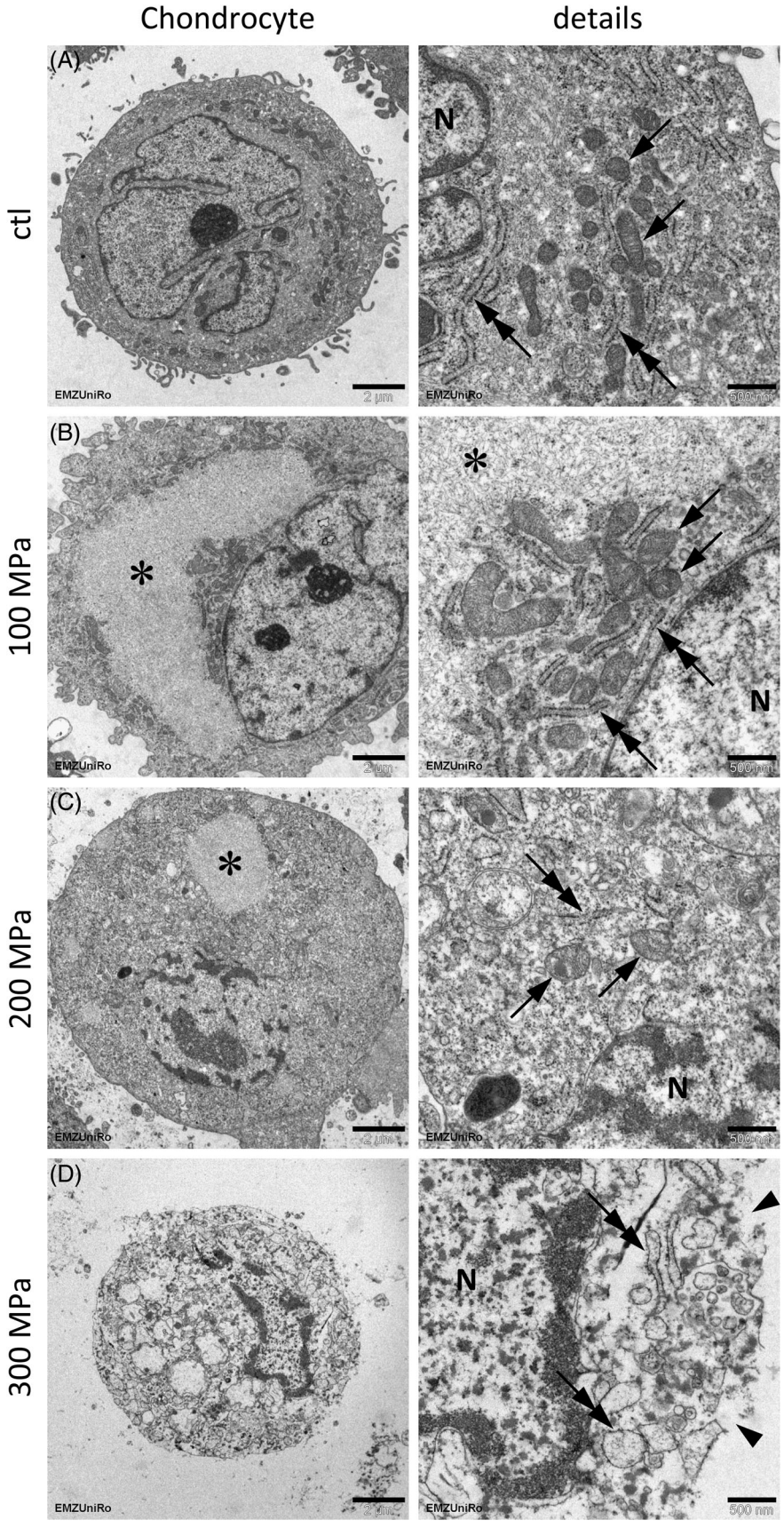

FIGURE 3 Transmission electron microscopy analysis of human chondrocytes treated with high hydrostatic pressure. Overview images of cross sections of representative chondrocytes and respective details of their organelle ultrastructure are shown (A–D). Chondrocytes were treated at 100 MPa (B), 200 MPa (C), 300 MPa (D), or were left untreated in atmospheric pressure as controls (ctl) (A). Compared to controls accumulations of cytoskeletal elements (asterisks) are observed at pressures of 100 and 200 MPa along with progressive organelle damage, for example, of mitochondria (arrows) and rough endoplasmatic reticulum (double arrows) as well as heterochromatin accumulation in the nuclei (N) highlighting general organelle and membrane compartment damage, including large membrane perforations (arrowheads) at 350 MPa. Scale bar: 2 µm and 500 nm for details.

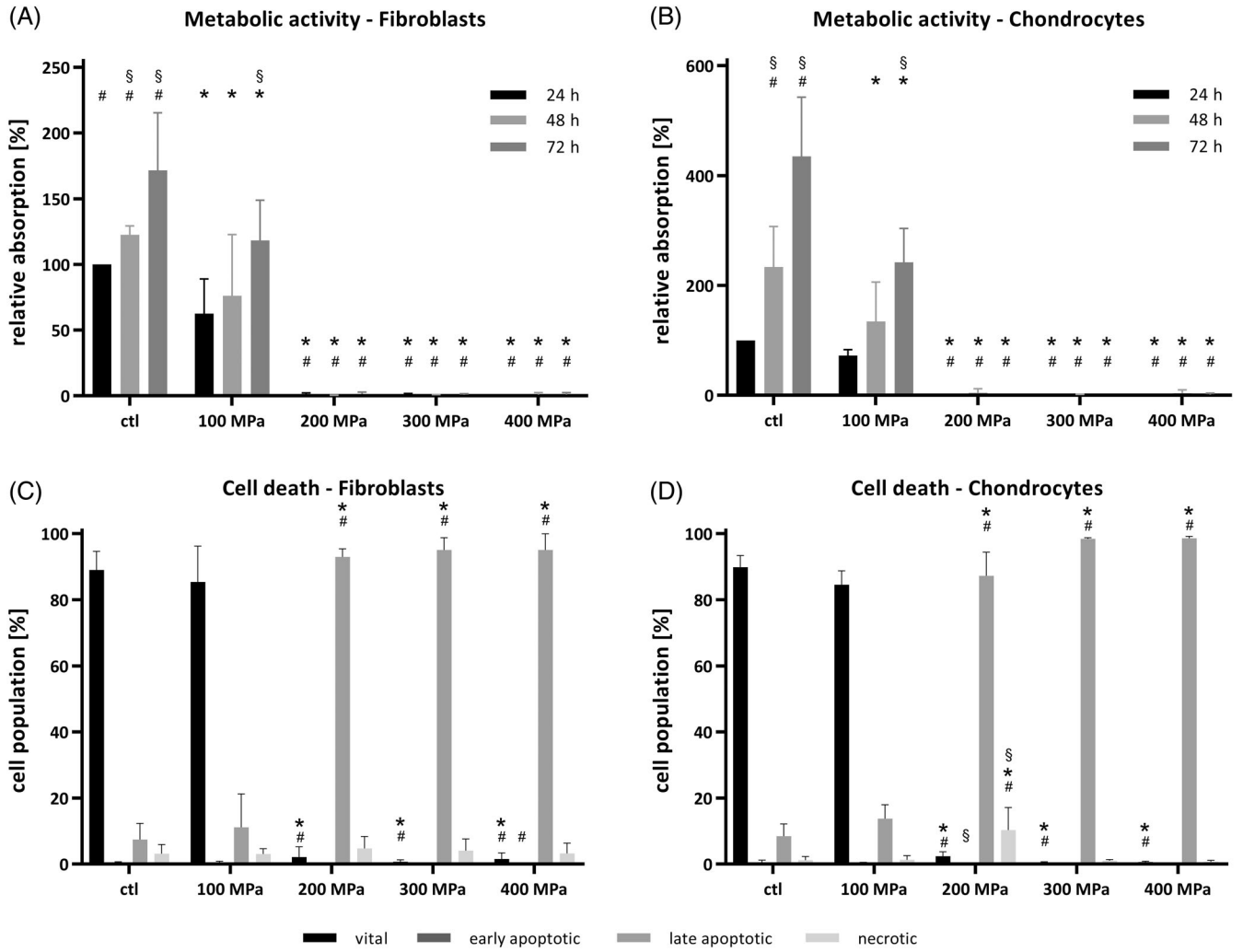

FIGURE 4 Impact of high hydrostatic pressure on viability of human fibroblasts and chondrocytes. This figure illustrates the effects of high hydrostatic pressure up to 400 MPa on human fibroblasts (A, C) and chondrocytes (B, D). Following pressure exposure, cells were analyzed immediately (0 h-samples, C, D) or incubated at 37°C and 5% CO_2 for 24, 48, and 72 h (A, B). Metabolic activity was assessed using the Water Soluble Metrazolium (WST)-1 assay (A, B), while cell viability was analyzed through APC annexin-V/propidium iodide flow cytometry (C, D). Data are presented as mean values with standard deviations. $n = 5$, two-way ANOVA with Dunnett's or Tukey's multiple comparisons test (A, B), mixed-effects analysis (C) or two-way ANOVA (D) with Sidak's multiple comparisons test, *$p < .05$: Untreated control (ctl) versus different HHP-treatments, #$p < .05$: 100 MPa versus different HHP-treatments, §$p < .05$: 24 versus 48 or 72 h (A, B), 0 versus 24 h (C, D: comp. Supplement Figure A2).

significantly to 242.10 ± 61.57% (100 MPa), fell below the detection limit (200 and 300 MPa), and was 1.21 ± 2.70% after HHP-treatment at 400 MPa ($p < .05$ vs. ctl/100 MPa). All unmentioned measured values can be found in the supplementary material Table A2.

3.3 | Time-dependent metabolic activity assessment

The metabolic activity of fibroblasts and chondrocytes decreased after HHP-treatment at 100 MPa compared to the untreated control, but recovered over time after this initial decrease (Figure 4A,B). For both, fibroblasts and chondrocytes, there was no significant increase over time in the 200, 300, and 400 MPa groups ($p > .05$ vs. 24 h, Supplement Table A3). In detail, the absorption of metabolic activity increased in the fibroblasts and chondrocytes compared to the 24 h samples after 48 and 72 h in the control and 100 MPa groups. For the fibroblasts, the metabolic activity increased significantly for the control group to 122.60 ± 6.74% after 48 h ($p < .05$ vs. 24 h) and to 171.60 ± 43.70% after 72 h ($p < .05$ vs. 24 h). For the 100 MPa group, the metabolic activity increased starting at 62.48 ± 26.47% after 24 h to 76.11 ± 46.53% after 48 h ($p = .50$ vs. 24 h) and significantly to 118.30 ± 30.49% after 72 h ($p < .05$ vs. 24 h). For the chondrocytes, the metabolic activity increased significantly for the control group to 233.80 ± 73.33% after 48 h ($p < .05$ vs. 24 h) and to 435.10 ± 107.50% after 72 h ($p < .05$ vs. 24 h). For the 100 MPa group, the metabolic activity increased starting at 72.42 ± 10.83% after 24 h to 134.20

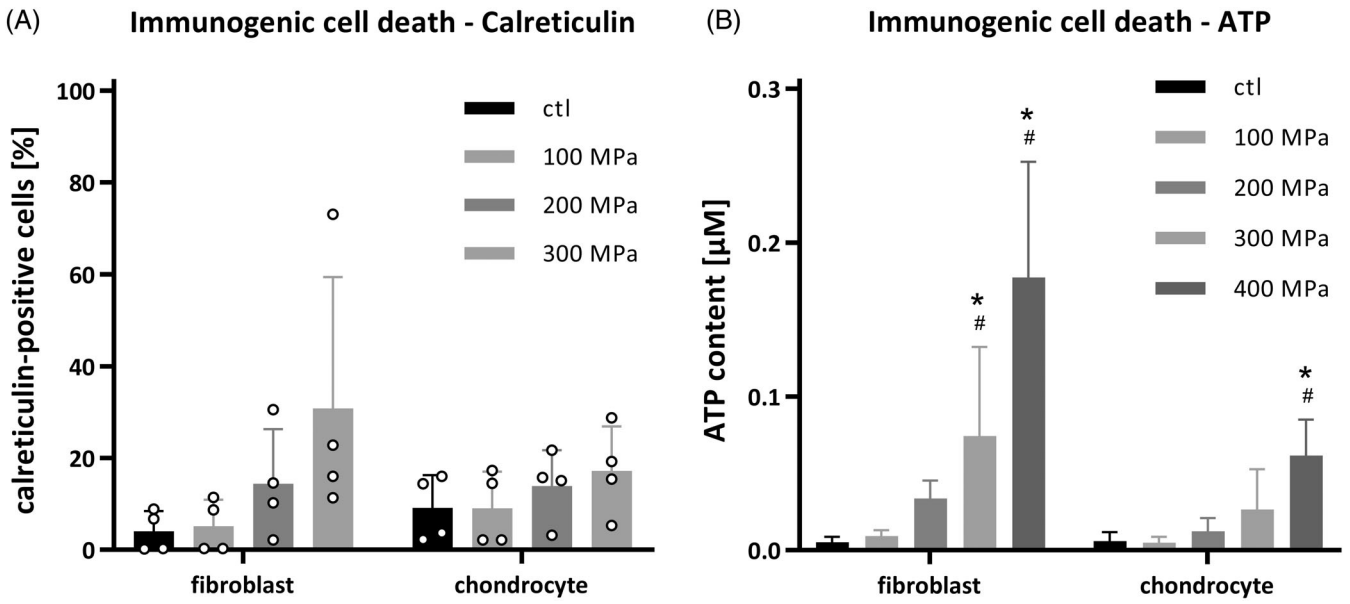

FIGURE 5 High hydrostatic pressure-induced immunogenic cell death in human fibroblasts and chondrocytes. Human fibroblasts and chondrocytes were exposed to high hydrostatic pressures up to 400 MPa. Calreticulin presence was assessed by flow cytometry (A), and ATP levels were determined from supernatants (B). Data are presented as mean values with standard deviations. (A) $N = 4$, (B) $N = 5$, RM one-way ANOVA with Dunnett's multiple comparisons test except (B), chondrocytes: Friedman test with Dunn's multiple comparisons, *$p < .05$ versus untreated control (ctl); #$p < .05$ versus 100 MPa.

± 71.70% after 48 h ($p = .18$ vs. 24 h) and significantly to 242.10 ± 61.57% after 72 h ($p < .05$ vs. 24 h).

3.4 | Flow cytometric analysis of cell death

Flow cytometry was employed to differentiate between apoptosis and necrosis (Figure 4C,D and Supplement Figures A2 and A3). Subsequent to HHP-treatment, 89.58 ± 5.63% of untreated fibroblasts and 89.84 ± 3.52% of untreated chondrocytes were vital. 7.49 ± 4.86% of the fibroblasts and 8.45 ± 3.72% of the chondrocytes were late apoptotic. After HHP-treatment at 100 MPa, a similar cell distribution was observed ($p > .05$ vs. ctl, Supplement Tables A4 and A5). However, following 200 MPa treatment, vital cells significantly decreased to 2.18 ± 3.10% for fibroblasts and 2.37 ± 1.34% for chondrocytes, with a corresponding increase in late apoptotic cells for fibroblasts to 93.00 ± 2.44% and chondrocytes to 87.20 ± 7.23% ($p < .05$ vs. ctl/100 MPa). The proportion of early apoptotic and necrotic cells remained largely unchanged ($p > .05$, except necrotic chondrocytes: ctl/100 MPa vs. 200 MPa: $p < .05$, Supplement Tables A4 and A5). Treatments at 300 and 400 MPa yielded analogous results, with vitality dropping to 1.58 ± 1.86% for fibroblasts and 0.61 ± 0.27% for chondrocytes at 400 MPa ($p < .05$ vs. ctl/100 MPa). The proportion of early apoptotic and necrotic cells remained largely unchanged ($p > .05$ vs. ctl/100 MPa, except early apoptotic fibroblasts: 100 vs. 400 MPa: $p < .05$, Supplement Tables A4 and A5). Analysis 24 h after HHP-treatment revealed similar trends (Supplement Figure A3, Tables A6 and A7). The comparison between 0 and 24 h samples only showed a significant difference in early apoptotic and necrotic chondrocytes when treated with 200 MPa (Supplement Table A5). All unmentioned measured values or p-values can be found in the supplementary material Tables A4–A7.

3.5 | Analysis of immunogenic cell death markers

For further analysis of cell death, investigation into the characteristics of immunogenic cell death included examining calreticulin translocation and ATP release post HHP-treatment (Figure 5). Both calreticulin translocation and ATP release exhibited a pressure-dependent increase. Calreticulin-positive fibroblasts demonstrated a stepwise yet non-significant increase, starting at 4.04 ± 4.46% in the untreated control. Calreticulin-positive fibroblasts rose to 5.18 ± 5.73% post 100 MPa treatment, further increased to 14.40 ± 11.92% post 200 MPa, and reached 30.81 ± 28.54% post 300 MPa treatment ($p > .05$, Supplement Table A8). Concerning the chondrocytes, the calreticulin-positive cells were 9.12 ± 7.12% in the untreated control, 9.04 ± 8.02% post 100 MPa treatment, 13.94 ± 7.75% post 200 MPa treatment, and reached 17.19 ± 9.67% post 300 MPa treatment ($p > .05$, Supplement Table A8).

The extracellular ATP amount of fibroblasts showed a stepwise increase, starting at 0.005 ± 0.004 µM for the untreated control. The ATP amount rose to 0.009 ± 0.004 µM (100 MPa) and 0.034 ± 0.012 µM (200 MPa) ($p > .05$ vs. ctl/100 MPa, Supplement Table A9). Furthermore, the extracellular ATP amount increased significantly to 0.074 ± 0.058 µM after treatment at 300 MPa and to 0.177 ± 0.075 µM at 400 MPa ($p < .05$ vs. ctl/100 MPa). For the chondrocytes, the extracellular ATP amount was 0.006 ± 0.006 µM in

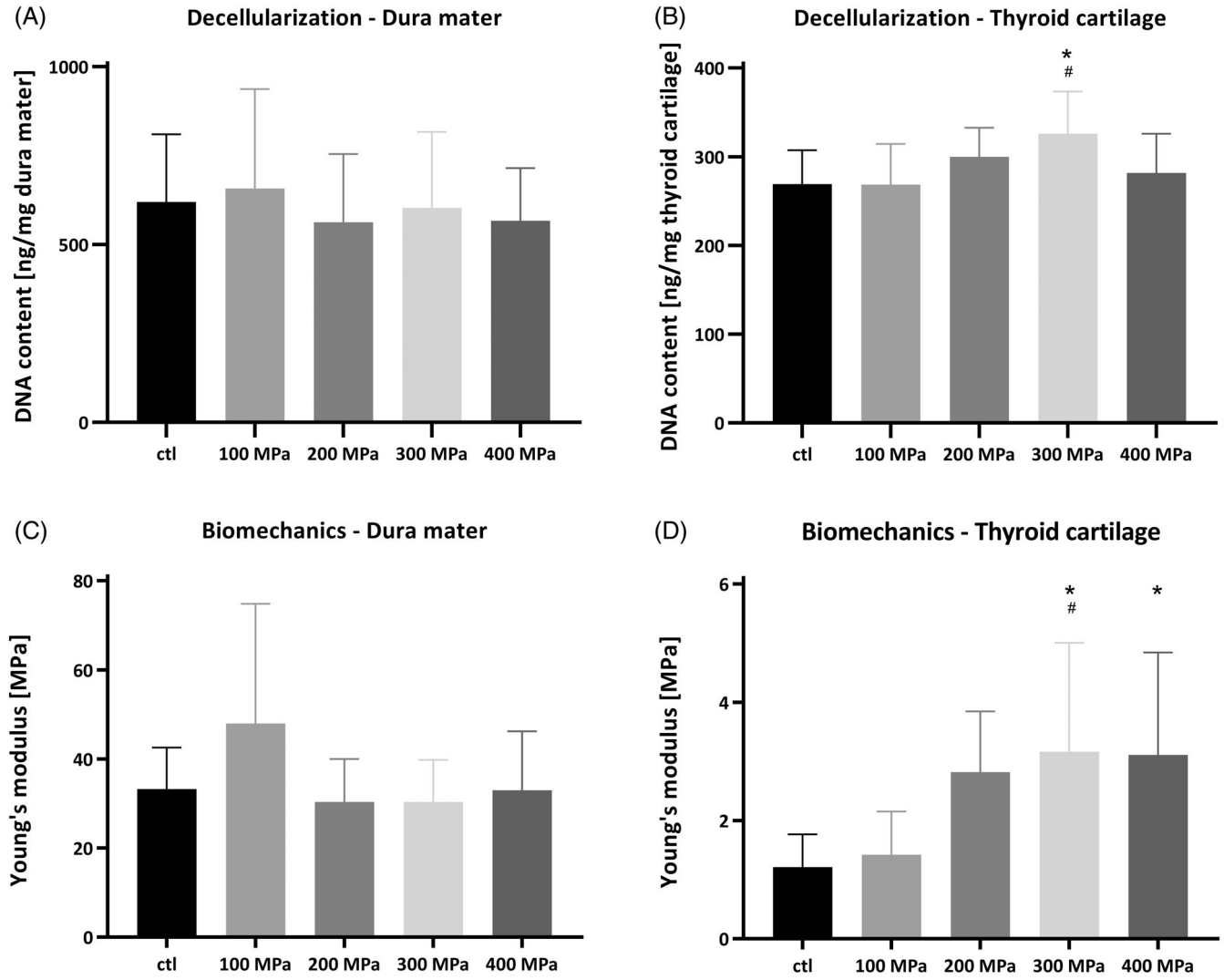

FIGURE 6 Stability of DNA content and biomechanical properties in tissues exposed to high hydrostatic pressure. DNA content (A, B) and biomechanical properties (C, D) in porcine dura mater (A, C) and thyroid cartilage (B, D) was measured after treatment with pressures up to 400 MPa and compared to untreated controls (ctl). For the dura mater, a uniaxial tensile test was performed, for thyroid cartilage an unconfined compression test. Data are presented as mean values with standard deviations. Dura mater (A) ctl: $N = 16$, treated: $N = 8$, (C) ctl: $N = 24$, treated: $N = 9$, thyroid cartilage (B): Ctl: $N = 11$, treated: $N = 8$; (D) ctl: $N = 11$, 100 MPa: $N = 9$, 200 MPa: $N = 8$, 300/400 MPa: $N = 10$, Ordinary one-way ANOVA with Dunnett's (A, B) or Tukey's (C, D) multiple comparisons test, *$p < .05$ versus ctl; #$p < .05$ versus 100 MPa.

the untreated control and rose to 0.005 ± 0.004 µM (100 MPa), 0.012 ± 0.009 µM (200 MPa) and 0.027 ± 0.026 µM (300 MPa) ($p > .05$, Supplement Table A9). 400 MPa treatment resulted in a significant difference with an extracellular ATP amount of 0.06 ± 0.23 µM ($p < .05$ vs. ctl/100 MPa).

3.6 | Tissue decellularization and matrix integrity

In order to assess potential decellularization resulting from HHP-treatment, the DNA content was determined (Figure 6A,B). The DNA content of the dura mater remained stable after HHP-treatment. In the untreated control, the DNA content was measured at 620.10 ± 190.40 ng/mg. Following exposure to 100 MPa, the DNA content was 658.00 ± 279.00 ng/mg. At 200 MPa, it was 562.70 ± 192.20 ng/mg, at 300 MPa 603.20 ± 214.00 ng/mg, and at 400 MPa 566.80 ± 148.50 ng/mg ($p > .05$, Supplement Table A10). The DNA content in the thyroid cartilage also remained stable after HHP-treatment with one exception after treatment with 300 MPa. The measured DNA content was 269.20 ± 38.08 ng/mg in the untreated control and 268.50 ± 45.88 ng/mg subsequent to 100 MPa, 299.70 ± 32.87 ng/mg subsequent to 200 MPa, 325.80 ± 47.66 ng/mg subsequent to 300 MPa, and 281.80 ± 44.21 ng/mg subsequent to 400 MPa ($p > .05$, except $p < .05$ for 300 MPa vs. ctl/100 MPa, Supplement Table A10). In dura mater, neither a significance nor a pressure-dependent trend was apparent. In thyroid cartilage, there was one significant treatment, but no pressure-dependent trend. In addition, the hematoxylin and eosin-stained tissues post treatment up

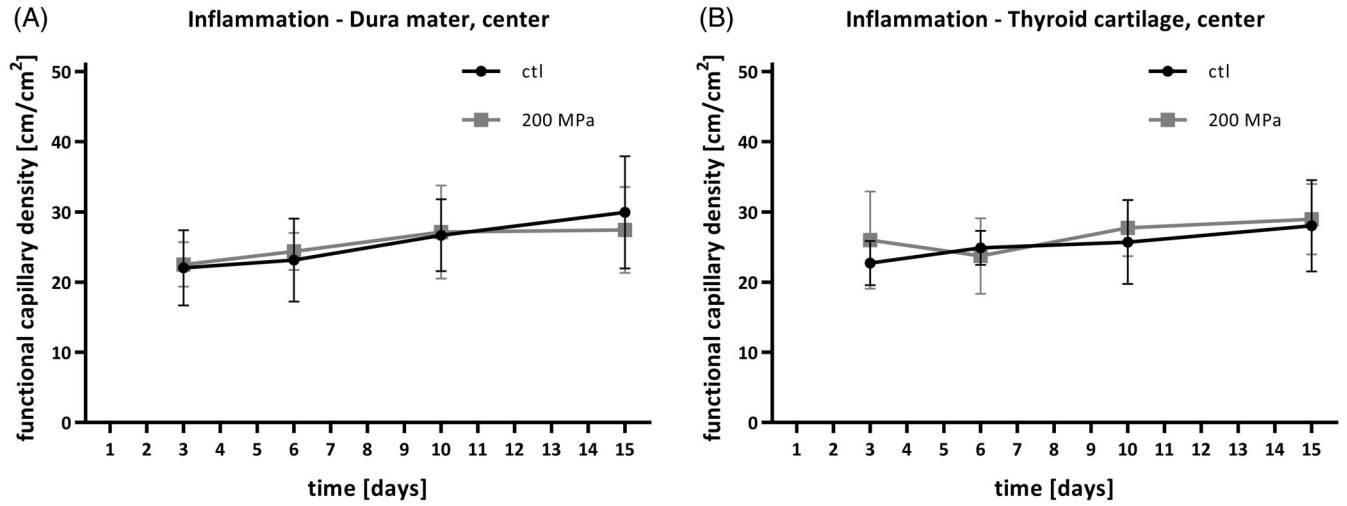

FIGURE 7 In vivo assessment of inflammation following implantation of high hydrostatic pressure-treated tissues. The inflammation originating from the implanted porcine dura mater (A) and the implanted porcine thyroid cartilage (B) treated with 200 MPa was evaluated using the mouse dorsal skinfold chamber model. Treated and untreated (ctl) tissue samples were implanted, and functional capillary density (FCD) was analyzed through intravital microscopy on day 3, 6, 10, and 15 post implantation. FCD was determined within one field of view (20×) to the implanted tissue (center). Data are presented as mean values with standard deviations. Dura mater ctl: $N = 13$, 200 MPa: $N = 16$, thyroid cartilage ctl: $N = 10$, 200 MPa: $N = 12$; two-way ANOVA with Sidak's multiple comparisons test, $p < .05$: Tests show no significant difference between ctl and 200 MPa, as well as between FCD near and in the peripheral area of the HHP-treated graft (comp. Supplement Figure A5).

to 400 MPa exhibited only minor changes, maintaining structural integrity (Supplement Figure A4). In depth, scanning electron micrographs of thyroid cartilage chondrocytes situated in the extracellular matrix revealed obvious structural damages of the cells from pressures of 200 MPa onwards. Similar to the observations made on the isolated fibroblast and chondrocytes these alterations included perforations of the cell membrane increasing in frequency with the pressure load at 200 and 300 MPa resulting in complete membrane disintegrity at 400 MPa. In contrast, the structure of the extracellular matrix remained largely unchanged (Supplement Figure A5).

3.7 | Biomechanical properties

The biomechanical properties were analyzed by an uniaxial tensile test for dura mater or fascia lata and an unconfined compression test for thyroid cartilage (Figure 6C,D). The Young's modulus of the dura mater remained stable after HHP-treatment. In the untreated control, the Young's modulus was measured at 33.25 ± 9.33 MPa. Following exposure to 100 MPa, the Young's modulus was 47.94 ± 26.87 MPa. At 200 MPa, it was 30.35 ± 9.63 MPa, at 300 MPa 30.33 ± 9.47 MPa, and at 400 MPa, 32.95 ± 13.27 MPa ($p > .05$, Supplement Table A11). The Young's modulus was further measured to compare HHP-treated human fascia lata with the commercially available, gamma-irradiated Tutoplast® Fascia lata Tissue Matrix (Supplement Figure A6). In the untreated control of the HHP-treated fascia lata, the Young's modulus was measured at 58.70 ± 35.97 MPa. Following exposure to 100 MPa, the Young's modulus was 40.45 ± 23.72 MPa. At 200 MPa, it was 28.63 ± 21.27 MPa, at 300 MPa 67.47 ± 32.74 MPa, and at 400 MPa, 39.01 ± 25.19 MPa. The Young's modulus of the Tutoplast® Fascia lata Tissue Matrix was measured at 61.68 ± 16.77 MPa ($p > .05$, Supplement Table A12).

The Young's modulus of thyroid cartilage showed stepwise increase, starting at 1.21 ± 0.55 MPa for the untreated control. The Young's modulus rose to 1.42 ± 0.733 MPa (100 MPa) and 2.82 ± 1.03 MPa (200 MPa) ($p > .05$ vs. ctl/100 MPa, Supplement Table A11). Furthermore, the Young's modulus increased significantly to 3.17 ± 1.84 MPa after treatment at 300 MPa ($p < .05$ vs. ctl/100 MPa) and was 3.11 ± 1.73 MPa after treatment at 400 MPa ($p < .05$ vs. ctl, $p = .05$ vs. 100 MPa). The statistical analysis revealed a significant difference from the control group starting at a treatment level of 300 MPa, indicating an increasing stiffness and reduced damping behavior of the cartilage.

3.8 | In vivo analysis of inflammation

An animal study focusing on the in vivo effects of HHP-treated tissues concentrated on FCD as an indicator of inflammation was performed. Notably, in the mouse model the FCD measurements near both dura mater and thyroid cartilage exhibited no substantial variation between the untreated control and the 200 MPa-group over time (Figure 7). FCD near to the dura mater, determined by the automated image analysis, was 22.03 ± 5.34 cm/cm^2 in the untreated control and 22.52 ± 3.26 cm/cm^2 at 200 MPa 3 days post-implantation. FCD rose to 29.95 ± 7.98 cm/cm^2 (ctl) and 27.42 ± 6.12 cm/cm^2 (200 MPa) by the 15th day ($p > .05$, ctl vs. 200 MPa, Supplement Table A14). Similarly, FCD measurements near the thyroid cartilage commenced at 22.73 ± 3.14 cm/cm^2 (ctl) and 25.99 ± 6.93 cm/cm^2 (200 MPa) 3 days following implantation. FCD increased to 28.03 ± 6.50 cm/cm^2 (ctl)

and 28.95 ± 5.02 cm/cm^2 (200 MPa) by day 15 ($p > .05$, ctl vs. 200 MPa, Supplement Table A14). All measured values can be found in the supplementary material Table A13. Peripheral area analysis yielded similar non-significant differences (Supplement Figure A7 and Tables A15 and A16). Furthermore, there was no significant difference when comparing the FCD near and in the peripheral area of the implanted HHP-treated tissue ($p > .05$, Figure 7 and Supplement Figure A7, Table A17). In addition, a manual analysis was used to validate the automated image analysis for determining the FCD. The standard deviations are quite constant for both methods and there is no significant difference between the two experimental groups (Supplement Figure A8, Tables A18 and A19). The hematoxylin and eosin-stained histological images of the tissues after 15 days in the dorsal skinfold chamber of the mouse confirm that there are no significant differences in the tissue after implantation of HHP- and untreated tissues (Supplement Figure A9).

4 | DISCUSSION

Functional and esthetic reconstruction in head and neck surgery presents a significant challenge.[4] Soft tissue and cartilage grafts are an integral part in head and neck cancer reconstruction, skull base repair, and performing nasal, ear, tracheal, and facial surgeries, notably for correcting tracheal defects in children.[1,2,45–48] The current gold standard of using autologous material for reconstruction is naturally limited and associated with donor site morbidity.[7] Allo- and xenogenic materials are significant alternatives, continuously undergoing improvements in quality and biological safety.[49] In the European Union, allografts are subject to mandatory processing protocols, including sterilization procedures that may compromise the integrity of the matrix and biomechanical properties.[14] The use of HHP on allogenic material may be an effective alternative because HHP is recognized for its capacity to preserve the structural and biomechanical integrity of the tissue.[28,50]

This study analyzed the HHP processing of fascia and cartilage grafts. Specifically, it focused on assessing HHP effects on cell structure, cell viability and devitalization, biomechanical characteristics, and immunogenicity of the processed grafts.

The devitalization effects of HHP are meticulously dose-dependent, with a critical threshold at 200 MPa. At this pressure level, HHP induced notable structural alterations in fibroblasts and chondrocytes. At lower pressures such as 100 MPa, FESEM images did not show morphological differences of the cell surface structures compared to the control group. With pressure levels exceeding 200 MPa, the membrane integrity decreased and the permeability increased. These structural changes also affected the metabolism of the cells. Metabolic activity, as measured by WST-1 cell proliferation assay, decreased after exposure to 100 MPa, but recovered over time. In contrast, HHP-treatment at 200 MPa resulted in a significant decrease in metabolic activity after 24 h to 0.02 ± 1.51% for fibroblasts and below the detection limit for chondrocytes. Over time, no cell recovery or proliferation was observed. This was confirmed by light microscopy, as no adherent cells were present after treatment at 200 MPa. HHP-treatment at 100 MPa results in reversible cell damage while 200 MPa leads to irreversible cell death.

At 200 MPa, there is a shift toward late-stage apoptotic cells, highlighting a specific cellular response to this pressure level. HHP induces specific types of cell death, either apoptotic or necrotic, based on the level of pressure applied. At 100 MPa, HHP-treatment did not induce apoptosis or necrosis in cells compared to the untreated control at 0 h. However, at this time point, fibroblast and chondrocyte vitality decreased to 2% and further to 1% 24 h after treatment at 200 MPa. For pressure levels exceeding 200 MPa, late apoptotic cell death predominated, with at least 90% for fibroblasts and 92% for chondrocytes observed 24 h after treatment. Consequently, HHP-technology enables specific devitalization at 200 MPa, aligning with sterilization requisites mandated by Directive 2004/23/EC of the European Parliament and the Council.

HHP-treatment preserves the structure of the matrix but does not remove cell debris from the tissue. The structure of the dura mater remained unchanged after HHP-treatment up to 400 MPa, as can be seen in the histological images (Supplement Figure A4). Likewise, no effect on the biomechanical properties of the dura mater due to HHP was observed in the uniaxial tensile test. HE stain of the thyroid cartilage showed that the architecture and layering of the cartilage remained unchanged even after treatment at 400 MPa. In the unconfined compression test, no significant change in Young's modulus of the cartilage could be demonstrated up to 200 MPa. However, although cells within the tissues were devitalized, they were not removed from the tissue structure. The DNA content did not decrease and the HE stain confirmed that cells were still present. The process of devitalizing cells without removing them (decellularization) leaves cellular components within the matrix, which could potentially initiate inflammatory responses following transplantation.[51] Enclosed proinflammatory cytokines such as IL-6 may also contribute to such a response.

This study observed a pressure-dependent increase in markers of immunogenic cell death. HHP-treatment resulted in devitalization with retention of cellular components within the tissue matrix. This approach offers potential benefits for tissue-specific remodeling due to the preservation of the original extracellular matrix. However, it is important to highlight that proinflammatory cytokines and cell remnants remain within the matrix, posing a risk of initiating inflammatory responses. Indeed, the residual devitalized cells display markers characteristic of immunogenic cell death. Specifically, the study observed calreticulin translocation, a crucial process facilitating phagocytosis by dendritic cells, and ATP release, which is a signal for dendritic precursor cells and macrophages.[52] Both markers demonstrated a pressure-dependent increase, suggesting the occurrence of immunogenic cell death. Likewise, proinflammatory cytokines such as IL1-α, IL-6, and MCP-1 were detected after HHP-treatment, whereby only MCP-1 reached notable concentrations. MCP-1 plays a role in recruiting monocytes and other immune cells to sites of inflammation. However, other cytokines such as IL-1β and IL-8 were not detected. As a result, inflammation may occur after HHP-treatment, which could prevent tissue-specific differentiation and remodeling.

In vivo investigations revealed an absence of inflammatory responses to HHP-treated tissue, indicating a favorable biological response. Although immunogenic cell death was observed in vitro, no signs of inflammation were detected in vivo after transplantation of xenogenic HHP-treated tissue. In the mouse model, no increase in FCD was detected within the peri-implant tissue when compared with peripheral areas, nor in comparison to the untreated graft. The residual cells and cytokines seem biologically insignificant in vivo, likely due to the low cellular density of fascia and cartilage and the cross-species conservation of matrix components. This is further supported by the fact that the transplantation of fresh tissue is permitted in certain countries.[53,54] It appears that allo- or xenogenic transplantation of supporting tissue is predominantly bioinert. This suggests that HHP-devitalized tissue can be transplanted directly without any additional processing steps.

In comparison to standard tissue graft processing, HHP offers efficient devitalization and rapid processing while maintaining functional matrix integrity. Common processing methods are chemical (e.g., Tris–HCl and SDS) or physical (e.g., freeze–thaw cycles or γ-irradiation) approaches.[9,55,56] The preparation process takes several days to weeks, while HHP-treatment lasts only 10 min. Moreover, conventional processing may result in the degradation of the biomechanical properties.[14] Freeze–thaw cycles can form crystals, which can change the collagen network integrity.[9] Similarly, gamma-irradiation induces alterations in the biomechanical properties of soft tissues, leading to a reduction in strength and stiffness.[57] However, in the uniaxial tensile test, no significant difference in the biomechanical properties of gamma-irradiated Tutoplast® Fascia lata Tissue Matrix was observed compared to HHP-treated human fascia lata (Supplement Figure A6). Furthermore, HHP-treatment of bone cylinders for 30 min at 300 MPa did not have any negative effect on the biomechanics.[58] Histological analyses of kidney sections showed the best matrix integrity and stability after HHP-treatment compared to other common methods such as freeze–thaw cycles or chemical treatment.[50] Overall, HHP offers advantages over other methods in terms of devitalization efficiency, functional matrix integrity, reproducibility, time, effort and costs.

The devitalization threshold of 200 MPa is consistent with recent research indicating a comparable response among various mammalian cells to these pressure ranges. For human fibroblasts, chondrocytes, and osteoblasts, complete cell death at 300 MPa has been described.[31,59,60] Diehl et al.[60] reported that human fibroblasts and osteoblasts undergo approximately 50% cell death when subjected to pressures ranging from 130 to 145 MPa. In contrast, the findings of Waletzko et al. did not corroborate this observation. In their study, a pressure of 100–150 MPa was found to exert no significant impact on the viability of human chondrocytes and osteoblasts.[31,60] Consistent with the latter observations, the present study identified no significant decrease in cell viability following exposure to a pressure of 100 MPa. A pressure of 200 MPa was required to reduce the viability of fibroblasts and chondrocytes to a minimal fraction. Similar findings have been reported in other studies, with less than 5% of chondrocytes and osteoblasts maintaining viability following exposure to pressures ranging from 250 to 300 MPa.[31] Even when fibroblasts were pre-treated at temperatures of −4 or −8°C and subsequently subjected to a pressure of 200 MPa, 2%–3% of the cells retained viability.[61]

When the amplitude of pressure was adequately high, HHP emerged as an effective alternative compared to other devitalization methods. In a comparative analysis of HHP, gamma irradiation, and ethanol treatment on tumor cells, it was found that irradiation at doses up to 150 Gy resulted in a 50% reduction in cell viability. While ethanol treatment exhibited significant toxicity, some cells remained viable and were capable of subsequent proliferation. Conversely, 300 MPa HHP achieved complete devitalization.[62] In general, HHP devitalization exhibits considerable cell specificity. For tumor cells 300 MPa was necessary for safe oncologic devitalization. At 200 MPa, more than 20% of the cells remained viable, suggesting that tumor cells are more resistant to HHP than fibroblasts and chondrocytes.[59,60,62]

The exact mechanisms underlying cell death remain incompletely elucidated. It has been noted that damage resulting from HHP-treatments up to 300 MPa tends to be reversible, whereas damage surpassing this threshold becomes irreversible. The absence of reversible cell death following treatment at 300 MPa aligns with prior observations indicating impairment of membrane and protein structure at this pressure level.[27,31] Significant membrane damage is also visible in this study at a pressure of 200 MPa in FESEM and TEM images. Within the scope of HHP-treatment spanning 150–300 MPa, initial damage predominantly affects quaternary structures, progressing to impairments in tertiary structures beginning at 200 MPa.[63,64] Such alterations can be reversible. For irreversible damage to secondary structures, pressures exceeding 700 MPa are necessary. In addition, the lack of recovery can be attributed to DNA double-strand breaks, a phenomenon observed in tumor cells.[62]

Histological analysis revealed that the dura mater and thyroid cartilage structure remained unchanged after HHP-treatment. Additionally, there were no significant alterations in biomechanical properties during tensile and compression tests up to 200 MPa. HHP effectively preserved the functional integrity of the ECM. However, this does not exclude the possibility of alterations in molecular morphology that could have immunological significance. Nevertheless, these alterations do not seem to affect the function or integration of the HHP-treated tissues. Watanabe et al.[65] showed that the compressive modulus of menisci did not change significantly even after treatment with 1000 MPa for 30 min. No negative effects on biomechanical properties have also been found for bone tissue after HHP-treatment at 300 MPa, and HHP has been identified as the best method for kidney slices in terms of matrix integrity and stability.[50,58] Further, Hiemer et al. demonstrated by histologic, immunohistochemical, and FESEM analyses that HHP preserves cartilage tissue integrity and ECM proteins such as collagen type II and aggrecan, with no structural changes or damage observed. Salti et al. found that HHP, when used in combination with chemical reagents (including SDS, sodium deoxycholate, and trypsin) effectively preserves the ECM structure and collagen content of precision-cut kidney slices during decellularization, despite

a significant loss of glycosaminoglycans. Previous studies have already shown that treatment of the tissue with SDS, sodium deoxycholate or trypsin leads to a significant reduction in the GAG content.[66,67] Diehl et al. confirmed that HHP-treated fibronectin, vitronectin, and type I collagen in bone tissue maintain had no adverse effects treatment and retained their functionality, even enhancing cell proliferation. Similarly, Waletzko-Hellwig et al. observed no significant differences in collagen type I content in bone tissue post HHP treatment, indicating that collagen structure remains intact.[28,50,68,69] For these reasons, HHP is also widely used in the food industry for decontamination while preserving taste and vitamins.[24–26]

The preservation of structural integrity following HHP-treatment was associated with the absence of cell removal, as indicated by stable DNA content in both the dura mater and thyroid cartilage after pressurization up to 400 MPa. This lack of reduction in DNA content has also been demonstrated in other studies.[61,65] Furthermore, TEM analysis in this present study showed that significant progressive changes in the chromatin and nuclear structure are caused by the HHP-treatment which eventually may result in irreversible functional damage. In the study by Sutherland et al.,[70] it was noted that HHP-treatment alone leads to tissue devitalization, necessitating a subsequent wash step for decellularization. Cell devitalization without decellularization implies the presence of cellular components within the matrix, which may potentially trigger inflammation after transplantation.[51] Proinflammatory cytokines such as IL-1 and IL-6 could also contribute to such a response. However, in the study conducted by Hiemer et al.,[68] a degradation of DNA was observed over time following HHP-treatment, whereas the DNA content of the untreated control remained unchanged. This finding should be considered in future research.

Tissue replacement materials must have low to negligible immunogenicity to avoid rejection by the recipient. Therefore, the transplant should be as immunologically inert as possible. Cell death is a factor that can trigger immunological processes, so the devitalization process should not have a necrotic effect, as this would lead to inflammatory responses, such as the release of damage-associated molecular patterns (DAMPS), which stimulate the pro-inflammatory response.[71] When using tissue replacement materials, it is advisable to avoid these, as they may cause a strong immune reaction in the recipient.[72,73] In this study, calreticulin and ATP increased in a pressure-dependent manner and the proinflammatory cytokines such as IL-1α and IL-6 were detectable, while IL-1β remained below the detection limit. The literature describes the ATP and calreticulin content, as well as the investigation of cytokines in association with HHP for tumor cells. Maletzki et al.[52,62] found a pressure-dependent increase in ATP and calreticulin, while Fucikova et al. showed an increase in ATP, calreticulin, IL-1β, and IL-6 compared to the control after pressure treatment. In conclusion, HHP triggers immunogenic cell death in tumor cells. In the field of biomaterials, the extent of rejection is determined by a range of factors. The type of transplantation is the primary factor, with a distinction between tissue and organ transfer. Other factors are the genetic disparity between donors and recipients, characterized by histocompatibility on chromosomes, the amount of transplanted tissue, the tissue-specific antigenicity, the recipient organ or transplant bed, and the level of the recipient's immune reactivity, are additional important factors. Generally, from an immunological standpoint, only a minor rejection response is anticipated for cartilage and connective tissue transplants.[74] It is assumed that the dense cartilage ECM hinders immune cells from recognizing chondrocyte antigens. Furthermore, the ECM predominantly comprises type II collagen, which is phylogenetically highly conserved and may represent an additional layer of immune privilege.[75,76] The study used xenogenic porcine dura mater and thyroid cartilage grafts, which are readily available in large quantities and can be sourced from young animals, making them preferable for use in regenerative medicine. In contrast, allogenic tissue is more limited, typically sourced from elderly donors, and may have greater variability between batches. However, the use of xenogenic material may pose a risk to immunogenic tissue and the transmission of xenogenic diseases, which have to be avoided.[77,78]

The present study has several limitations. The conducted experiments were carried out using cells in suspension. Devitalization begins at 200 MPa, resulting in a notable alteration in cell structure. Whether this phenomenon occurs similarly in adherent cells remains unclear. Additionally, in further studies, the intervals between the applied pressure values could be reduced to determine a more precise critical pressure amplitude. However, the isostatic effect of HHP implies that cell death mechanisms are the same in all cells and complex tissue. In this study, functional integrity of the ECM was demonstrated using histology and FESEM images as well as biomechanics. The molecular integrity of the ECM was not assessed in these experiments. Therefore, future studies should focus on examining ECM components such as collagen and glycosaminoglycans to validate our findings and ensure that ECM integrity is preserved following HHP treatment. Furthermore, the study concludes that HHP is not a suitable method for decellularization. Cells remain within the matrix following HHP-treatment, and the study did not investigate whether these residual matrix-bound cells have an influence on subsequent recellularization. However, the in vivo test results presented in this study suggest that these remaining cells are not significant. If decellularization is necessary, a combination with chemical reagents, for example, may be considered.[65,79] Commercial allografts are available for fascia lata, which were biomechanically equivalent to the HHP-treated product. However, there is no effective processing method for cartilage. Therefore, alternative approaches may be necessary for cartilage. The use of fresh tissue is both practically and legally permissible in some countries.[53,54] The additional devitalization using HHP could further enhance safety and increase the global adoption of cartilage replacement materials.

This study focuses on the analysis of fresh cartilage without degeneration, which is needed in head and neck surgery. In contrast, previous research used deteriorated cartilage samples sourced from elderly individuals with osteoarthritis. Additionally, for the first time, this study expands the knowledge of the effects of HHP-treatment on the examination of the porcine dura mater, which can be a readily available and cost-effective alternative to the fascia lata. Moreover,

this study confirmed the devitalization effect while maintaining matrix stability, integrity, and biomechanical properties. Additionally, there has been limited research on the immunological effects of HHP-treatment on human cells. Although markers of immunogenic cell death have been studied in tumor cells, they have not yet been investigated in fibroblasts and chondrocytes. The intravital measurements carried out in this study provide new insights into angiogenesis and inflammation over time after transplantation. HHP is a promising method due to its low cost, low effort, and high reproducibility.

HHP-treatment is quick, reproducible, and has minimal effort. Additionally, HHP enables specific and uniform devitalization as it acts isostatically and instantaneously. Furthermore, compliance with legally mandated sterilization steps for tissues is achieved through HHP technology, while preserving matrix integrity, stability, and biomechanical properties. Good biocompatibility is also ensured, without the need for additional decellularization steps. The use of xenogenic instead of allogenic tissue could also reduce costs for clinical applications. Overall, the adoption of xenogenic, HHP-treated tissue holds the potential for increased and expedited availability of transplant materials in clinical settings.

Future research should prioritize long-term studies on HHP-treated tissues to assess chronic foreign body responses and cytokine concentration comprehensively. Additionally, the revitalization of treated tissues warrants further exploration. A notable strategy for enhancing recellularization, particularly in cartilage, may involve laser technology. The compact nature of cartilage matrix inhibits cellular infiltration, but laser-assisted creation of precise hole patterns and sizes facilitates this process without inducing significant thermal ablation.[80] Furthermore, ensuring microbiological safety constitutes a critical research domain. Identifying target bacteria and acknowledging the distinct responses of various bacterial forms, such as Gram-negative and Gram-positive bacteria, to HHP-treatment, along with spore considerations, is essential for developing microbiologically secure tissue replacement materials.[81]

5 | CONCLUSION

HHP-treatment exceeding 200 MPa devitalizes fibroblasts and chondrocytes with structural alterations at cellular level. The predominant mode of cell death is late apoptosis, with indications of immunogenic cell death. Moreover, HHP-treatment at 200 MPa preserves the ECM structure and biomechanical properties of the dura mater and thyroid cartilage. Consequently, this pressure proves optimal for in vivo investigations, with no observed inflammatory response in the xenogenic model, indicating a favorable biological response to HHP-treated tissue. In conclusion, HHP represents a promising technology for tissue replacement materials.

ACKNOWLEDGMENTS

This work received support from the Core Facility for Cell Sorting and Cell Analysis, Rostock University Medical Center through their guidance and provision of the necessary equipment, the Core Facility Central Animal Facility of the Rudolf-Zenker-Institute for Experimental Surgery, Rostock University Medical Center for the care of the animals during the experiments and was supported by the Institute of Anatomy, Rostock University Medical Center for providing the body donors. In addition, this work was supported with TEM analysis (Dr. Marcus Frank) and TEM sample preparation (Ute Schulz) by the Electron Microscopy Centre Rostock as well as by the Flow Cytometry Facility, a core facility of the Interdisciplinary Center for Clinical Research (IZKF) Aachen within the Faculty of Medicine at RWTH Aachen University. Images were created with BioRender.com (agreement numbers: AP26OAPWC1—Figure 1).

FUNDING INFORMATION

The collaborative research project HOGEMA was supported by the European Social Fund (grant number: ESF/14-BM-A55-0016/18), and the Ministry of Education, Science and Culture of Mecklenburg-Vorpommern, Germany as well as the German Research Foundation (grant number: 456590961).

CONFLICT OF INTEREST STATEMENT

The authors declare no conflict of interest.

DATA AVAILABILITY STATEMENT

The data that support the findings of this study are available from the corresponding author upon reasonable request.

ORCID

Friederike Kalle https://orcid.org/0009-0007-3677-5755
Anika Jonitz-Heincke https://orcid.org/0000-0001-9318-4264

REFERENCES

1. Firat C, Gurlek A, Aydin NE, Aydn NE. Viability of cartilage grafts in various forms. *J Craniofac Surg*. 2011;22:1666-1670. doi:10.1097/SCS.0b013e31822f3b1f
2. Liu Y, Zhou G, Cao Y. Recent progress in cartilage tissue engineering—our experience and future directions. *Engineering*. 2017;3:28-35. doi:10.1016/J.ENG.2017.01.010
3. Tarhan E, Cakmak O, Ozdemir BH, Akdogan V, Suren D. Comparison of AlloDerm, fat, fascia, cartilage, and dermal grafts in rabbits. *Arch Facial Plast Surg*. 2008;10:187-193. doi:10.1001/archfaci.10.3.187
4. Albrecht T, Wallner F. Rekonstruktionsmöglichkeiten nach Verletzungen der Kopf-Hals-Region. *HNO*. 2023;71:57-62. doi:10.1007/s00106-022-01230-5
5. Strüder D, Ebert J, Kalle F, et al. Head and neck cancer: a study on the complex relationship between QoL and swallowing function. *Curr Oncol*. 2023;30:10336-10350. doi:10.3390/curroncol30120753
6. Staudenmaier R. Optimierung der Ohrmuschelrekonstruktion mit autologem Rippenknorpel. *Erfahrung Aus 120 Fällen*, *HNO*. 2006;54:749-755. doi:10.1007/s00106-005-1372-5
7. Kashkouli MB. A novel technique for small-incision fascia lata harvesting without a fasciatome for the frontalis suspension procedure. *Orbit*. 2007;26:203-206. doi:10.1080/01676830701376122
8. European Parliament and the Council. Directive 2004/23/EC on setting standards of quality and safety for the donation, procurement, testing, processing, preservation, storage and distribution of human tissues and cells. *Off J Eur Union*. 2004;L102:48-58.
9. Benders KEM, van Weeren PR, Badylak SF, Saris DBF, Dhert WJA, Malda J. Extracellular matrix scaffolds for cartilage and bone

regeneration. *Trends Biotechnol*. 2013;31:169-176. doi:10.1016/j.tibtech.2012.12.004

10. Fawzi-Grancher S, Goebbels RM, Bigare E, et al. Human tissue allograft processing: impact on in vitro and in vivo biocompatibility. *J Mater Sci Mater Med*. 2009;20:1709-1720. doi:10.1007/s10856-009-3726-0
11. Lansdown DA, Riff AJ, Meadows M, Yanke AB, Bach BR. What factors influence the biomechanical properties of allograft tissue for ACL reconstruction? A systematic review. *Clin Orthop Relat Res*. 2017;475:2412-2426. doi:10.1007/s11999-017-5330-9
12. Putzer D, Huber DC, Wurm A, Schmoelz W, Nogler M. The mechanical stability of allografts after a cleaning process: comparison of two preparation modes. *J Arthroplasty*. 2014;29:1642-1646. doi:10.1016/j.arth.2014.03.028
13. Shang X, Wang H, Li J, Li Q. Progress of sterilization and preservation methods for allografts in anterior cruciate ligament reconstruction. *Chin J Reparat Reconstruct Surg*. 2019;33:1102-1107. doi:10.7507/1002-1892.201903078
14. Mickiewicz P, Binkowski M, Bursig H, Wróbel Z. Preservation and sterilization methods of the meniscal allografts: literature review. *Cell Tissue Bank*. 2014;15:307-317. doi:10.1007/s10561-013-9396-7
15. DuRaine GD, Brown WE, Hu JC, Athanasiou KA. Emergence of scaffold-free approaches for tissue engineering musculoskeletal cartilages. *Ann Biomed Eng*. 2015;43:543-554. doi:10.1007/s10439-014-1161-y
16. Shibuya N, Jupiter DC. Bone graft substitute: allograft and xenograft. *Clin Podiatr Med Surg*. 2015;32:21-34. doi:10.1016/j.cpm.2014.09.011
17. Arzi B, DuRaine GD, Lee CA, et al. Cartilage immunoprivilege depends on donor source and lesion location. *Acta Biomater*. 2015;23:72-81. doi:10.1016/j.actbio.2015.05.025
18. Fischer M, Bortel E, Schoon J, et al. Cold physical plasma treatment optimization for improved bone allograft processing. *Front Bioeng Biotechnol*. 2023;11:1264409. doi:10.3389/fbioe.2023.1264409
19. Kani KK, Porrino JA, Chew FS. Meniscal allograft transplantation: a pictorial review. *Curr Probl Diagn Radiol*. 2022;51:779-786. doi:10.1067/j.cpradiol.2021.09.008
20. Theodoulou MH, Bohman L. Allograft cartilage replacements. *Clin Podiatr Med Surg*. 2018;35:281-293. doi:10.1016/j.cpm.2018.02.003
21. Kurokawa S, Hashimoto Y, Funamoto S, et al. In vivo recellularization of xenogeneic vascular grafts decellularized with high hydrostatic pressure method in a porcine carotid arterial interpose model. *PLoS One*. 2021;16:e0254160. doi:10.1371/journal.pone.0254160
22. Hindle P, Hendry JL, Keating JF, Biant LC. Autologous osteochondral mosaicplasty or TruFit plugs for cartilage repair. *Knee Surg Sports Traumatol Arthrosc Off J ESSKA*. 2014;22:1235-1240. doi:10.1007/s00167-013-2493-0
23. Krueger S, Achilles S, Zimmermann J, Tischer T, Bader R, Jonitz-Heincke A. Re-differentiation capacity of human chondrocytes in vitro following electrical stimulation with capacitively coupled fields. *J Clin Med*. 2019;8(11):1771. doi:10.3390/jcm8111771
24. San Martín MF, Barbosa-Cánovas GV, Swanson BG. Food processing by high hydrostatic pressure. *Crit Rev Food Sci Nutr*. 2002;42:627-645. doi:10.1080/20024091054274
25. Rendueles E, Omer MK, Alvseike O, Alonso-Calleja C, Capita R, Prieto M. Microbiological food safety assessment of high hydrostatic pressure processing: a review. *LWT—Food Science and Technology*. 2011;44:1251-1260. doi:10.1016/j.lwt.2010.11.001
26. Yamamoto K. Food processing by high hydrostatic pressure. *Biosci Biotechnol Biochem*. 2017;81:672-679. doi:10.1080/09168451.2017.1281723
27. Rivalain N, Roquain J, Demazeau G. Development of high hydrostatic pressure in biosciences: pressure effect on biological structures and potential applications in biotechnologies. *Biotechnol Adv*. 2010;28:659-672. doi:10.1016/j.biotechadv.2010.04.001
28. Waletzko-Hellwig J, Pohl C, Riese J, et al. Effect of high hydrostatic pressure on human trabecular bone regarding cell death and matrix integrity. *Front Bioeng Biotechnol*. 2021;12:730266.
29. van de Sande MAJ, Bovée JVMG, van Domselaar M, van Wijk MJ, Sanders I, Kuijper E. Successful disinfection of femoral head bone graft using high hydrostatic pressure. *Cell Tissue Bank*. 2018;19:333-340.
30. Frey B, Janko C, Ebel N, et al. Cells under pressure—treatment of eukaryotic cells with high hydrostatic pressure, from physiologic aspects to pressure induced cell death. *Curr Med Chem*. 2008;15:2329-2336. doi:10.2174/092986708785909166
31. Waletzko J, Dau M, Seyfarth A, et al. Devitalizing effect of high hydrostatic pressure on human cells—influence on cell death in osteoblasts and chondrocytes. *Int J Mol Sci*. 2020;21:3836.
32. Weiss E-M, Frey B, Rödel F, et al. Ex vivo- and in vivo-induced dead tumor cells as modulators of antitumor responses. *Ann N Y Acad Sci*. 2010;1209:109-117. doi:10.1111/j.1749-6632.2010.05743.x
33. Seitz C, Rückert M, Deloch L, et al. Tumor cell-based vaccine generated with high hydrostatic pressure synergizes with radiotherapy by generating a favorable anti-tumor immune microenvironment. *Front Oncol*. 2019;9:805. doi:10.3389/fonc.2019.00805
34. Kampmann A, Lindhorst D, Schumann P, et al. Additive effect of mesenchymal stem cells and VEGF to vascularization of PLGA scaffolds. *Microvasc Res*. 2013;90:71-79. doi:10.1016/j.mvr.2013.07.006
35. Knapik A, Kornmann K, Kerl K, et al. In vivo evaluation of wound bed reaction and graft performance after cold skin graft storage: new targets for skin tissue engineering. *J Burn Care Res*. 2014;35:e187-e196. doi:10.1097/BCR.0b013e3182a226df
36. Laschke MW, Augustin V, Kleer S, Tschernig T, Menger MD. Locally applied macrophage-activating lipopeptide-2 (MALP-2) promotes early vascularization of implanted porous polyethylene (Medpor®). *Acta Biomater*. 2014;10:4661-4669. doi:10.1016/j.actbio.2014.07.004
37. Laschke MW, Schank TE, Scheuer C, et al. Three-dimensional spheroids of adipose-derived mesenchymal stem cells are potent initiators of blood vessel formation in porous polyurethane scaffolds. *Acta Biomater*. 2013;9:6876-6884. doi:10.1016/j.actbio.2013.02.013
38. Laschke MW, Augustin VA, Sahin F, et al. Surface modification by plasma etching impairs early vascularization and tissue incorporation of porous polyethylene (Medpor®) implants. *J Biomed Mater Res B Appl Biomater*. 2016;104:1738-1748. doi:10.1002/jbm.b.33528
39. Schumann P, Lindhorst D, von See C, et al. Accelerating the early angiogenesis of tissue engineering constructs in vivo by the use of stem cells cultured in matrigel. *J Biomed Mater Res A*. 2014;102:1652-1662. doi:10.1002/jbm.a.34826
40. Laschke MW, Vollmar B, Menger MD. The dorsal skinfold chamber: window into the dynamic interaction of biomaterials with their surrounding host tissue. *Eur Cell Mater*. 2011;22:147-167. doi:10.22203/eCM.v022a12
41. Grambow E, Leppin C, Leppin K, et al. The effects of hydrogen sulfide on platelet-leukocyte aggregation and microvascular thrombolysis. *Platelets*. 2017;28:509-517. doi:10.1080/09537104.2016.1235693
42. Xie W, Lorenz M, Poosch F, et al. 3D-printed lightweight dorsal skin fold chambers from PEEK reduce chamber-related animal distress. *Sci Rep*. 2022;12:11599. doi:10.1038/s41598-022-13924-5
43. Strüder D, Grambow E, Klar E, Mlynski R, Vollmar B. Intravital microscopy and thrombus induction in the earlobe of a hairless mouse. *J Vis Exp JoVE*. 2017;2:55174. doi:10.3791/55174
44. Bankhead P, Loughrey MB, Fernández JA, et al. QuPath: open source software for digital pathology image analysis. *Sci Rep*. 2017;7:16878. doi:10.1038/s41598-017-17204-5
45. Gan W, Xiang Y, Lv D, et al. Complex reconstruction technique applied in advanced head and neck cancer. *Medicine (Baltimore)*. 2020;99:e18810. doi:10.1097/MD.0000000000018810
46. Alicandri-Ciufelli M, Serafini E, Pavesi G, et al. Cadaver homologous banked fascia lata in skull base reconstruction: preliminary

multidisciplinary experiences. *Indian J Otolaryngol Head Neck Surg*. 2023;75:941-946. doi:10.1007/s12070-023-03517-7
47. Monnier P. Pediatric airway surgery: management of laryngotracheal stenosis in infants and children. *Egypt J Otolaryngol*. 2014;30:188-190. doi:10.1007/BF03546434
48. Doody J, Alkhateeb A, Balakrishnan K, et al. International Pediatric Otolaryngology Group (IPOG) consensus recommendations: management of suprastomal collapse in the pediatric population. *Int J Pediatr Otorhinolaryngol*. 2020;139:110427. doi:10.1016/j.ijporl.2020.110427
49. Ahmed N, Eras V, Pruß A, Perka C, Brune J, Vu-Han T-L. Allografts: expanding the surgeon's armamentarium. *Cell Tissue Bank*. 2023;24:273-283. doi:10.1007/s10561-022-10015-7
50. Salti H, Kramer L, Nelz S-C, et al. Decellularization of precision-cut kidney slices-application of physical and chemical methods. *Biomed Mater*. 2023;18:025004. doi:10.1088/1748-605X/acb02e
51. Schreiter J, Meyer S, Schmidt C, Schulz RM, Langer S. Dorsal skinfold chamber models in mice. *GMS Interdiscip Plast Reconstr Surg DGPW*. 2017;6:Doc10. doi:10.3205/iprs000112
52. Fucikova J, Kepp O, Kasikova L, et al. Detection of immunogenic cell death and its relevance for cancer therapy. *Cell Death Dis*. 2020;11:1013. doi:10.1038/s41419-020-03221-2
53. Milkovich J, Ahmad J. A Canadian experience with off-the-shelf, aseptically processed, costal cartilage segment allografts in complex rhinoplasty. *Aesthet Surg J Open Forum*. 2022;4:ojac085. doi:10.1093/asjof/ojac085
54. Rohrich RJ, Abraham J, Alleyne B, Bellamy J, Mohan R. Fresh frozen rib cartilage grafts in revision rhinoplasty: a 9-year experience. *Plast Reconstr Surg*. 2022;150:58-62. doi:10.1097/PRS.0000000000009203
55. Kheir E, Stapleton T, Shaw D, Jin Z, Fisher J, Ingham E. Development and characterization of an acellular porcine cartilage bone matrix for use in tissue engineering. *J Biomed Mater Res A*. 2011;99:283-294. doi:10.1002/jbm.a.33171
56. Yang Q, Peng J, Guo Q, et al. A cartilage ECM-derived 3-D porous acellular matrix scaffold for in vivo cartilage tissue engineering with PKH26-labeled chondrogenic bone marrow-derived mesenchymal stem cells. *Biomaterials*. 2008;29:2378-2387. doi:10.1016/j.biomaterials.2008.01.037
57. Rihn JA, Irrgang JJ, Chhabra A, Fu FH, Harner CD. Does irradiation affect the clinical outcome of patellar tendon allograft ACL reconstruction? *Knee Surg Sports Traumatol Arthrosc*. 2006;14:885-896. doi:10.1007/s00167-006-0036-7
58. Waletzko-Hellwig J, Saemann M, Schulze M, Frerich B, Bader R, Dau M. Mechanical characterization of human trabecular and formed granulate bone cylinders processed by high hydrostatic pressure. *Materials (Basel)*. 2021;14:1069.
59. Naal F-D, Mengele K, Schauwecker J, et al. High hydrostatic pressure-induced cell death in human chondrocytes and chondrosarcoma cells. *Anticancer Res*. 2005;25:1977-1982.
60. Diehl P, Schmitt M, Blümelhuber G, et al. Induction of tumor cell death by high hydrostatic pressure as a novel supporting technique in orthopedic surgery. *Oncol Rep*. 2003;10:1851-1855. doi:10.3892/or.10.6.1851
61. Zemmyo D, Yamamoto M, Miyata S. Efficient decellularization by application of moderate high hydrostatic pressure with supercooling pretreatment. *Micromachines (Basel)*. 2021;12:1486. doi:10.3390/mi12121486
62. Maletzki C, Freiin Grote V, Kalle F, et al. Establishing safe high hydrostatic pressure devitalization thresholds for autologous head and neck cancer vaccination and reconstruction. *Cell Death Discov*. 2023;9:390. doi:10.1038/s41420-023-01671-z
63. Rodiles-López JO, Arroyo-Maya IJ, Jaramillo-Flores ME, et al. Effects of high hydrostatic pressure on the structure of bovine alpha-lactalbumin. *J Dairy Sci*. 2010;93:1420-1428. doi:10.3168/jds.2009-2786
64. Breda A, Valadares NF, Souza ON, Garratt RC. Chapter A06. *Protein Structure, Modelling and Applications: Why is It Important to Study Proteins? Explosion of Biological Sequence and Structure Data, Bioinformatics in Tropical Disease Research: A Practical and Case-Study Approach*; 2008:1-34.
65. Watanabe N, Mizuno M, Matsuda J, et al. Comparison of high-hydrostatic-pressure decellularized versus freeze-thawed porcine menisci. *J Orthop Res*. 2019;37:2466-2475.
66. Fischer I, Westphal M, Rossbach B, et al. Comparative characterization of decellularized renal scaffolds for tissue engineering. *Biomed Mater*. 2017;12:45005. doi:10.1088/1748-605X/aa6c6d
67. Poornejad N, Schaumann LB, Buckmiller EM, et al. The impact of decellularization agents on renal tissue extracellular matrix. *J Biomater Appl*. 2016;31:521-533. doi:10.1177/0885328216656099
68. Hiemer B, Genz B, Jonitz-Heincke A, et al. Devitalisation of human cartilage by high hydrostatic pressure treatment: subsequent cultivation of chondrocytes and mesenchymal stem cells on the devitalised tissue. *Sci Rep*. 2016;6:33747.
69. Diehl P, Schmitt M, Schauwecker J, et al. Effect of high hydrostatic pressure on biological properties of extracellular bone matrix proteins. *Int J Mol Med*. 2005;16:285-289.
70. Sutherland AJ, Converse GL, Hopkins RA, Detamore MS. The bioactivity of cartilage extracellular matrix in articular cartilage regeneration. *Adv Healthc Mater*. 2015;4:29-39. doi:10.1002/adhm.201400165
71. Elmore S. Apoptosis: a review of programmed cell death. *Toxicol Pathol*. 2007;35:495-516. doi:10.1080/01926230701320337
72. Kono H, Rock KL. How dying cells alert the immune system to danger. *Nat Rev Immunol*. 2008;8:279-289. doi:10.1038/nri2215
73. Yang Y, Jiang G, Zhang P, Fan J. Programmed cell death and its role in inflammation. *Mil Med Res*. 2015;2:12. doi:10.1186/s40779-015-0039-0
74. Brusis T. Die erste allogene Trachealtransplantation beim Menschen vor 45 Jahren Vorgehen, Verlauf und Ergebnis. *HNO*. 2023;71:763-766. doi:10.1007/s00106-023-01374-y
75. Niemietz T, Zass G, Hagmann S, Diederichs S, Gotterbarm T, Richter W. Xenogeneic transplantation of articular chondrocytes into full-thickness articular cartilage defects in minipigs: fate of cells and the role of macrophages. *Cell Tissue Res*. 2014;358:749-761. doi:10.1007/s00441-014-1982-x
76. Smith B, Sigal IR, Grande DA. Immunology and cartilage regeneration. *Immunol Res*. 2015;63:181-186. doi:10.1007/s12026-015-8720-7
77. Sicari BM, Johnson SA, Siu BF, et al. The effect of source animal age upon the in vivo remodeling characteristics of an extracellular matrix scaffold. *Biomaterials*. 2012;33:5524-5533. doi:10.1016/j.biomaterials.2012.04.017
78. Wang RM, Johnson TD, He J, et al. Humanized mouse model for assessing the human immune response to xenogeneic and allogeneic decellularized biomaterials. *Biomaterials*. 2017;129:98-110. doi:10.1016/j.biomaterials.2017.03.016
79. Sánchez JC, Díaz DM, Sánchez LV, et al. Decellularization and in vivo recellularization of abdominal porcine fascial tissue, tissue. *Eng Regen Med*. 2021;18:369-376. doi:10.1007/s13770-020-00314-z
80. Nürnberger S, Schneider C, Keibl C, et al. Repopulation of decellularised articular cartilage by laser-based matrix engraving. *EBioMedicine*. 2021;64:103196. doi:10.1016/j.ebiom.2020.103196
81. Loeffler H, Waletzko-Hellwig J, Fischer R-J, et al. Systematic enhancement of microbial decontamination efficiency in bone graft processing by means of high hydrostatic pressure using *Escherichia*

coli as a model organism. *J Biomed Mater Res B Appl Biomater*. 2024; 112:e35383. doi:10.1002/jbm.b.35383

SUPPORTING INFORMATION

Additional supporting information can be found online in the Supporting Information section at the end of this article.

How to cite this article: Kalle F, Stadler VP, Brach JK, et al. High hydrostatic pressure treatment for advanced tissue grafts in reconstructive head and neck surgery. *J Biomed Mater Res*. 2024;1-19. doi:10.1002/jbm.a.37791

scientific reports

Check for updates

OPEN

3D-printed lightweight dorsal skin fold chambers from PEEK reduce chamber-related animal distress

Wentao Xie[1,2], Matthias Lorenz[3], Friederike Poosch[4], Rupert Palme[5], Dietmar Zechner[1], Brigitte Vollmar[1], Eberhard Grambow[1,6]✉ & Daniel Strüder[1,4]

The dorsal skinfold chamber is one of the most important in vivo models for repetitive longitudinal assessment of microcirculation and inflammation. This study aimed to refine this model by introducing a new lightweight chamber made from polyetheretherketone (PEEK). Body weight, burrowing activity, distress, faecal corticosterone metabolites and the tilting angle of the chambers were analysed in mice carrying either a standard titanium chamber or a PEEK chamber. Data was obtained before chamber preparation and over a postoperative period of three weeks. In the early postoperative phase, reduced body weight and increased faecal corticosterone metabolites were found in mice with titanium chambers. Chamber tilting and tilting-related complications were reduced in mice with PEEK chambers. The distress score was significantly increased in both groups after chamber preparation, but only returned to preoperative values in mice with PEEK chambers. In summary, we have shown that light chambers reduce animal distress and may extend the maximum dorsal skinfold chamber observation time. Chambers made of PEEK are particularly suitable for this purpose: They are autoclavable, sufficiently stable to withstand rodent bites, inexpensive, and widely available through 3D printing.

The dorsal skinfold chamber is an essential model for in vivo microcirculation analysis[1]. Researchers investigated inflammation[2–4], thrombogenesis[5–7], wound healing[8,9], angiogenesis, biomaterials[10] and tumor vascularisation[11–13] using the dorsal skinfold chamber[14–16]. Repetitive intravital visualisation of the microvascular dynamics is the major advantage of the model (Fig. 1).

Repetitive intravital microscopy without repetitive surgery requires the continuous exposition of the prepared vascular bed. The skinfold chamber on the back of the laboratory animal ensures optimal conditions for repetitive intravital microscopy[17]. The standard chamber comprises two titanium frames fixing the extended dorsal skin in the back's midline. During chamber implantation, the first frame is sutured to one side of the dorsal skinfold. The skin, the subcutaneous tissue, and the striated panniculus carnosus muscle on one side of the dorsal skinfold are removed. Then, microsurgery exposes the vessels of the opposite panniculus carnosus muscle. Finally, screws are punched through the dorsal skinfold to connect the second frame of the chamber and the observation window is filled with saline followed by sealing with a coverslip.

The major limitation of the model is the physical burden of the chamber, which leads to animal immobilization and distress. The titanium dorsal skinfold chamber is 4 cm long, 3 cm high, and weighs 3.8 g. The weight matches up to 20% of the mouse's body weight (20–30 g). Weight and skin stretching may lead to restricted breathing, immobilization, and pain. The severity of any dorsal skinfold chamber experiment is considered at least moderate. Therefore, the reputation of the model as a standard in microvascular research has been contested in the context of 3R (refinement, reduction, replacement)[18].

Lateral tilting of the dorsal skinfold chamber is another important limitation and strongly related to animal distress[17]. Weight, the chamber's high center-of-gravity, and overstretching of the skin (in particular at the fixation

[1]Institute for Experimental Surgery, Rostock University Medical Center, 18057 Rostock, Germany. [2]Department of Vascular and Thyroid Surgery, Department of General Surgery, The First Affiliated Hospital of Anhui Medical University, Hefei 230022, China. [3]Faculty of Engineering, Technology, Business and Design, University of Applied Sciences, 23966 Wismar, Germany. [4]Department of Otorhinolaryngology, Head and Neck Surgery "Otto Koerner", Rostock University Medical Center, 18057 Rostock, Germany. [5]Unit of Physiology, Pathophysiology and Experimental Endocrinology, Department of Biomedical Sciences, University of Veterinary Medicine Vienna, 1210 Vienna, Austria. [6]Department of General, Visceral, Thoracic, Vascular and Transplantation Surgery, Rostock University Medical Center, Schillingallee 35, 18057 Rostock, Germany. ✉email: eberhard.grambow@med.uni-rostock.de

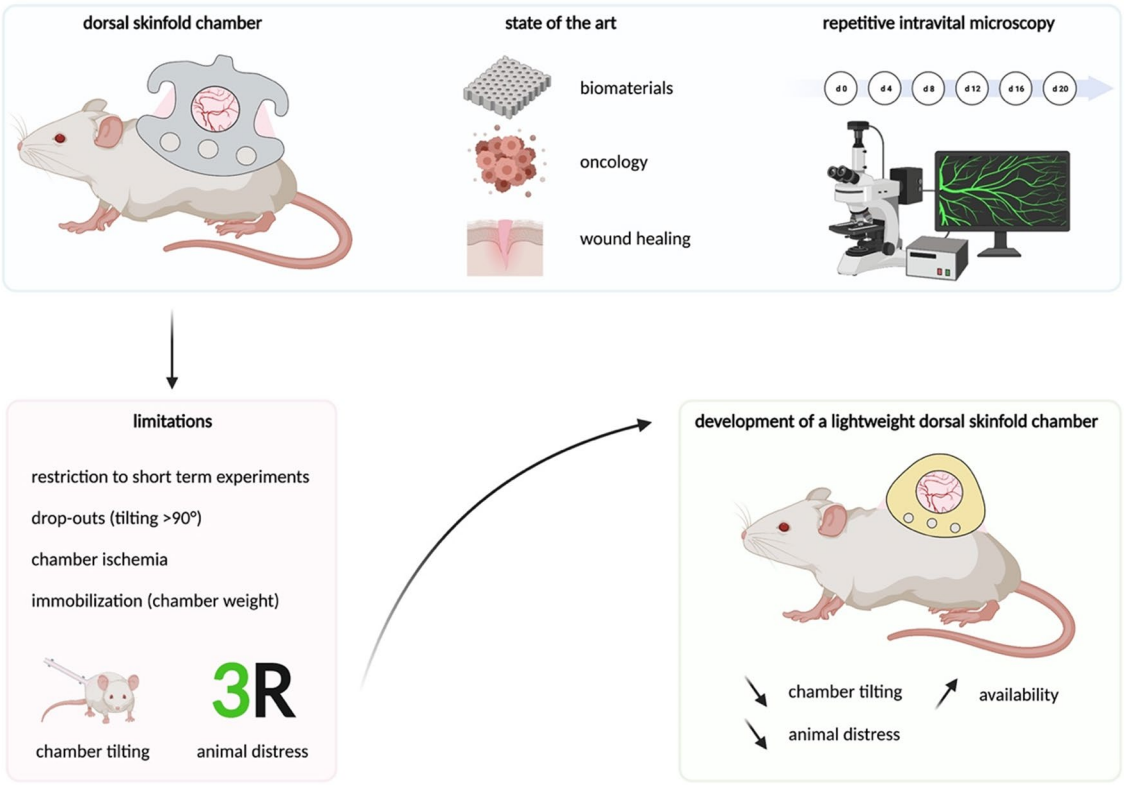

Figure 1. Application and limitations of the dorsal skinfold chamber. The model enables continuous observation of microvascular parameters by intravital microscopy. The major limitations are animal distress and restriction to short-term experiments. To improve animal welfare and extend the observation time, a lightweight, 3D-printable PEEK chamber was developed. Figure created with BioRender.com.

screws) lead to lateral tilting of the chamber in the second week after dorsal skinfold chamber preparation. Tilting comprises perfusion and causes animal distress (immobilization, pain). Chamber tilting of > 50° must be scored in the severity assessment and tilting of > 100° considered as an abort criterion. Therefore, experiments of up to 21 days are associated with high dropouts (20% in the third week) and low reliability (infections, ischemia). Experiments of longer than 21 days are impossible with standard chambers[19,20].

To overcome these limitations, the chambers were continuously revised. Schreiter et al. reviewed the developments until 2017[1]. While 63% of the dorsal skinfold chamber studies were from German-speaking countries and mostly used titanium chambers, smaller titanium chambers are already standard in the US[1]. Research groups from Sweden and Asia proposed more advanced plastic chambers made from plexiglass, dacron and polyetheretherketone (PEEK)[1].

For many years, PEEK has been used successfully in medicine as a replacement material for titanium to fabricate surgical devices, implants and prostheses[21,22]. PEEK is a linear, semi-crystalline polymer that exhibits excellent mechanical and thermal properties. PEEK is bioinert and durable (lack of thermal aging and chemical resistance).

Although many publications point out disadvantages of large titanium chambers, they are still used in most studies: Between 2017 and 2021, only four of 76 studies used non-titanium chambers (70 titanium, 3 plastic, 1 steel wire, 2 no information given; Suppl. Table S1)[23–26].

One factor in the limited distribution of improved dorsal skinfold chamber is that previous research on chamber refinement missed quantifying the actual impact on animal distress. Existing titanium chamber stocks and poor availability of plastic chambers are further factors, which hindered comprehensive implementation of refined dorsal skinfold chambers.

The goal of the present study was the design and evaluation of a lightweight PEEK dorsal skinfold chamber to reduce animal distress and preserve repetitive intravital microscopy quality. We introduce a 3D printed design with unrestricted access and evaluate animal distress compared with traditional chambers. Therefore, the pilot study assessed specific dorsal skinfold chamber parameters (intravital microscopy quality, chamber tilting) and general distress parameters (weight loss, corticosterone levels, behaviour, distress score). As bridging technology, the PEEK chamber may improve future in vivo research until sufficient in vitro and in virtuo models are established.

	Titanium chamber	PEEK chamber
Weigth (g)	3.8	1.5
Height (mm)	36 × 24	24 × 20
Transdermal screws	3	–
Price (€)	30–110	5

Table 1. Comparison of the titanium and PEEK chamber.

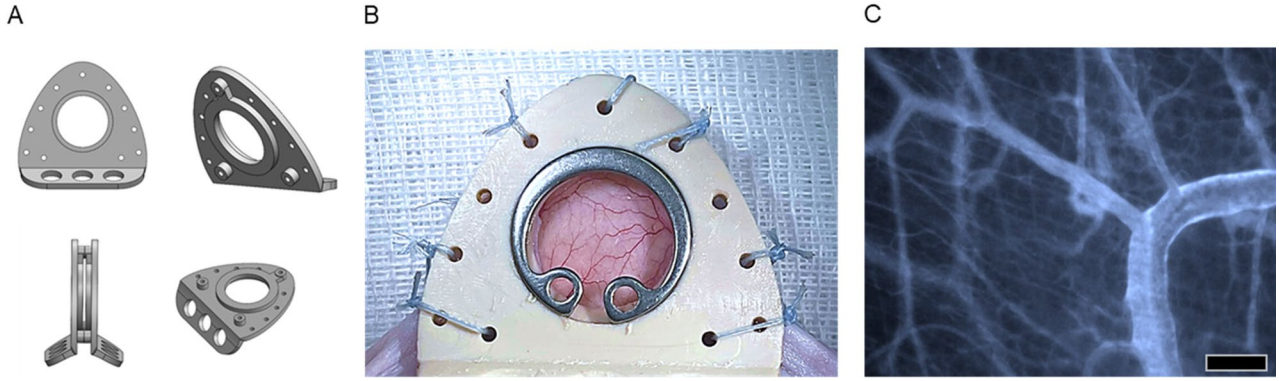

Figure 2. Exemplary design of the PEEK chamber. (**A**) Model of the scaled-down and 3D-printable PEEK chamber (created with SolidWorks). (**B**) The extrusion printed PEEK chamber was ground to remove superficial irregularities and implantated into the test animal. (**C**) Representative intravital microscopy image of a PEEK chamber on day 3. Bar represents 100 µm.

Results

This study examined animal distress of standard titanium dorsal skinfold chambers compared to a 3D printed design made of PEEK. Preparation of the chamber and intravital microscopy were comparable. PEEK chambers showed no signs of bites, chews or any other manipulation by the mice. In terms of lateral chamber tilting, animal weight loss and corticoid levels, the PEEK chamber was markedly superior.

The new PEEK chamber was designed lower and lighter than titanium chambers (approx. 1.5 g instead of 3.8 g). The chamber was 3D-printed cost-effectively according to a reproducible protocol (€5.30 /chamber). The costs were lower compared to milled titanium chambers (€30–€110). The design and the low weight allowed the PEEK chamber to be secured with sutures (Table 1). Robust suture material (FiberWire, Arthrex, Munich, Germany) attached with multiple knots reliably fixed the chamber for 21 days (Fig. 2). The traumatic transdermal insertion of titanium screws was obsolete. The duration and difficulty of chamber implantation was comparable to the titanium chamber (20 min). PEEK is bioinert and autoclavable; wound infections did not occur in the pilot study, even with repeated use of autoclaved chambers.

PEEK chambers significantly reduced lateral tilting in the third week (Fig. 3). In the first week, both preparations were stable in the median plane; the titanium group even showed slightly less tilting (PEEK: 15°/9°–35°; titanium: 5°/0°–28°, $p = 0.1688$; median/95% confidence interval). None of the chambers tilted by > 45° in the first week. In the second week, one PEEK chamber tilted moderately by 72° and one titanium chamber tilted severely by 102°. The other five of six chambers in the respective groups remained stable with less than 20° deviation. In the third week, the deviation of the moderately tilted PEEK chamber remained stable, and another PEEK chamber tilted likewise. Four of six PEEK chambers showed no deviation even after 21 days. In the titanium group, however, the tilting angle increased markedly in five of six animals. In three of six titanium chamber animals, the chamber deviated to about 90° and the skin around the screws had stretched to large defects. The median tilting of the titanium chambers was significantly greater than tilting of the PEEK chambers in the third week (PEEK: 8.5°/0°–62°; titanium: 67°/10°–129°, $p < 0.05$).

Postoperative weight loss was significantly reduced in PEEK chamber mice (Fig. 4A). While significant weight loss occurred postoperatively in all animals, weight loss was lower with PEEK chambers (PEEK: − 6.12%/− 14.46 to 1.06%; titanium: − 14.69%/− 18.95 to 8.77%; $p < 0.05$). The body weight of PEEK chamber mice recovered already in the middle phase (2.46%/− 0.47 to 9.07%). Titanium chamber animals did not fully recover from the high initial weight loss until the late phase (− 3.33%/− 25.68% to 5.10%). Additionally, the weight loss of titanium chamber approached 20%, which is considered as an abort criterium.

Similar beneficial results for the PEEK chamber were found for faeces corticosterone metabolites (FCMs; Fig. 4B). In the PEEK group, only two animals experienced a slight increase in FCMs during the early phase (147%/121–281% $p = 0.13$). In contrast, early phase FCMs in mice with titanium chambers increased fourfold compared to baseline (baseline: 100%, early phase: 368%/248–587%; $p < 0.05$). In the middle and late phase, FCM values in both groups returned to the baseline (Fig. 4B). The direct comparison between PEEK and titanium chambers revealed a significant increase of titanium chamber FCMs in the early phase (PEEK: 147%/121–281%;

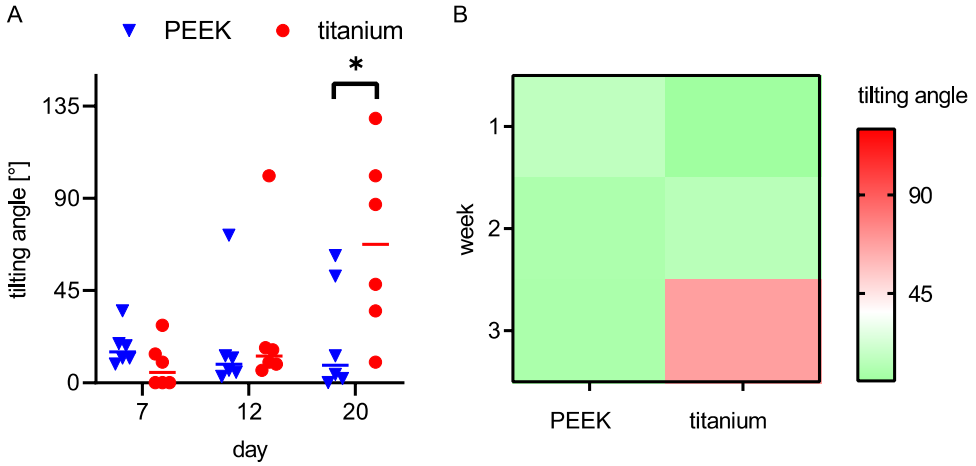

Figure 3. Lateral chamber tilting. PEEK and titanium chamber tilting angles over time are given as individual values (**A**) and as a heatmap indicating high risk for lateral chamber tilting (**B**). PEEK chambers significantly reduced lateral tilting in the third week, while tilting in both chambers was comparable for 12 days. This is further visualized in the heat map (**B**). Differences between the groups were analysed by multiple t-tests (Holm-Sidak), *$p < 0.05$, PEEK: $n = 6$, titanium: $n = 6$.

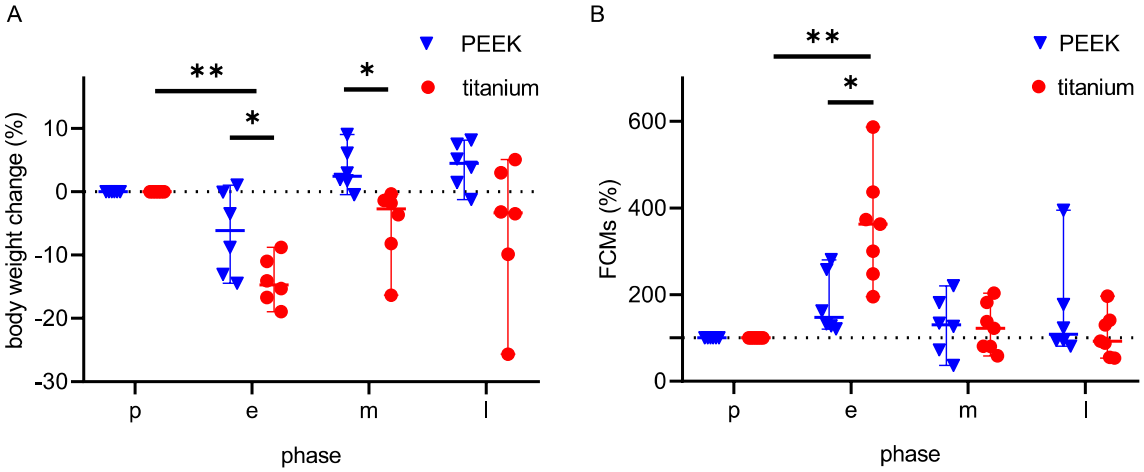

Figure 4. Changes in body weight and faecal corticosterone metabolite (FCM) concentrations after dorsal skinfold chamber implantation. Individual values are given over time in a preoperative phase (p), early postoperative phase (e), middle postoperative phase (m) and late postoperative (l) phase. Body weight change (**A**) between each time point was analysed by RM one-way ANOVA on ranks followed by Dunn's correction, and the difference between each group was analysed by unpaired t test followed by two-tailed P value tests. FCM concentrations (**B**) between each time point was analysed by Friedman test followed by Dunn's correction, and the difference between each group was analysed by unpaired t test followed by two-tailed P value tests. *$p < 0.05$; **$p < 0.05$; PEEK: $n = 6$, titanium: $n = 6$.

titanium: 368%/248–587%, $p < 0.05$), while FCMs were comparable in the middle (PEEK: 130%/37–220%; titanium: 101%/59–203%, $p = 0.31$) and late phase (PEEK: 108%/81–395%; titanium: 90%/54–196%, $p = 0.85$).

Specific distress scoring and burrowing assessment did not show differences between titanium and the PEEK chambers (Fig. 5). Distress values remained low, with maximum 7/66 points for PEEK and 6/66 points for titanium chambers ($p > 0.8268$). In both groups, the distress score increased slightly in the early phase and declined in the middle and late phase. Likewise, burrowing started with relatively high baseline values (PEEK: 108 g/57–195 g; titanium: 196 g/105–200 g, $p = 0.06$). Postoperative burrowing decreased significantly in both groups (PEEK: $p < 0.05$; titanium: $p = 0.05$, vs. baseline). Burrowing remained decreased markedly throughout the observation time in both groups (PEEK: 61 g/13–192 g; titanium: 36 g/20–56 g).

In summary, the PEEK chamber is easily available and maintains the high quality of intravital vascular imaging. The PEEK chamber's flat and lightweight design can reduce animal distress and prolong the maximum duration of the experiment.

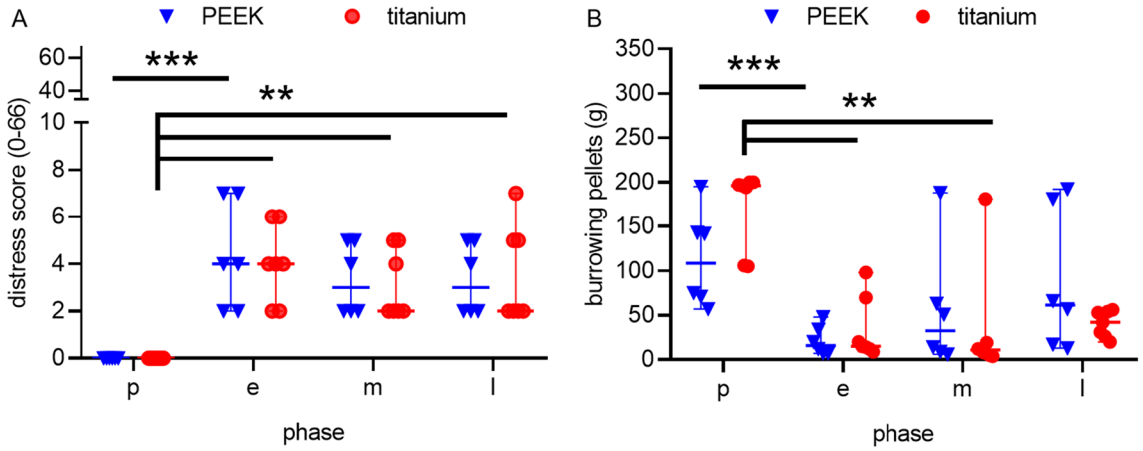

Figure 5. Distress Score and burrowing activity after dorsal skinfold chamber implantation. Individual values are given over time in a preoperative phase (p), early postoperative phase (e), intermediate postoperative phase (m) and late postoperative (l) phase. Specific distress scoring and burrowing assessment did not show differences between the titanium and the PEEK chamber. Distress score (**A**) and burrowing activity (**B**) at each time point were compared by Friedman test followed by Dunn's correction and the difference between each group was analysed by unpaired t test (Holm-Sidak). $^{**}p < 0.05$, $^{***}p < 0.05$; PEEK: n = 6, titanium: n = 6.

Discussion

The dorsal skinfold chamber is a major model for repetitive examination of vascular changes and inflammation. However, the dorsal skinfold chamber causes considerable stress for the test animals. Therefore, the model is not only criticized by animal welfare groups. This criticism is understandable, since many improved models have already been published, but mainly the classical titanium chamber is used[17,23,24,27–29]. For the widespread establishment of plastic chambers, a simple manufacturing protocol has been lacking on the one hand and proof of superiority in distress reduction on the other.

Here, we present a simple 3D-printed model made of PEEK. We show that the PEEK chamber reduces distress and extends maximum observation time.

The surgical demands and the quality of intravital microscopy are equivalent in PEEK and titanium chambers. When implanting the PEEK chamber, penetration of the skinfold with screws can be omitted, because of the chamber's light weight. In titanium chambers, screws cause penetrating holes at the base of the skinfold, which are associated with chamber tilting. The PEEK chamber is fixed by tear resistant sutures, which the test animal cannot reopen (FibreWire, Arthrex, Munich, Germany). These sutures cause less trauma than previously used screws. After chamber implantation, the experiments run without differences to titanium chambers. In particular, there are no differences in the quality of the repetitive intravital fluorescence microscopy.

The most common complication of dorsal skinfold chamber experiments is lateral tilting of the chamber during the second week[17]. By the third week, 50% of the titanium chambers tilt to a position of > 90°, which causes animal immobilization. In all PEEK chambers, tilting remained below 90° for three weeks. The only PEEK chamber that had a tilting of 50° in the second week remained constant in the following week. This is clearly because of the reduced weight. In contrast, titanium chambers continued tilting over time. Therefore, the stable position of PEEK chambers could extend the maximum duration of future experiments to four or five weeks.

Besides decreased tilting in the third week, the use of PEEK chambers also reduced distress for the experimental animals in the postoperative period. Postoperative weight loss is significantly higher in titanium chamber animals and does not return to baseline values over three weeks. With PEEK chambers, on the other hand, the test animals reach their original weight as early as the second week. Consistent with our data, previous research described up to 15% postoperative weight loss for titanium chambers and decreased weight loss for non-metal dorsal skinfold chambers[30–32].

This difference in stress was confirmed by FCM measurement, a non-invasive measure of adrenocortical activity[33]. FCMs increased significantly after implantation of a titanium chamber while only a slight increase in FCMs was observed for PEEK chambers. Therefore, postoperative stress was primarily related to the titanium chamber and not to the surgery itself. In the intermediate and late phase, FCMs returned to baseline values in both groups. The design of future titanium chamber experiments should consider increased postoperative stress as a potential bias[34].

In contrast to FCMs and body weight changes, mice in both groups did not differ in burrowing activity nor distress score. The distress score remained at a low level after the operation. The postoperative increase of 7/66 points in the distress score was statistically significant. However, the values remained in the lower range of the score.

To our knowledge, this study is the first to investigate the distress of laboratory animals with dorsal skinfold chambers. Despite the lack of data on animal distress, many chamber improvements have already been published. These improvements were supposed to reduce animal distress and to enable MRI imaging. A simple development is a smaller titanium frame with an equally large observation window[29]. These smaller titanium chambers are sold commercially in the United States (small dorsal kit SM100, APJ Trading Co., Ventura, CA, USA). Schreiter

et al. describe the advantages of a self-designed small titanium chamber: postoperatively no recovery period was necessary, younger animals could be used and their stress was supposed to be reduced[1]. However, titanium chambers are not MRI compatible and screw fixation is necessary. Furthermore, titanium is difficult to process and cannot be manufactured in life science facilities.

Innovative developments are chambers made of plastic, which have been used for years in Japan and the US. The first plastic chamber made of Duracon was described in 2003 by Ushiyama et al.[17]. The publication illustrated reduced tilting and supposed distress reduction, because of the lightweight Duracon material. However, quantification of tilting and distress was not performed. In addition, these early plastic chambers continued to use screw fixation[17,35]. These screws penetrate the skin and cause large wounds at the chamber basis.

A further weight reduction was achieved by using thermoplastic PEEK. PEEK is characterized by a high flexural modulus (3738 MPa) and tensile strength (100 MPa) compared to Duracon (2500 MPa, 87 MPa) and acrylic glass (3210 MPa, 75 MPa)[36]. PEEK can therefore resist the bite of rodents. Furthermore, PEEK can be fabricated with additive manufacturing processes, which results in further advantages such as a high degree of geometric freedom, low production costs and the flexibility regarding the unique or single-part production[37].

The first lightweight PEEK chambers were introduced by Gaustad et al. and Seynhaeve et al.[23,28]. The PEEK chamber weight was as low as 1 g and 1.1 g, respectively. The chambers were fixed using sutures (Gaustad) or small screws (Seyhaeve). Mice fitted with the chambers showed a full capacity of motion, climbed, and gained weight as mice without chambers. We observed similar positive effects for PEEK chambers (body weight, climbing, mobility). In addition, we verified reduced distress using a standardized protocol. We have repetitively measured chamber tilting and found that the PEEK chambers significantly reduce tilting in the third week of the experiment. Lightweight chambers with reduced lateral tilting enable increased observation times of up to one month[27]. This is especially relevant for biomaterial and oncology research: dorsal skinfold chamber observation times of three to five weeks could enable to study long-term biomaterial integration (fibrosis, giant cell formation, implant vascularization)[38]. In oncology, longer observation times could significantly improve the model, since the growth of tumor cells already preoccupies large parts of the current maximum observation time[39].

The reduction in tilting was significant, although the measurement method had limitations, as the chamber position depends on the body position. The measurement was performed on anaesthetized animals in an upright position with all feet on the ground. However, when positioning the animals, slight deviations of the angles occurred.

Another limitation of the study is that the standardized distress score does not focus on the immobilization of the test animals. However, the impediment of free movement, because of tilting and chamber weight, probably represents the main restriction for the experimental animals. Electronically recording of the animal mobility through tracking systems or recording of the time spent climbing the cage could increase the power of the stress analysis. However, using standardized distress scores enables comparisons to previous experiments.

The low number (n = 6) of test animals may be considered another limitation of the study. However, the PEEK chamber was significantly superior in major outcomes, such as tilting and weight loss. Therefore, no additional experimental animals had to be included. Another limitation related to the study design is that the PEEK and the titanium chambers have different sizes. Hence, all conclusions are related to the design (height, weight), but not to the material (PEEK vs. titanium). Low and lightweight titanium chambers may also decrease animal distress compared to large standard titanium chambers. Yet, we consider PEEK a more suitable material because it increases availability, enables imaging, and decreases costs. These main advantages render a light titanium group obsolete.

Conclusion. In experiments with dorsal skinfold chambers, the animals are particularly stressed by classical titanium chambers. This setup should be revised, in the context of 3R. Despite the development of smaller and lighter chambers, most dorsal skinfold chamber experiments in recent years have continued to use titanium chambers. We have shown that lighter chambers can significantly reduce animal distress and even extend the maximum experiment duration. Chambers made of PEEK are particularly suitable for this purpose: They are autoclavable, sufficiently stable to withstand rodents, inexpensive, and widely available through 3D printing.

Methods

PEEK chamber printing. The PEEK chamber was designed for geometric shape improvement, weight reduction, and optimization for additive manufacturing using SolidWorks (Dassault Systèmes, Waltham, MA, USA). The Fused Filament Fabrication (FFF) process and the printer Minifactory ultra (miniFactory Oy LTD, Seinäjoki, Finland) were used for chamber printing. The design (*.stl file) was imported to Simplify3d (Simplify3d, Ohio, US). Biocompatible and steam sterilizable PEEK filament Intamsys Funmat HT (INTAMSYS Technology Co. Ltd, Shanghai, China) with a flexural modulus of 3738 MPa and tensile strength of 100 MPa was chosen. The material-dependent printing parameters were 230 °C chamber temperature, 190 °C bed temperature, 420 °C nozzle temperature 0.4 mm nozzle diameter, and 18 mm/s printing speed. Slicing was done according to the manufacture settings with a corresponding layer thickness of 250 µm. A brim of 3 mm gave optimal hold to the chamber on the printer bed. To ensure a plane chamber surface for skin contact side, the bottom of the chamber was placed on the printer glass bed for slicing. An extrusion multiplexer of 1.02 was set to fill production-related gaps between the filaments in the x–y direction (see supplementary PEEK chamber 3D printing protocol). Irregularities on the top side (window side) were ground manually after the printing process (printed chamber before polishing shown in supplementary Figure S1 and polished surface shown in Fig. 2B). Seven holes of 1 mm diameter were drilled into the frames for suture chamber fixation using a template. Before experimental use, the chamber was visually proved and post processed by steam sterilization.

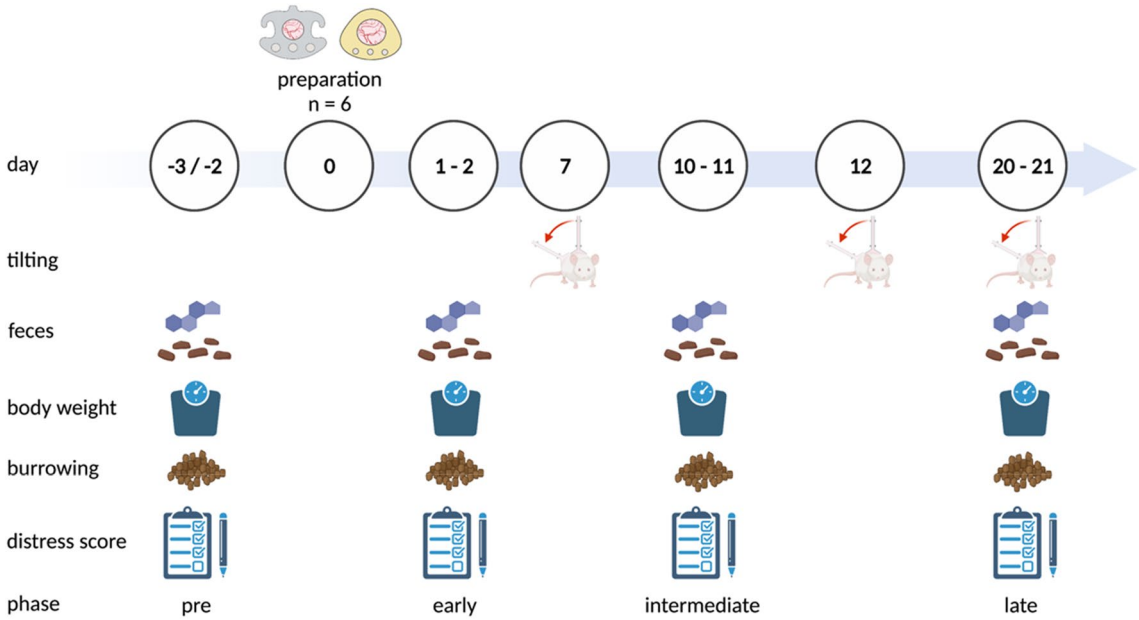

Figure 6. Experimental design. The dorsal skinfold chambers were implanted on day 0. Tilting angles were assessed on day 7, 12 and 21. Collection of faeces, body weight measurement, burrowing analysis and distress scoring were performed in a preoperative, early, intermediate, and late postoperative phase. Figure created with BioRender.com.

Animals and ethics statement. All in vivo experiments were conducted in accordance with the German legislation on protection of animals (7221.3-1-012/20) and the NIH Guide for the Care and Use of Laboratory Animals (Institute of Laboratory Animal Resources, National Research Council). Male hairless SKH1/hr mice (6–10 weeks of age and weight of 25–30 g) were used for all experiments. The animals were housed individually in a specific pathogen-free facility with a twelve-hour light–dark cycle and access to standard laboratory chow and water ad libitum.

Study design. Twelve mice were randomly allocated to two experimental groups: titanium chamber and PEEK chamber. Each animal was one experimental unit and examined independently using body weight, faecal corticosterone metabolites (FCMs), burrowing activity and clinical distress scores on days 1/2, 10/11 and 20/21 after dorsal skinfold chamber preparation. Following distress and tilting measurements on day 21, mice were sacrificed (Fig. 6).

Experimental procedures. Dorsal skinfold chamber implantation: Mice were anesthetized by an intraperitoneal (ip) injection of ketamine/xylazine (90/10 mg/kg bw) and positioned on a heating pad (37.8 °C). Microsurgery for dorsal skinfold titanium chamber implantation has been described before[5]. The significant change in the proposed model is the preparation without screws: After disinfection of the dorsal skin (Octeniderm, Schülke & Mayr GmbH, Norderstedt, Germany) and marking of the median line, a skin bilayer was stretched in the median line. Subsequently, the back of the PEEK chamber was sutured to the skin fold through the preformed holes (FiberWire, Arthrex, Munich, Germany). The preparation area was color-marked and the microsurgical preparation of the front side was performed. After completion of the preparation, the front of the chamber was placed congruently and fixed by three sutures connecting both chamber frames (Fig. 2).

Chamber tilting. For chamber tilting analysis, animals were sedated in an isoflurane chamber for approximately ten seconds on days 7, 12, and 20/21. The sedated animals were positioned upright, with all feet on the floor. In the upright position, the animals were photographed from behind. In Photoshop software (Adobe Inc., San José, U.S.), the lateral tilting angle was measured in degrees of deviation from a vertical line.

Body weight. The body weight was measured on a scale (EMB 200-2, Kern & Sohn, Balingen, Germany) at 9:00–9:30 am. Percent change in body weight was determined by comparison with body weight in the preoperative phase.

Distress score. Since handling may affect animal distress, the distress score was assessed before weighting. The distress score sheet comprises body weight, general condition, spontaneous behaviour, flight behaviour and process-specific criteria, as previously published[40]. (Suppl. Tables S2 and S3).

Burrowing. To quantify the burrowing activity, a tube (length: 15 cm, diameter: 6.5 cm) filled with 200 ± 1 g of food pellets (ssniff Spezialdiaeten GmbH, Soest, Germany) was placed in the left back corner of the cages 3 h before the dark phase at 04:00–04:10 pm. Despite the implanted chambers, mice had free access to these pellets throughout the whole observation time. The weight of the food pellets (g) left in the tube was measured on the next day.

Faecal corticosterone metabolites (FCMs). After weighting, the bedding with old faeces was removed and replaced by fresh beddings. After 24 h, at least 400 mg faeces were collected per cage. The faeces were dried for 4 h at 65 °C and kept at − 20 °C until further processing. 50 mg of homogenized, dried faeces were extracted with 1 mL of 80% methanol and FCMs analyzed with a 5α-pregnane-3β, 11β, 21-triol-20-one enzyme immunoassay[41,42]. FCMs were evaluated blinded, and the percentage of FCMs was determined by comparison to respective FCM concentrations in the pre-operative phase.

Intravital microscopy. Representative intravital microscopy was performed on day 3. Mice were anesthetized and placed on a plexiglass pad with integrated heating. For the visualization of the microvascular system fluorescein isothiocyanate–labeled (FITC)-dextran (0.05 ml, 5%, MW: 150 kD) was injected into the lateral tail vein (or into the retrobulbar venous plexus if tail vein injection failed). Intravital microscopy was performed with 50-, 100- and 200-fold magnification using an Axiotech vario microscope (Carl Zeiss AG, Oberkochen, Germany) with a 100-W HBO mercury lamp with a blue filter (excitation, 450–490 nm; emission, 520 nm) The microscopic images were recorded on DVD (DMR-EX99V, Panasonic, Kadoma, Japan) using a charge-coupled video camera (FK 6990A-IQ, Pieper, Berlin, Germany) for off-line evaluation.

Statistics. Data were graphed and analyzed with GraphPad Prism (version 8.0.1, GraphPad Software Inc., San Diego, CA, U.S.) and were presented as median and 95% confidence interval. The characteristics of data were assessed by Shapiro Wilk test. When analyzing the influence of time on the dependent variables, a Friedman Test was performed (corrections of multiple comparisons using Dunn test) in tilting angles, burrowing activity, percentage of FCMs and distress score, and a one-way repeated measure ANOVA was performed (corrections of multiple comparisons using Tukey test) in the percentage of body weight change analysis. When analyzing the influence of the chambers on the dependent variables, a Mann Whitney Rank sum test (for non-parametric data) or unpaired t test (for parametric data) was used. Differences with $p < 0.05$ were considered significant. Data are given as median/95% confidence interval.

Data availability

The datasets generated and analyzed during the current study are available from the corresponding author on reasonable request.

Received: 18 November 2021; Accepted: 30 May 2022
Published online: 08 July 2022

References

1. Schreiter, J., Meyer, S., Schmidt, C., Schulz, R. M. & Langer, S. Dorsal skinfold chamber models in mice. *GMS Interdiscip. Plast. Reconstr. Surg. DGPW* **6**, DOC10 (2017).
2. Pappelbaum, K. I. *et al.* Ultralarge von Willebrand factor fibers mediate luminal *Staphylococcus aureus* adhesion to an intact endothelial cell layer under shear stress. *Circulation* **128**, 50–59 (2013).
3. Butschkau, A. *et al.* Contribution of protein Z and protein Z-dependent protease inhibitor in generalized Shwartzman reaction. *Crit. Care Med.* **41**, e447–e456 (2013).
4. Hillgruber, C. *et al.* Blocking von Willebrand factor for treatment of cutaneous inflammation. *J. Invest. Dermatol.* **134**, 77–86 (2014).
5. Kram, L., Grambow, E., Mueller-Graf, F., Sorg, H. & Vollmar, B. The anti-thrombotic effect of hydrogen sulfide is partly mediated by an upregulation of nitric oxide synthases. *Thromb. Res.* **132**, e112–e117 (2013).
6. Grambow, E. *et al.* Effect of the hydrogen sulfide donor GYY4137 on platelet activation and microvascular thrombus formation in mice. *Platelets* **25**, 166–174 (2014).
7. Ampofo, E. *et al.* Role of protein kinase CK2 in the dynamic interaction of platelets, leukocytes and endothelial cells during thrombus formation. *Thromb. Res.* **136**, 996–1006 (2015).
8. Hergert, B., Grambow, E., Butschkau, A. & Vollmar, B. Effects of systemic pretreatment with CpG oligodeoxynucleotides on skin wound healing in mice. *Wound Repair Regen.* **21**, 723–729 (2013).
9. Sorg, H., Grambow, E., Eckl, E. & Vollmar, B. Oxytocin effects on experimental skin wound healing. *Innov. Surg. Sci.* **2**, 219–232 (2017).
10. Dau, M. *et al.* Collagen membranes of dermal and pericardial origin-In vivo evolvement of vascularization over time. *J. Biomed. Mater. Res. A* **108**, 2368–2378 (2020).
11. Hightower, C. M. & Intaglietta, M. The use of diagnostic frequency continuous ultrasound to improve microcirculatory function after ischemia-reperfusion injury. *Microcirculation* **14**, 571–582 (2007).
12. Püschel, A., Lindenblatt, N., Katzfuss, J., Vollmar, B. & Klar, E. Immunosuppressants accelerate microvascular thrombus formation in vivo: role of endothelial cell activation. *Surgery* **151**, 26–36 (2012).
13. Hillgruber, C. *et al.* Blocking neutrophil diapedesis prevents hemorrhage during thrombocytopenia. *J. Exp. Med.* **212**, 1255–1266 (2015).
14. Baron, V. T., Welsh, J., Abedinpour, P. & Borgström, P. Intravital microscopy in the mouse dorsal chamber model for the study of solid tumors. *Am. J. Cancer. Res.* **1**, 674–686 (2011).
15. Nesbitt, H. *et al.* The unidirectional hypoxia-activated prodrug OCT1002 inhibits growth and vascular development in castrate-resistant prostate tumors. *Prostate* **77**, 1539–1547 (2017).

16. Peng, W. *et al.* Targeted photodynamic therapy of human head and neck squamous cell carcinoma with anti-epidermal growth factor receptor antibody Cetuximab and Photosensitizer IR700DX in the mouse skin-fold window chamber model. *Photochem. Photobiol.* **96**, 708–717 (2020).
17. Ushiyama, A., Yamada, S. & Ohkubo, C. Microcirculatory parameters measured in subcutaneous tissue of the mouse using a novel dorsal skinfold chamber. *Microvasc. Res.* **68**, 147–152 (2004).
18. Russell, W. M. & Burch, R. L. *The Principles of Humane Experimental Technique* (Methuen, 1959).
19. Michael, S., Sorg, H., Peck, C.-T., Reimers, K. & Vogt, P. M. The mouse dorsal skin fold chamber as a means for the analysis of tissue engineered skin. *Burns* **39**, 82–88 (2013).
20. Alieva, M., Ritsma, L., Giedt, R. J., Weissleder, R. & van Rheenen, J. Imaging windows for long-term intravital imaging: General overview and technical insights. *Intravital* **3**, e29917 (2014).
21. Guo, F. *et al.* Biomechanical evaluation of a customized 3D-printed polyetheretherketone condylar prosthesis. *Exp. Ther. Med.* **21**, 348 (2021).
22. Alqurashi, H. *et al.* Polyetherketoneketone (PEKK): An emerging biomaterial for oral implants and dental prostheses. *J. Adv. Res.* **28**, 87–95 (2021).
23. Seynhaeve, A. L. B. & ten Hagen, T. L. M. Intravital microscopy of tumor-associated vasculature using advanced dorsal skinfold window chambers on transgenic fluorescent mice. *J. Vis. Exp.* **131**, e55115 (2018).
24. Gu, J.-M. *et al.* Blockade of placental growth factor reduces vaso-occlusive complications in murine models of sickle cell disease. *Exp. Hematol.* **60**, 73-82.e3 (2018).
25. Tong, F. *et al.* Hypo-fractionation radiotherapy normalizes tumor vasculature in non-small cell lung cancer xenografts through the p-STAT3/HIF-1 alpha signaling pathway. *Ther. Adv. Med. Oncol.* **12**, 1758835920965853 (2020).
26. Nawijn, C. *et al.* Multi-timescale microscopy methods for the characterization of fluorescently-labeled microbubbles for ultrasound-triggered drug release. *J. Vis. Exp.* **172**, e62251 (2021).
27. Axelsson, H., Bagge, U., Lundholm, K. & Svanberg, E. A one-piece plexiglass access chamber for subcutaneous implantation in the dorsal skin fold of the mouse. *Int. J. Microcirc. Clin. Exp.* **17**, 328–329 (1997).
28. Gaustad, J.-V., Brurberg, K. G., Simonsen, T. G., Mollatt, C. S. & Rofstad, E. K. Tumor vascularity assessed by magnetic resonance imaging and intravital microscopy imaging. *Neoplasia* **10**, 354–362 (2008).
29. Choi, M., Chung, T., Choi, K. & Choi, C. Dynamic fluorescence imaging for multiparametric measurement of tumor vasculature. *J. Biomed. Opt.* **16**, 046008 (2011).
30. Shan, S. *et al.* Preferential extravasation and accumulation of liposomal vincristine in tumor comparing to normal tissue enhances antitumor activity. *Cancer Chemother. Pharmacol.* **58**, 245–255 (2006).
31. Gelaw, B. & Levin, S. Wound-induced angiogenesis and its pharmacologic inhibition in a murine model. *Surgery* **130**, 497–501 (2001).
32. Leunig, M., Yuan, F., Gerweck, L. E. & Jain, R. K. Effect of basic fibroblast growth factor on angiogenesis and growth of isografted bone: Quantitative in vitro-in vivo analysis in mice. *Int. J. Microcirc. Clin. Exp.* **17**, 1–9 (1997).
33. Palme, R. Non-invasive measurement of glucocorticoids: Advances and problems. *Physiol. Behav.* **199**, 229–243 (2019).
34. Ibarguen-Vargas, Y., Surget, A., Touma, C., Palme, R. & Belzung, C. Multifaceted strain-specific effects in a mouse model of depression and of antidepressant reversal. *Psychoneuroendocrinology* **33**, 1357–1368 (2008).
35. Leung, H. M., Schafer, R., Pagel, M. M., Robey, I. F. & Gmitro, A. F. Multimodality pH imaging in a mouse dorsal skin fold window chamber model. *Proc. SPIE Int. Soc. Opt. Eng.* **8574**, 85740L (2013).
36. Roderick, R., Xavier, B., Philippe, B., Olli, P. & Riku, H. Semi-crystalline Kepstan® PEKK seals via fused filament fabrication on the miniFactory Ultra®. https://www.extrematerials-arkema.com/files/live/sites/arkema_extrematerials/files/downloads/brochures/kepstan-brochures/kepstan-br-semicrystalline-kepstan-pekk-seals-optimized.pdf (2021).
37. Vaezi, M. & Yang, S. Extrusion-based additive manufacturing of PEEK for biomedical applications. *Virtual Phys. Prototyp.* **10**, 123–135 (2015).
38. Laschke, M. W. & Menger, M. D. The dorsal skinfold chamber: A versatile tool for preclinical research in tissue engineering and regenerative medicine. *Eur. Cell. Mater.* **32**, 202–215 (2016).
39. Boucher, Y., Leunig, M. & Jain, R. K. Tumor angiogenesis and interstitial hypertension. *Cancer Res.* **56**, 4264–4266 (1996).
40. Xie, W. *et al.* Diagnostic ability of methods depicting distress of tumor-bearing mice. *Animals (Basel)* **11**, 2155 (2021).
41. Touma, C., Sachser, N., Möstl, E. & Palme, R. Effects of sex and time of day on metabolism and excretion of corticosterone in urine and feces of mice. *Gen. Comp. Endocrinol.* **130**, 267–278 (2003).
42. Touma, C., Palme, R. & Sachser, N. Analyzing corticosterone metabolites in fecal samples of mice: A noninvasive technique to monitor stress hormones. *Horm. Behav.* **45**, 10–22 (2004).

Acknowledgements

We thank the staff of the Rudolf-Zenker-Institute for Experimental Surgery for the care of the animals during the experiments and Edith Klobetz-Rassam for FCM analysis.

Author contributions

D.S., E.G., D.Z. and B.V. conceived and designed the experiments; W.X., M.L. and F.P. performed the experiments. R.P., W.X., D.S. and E.G. analyzed the data. M.L., and R.P. contributed materials/analysis tools; D.S., E.G. and W.X. wrote the paper. All authors approved the final version of the manuscript.

Funding

Open Access funding enabled and organized by Projekt DEAL. This joint research project HOGEMA is supported by the European Social Fund (ESF), reference: ESF/14-BM-A55-0012/18, and the Ministry of Education, Science and Culture of Mecklenburg-Vorpommern, Germany. Evaluation of distress was supported by the Deutsche Forschungsgemeinschaft (DFG research group FOR 2591, ZE 712/1-1, ZE 712/1-2, VO 450/15-1 and VO 450/15-2).

Competing interests

The authors declare no competing interests.

Additional information

Supplementary Information The online version contains supplementary material available at https://doi.org/10.1038/s41598-022-13924-5.

Correspondence and requests for materials should be addressed to E.G.